Steam Generator Thermal Performance Degradation Case Studies

TR-110018

Final Report, July 1998

EPRI Project Manager
G. Srikantiah

EPRI 3412 Hillview Avenue, Palo Alto, CA 94304, PO Box 10412, Palo Alto, CA 94303, U.S.A. 800.313.3774 or 650.855.2000, www.epri.com

DISCLAIMER OF WARRANTIES AND LIMITATION OF LIABILITIES

ORGANIZATION(S) THAT PREPARED THIS REPORT

Dominion Engineering, Inc.

ORDERING INFORMATION

Requests for copies of this report should be directed to the EPRI Distribution Center, 207 Coggins Drive, P.O. Box 23205, Pleasant Hill, CA 94523, (510) 934-4212.

CITATIONS

This report was prepared by

Dominion Engineering, Inc.
6862 Elm Street
McLean, Virginia 22101

Authors
M. A. Kreider
G. A. White
R. D. Varrin, Jr.

This report describes research sponsored by EPRI.

The report is a corporate document that should be cited in the literature in the following manner:

Steam Generator Thermal Performance Degradation Case Studies, EPRI, Palo Alto, CA: 1998. TR-110018.

REPORT SUMMARY

The steam generator performance degradation case studies in this report form the foundation for an industry thermal performance database. The database's plant-specific information can help utilities identify causes of thermal performance degradation and develop remedial measures.

Background

During the last several years, a significant number of pressurized water reactor (PWR) plants have exhibited decreases in secondary-side steam generator steam pressure. In some cases, the decreases have caused reduced high-pressure turbine pressure and, hence, reduced electrical generating capacity. A reduction of one percent in electrical generating capacity in a typical PWR is equivalent to roughly $2 million per year in replacement power costs, creating a significant impact on utility revenue. In one plant, secondary pressure loss of nearly 80 psi occurred; chemical cleaning of the steam generator restored most of this pressure loss. Secondary tube deposits were the primary cause of this plant's pressure loss. However, secondary deposits are not necessarily the primary cause of thermal performance degradation, as this study demonstrates.

Objectives

To collect and evaluate plant performance history data from three selected plants; to perform a global fouling factor analysis; to quantitatively evaluate the best-estimate and bounding pressure decreases associated with all potential causes of steam pressure degradation for each plant in the study; to analyze available tube deposit data and calculate the thermal resistance of the deposit layers; and, to correlate changes observed in the thermal performance in one plant with historical Dimethylamine (DMA) addition.

Approach

Investigators applied a global fouling factor analysis method to quantify degradation in steam generator performance. In addition to the detailed study of fouling effects due to secondary deposits, this method accounts for changes in thermal power, primary temperatures, heat transfer area (for example, due to tube plugging), and their effect on performance degradation. Inputs to this analysis are thermal hydraulic design data and plant instrument measurements recorded over the operating life of the plants. These measurements include steam pressure, primary temperatures, feed water flow rate, and

the number of plugged and sleeved tubes for each outage. In addition to the fouling factor analysis, investigators studied other potential factors that may contribute to steam pressure degradation.

Results

The report details relative contributions to thermal performance degradation (indicated by steam pressure decreases) in three selected plants due to secondary fouling and other sources. These additional sources include power uprates, primary temperature changes or errors, and tube plugging, each source acting alone or in combination. Fouling due to secondary deposits can be a significant cause and, in fact, may be the major cause of documented pressure loss at one plant.

EPRI Perspective

Steam generator thermal performance degradation—manifested by steam pressure decreases—can be a potential cause of lost generating capacity in PWRs. This pilot study identified factors that may contribute to performance degradation. The three plants in the study were a feed ring design plant (Union Electric's Model F plant, Callaway), a preheat design (Houston Lighting and Power's Model E plant, STP) and an older model 51 (TVA's Sequoyah). Analysts selected these plants based on the severity of their pressure loss and other factors. A fourth plant, TU Electric's Comanch Peak, was added later to evaluate potential effects of DMA soaks on performance.

The study showed that none of the plants suffered severe fouling due to secondary deposits, though it was a contributing factor. Major causes included power uprates, hot leg temperature streaming, and primary temperature decrease. Tracking the global fouling factor, installing more accurate instrumentation, and characterizing the secondary deposit properties can all aid in evaluating and remedying potential causes. The plant-specific information and analysis results add to the industry database of thermal performance information, thereby helping utilities identify causes of—and prepare remedial measures for—potential thermal performance degradation.

TR-110018

Interest Categories

Steam generators
Plant thermal performance

Keywords

Sludge
Fouling
Performance degradation
Steam generators
Thermal performance
Steam pressure loss

ABSTRACT

In order to further understanding of steam generator (SG) thermal performance degradation, which can cause SG steam pressure decreases and potentially lost electrical generating capacity, case studies of the SGs at three US plants were performed: Callaway (Westinghouse Model F), Sequoyah 1 (Westinghouse Model 51), and South Texas 1 (Westinghouse Model E2). In addition, results from a previous analysis of San Onofre 2 (CE Model 3410) are summarized. Another plant, Comanche Peak 2 (Westinghouse Model D5), was later added to the study, in part to evaluate the potential effects of dimethylamine (DMA) soaks on SG performance. For each plant, historical thermal-hydraulic data were collected to facilitate calculation of the global fouling factor over the operating life. Associated fouling-factor uncertainty analyses were performed to determine whether the calculated values represent significant fouling or whether uncertainty in key variables (e.g., steam pressure or feedwater flow rate) could be responsible for calculated fouling. In tandem with the fouling-factor analyses, a study evaluated for each plant the potential causes of pressure loss, including not only secondary fouling, but also tube plugging, temperature changes, measurement error, and others.

The results of the analyses indicate that only San Onofre 2 suffered severe SG fouling due to secondary deposits. At Callaway, about half of a net pressure loss of about 30 psi resulted from a 4.5% power uprate instituted in 1988. Other factors, including reactor hot-leg temperature streaming and an increase in separator/dryer pressure drop, played a lesser role. At Sequoyah 1, hot-leg temperature streaming and tube plugging were the main causes of a 25-psi steam pressure decrease between early operation and a 1995 chemical cleaning, while secondary deposits were probably playing a small role (10 psi or less). A pressure loss of over 60 psi at South Texas 1 was mainly the result of primary temperature decreases. An 11-psi loss at Comanche Peak 2 was chiefly due to a slight primary temperature decrease and other minor factors (e.g., hot-leg temperature streaming). Due to the low level of fouling, no substantial thermal performance increases were noted (or should have been expected) due to the use of DMA. However, very low iron feedwater concentrations resulted after the institution of DMA, delaying the onset of potentially resistive tube scale in the future. Further, the high-concentration DMA soak during the second refueling outage correlated well with two fouling factor transients—potentially indicating that DMA can increase scale porosity and then break up and remove such scale.

As shown by these case studies, various factors other than secondary deposits can also cause pressure loss. Tracking the global fouling factor, installing more accurate instrumentation, and characterizing secondary deposit properties can all aid in evaluating and remedying potential causes. The plant-specific information presented in this report serves to build the industry database of thermal performance information, thereby helping other utilities identify causes of—and prepare remedial measures for—their own potential SG thermal performance degradation.

ACKNOWLEDGMENTS

This study could not have been performed without the generous help of Union Electric, Tennessee Valley Authority, Houston Lighting and Power, and Texas Utilities Electric, who provided essential plant data and information. The authors would also like to thank the following people for their time and effort spent in providing support on this project: Steve Ewens and Warren Witt of Union Electric for their assistance with Callaway; Gary Boles, Rick Mooney, Ken Hurt, David James, Rick Rogers, and Lisa Williams with TVA for their assistance with Sequoyah 1; Ron Baker, Craig Uhrich, Ulhas Patil, and Jay Eichenlaub of Houston Lighting and Power for their help with South Texas 1; and Bill Fellers, Joe Wooten, Tim Robbins, Greg Nichols, Al Saunders, and Ron Greenthaler for aiding the Comanche Peak study presented in Appendix D. In addition, we would also like to recognize the contributions of Southern California Edison, especially Al Matheny and Michael Schwaebe, whose help allowed presentation of the SONGS 2 and 3 results.

CONTENTS

LIST OF FIGURES

LIST OF TABLES

1

INTRODUCTION

Purpose and Scope

Within the last several years, a significant number of PWR plants have begun to observe decreases in secondary-side steam generator (SG) steam pressure. In some cases, the pressure decreases have been sufficient to cause reduced HP turbine pressure and hence reduced electrical generating capacity. These reductions have been as large as several percent at some plants. Because a 1% reduction in the electrical generating capacity of a typical PWR is equivalent to roughly $2 million per year in terms of the cost of replacement power, this phenomenon can have a significant impact on utility revenue. As a result of this problem, some utilities have attempted to determine the root cause(s) of the performance degradation. One example is Southern California Edison, whose San Onofre Nuclear Generating Station (SONGS) Units 2 and 3 recorded pressure losses of nearly 80 psi compared to early cycles prior to recent chemical cleanings at each unit. As documented in References (1) and (2), the primary cause of the SONGS pressure losses prior to the chemical cleanings was secondary tube deposits. However, as is shown in Reference (3) and later in this report, secondary deposits are not necessarily the primary cause of SG thermal performance degradation for all plants.

This effort represents progress towards a better understanding of SG thermal performance degradation throughout the nuclear industry. It comprises an evaluation of the SGs at three plants: Callaway (Westinghouse Model F), Sequoyah Unit 1 (Westinghouse Model 51), and South Texas Project Unit 1 (Westinghouse Model E2). In addition, the key results from a previous analysis of the SONGS 2 SGs (CE Model 3410) are also presented for comparative purposes. Another plant, Comanche Peak 2 (Westinghouse Model D5), was later added to the study to determine the effects of dimethylamine (DMA) addition on SG thermal performance. These results are presented in Appendix D. This selection of plants represents a variety of the PWR designs used throughout the industry.

The first part of the SG thermal performance evaluation is a global fouling factor analysis performed for each of the subject plants. The global fouling factor is a measure of how much the performance of the SGs has degraded. Because it accounts for changes in thermal power, primary temperatures, and heat-transfer area (e.g.,

plugging), it allows more insight into potential fouling than SG steam pressure alone.* Inputs to this analysis consist of thermal-hydraulic design information as well as plant data recorded over the operating life of the plants, including steam pressure, primary temperatures, feedwater flow rate, and the number of plugged tubes for each outage.

In addition to the fouling factor analysis, an analysis of available secondary tube deposit characterization data for each of the subject plants is performed to determine independently what portion of the observed performance losses can be attributed to secondary deposits. In view of the results, a detailed accounting of all postulated causes of steam pressure degradation at each plant is performed. This breakdown yields the fraction of the observed steam pressure decrease at each plant that is attributable to secondary tube fouling and the fractions that result from other factors.

Motivation for Analyzing Performance Degradation

As discussed above, thermal performance degradation can have a significant impact on utility revenue if the plant is unable to produce 100% of its rated electrical generating capacity. In addition, severe pressure loss can require the utility to re-evaluate operating limits or modify technical specifications (e.g., for thermal power, steam generator pressure, or primary-to-secondary differential pressure). In some cases, modifications to the secondary cycle could even be required. Because of these concerns, it is in the interest of most utilities to evaluate the potential causes of actual and possible future performance degradation in order to prepare remedial strategies, if needed.

As described in more detail in Chapter 3**,** performance degradation is not always caused by secondary-side tube deposits. Callaway, one of the plants examined in this study, performed a chemical cleaning in 1995 in part to remedy SG thermal performance degradation and observed a slight *decrease* in SG steam pressure following the cleaning. Although this result was contrary to industry expectation, the results presented later in this report confirm that this outcome is consistent with the available thermal performance data. On the other hand, secondary-side deposits were the primary cause of performance degradation at SONGS 2 and 3, as is discussed in greater detail in Chapter 7.

As these two contrasting cases indicate, SG performance degradation is a plant-specific issue, due not only to design differences from plant to plant, but also due to the plant-specific nature of deposits within SGs. For those plants which are already experiencing significant pressure loss, it is important to determine which of the potential causes are responsible for the performance degradation. Accurate

* Greater detail on the global fouling factor methodology is provided in Chapter 4.

determinations of the causes of thermal performance degradation can save the utility considerable expense by either (1) showing that an expensive deposit removal strategy (e.g., chemical cleaning) is unwarranted from the viewpoint of thermal performance degradation because it would not restore performance, or (2) confirming that secondary deposits are in fact the chief cause of a thermal performance problem. In this case, deposit removal is likely to be less expensive than the alternative cost (e.g., lost electrical generating capacity, secondary-cycle modifications to prevent increasing power losses, etc.). For plants that have not experienced extreme pressure loss, meaningful information can still be obtained by examining the issue before the plant is power limited, e.g., the knowledge that problems are likely to occur within a certain time period.

Primary Goals and Objectives

The major aims of this report are the following:

- Report the results of fouling factor calculations for the operating histories of Callaway, Sequoyah 1, South Texas 1, and Comanche Peak 2 (Appendix D).
- Perform an uncertainty analysis for the calculated fouling factor at each plant.
- Analyze available secondary tube deposit characterization data for each plant in order to predict the associated thermal resistance of such layers.
- Quantitatively evaluate the best-estimate and bounding pressure decreases (or increases) associated with all potential causes of steam pressure degradation for each plant in the study.
- Compare the key results for each plant in the study. In addition, the results for SONGS 2 will also be discussed.
- Examine the measurement instruments and techniques used at each plant, in part to help determine recommended actions for standardizing plant thermal performance data collection.
- Correlate any changes in observed SG thermal performance with the historical addition of DMA at Comanche Peak 2. These results appear in Appendix D.

Report Organization

The remainder of the report is broken into the following chapters:

1. **Summary of Results and Conclusions (Chapter 2)**

   A brief overview of the fouling factor results and the pressure loss breakdown (by cause) for each plant is presented. In addition, recommendations for industry action such as standardization of plant data collection are summarized.

2. **Background—Steam Generator Performance Degradation (Chapter 3)**

   SG thermal performance degradation has only recently surfaced as a major issue as corrosion and tube plugging continue to increase at many plants. A number of utilities have used different strategies to reverse decreasing thermal performance with varying degrees of success. The potential role of secondary-side tube deposits and other causes of SG thermal performance degradation are discussed in a historical context in this chapter. As the Callaway experience demonstrated, tube scale is not necessarily the only cause of SG pressure decreases.

3. **Global Fouling Factor Analysis (Chapter 4)**

   In order to quantitatively evaluate the heat-transfer performance of the steam generators, the overall heat-transfer equation for pure counterflow heat exchangers is employed, where Q is the thermal power, U is the overall heat-transfer coefficient, A is the total heat-transfer area (referenced to the tube OD surface), and ΔT_{lm} is the log-mean temperature difference (LMTD):

   $$Q = UA\Delta T_{lm} \qquad \text{(eq. 1-1)}$$

   The parameter U, or its inverse R'', can be used to track the performance of the SGs. The fouling factor is typically defined as the change in R'' (i.e., $R'' - R_0''$, where R_0'' is the value of R'' when the SGs are new). In order to facilitate this calculation, plant instrument measurements (e.g., hot and cold-leg temperatures, feedwater flow rate, secondary-side pressure, etc.) are collected. Subsequent calculation of the fouling factor at different points in time as the SGs age reveals trends in fouling. Although useful, this technique for evaluating SG performance does have limitations that should be recognized: (1) subcooling of the feedwater is neglected, and (2) changes in pressure drop between the tube bundle and the SG outlet (e.g., due to increased clogging of the moisture separators and dryers) are commonly ignored although they too can impact thermal performance. Absent pertinent data, these two effects cannot be evaluated directly using this methodology.

   In addition to completing the fouling factor calculation itself, it is also important to determine the potential effects of measurement errors. This is achieved

through the use of uncertainty analyses, which consider uncertainties in all measured values upon which Eq. [1-1] depends.

4. **Tube Deposit Thermal Properties (Chapter 5)**

   The thermal resistance associated with corrosion layers on both the ID and OD surfaces of SG tubes can potentially cause a significant decrease in heat-transfer capability. The effects of primary-side (ID) films are investigated in light of industry data. The effects of secondary tube scale are evaluated using available data that characterize the tube scale at the subject plants (e.g., thickness, composition, morphology). Note that the estimated pressure loss associated with particular deposit thermal properties is independent of the calculated fouling factor and may be used as confirmation that secondary deposits are (or are not) causing significant thermal performance degradation at each plant.

5. **Causes of SG Steam Pressure Loss (Chapter 6)**

   With the information compiled in #3 above, the dependence of SG pressure on those factors appearing explicitly in the fouling factor equations is computed by using partial derivatives calculated from Eq. [1-1]. In this fashion, changes in SG pressure can be directly correlated to changes in fouling factor, plugged tubes, primary-fluid temperature, and thermal power. These dependencies are critical in estimating how much pressure loss can be attributed to SG tube fouling or other causes.

   In order to accurately assess the meaning of the fouling factor calculations, the effects of other factors on SG pressure are also investigated in light of the calculated results. These factors include

   - different-from-nominal design parameter values (e.g., SG tube wall thickness and thermal conductivity variations)
   - tube surface fouling (both primary-side and secondary-side)
   - fouling of tube supports (which affects the recirculation ratio)
   - steam pressure measurement uncertainty
   - moisture separator/dryer fouling
   - hot-leg temperature streaming
   - divider-plate leakage
   - reactor power calibration error

- feedwater subcooling (since it is ignored in the fouling factor calculations)

Realistically evaluating how much of a given thermal performance problem can be attributed to each of the above causes facilitates informed decisions on the implementation of remedial measures at a particular plant.

6. **Plant Comparisons (Chapter 7)**

   Key results from the calculations described in Chapters 4, 5, and 6 for the three original subject plants as well as SONGS 2 are compared and contrasted.

7. **Plant Thermal Performance Measurements (Chapter 8)**

   The methods and instruments used to measure secondary steam pressure, primary temperatures (T_{hot} and T_{cold}), and feedwater mass flow rate are compared for the subject plants. Errors associated with these variables have the largest impact on the uncertainty in calculated fouling factor. As a result of these comparisons, a list of recommended actions for improving plant thermal performance data is developed.

8. **Remedial Measures for Improving Heat Transfer (Chapter 9)**

   A series of suggested actions for reversing or counteracting thermal performance degradation is explored in this chapter, including chemical cleaning, mechanical cleaning, T_{hot} increases, feedwater heater bypasses, etc.

9. **References (Chapter 10)**

   This chapter includes all sources explicitly referenced in the report along with a few additional related sources.

2

SUMMARY OF RESULTS AND CONCLUSIONS

Fouling Factor and SG Pressure Loss Results

The results of fouling factor calculations and associated uncertainty analyses performed for Callaway, Sequoyah 1, South Texas 1, SONGS 2, and Comanche Peak 2 are summarized in Table 2-1. With a negative fouling factor that increased following chemical cleaning, Callaway exhibits fouling behavior suggestive of heat-transfer enhancing secondary tube deposits. At Sequoyah 1, the fouling factor is somewhat higher than at Callaway. Although the fouling factor increased slightly following chemical cleaning, the slight net increase since early operation suggests a low positive thermal resistance. However, the ambiguity of the available data make it impossible to say definitively whether Sequoyah 1 scale was slightly resistive or essentially had no effect. The South Texas 1 fouling factor is also small; considering the uncertainty, little or no sustained fouling due to tube deposits is believed to be present. In contrast to these plants, SONGS 2 exhibited a large computed fouling factor well in excess of the calculated uncertainty, indicating that secondary tube deposits were causing significant loss of heat-transfer capability prior to chemical cleaning in 1996–97. Comanche Peak 2, examined in Appendix D, exhibited very little net fouling. An 11-psi decrease there is attributable to a slight primary temperature decrease and other minor causes.

Table 2-1
Computed Fouling Factors (10^{-6} h-ft^2-°F/BTU)

Value	Callaway		Sequoyah 1		South Texas 1	SONGS 2	Comanche Peak 2
	Before CC	After CC	Before CC	After CC	Mid-1996	Before CC	Mid-1997
Best Estimate	–28	–5	+21	+42	+30	+172	+9
Computed Uncertainty	±19	±19	±24	±24	±62	±48	±31
Lower-Bound Estimate	–47	–24	–3	+18	–32	+124	+40
Upper-Bound Estimate	–9	+14	+45	+66	+92	+220	–22

In Table 2-2, the major sources of steam pressure degradation are summarized for the five plants. Significant observations regarding this table include

- The observed pressure loss at Callaway is chiefly the result of a 4.5% power uprate instituted in 1988. Other factors, including hot-leg streaming and separator/dryer pressure drop, play a lesser role. Secondary deposits are not a primary cause of pressure loss; prior to chemical cleaning they were most likely somewhat *beneficial* to heat transfer.

- Hot-leg streaming and tube plugging were responsible for two-thirds of the steam pressure loss at Sequoyah 1 prior to chemical cleaning. Secondary deposits are believed to have caused a modest degree of pressure loss (10 psi) although this conclusion is somewhat uncertain.

Table 2-2
Summary of Pressure Loss Breakdowns—Major Causes

Cause	Callaway		Sequoyah 1		South Texas 1	SONGS 2	Comanche Peak 2
	Before CC	After CC	Before CC	After CC	Mid-1996	Before CC	Mid-1997
Tube Plugging	1	2	4	7	2	12	0
Power Uprate	15	15	0	0	0	0	0
Primary Temp. Variation	1	3	0	1	52	–5	6
Secondary Tube Fouling	–5	4	10	4	0	72	0
Hot-Leg Streaming	4	4	15	15	13	0	4
Addit'l Separator/Dryer ΔP	4	4	0	0	0	4	0
Balance[1]	–3	–3	–4	9	–4	–6	1
Total Loss (psi)[2]	17	28	25	36	63	77	11

[1] This category represents the pressure loss (or gain, if negative) required to make the total agree with the actual observed loss. It includes the sum of other minor causes that are not explicitly listed here. It also includes the error associated with any of the attributed causes (e.g., based on the restart pressure after chemical cleaning, the SONGS 2 tube scale was likely only responsible for about 57 psi of pressure loss rather than the estimated 72).

[2] Totals may not equal the sums of the individual causes due to rounding.

- The pressure loss at South Texas 1 is mainly the result of primary temperature decreases. A 4°F decrease was intentionally imposed to reduce the rate of tube degradation, and an additional 1°F resulted from loop asymmetry and a change in temperature control scheme. Very thin secondary deposits are believed to be causing little or no loss of SG steam pressure.

- Highly resistive secondary deposits were responsible for a large portion of the 77-psi steam pressure decrease observed at SONGS 2 prior to a recent chemical cleaning. Tube plugging is playing a lesser role.

- About half of the 11-psi pressure decrease observed at Comanche Peak 2 is attributable to a slight decrease in primary temperature. Other minor causes, including hot-leg temperature streaming and primary and secondary tube deposits, are likely responsible for the remainder.

General Conclusions

As a result of this study, the following items become evident:

1. The principal causes of thermal performance degradation can vary greatly from plant to plant.

2. Except for plants that have instituted T_{hot} changes, large steam pressure losses (i.e., >50 psi) are likely the result of consolidated low-porosity inner secondary deposit layers. SONGS 2 is an example.

   Small or moderate steam pressure losses (i.e., <30 psi) are often the product of several factors, such as tube plugging, primary temperature fluctuations (e.g., hot-leg streaming), power uprates, and slightly or moderately resistive tube deposits. Callaway and Sequoyah 1 are examples.

3. The relatively large transients in steam pressure and fouling factor that are often observed following outages and trips (e.g., those observed at South Texas 1) cannot be satisfactorily explained with currently available information. However, three plausible explanations include: 1) cyclic variations in hot-leg streaming due to changes in core flow patterns, 2) cyclic fouling and de-fouling of the preheater, and 3) partial deposit exfoliation coupled with steam blanketing. In any case, long-term performance trends are more likely to have a significant economic impact on most utilities than such transients are.

4. Preheater SGs have unique performance issues due to the possible clogging of flow paths in the preheater section. These include

   a. Changes in the ratio of flow rates exiting the top and bottom of the preheater (i.e., flow maldistribution).

   b. Changes in flow patterns within the preheater that may reduce the heat-transfer coefficient of the preheater.

c. Changes in the percentage of flow sent to the upper internals as opposed to the preheater. Prior to initial startup, Comanche Peak 2 changed this flow split from the design 90%/10% to 85%/15%. This change is responsible in part for the lower-than-expected heat-transfer margin observed during early operation (i.e., an estimated 5–10 psi decrease in steam pressure versus the design pressure). Note that this issue is not relevant for Model E2s (e.g., South Texas 1) which do not send any feedwater flow to the upper internals.

5. Plant instrument data and secondary tube scale characteristics are important and should be tracked even for plants that currently do not have significant pressure loss.

6. Field and laboratory experience suggests that full-bundle chemical cleaning is effective at returning SG thermal performance approximately to start-up levels. Fouling factor calculations at Callaway and SONGS 2 and 3, as well as heat-transfer tests performed on pulled tubes from Ginna (4), support this conclusion.

7. The experience at Comanche Peak 2 suggests that the addition of DMA to the SG feedwater can decrease feedwater iron concentrations to very low levels—thereby helping to delay or prevent the formation of resistive tube scale. Notable fouling factor transients mat also mean that DMA is capable of increasing scale porosity and/or removing scale from SG tubes.

Recommended Industry Actions

To address current and potential future thermal performance degradation, utilities should consider the following actions as applicable to their particular plants:

1. Using available past data, compute the global fouling factor since the beginning of operation in the manner described in this report. The presence of thermally resistive secondary tube deposits may be revealed by examining the fouling factor history (e.g., SONGS 2). Data from early cycles are particularly important because they can reveal whether the SGs were initially performing at the level suggested by the thermal-hydraulic design values.

2. Continue to track the fouling factor during future operating cycles in order to identify potential problems early. Due to the nature of the fouling factor, variations in primary temperature, tube plugging, and thermal power are accounted for, so increases in the fouling factor imply other root causes (e.g., secondary deposits, additional separator/dryer pressure drop, etc.; see Chapter 6 for details on possible causes of pressure loss). The most useful fouling factor history will require keeping records of plant instrument data for full-power operation at least once per week because of typical data scatter (see the bottom of p. 8-10).

3. As part of #2 above, determine and record actual measurement uncertainties (not administrative limits), particularly for primary temperatures, SG steam pressure, and feedwater flow rate. This information will allow calculation of the fouling factor uncertainty, which is necessary for assessing the importance of the calculated fouling factor.

4. Consider instruments to measure additional performance parameters, including:

   a. The actual pressure drop between the tube bundle and the steam pressure measurement location. This information can help determine whether separator/dryer pressure drop, for example, has increased compared to the design value.

   b. Recirculation ratio. Uncommonly tracked, the recirculation ratio can indicate whether flow decreases due to tube support clogging are occurring. Methods that have been used for measuring recirculation ratio include: 1) measuring the velocity in the downcomer with ultrasonic techniques, 2) measuring the downcomer fluid temperature, and 3) using tracer techniques.

   c. The flow distribution in preheater SGs. Significant changes may indicate preheater baffle plate clogging and/or unclogging.

5. Gather tube scale characterization data frequently. This will help provide independent confirmation that the calculated fouling factor is (or is not) being caused by secondary deposits. Collecting information at multiple times will allow changes in scale properties to be evaluated, potentially helping determine how future fouling rates are likely to change. The primary properties of interest are thickness, composition (i.e., percentage of each compound present), porosity, pore size distribution, and internal structure (revealed through metallographic cross sections, for example). Visual inspections may also provide useful information (e.g., thickness uniformity, tube support fouling, etc.).

   Tracking impurity ingress concentrations (particularly iron and copper) provides information for an independent assessment of deposit loading by facilitating an independent estimate of the average deposit thickness. This estimate can be used to confirm thickness measurements that might be available for a limited number of flake samples that are not necessarily representative of the entire tube bundle. Time histories of impurity concentrations can also be used to evaluate the effects of alternate amines (e.g., ETA or DMA). Note that transient increases in impurity concentrations during plant startups are often relatively large and should be considered in such analyses.

6. Consider changes in instrumentation that will reduce the uncertainty associated with calculated fouling factors. Such changes might include redundant

temperature elements for T_{hot} and T_{cold} (in part to help identify hot-leg temperature streaming), more accurate pressure transducers (±2 psi), redundant feedwater flow measurements (e.g., leading-edge flow meters (LEFMs)), and measurements of primary mass flow rate. See p. 8-9 for additional detail.

7. Consider the use of DMA or ETA as an alternate amine. As indicated in Appendix D, the experience at Comanche Peak suggests that DMA has the ability to reduce feedwater iron concentrations and, at least in some cases, increase scale porosity and/or weaken and remove existing scale layers. Although long-term heat-transfer increases did not result at Comanche Peak 2 (due to already low fouling levels), plants with resistive scale layers may reap significant heat-transfer benefits. ETA may have similar benefits; evidence suggests that the fouling rate at Callaway leveled off after the institution of ETA.*

8. Consider developing or refining a thermal-hydraulic model specific to the plant of interest to determine how variables like pressure, flow velocity, quality, and scale deposits are likely to vary throughout the bundle. Such a model can also potentially indicate the beneficial or detrimental effects of tube support and preheater baffle plate clogging and unclogging. The ATHOS code, originally developed by EPRI during the 1980s, represents an industry-standard tool. References (5) and (6) provide additional detail.

9. For plants that have little remaining heat-transfer margin (or are fouling rapidly), perform preliminary economic evaluations to identify attractive remedies or countermeasures against thermal performance degradation. Such evaluations should include chemical cleaning, mechanical cleaning, T_{hot} increases, secondary-cycle modifications (e.g., turbine modifications or feedwater heater bypass), and SG replacement as potential options. Also required as an input is the predicted progression of tube plugging and/or sleeving due to corrosion mechanisms, which can be accomplished using statistical methods (see Reference (7)).

---

* Because a pressure pulse cleaning (PPC) was also employed during the same outage as the initial use of ETA, it is possible that this cleaning, alone or in combination with the use of ETA, is responsible for the reduction in fouling rate at Callaway.

3

BACKGROUND - STEAM GENERATOR PERFORMANCE DEGRADATION

SGs are well recognized as one of the most vulnerable components in the pressurized water reactor (PWR) nuclear steam supply system (NSSS) due to the susceptibility of SG tube materials to corrosion. While the integrity problems associated with SG tube corrosion (e.g., intergranular attack (IGA), stress corrosion cracking (SCC), denting, etc.) have received most of the utility focus over the past 25 years, losses in plant electrical generating capacity due to what is often suspected to be secondary-side fouling have garnered widespread attention in the US, Europe, and Japan since about 1990. Gradual losses in steam pressure totaling over 100 psi from peak performance pressures have been reported (8, 9). In addition to gradual decreases in steam pressure, some plants experience sharp declines in steam pressure following restarts after refueling outages or plant trips, followed by partial recovery during subsequent operation and then a more gradual decline over the course of the operating cycle. The net effect is a decrease in pressure compared to the same points in the previous cycle. Typical trends in steam pressure reductions and the restart transient phenomenon are illustrated in Figure 3-1.

Definition of Thermal Performance Degradation

Before analyzing SG thermal performance degradation, it is instructive to first develop a working definition. In a narrow sense, it can be defined as a decrease in the overall SG tube bundle heat-transfer coefficient. Stated another way, it is a loss of capacity to transfer heat given constant primary and secondary inlet temperatures, pressures, and mass flow rates. More broadly:

Thermal performance degradation can refer to a decrease in SG outlet pressure and/or thermal power,* which can be caused by three different sources:

- **Decrease in overall tube bundle heat transfer coefficient**
- **Other sources within the SG shell (e.g., extra moisture separator pressure drop)**
- **External sources (e.g., hot-leg temperature streaming)**

* Note that excessive moisture carryover, steam carryunder, and water-level oscillations may also be considered forms of SG performance degradation.

In this report, we will be concerned with evaluating all three of these potential sources.

Secondary-Side Deposits

Until recently, many utilities and NSSS vendors had assumed that lost SG thermal performance was due exclusively to the presence of secondary tube scale deposits. This conclusion was generally consistent with the fact that nearly all of the plants and SG designs experiencing performance degradation have reported the presence of these deposits, which typically consist of iron oxides, copper metal, hardness species, and a host of minor constituents including alumino-silicates, salts, debris, and organics (see *Characterization of PWR Steam Generator Deposits,* EPRI Report TR-106048 (10), for more information). In addition, the role of secondary deposits in causing heat-transfer degradation was confirmed for the Ginna plant in the early 1990s (see EPRI Report TR-100866 (4)). Experiments documented in Reference (4) showed that fouling caused by corrosion products and impurities on the secondary side of SG tube surfaces was primarily responsible for the performance degradation at Ginna.

Based on the belief that secondary-side tube deposits are chiefly responsible for thermal performance losses, utilities have attempted to remedy decreasing heat transfer capability by reducing the current and future accumulation of secondary-side deposits in their SGs. Several utilities have opted to mechanically clean the deposits from the tube surfaces. Others have employed full-height chemical cleaning. (Although most plants that have chemically cleaned their SGs have done so to address specific corrosion concerns rather than thermal performance problems, the results of their experiences can still be revealing with regard to thermal performance since chemical cleaning usually removes almost all of the corrosion products from tube surfaces.) In addition, some utilities have attempted to loosen or alter the intrinsic structure of tube scale through the addition of morpholine and/or dimethylamine (DMA) on line or before, during, and after shutdowns for refueling. (See Appendix D for an analysis of Comanche Peak 2, which has used morpholine and DMA as feedwater additives.)

Until the recent chemical cleanings at SONGS 2 and 3 in 1996-97, the effectiveness of these measures as a means of increasing thermal performance remained somewhat in question, which in turn cast doubt on the inherent role of secondary deposits in causing SG thermal performance degradation. In fact, simple attempts to correlate fouling behavior with the amount of corrosion product ingress or tube scale thickness are not always successful. For instance, some plants with tube scale thicknesses of 10 to 15 mils have not experienced any decrease in generating capacity, while other plants with as little as 3 to 4 mil thick deposits (or less) have experienced heat transfer degradation. This seemingly paradoxical behavior can be explained, at least in part, by realizing that some plants have much more design margin to accommodate fouling than others do. In addition, not all plants behave similarly with regard to long-term trends in performance degradation. Figure 3-2 summarizes three possible progressions of heat-

exchanger fouling, some of which have been observed in PWR SGs: linearly increasing, falling rate, and asymptotic. The top illustration (a) depicts these trends in terms of the fouling factor, which increases as the heat exchanger fouls. The lower illustration (b) shows the same trends as they would be reflected by SG steam pressure, which falls as the SG fouls. If a plant were to experience asymptotic fouling, it is possible that a steady-state condition could develop after which time no further degradation in steam pressure is experienced. Many utilities today are hopeful that such behavior will occur at their plants. However, little or no research as to whether asymptotic behavior occurs in SGs has been conducted.

Other potentially confusing evidence regarding the causal role of secondary deposits in thermal performance degradation concerns utilities' efforts to lower corrosion product transport to the SGs. In the late 1980s, some utilities successfully sought to reduce corrosion product transport by switching to alternate amines such as ETA and morpholine. It was predicted that as a result, the rate of reduction in SG steam pressure at plants affected by fouling would decrease or that fouling would reach an asymptotic value. However, neither of these trends was consistently observed by the majority of plants that have adopted new feedwater chemistry strategies (8). Little or no effect on trends in fouling factor or SG steam pressure has been observed at a number of plants despite reduced corrosion product transport.* This lack of change may be due to the densification of existing tube scale over time, a process known as scale ripening. Ripening occurs as soluble iron species, silicates, and hardness species are carried through the tube scale via pores, effectively filling the pores near the tube wall surface and thereby creating a more insulating corrosion layer. The rate of scale ripening in existing tube scale may not be controlled by the concentration of corrosion products on the secondary side, but by mass diffusion through the tube scale pores. Consequently, corrosion product transport alone may not always control the rate of heat transfer degradation.

A further example of the uncertain role of deposits with regard to heat transfer in SGs occurred in 1995 when the Callaway Plant, a 1240 MWe PWR owned and operated by Union Electric, expected to restore lost steam pressure by chemically cleaning the secondary side of their SGs. The objective was to remove an estimated 4 mils of tube scale that was believed to be the root cause of their SG thermal performance problems. At the completion of the cleaning, during which approximately 5,000 pounds of deposits were removed from each of the four SGs, secondary-side visual inspections confirmed that essentially all deposits had been removed and tube surfaces were cleaned to what appeared to be bare metal. Much to the utility's surprise, the plant

---

* One notable exception is Callaway, which experienced a decrease in the fouling rate coincident with the introduction of ETA in the feedwater. Note, though, that Callaway also performed a pressure pulse cleaning (PPC) during this outage, which may have been partly (or even fully) responsible for the change in fouling rate.

restarted after the cleaning only to have an even greater reduction in steam pressure compared to the pressure loss observed prior to the cleaning. As is described in more detail on pp. 7-1 and 7-2, analysis of Callaway thermal performance and tube scale data reveals that a 4.5% power uprate, a small design margin against fouling, tube deposits that were slightly heat-transfer enhancing (prior to removal by chemical cleaning), and a few other minor factors combined to produce a loss of power generating capacity with essentially no net secondary tube fouling.

Further evidence for the correlation of secondary tube deposits with performance degradation is provided in Figure 3-3. Shown there is the observed SG steam pressure decrease for ten US plants graphed as a function of predicted heat-transfer margin "consumed" by fouling and tube plugging.* The consumed margin values are based on available tube plugging and deposit loading information (e.g., based on chemical cleaning results or scale measurements). Note that increasing amounts of consumed margin correlate well with pressure decreases, suggesting that thicker deposits tend to cause thermal performance degradation.

Other Possible Causes of Performance Degradation

The failure of ETA-based chemistry control to decrease the rate of steam pressure loss at several plants and particularly the events at Callaway have led to speculation within the industry that perhaps secondary-side tube scale deposits are not always the root cause of thermal performance degradation. Other possible causes include:

1. Tube support blockages, which could reduce recirculation ratios and therefore secondary velocities upward through the SG tube bundle, thereby reducing heat-transfer coefficients.

2. Primary-side tube fouling, which would have the same effect as secondary-side fouling but with the heat transfer resistance occurring on the tube ID wall.

3. Extra moisture separator/dryer pressure drop due to dryer/drain clogging or separator erosion and/or fouling.

4. Error in applied primary temperature due to temperature measurement error, hot-leg temperature streaming, and/or divider plate leakage in the primary channel head. Hot-leg streaming is a phenomenon that can occur if the hot-leg flow is particularly non-uniform across the section where its temperature is measured, allowing the hot-leg RTD to detect hotter-than-average coolant from the core that passes adjacent to the RTD well location. This is most relevant to Westinghouse

* None of the plants in Figure 3-3 has tube plugging excessive enough to cause the observed pressure losses.

low-neutron leakage cores (limited thermal mixing) that also use hot-leg temperature as an input to a reactor control regime based on the average of hot-leg and cold-leg temperatures (i.e., T_{ave} controlled plants). Steam cycle programs that use this hot-leg temperature data interpret the effect as a reduction in heat transfer based on the higher-than-actual primary to secondary side temperature difference. Calculations by at least one NSSS vendor have suggested that this effect can account for up to 10 psi of SG pressure "loss."

5. Error in reactor thermal power calibration due to feedwater flow and temperature measurement error (including venturi meter fouling), blowdown flow measurement error, and uncertainty in the outlet steam quality.

6. Variations in feedwater temperature (degree of subcooling).

7. Loss of heat-transfer area due to tube plugging (and to a much lesser extent sleeving).

8. Operation at lower primary temperatures compared to design values. Although nearly the same thermal power may be generated if the primary temperatures are lower, SG steam pressure can decline significantly as a by-product.

9. Increases in reactor thermal power including plant uprates.

10. Nonuniformities in temperature among primary loops (if a maximum (auctioneer) T_{ave} control scheme is used).

11. For preheater SGs, variations in the flow distribution exiting the preheater.

Figure 3-4 summarizes these possible causes of performance degradation. Later chapters of this report consider these factors as potential causes of SG thermal performance degradation at Callaway, Sequoyah 1, South Texas 1, and Comanche Peak 2 (Appendix D). In addition, the results of a previous study performed for SONGS Unit 2 will also be summarized.

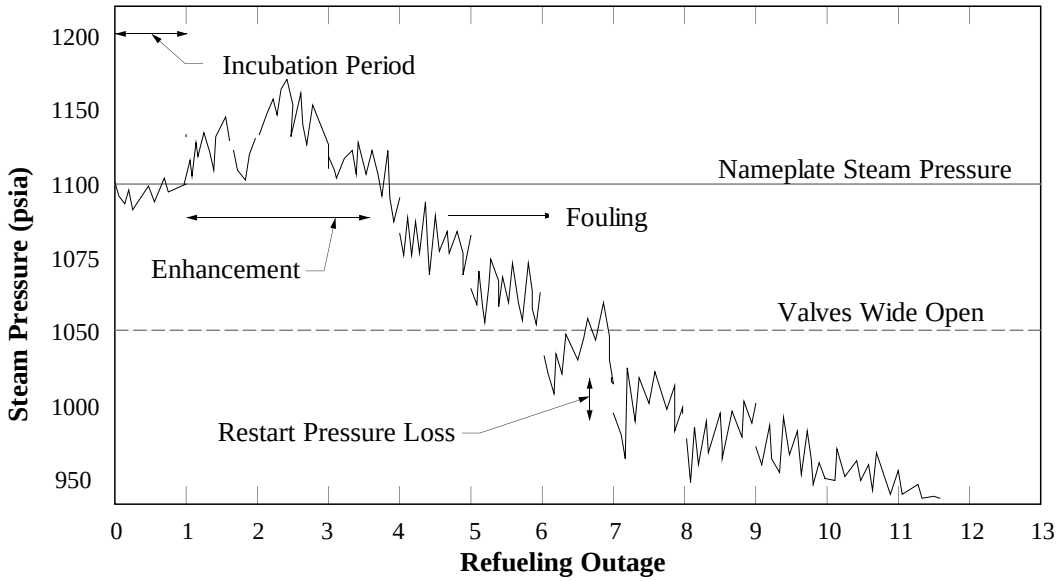

Figure 3-1
Example of Typical Steam Pressure Behavior in RSGs

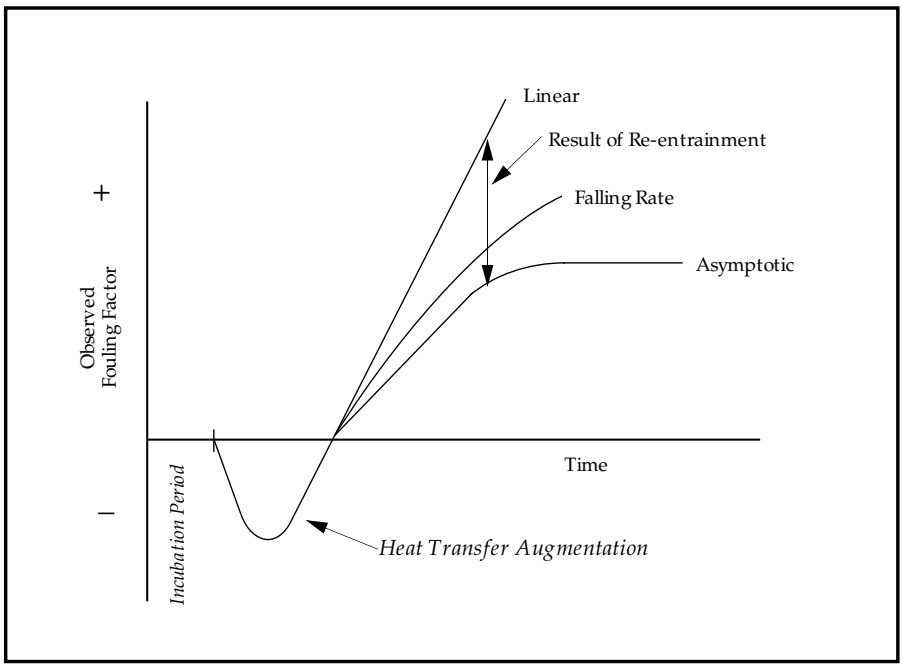

(a) Fouling Factor

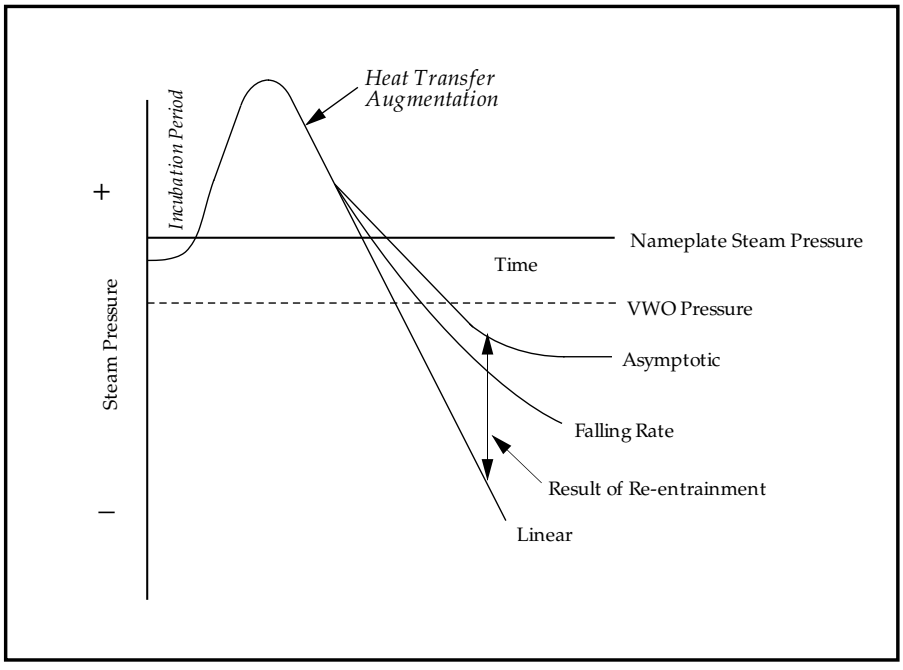

(b) Steam Pressure

Figure 3-2
Typical Fouling Trends Observed in Heat Exchanger Equipment

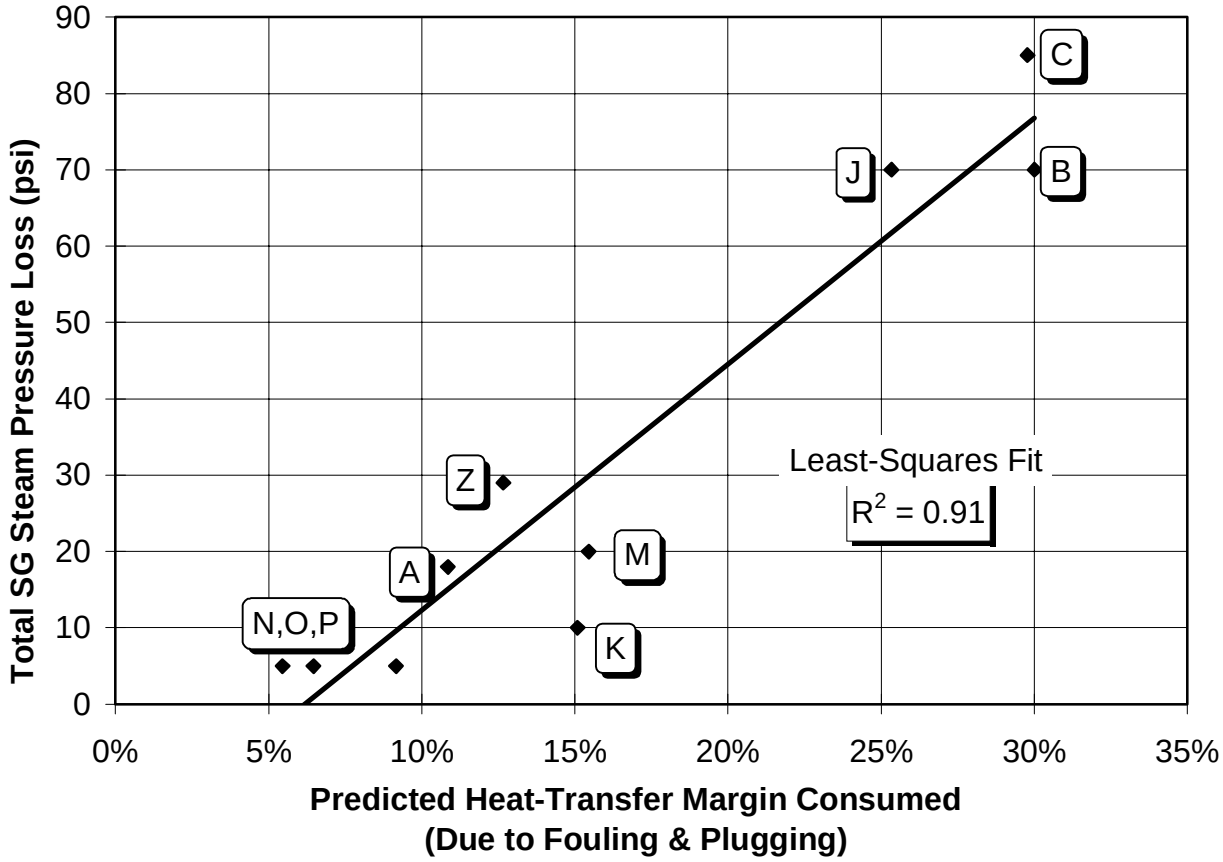

Figure 3-3
Correlation Between SG Steam Pressure Loss and Predicted Heat-Transfer Margin Consumed

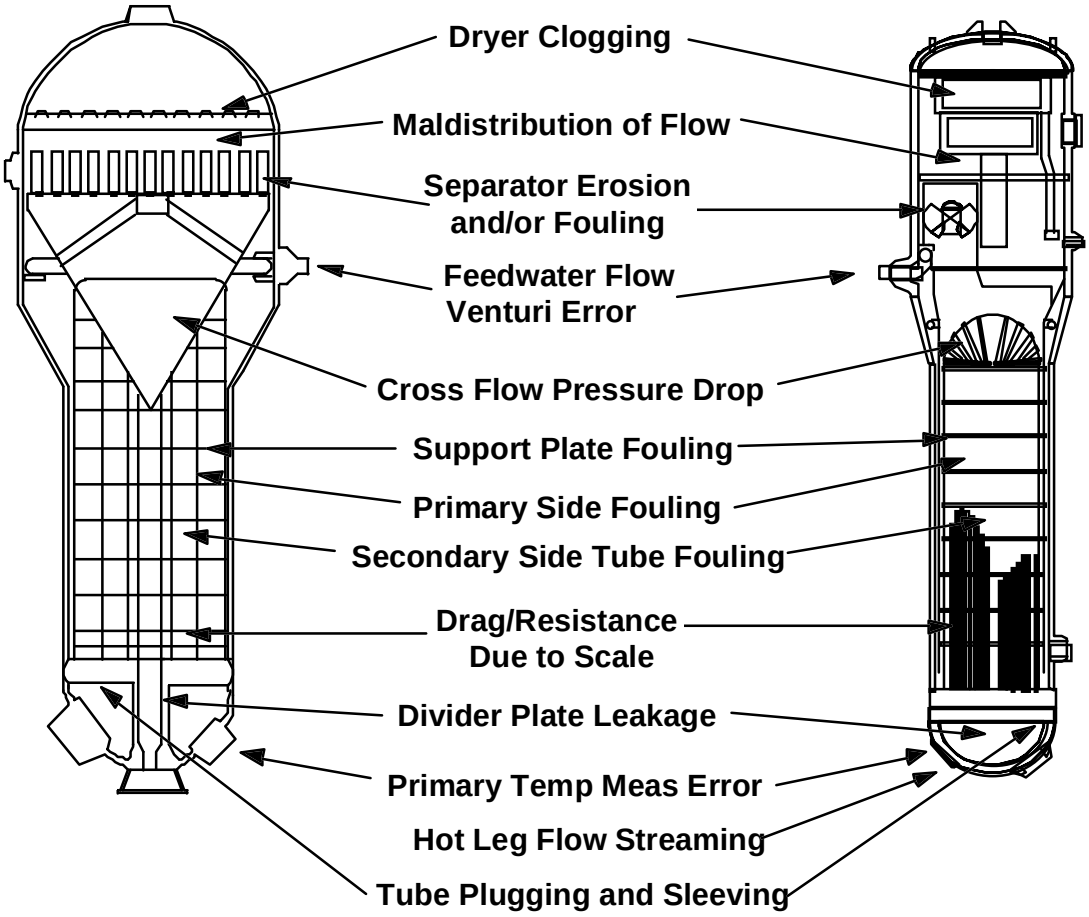

Figure 3-4
Summary of Potential Causes of SG Performance Degradation

4

GLOBAL FOULING FACTOR ANALYSIS

An exact quantitative measure of the heat-transfer effects of secondary deposits is difficult to obtain due to the complex nature of SG thermal hydraulics. Accurate modeling of the details requires sophisticated thermal-hydraulics software specially designed for the SG geometry (e.g., ATHOS); even then, significant assumptions must be made. However, important insight into the performance of SGs can be achieved with the use of the standard global heat-transfer equation. Development of this approach is described below.

Fouling Factor Methodology

The purpose of a fouling factor calculation is to quantify the degradation of the ability of a heat exchanger to transfer heat. At a local level, the ability to transfer heat from the primary coolant to the secondary fluid is given by the local heat transfer coefficient U_{local}:

$$q'' = U_{local}\left(T_{prim} - T_{\sec}\right) \qquad \text{(eq. 4-1)}$$

where q'' is the local heat flux. This equation can also be written in terms of the local resistance to heat transfer R''_{local}:

$$q'' = \frac{T_{prim} - T_{\sec}}{R''_{local}} \qquad \text{(eq. 4-2)}$$

The local resistance is made up of the conductive resistance of the tube wall, the boundary layer resistances of the primary and secondary fluids, and the resistances resulting from the accumulation of any deposit layers on the inside and outside tube surfaces. The local fouling factor is the sum of these last two resistances and, in practice, is defined as the change in local resistance from the local resistance at initial operation:

$$R''_{f,local} = \Delta R''_{local} = R''_{local} - R''_{local,0} \qquad \text{(eq. 4-3)}$$

As the local fouling factor increases due to the accumulation of deposits, the driving temperature difference must increase at the same rate in order for the same heat flux to be transferred.

The local fouling analysis can be extended to a global fouling analysis of an entire heat exchanger by defining a global heat transfer coefficient U and a global heat transfer resistance R (or a global area-based resistance R''):

$$Q = UA\Delta T_m = \frac{\Delta T_m}{R} = \frac{A\Delta T_m}{R''} \qquad \text{(eq. 4-4)}$$

where Q is the total thermal power transferred, A is the active heat transfer area (defined using the outside tube surface area), and ΔT_m is the mean temperature difference between the two fluids. This equation is called the overall heat transfer equation.

Under certain assumptions, the mean temperature difference is equal to the log-mean temperature difference (LMTD), which is defined as

$$\Delta T_{lm} = F\frac{\Delta T_2 - \Delta T_1}{\ln\left(\Delta T_2 / \Delta T_1\right)} \qquad \text{(eq. 4-5)}$$

where ΔT_1 and ΔT_2 are the terminal temperature differences analogous to those for a pure counterflow heat exchanger and F is a factor less than or equal to one that accounts for the deviation from pure counterflow. This equation is strictly valid only if the local heat transfer coefficient is constant throughout the heat exchanger and the specific heat of each fluid can be considered constant. A commercial PWR steam generator does not strictly meet these two conditions because the secondary boundary layer resistance changes with the mode of heat transfer (boiling versus single-phase convection) and heat flux, flow rate, and quality (for boiling); and also because the specific heat of the secondary fluid jumps from a finite value to infinity at the inception of boiling. The first violation may cause only a slight uncertainty because the secondary boundary layer resistance is only about 15% of the total resistance. The effect of the second violation is illustrated in Figure 4-1, which shows the fluid temperature distribution of the primary and secondary fluids assuming pure counterflow. By using a log-mean temperature analysis, the secondary fluid temperature must be modeled as a logarithmic curve or as a constant. Figure 4-1 shows that the secondary fluid temperature distribution is best approximated by neglecting the subcooling of the fluid entering the bottom of the tube bundle from the downcomer. For a heat exchanger with the temperature of one fluid held constant by phase change, the factor F is one regardless of heat exchanger geometry.

Then the overall heat transfer equation for a PWR steam generator becomes

$$Q = UA\frac{\left(T_{hot} - T_{sat}\right) - \left(T_{cold} - T_{sat}\right)}{\ln\left(\frac{T_{hot} - T_{sat}}{T_{cold} - T_{sat}}\right)} \qquad \text{(eq. 4-6)}$$

or

$$Q = UA\frac{T_{hot} - T_{cold}}{\ln\left(\frac{T_{hot} - T_{sat}\left(p_{sat}\right)}{T_{cold} - T_{sat}\left(p_{sat}\right)}\right)} \qquad \text{(eq. 4-7)}$$

As was the local fouling factor, the global fouling factor is defined using the reduction in the overall heat transfer coefficient:

$$R_f'' = \Delta R'' = R'' - R_0'' = \frac{1}{U} - \frac{1}{U_0} \qquad \text{(eq. 4-8)}$$

The utility of this approach is that all the quantities which appear in the overall heat transfer equation and in the definition of global fouling factor are normally tracked for PWR steam generators. If the local fouling factor is relatively uniform throughout the steam generator, then the global fouling factor is equal to the local fouling factor with some relatively small error, most likely principally due to the neglect of the downcomer subcooling.* If the local fouling factor is not relatively uniform, then the global fouling factor is still a legitimate average value of the distribution of local fouling factors, but with a somewhat higher level of uncertainty.

Figures 4-2 and 4-3 illustrate the changes in resistance to heat transfer that occur during fouling. Figure 4-2 shows that the total resistance may increase over steam generator life to the point that the turbine throttle valves must be completely opened in order to lower the steam generator pressure and saturation temperature so that a large enough LMTD exists to transfer 100% thermal power. Further increases in resistance necessitate significant loss of electrical output unless remedial secondary cycle modifications are instituted. Figure 4-3 shows how the temperature difference from the primary coolant to secondary fluid must increase with fouling.

The extra resistance to heat transfer due to the presence of tube deposits can be quantified using a fouling factor analysis, and the steam generator performance improvement following deposit removal can be predicted. However, the following

---

* Note that the downcomer subcooling is significantly lower than the feedwater subcooling due to mixing of the feedwater with saturated liquid from the separators.

issues must be considered when using the fouling factor methodology on a PWR steam generator:

- FOULING FACTOR UNCERTAINTY. The fouling factor calculation may be subject to significant measurement error due mainly to the uncertainties in the primary temperatures, feedwater flow rate, and steam generator pressure. Therefore, a calculated fouling factor should be reported with an uncertainty tolerance.

- SOURCES OF PERFORMANCE DEGRADATION OTHER THAN FOULING. Sources of pressure loss other than fouling must be identified so that they are not attributed to the calculated fouling factor. The sources that are explicitly accounted for by the fouling factor calculation—tube plugging, power increases, and primary temperature decreases—are straightforward to identify. Sources that are not usually factored out, such as extra separator/dryer pressure drop, are more difficult to identify. This subject is treated in more depth in Chapter 6.

- POTENTIAL CHANGES IN BOUNDARY LAYER RESISTANCES. The global fouling factor does not distinguish between resistance due to fouling layers and that due to changes in thermal hydraulics. Therefore, effects such as changes in primary tube velocity due to plugging and changes in boiling heat transfer coefficient due to changes in recirculation ratio (change in velocity and quality) could have an effect.

- UNCERTAINTY IN FOULING FACTOR DUE TO NEGLECT OF SUBCOOLING. As discussed above, the fouling factor calculation does not capture the effect of variations in the degree of downcomer subcooling. Changes in subcooling affect the true mean temperature difference as well as the distribution of secondary side heat transfer coefficients. See Chapter 6 for more discussion on this topic.

- PRESENCE OF AN INTEGRAL PREHEATER. Certain issues specific to preheaters (e.g., fouling of the preheater baffle plates, difference in meaning of LMTD, etc.) must be considered before applying the global fouling factor methodology to SGs with preheaters (see below). South Texas 1—and also Comanche Peak 2, discussed in Appendix D—have preheaters integral to their SGs.

Preheater Steam Generators

Up to this point, no specific mention has been made regarding the distinction between feedring SGs and SGs with preheaters (or economizers). Callaway and Sequoyah 1 (and SONGS 2) all have feedring SGs, while the South Texas 1 and Comanche Peak 2 SGs have preheaters. There are a number of issues regarding application of the global fouling factor methodology to preheater SGs that need to be addressed.

Flow Distribution

All or most of the feedwater entering preheater SGs passes first through the preheater section before passing into the open portion of the tube bundle. For Model E2's (South Texas 1) and D5's (Comanche Peak 2), the flow is directed to the bottom portion of the preheater where most of it makes five or six passes through a counterflow arrangement before exiting the preheater at the top. A fraction of the flow exits the preheater at the bottom in what is known as the mixing region (see Figure 4-4). This design is termed a counterflow preheater. Commercial plants also use split flow and axial flow designs.

For optimal performance of the preheater, the ratio of the flow rate through the counterflow portion of the preheater to the flow rate into the mixing region must be maintained at a certain value. If the flow holes in the baffle plates become clogged or partially obstructed due to fouling, this ratio can change, potentially reducing the efficiency of the SG as a whole.* This phenomenon cannot be captured with the global fouling factor methodology outlined earlier in this chapter.

Log-Mean Temperature Difference

For feedring SGs, the use of T_{sat} for both the inlet and outlet secondary fluid temperature in Eq. [4-7] reflects neglect of the subcooling of the feedwater entering the feedring. As discussed earlier and shown in Figure 4-1, this error is usually moderately small and is the best approximation available if the global fouling factor is to be employed. For preheater SGs this error is larger because the degree of subcooling is significantly larger. Even more importantly, the presence of the preheater allows the steam temperature T_{sat} to approach the cold-leg temperature T_{cold}. This is because the feedwater reaches saturation at a relatively high elevation on the cold-leg side in a preheater tube bundle compared to a feedring tube bundle. The primary-side temperature at that elevation is significantly higher than the outlet temperature (T_{cold}). This permits T_{sat} to be higher than in a feedring unit, in which T_{sat} is limited to T_{cold} because saturation is reached at an elevation just above the tubesheet where the primary temperature is very close to T_{cold}. This phenomenon is illustrated in Figure 4-5 (adapted from Reference (11)), which shows how the primary and secondary temperatures vary along the length of the SG tubes. Note that feedwater exits the preheater at a point some distance from the cold-leg end, meaning that the subcooled feedwater can acquire heat from the primary fluid when it is significantly warmer than T_{cold}. This point is illustrated graphically in Figure 4-5 via the pinch point (closest approach between primary and secondary fluid temperatures), which moves from P_1 to P_2 due to the presence of the preheater. As a consequence, the final exit temperature at

---

* This effect is distinct from that caused by reduced heat transfer coefficient within the preheater due to fouling, which can itself lower the efficiency of the preheater and hence the SG.

the top of the preheater (i.e., the boiling temperature) can closely approach the cold-leg temperature. The result is that preheater SGs can produce higher steam pressures than feedring SGs given the same inlet conditions (i.e., they are more efficient). South Texas 1 is a good example of this phenomenon: the design value of T_{sat} (557.1°F) is less than 3°F below the design T_{cold} value (559.7°F).

The significance of this characteristic is that the calculated LMTD (as expressed in Eq. [4-7]), and hence the calculated fouling factor, are much more sensitive to changes in the cold-leg temperature than is the case for feedring SGs.* It is possible that for preheaters, a modified LMTD could be defined using an estimated primary temperature at the location where the secondary fluid exits the preheater in place of T_{cold}; however, such an alternate definition is beyond the scope of this effort. In spite of the added limitations of Eq. [4-7] when applied to preheater SGs, it is believed that the global fouling factor captures the essence of fouling behavior just as it does for feedring SGs, although with a greater degree of uncertainty.

Multiple Fouling Factors

Because the geometry and mode of heat-transfer inside the preheater are fundamentally different from the remainder of the SG, a more accurate global analysis might include several fouling factors with distinct LMTDs (e.g., one for the hot-leg side, one for the cold-leg side, one for the preheater, and one for the mixing region). This technique would be capable of revealing fouling in specific regions of the SG (e.g., in the preheater). However, use of a more detailed method like this requires fluid temperature measurements at more locations than just the hot-leg inlet and the cold-leg outlet. Such measurements are generally not available for the operating history of the plant, making the method difficult to apply. Use of this method may require several assumptions including flow rate distributions.

Design and Actual Measured Thermal-Hydraulic Data

In order to perform the fouling factor calculations, data describing the intended design operating parameters are required to determine a design "baseline" for expected performance. In addition, operating parameters recorded during full-power operation are required to calculate the actual performance, which can then be compared to the

---

* This is illustrated quantitatively in Tables 4-3a, 4-4, and 4-5, which have results of uncertainty analyses for Callaway, Sequoyah 1, and South Texas 1. Note that the sensitivity of R'' is much larger for STP 1 (43) than for either Callaway (16) or Sequoyah 1 (15).

predicted design baseline performance, or to the beginning-of-life actual performance, to generate a fouling factor.*

Design Data

Callaway: The relevant thermal-hydraulic design data used for the Callaway SGs are used to develop a baseline for the fouling factor and are summarized in Table 4-1. Note that the average bundle pressure (1012 psia) is calculated from the outlet pressure (1000 psia) and an estimate of the pressure difference between the middle of the bundle and the outlet. This estimate is based on measurements made at Wolf Creek, also a plant with Model F SGs (p. E-104 of Reference (12) and pp. 7-16 and 7-17 of Reference (13)).

Sequoyah 1: Information provided by the Tennessee Valley Authority (TVA) includes the relevant design characteristics of Sequoyah 1 as shown in Table 4-1.

South Texas 1: The design characteristics for this plant were provided by Houston Lighting and Power and are summarized in the rightmost column in Table 4-1.

Measured Operating Data

Data for full-power operation were provided by all three utilities for their respective plants. Data for Callaway spanned the time period from initial operation in December 1984 until April 1996. On average, about one set of measurements per operating week was provided; the largest single gap between measurements was 0.1 EFPY (36 EFPD). All data were provided in electronic form except for some of the Cycle 1 measurements.

For Sequoyah 1, data were provided in electronic spreadsheet form for dates between initial commercial operation in July 1981 until May 1996. Data were provided on average once per month over the entire period. However, three large gaps are present: January to May 1982 (0.3 EFPY), November 1983 to January 1989 (1.3 EFPY, including all of Cycle 3) and August 1991 to March 1992 (0.3 EFPY). For the remaining periods of operation, data were available on average about once every 2.5 weeks of operating time (about once per week during Cycles 1, 7, and 8). Note that values reported prior to March 1992 (i.e., for Cycles 1-5) reflect instantaneous measurements recorded at a specific time on the day in question. Data from Cycles 6–8 comprise time-averaged values (time averaging performed by TVA).

---

* It should be noted that the initial startup performance may not match the design baseline. Any such difference that contributes to the fouling factor cannot be attributed to secondary deposits, which do not exist at initial startup.

For South Texas 1, electronic data were provided covering the period from initial commercial operation in August 1988 until June 1996. As with Sequoyah 1, the overall average frequency was approximately once per month. However, there are four lengthy gaps between available data points: July to December 1989 (0.6 EFPY), February 1990 to April 1991 (0.5 EFPY), August 1992 to May 1994 (0.3 EFPY), and May to September 1994 (0.4 EFPY). Over the remaining periods, measurements were provided about once every two weeks of operating time. Note that HL&P reported data approximately once per hour for the days on which measurements were provided. For each such day, a single time that reflected near-100% power operation was selected for the fouling factor calculations.

Listed below are the items used in fouling factor calculations for each plant:

Outage Dates and EFPY

For each plant, the start and end dates of major outages (i.e., refueling outages, planned in-service inspections, and any forced outages lasting more than about 3 weeks) were compiled from References (14) and (15). The effective full-power years (EFPY) of operation at the start of each refueling outage were provided by the utilities or were taken from Reference (15). The EFPY value at the start of each major forced outage is estimated based on the date of the outage.* (Note that these estimates do take into account shorter outages not explicitly considered.)

Number of Plugged Tubes

The entire tube plugging history is included in the calculations for each plant. That is, the number of tubes plugged in each SG during each outage is an explicit part of the computation of available heat-transfer surface area for subsequent plant operation. This information was taken from Reference (15).

Primary Temperatures

Callaway: For each date, T_{hot}, T_{cold}, and T_{ave} were reported by Union Electric for each SG. However, because the T_{hot} values were wide-band measurements subject to significant uncertainty, the T_{ave} and T_{cold} values were used to back-calculate T_{hot} for the purposes of the fouling factor calculations.

Sequoyah 1: For all dates on which measurements were provided, T_{ave} was reported by TVA for each SG. In addition, for Cycles 1, 2, and 6–8 the primary temperature difference ΔT (T_{hot} - T_{cold}) was used to calculate T_{hot} and T_{cold}. For Cycles 4 and 5, only

---

* This was only necessary for Sequoyah 1 and South Texas 1; Callaway has not experienced a forced outage longer than about 2 weeks.

the average ΔT for all 4 loops was available. Thus, T_{cold} for each SG is taken as the average value. T_{hot} for each loop during these two cycles is calculated based on the actual T_{ave} and the average T_{cold}. In a couple of cases, ΔT was not available; in these cases the primary temperatures were estimated as the average of the preceding and the succeeding values.

South Texas 1: Both T_{hot} and T_{cold} measurements were directly provided by HL&P. Note, however, that these measurements are wide range and therefore are not as accurate as narrow-range values.

Feedwater Temperature

Single measurements were reported for each SG at each plant; all values are incorporated in the fouling factor calculations. (Note that for Callaway prior to March 1991, only the temperature at the feedwater header, which supplies all four loops, was provided. This temperature is used for each loop.)

Feedwater Pressure

Single measurements of feedwater pressure were provided for each loop at Sequoyah 1 and South Texas 1, but not for Callaway. These values were incorporated into the fouling factor calculations. (For Callaway, the design value of the pressure drop between the feedwater inlet and the SG outlet is used to estimate the actual feedwater pressure for each data point. This estimate is reasonable, particularly since the fouling factor calculation is not sensitive to the feedwater pressure.)

Feedwater Mass Flow Rate

Callaway: Single feedwater flow rates were provided for each loop.

Sequoyah 1: Single measurements for each loop were provided for Cycles 1 and 2, and two measurements were provided for Cycles 4 through 8. In all cases, the average measured rate is used in the fouling factor calculations.

South Texas 1: Three measurements were provided for each loop on most dates while one or two measurements were provided on the remaining dates. In all cases, the average measured rate is used in the fouling factor calculations.

Steam Mass Flow Rate

Although not necessary for computing the fouling factor, independent steam mass flow rate measurements (adjusted for blowdown flow) can be used as an alternative

to the feedwater flow rate. The alternative calculation can be used to check for consistency between feedwater and steam flow measurements.

Callaway: Single steam flow rates were provided for each loop.

Sequoyah 1: Single measurements for each loop were provided for Cycles 1 and 2, and two measurements were provided for Cycles 4 through 8. In all cases, the average measured rate is used in the fouling factor calculations.

South Texas 1: Two measurements were provided for each loop for all cycles except Cycle 1. In all cases, the average measured rate is used in the fouling factor calculations. Note that a correction for variations in density was applied by the authors to the raw data supplied by HL&P.

Blowdown Flow Rate

Callaway: Total blowdown flow for all four loops was reported by Union Electric. For the fouling factor calculations, it is assumed that this total flow is evenly distributed among the four loops.

Sequoyah 1: Consistent total blowdown measurements were provided by TVA for operation after 1992 (i.e., Cycles 6–8). As with Callaway, blowdown is assumed to be evenly distributed among the 4 loops. Prior to Cycle 6, blowdown is estimated using the average value for total blowdown recorded during Cycles 6–8.*

South Texas 1: Individual loop measurements were reported by HL&P; each is incorporated in the fouling factor calculations.

Steam Pressure

In all cases, secondary steam pressure is measured downstream of the SG outlets. Therefore, the measured values must be corrected for the pressure drop from the SG to the location of the measurement. (Note that all measurements reported as gage pressures (psig) are converted to absolute pressures (psia) for the purposes of the fouling factor calculations.)

Callaway: The main steam pressure recorded by instrumentation is converted to the pressure at the middle of the tube bundle (i.e., average tube bundle pressure) by applying the following corrections:

---

* Note that the fouling factor is relatively insensitive to changes in the blowdown flow rate because the feedwater flow rate is so much larger. As a result, this approximation is judged reasonable.

1. The loss due to flow through the piping between the SG outlet and the pressure transducers. This pressure drop is calculated using a modified Darcy Equation (corrected for the effects of changing density). Prior to July 1992, this correction is made explicitly in the fouling factor calculations. (See Appendix A for a discussion of the equation used to make the correction.) After July 1992, the pressure measurements reported by Union Electric already incorporate this correction.

2. Postulated additional separator/dryer pressure drop. Callaway performed measurements in February 1996 that indicate a total pressure drop of about 7 psi across the separators and dryers. This is compared to an original design value of approximately 3 psi. When computing the mid-bundle pressure, a fraction of this difference (7 – 3 = 4 psi) is added to the MS pressure measurements according to the time of the measurement (i.e., the correction increases linearly from zero at initial startup to 4 psi by February 1996).

3. Pressure drop between the middle of the tube bundle and the SG outlet nozzle. This is estimated to be 11.5 psi based on published literature for Model F steam generators (p. E-104 of Reference (12) and pp. 7-16 and 7-17 of Reference (13)).

4. For operation prior to March 1985, an added pressure drop of 20 psi is included to reflect the presence of start-up strainers on the main steam line.

Sequoyah 1: Like Callaway, steam pressure at Sequoyah is measured downstream of the SG outlet. For Cycles 1–2, a single measurement (or perhaps an average measurement) was reported for each loop. For Cycles 4–8, three separate measurements were reported for each loop. In all instances, the average value is used in the fouling factor calculations. For the Sequoyah 1 measurements, the pipe-loss correction between the SG outlet and the measurement location is approximately 5 psi. The additional pressure drop between the average bundle pressure and the SG outlet at Sequoyah is approximately 8 psi according to utility information. Measurements of the pressure drop between the top of the tube bundle and a location on the main steam piping have not changed significantly over the last several cycles, indicating that the separators have not dramatically fouled. Thus, no corrections for such fouling were made in the fouling factor calculations.

South Texas 1: Steam pressure at STP 1 is also measured downstream of the SG outlets. A total of three measurements for each loop were recorded; the average values were used in the fouling factor calculations. In this case, the required corrections from the measurements to the average bundle pressure are:

1. The loss due to flow through the piping between the SG outlet and the pressure transducers. According to HL&P, this pressure loss is about 10 psi to the downstream side of the outlet nozzle.

2. Pressure drop between the middle of the tube bundle and the SG outlet nozzle. Per HL&P, this differential is about 7 psi.

Calorimetric Thermal Power

Plant-computed thermal power measurements were provided for Callaway and Sequoyah 1, but not for South Texas 1. This quantity can be used as an alternative basis for computing the fouling factor. Such an alternative computation may be useful for discerning the effects of measurements errors.

Graphical representations for histories of the above measured parameters are provided at the end of this chapter. They include the following:

---

* The steam flow rate is calculated from reported feedwater and blowdown flow rates (i.e., steam flow rate equals feedwater flow rate less the blowdown flow rate). A ratio greater than 1 most likely indicates either a too-high feedwater measurement or a too-low steam flow measurement. A ratio less than 1 indicates the reverse.

Figure 4-16b. Historical Ratio of Calculated to Measured Steam Flow Rate at South Texas 1
Figure 4-17. Historical Feedwater Temperature at South Texas

Detailed discussions of these figures are provided at relevant locations in the remainder of the report.

Fouling Factor Calculations

With the data described in the preceding paragraphs, the fouling factor is calculated for the operating history of Callaway, Sequoyah 1, and South Texas 1. In all cases, the fouling factor is computed relative to the design value for the "clean" resistance R_0'', computed using the values in Table 4-1. The results are depicted in the following figures:

Callaway

Figure 4-18a. Historical Fouling Factor at Callaway (Using Feedwater Flow Measurements)
Figure 4-18b. Historical Fouling Factor at Callaway (Using Steam Flow Measurements)
Figure 4-18c. Historical Fouling Factor at Callaway (Using UE-Supplied Power)

The three figures do not differ significantly, indicating that feedwater flow measurements, steam flow measurements, and UE-calculated thermal power are all fairly consistent. Since Callaway has experienced some fouling of its feedwater venturis, Figure 4-18b is chosen as the basis for future discussion regarding the Callaway fouling factor. There are several noteworthy features on this graph:

- The fouling factor decreases sharply during the first cycle of operation. This may reflect the development of heat-transfer-enhancing deposits on the secondary side of the SG tubes.
- After the early decrease, the fouling factor remains near zero, or even slightly negative, during Cycles 2–4. During this time, Union Electric increased Callaway's power rating from 3425 MWt to 3579 MWt, thereby reducing the available margin against fouling and tube plugging.
- During startup after the end of cycle (EOC) 4 outage, the valves wide open (VWO) condition was reached, resulting in a decrease in electrical generating capacity. Note that there is no sharp increase in the average fouling factor marking this occasion. In fact, the fouling factor is only slightly positive at the beginning of Cycle 5.
- During Cycles 5 and 6, the fouling factor increased steadily until ETA was introduced in the feedwater and a pressure pulse cleaning was performed. Coincident with these changes, the fouling factor appears to level off.
- During the EOC 7 outage, a chemical cleaning of the SG secondary side was performed in each of the four SGs. Upon restart in Cycle 8, the fouling factor

goes through a step increase. This suggests that the deposits removed by the chemical cleaning were in fact beneficial to heat transfer (i.e., responsible for a decrease in the fouling factor). Thin deposits with particular composition and morphology may cause this behavior (see Chapter 5).

The net change in fouling factor (according to Figure 4-18b) between early operation and recent operation is –5 10^{-6} h-ft^2-°F/BTU, which is negligible given the uncertainties of the calculation (see **Fouling Factor Uncertainty Analysis** below). The net change just prior to chemical cleaning was –28 10^{-6}.

Sequoyah 1

Figure 4-19a. Historical Fouling Factor at Sequoyah 1 (Using Feedwater Flow Measurements)
Figure 4-19b. Historical Fouling Factor at Sequoyah 1 (Using Steam Flow Measurements)
Figure 4-19c. Historical Fouling Factor at Sequoyah 1 (Using TVA-Supplied Power)
Figure 4-19d. Historical Fouling Factor at Sequoyah 1 (Using Feedwater Flow and Corrected T_{hot})

Figures 4-19a and 4-19b are noticeably different, suggesting that feedwater and steam flow measurements are not in good agreement. This is confirmed in Figure 4-12b, which indicates substantial disagreement in Cycles 1, 4, and 5. Figure 4-19c is in good agreement with 4-19a, which is expected because TVA uses feedwater flow rate to calculate thermal power. Figure 4-19d is identical to 4-19a except that it also reflects a correction for a 2°F error in T_{ave} caused by hot-leg streaming beginning in Cycle 5. Note from the figures that this correction reduces the calculated fouling factor by about 23 10^{-6} h-ft^2-°F/BTU. Also, the overall change in fouling factor since early operation suggested by Figure 4-19d is about 42 10^{-6} (21 10^{-6} just prior to chemical cleaning).

South Texas 1

Figure 4-20a. Historical Fouling Factor at South Texas 1 (Using Feedwater Flow Measurements)
Figure 4-20b. Historical Fouling Factor at South Texas 1 (Using Steam Flow Measurements)

Except for Cycle 1 (for which no steam flow rate measurements were available), these two figures are in fairly close agreement. From Figure 4-20a, the fouling factor increase between early and recent operation is about 30 10^{-6} h-ft^2-°F/BTU.

Fouling Factor Uncertainty Analysis

There are potentially significant uncertainties in the plant instrument data required as inputs to the fouling factor calculation. As a result, a statistical uncertainty analysis is warranted when reporting the fouling factor calculations. The standard engineering approximation for calculating the uncertainty tolerance of a computed quantity uses the following equation:

$$\Delta_{statistical}(F) = \sqrt{\sum_{i=1}^{n}\left(\frac{\partial F}{\partial x_i}\right)^2 \Delta^2(x_i)} \qquad \text{(eq. 4-9)}$$

where F is a function of x_1 through x_n and $\Delta(x_i)$ is the engineering estimate of the uncertainty in the measured quantity x_i. The worst case uncertainty in the calculated quantity F is given by

$$\Delta_{worst\ case}(F) = \sum_{i=1}^{n} \left| \left(\frac{\partial F}{\partial x_i} \right) \Delta(x_i) \right| \qquad \text{(eq. 4-10)}$$

However, this quantity is considered overly conservative for the fouling factor calculation. More detailed discussion of the issues involved in calculating uncertainties is provided in Reference (16), including such topics as precision and bias errors and sensitivity calculations. Page 3-8 of Reference (12) comprises a discussion of measurement uncertainty issues specific to nuclear plants.

Uncertainty Inputs

In order to perform the calculation suggested by Eq. [4-9], values for each of the $\Delta(x_i)$ must be determined. These include the following:

- Primary temperatures T_{hot} and T_{cold}
- Feedwater temperature
- Feedwater mass flow rate
- Blowdown flow rate
- Feedwater pressure
- SG steam pressure
- Steam quality
- Heat-transfer area

The input values and the results of the uncertainty analysis for each plant are discussed below.

Callaway

Measurement tolerances are indicated in Table 4-2. Note that Table 3-2 of Reference (12) applies explicitly to Wolf Creek. However, Callaway and Wolf Creek are both examples of the standardized nuclear unit power plant system (SNUPPS) design.

Hence, these measurement tolerances are believed to be applicable to Callaway also. The tolerances marked "estimate" in Table 4-2 are based on engineering judgment. The results of the uncertainty analysis are shown in Table 4-3a. Note that the total statistical uncertainty in the fouling factor (±19 10^{-6} h-ft^2-°F/BTU) is larger in magnitude than the previously calculated fouling factor change over the life of the plant (–5 10^{-6}). From the lower portion of Table 4-3a, it is apparent that the uncertainty in SG steam pressure dominates the fouling factor uncertainty, while T_{cold}, T_{hot}, and feedwater flow rate play lesser roles. The remaining variables contribute very little to the total uncertainty. The fouling factor for Callaway (in 1996) is thus given by

$$R''_{f-Callaway} = -5 \pm 19\ 10^{-6}\, h - ft^2 - {}^\circ F / BTU \qquad \text{(eq. 4-11)}$$

The tolerances listed in the top portion of Table 4-2 probably reflect the use of recently calibrated instruments. It is possible during operation that the actual uncertainty may increase due to drift. The second section of Table 4-2 indicates how the fouling factor uncertainty changes if the tolerances on T_{hot}, T_{cold}, and SG pressure are doubled. Because these are the three primary contributors to the fouling factor uncertainty, it also doubles (to ±37 10^{-6}) as shown in Table 4-3b.

Sequoyah 1

Measurement tolerances are listed in Table 4-2, and the associated uncertainty analysis is shown in Table 4-4. Several of the uncertainty inputs were available in plant scaling and set point documents (References (17) through (20)). In this case, the uncertainties in T_{cold} and steam pressure are dominant, while feedwater flow rate and T_{hot} have minor contributions. The other variables contribute little to the fouling factor uncertainty. The calculated fouling factor may be completely reported for Sequoyah 1 (in 1996) as

$$R''_{f-Sequoyah} = 42 \pm 24\ 10^{-6}\, h - ft^2 - {}^\circ F / BTU \qquad \text{(eq. 4-12)}$$

South Texas 1

Measurement tolerances specific to South Texas 1 are shown in Table 4-2; the values are based on conversations with HL&P personnel or are best estimates based on engineering judgment. The associated uncertainty analysis is shown in Table 4-5. Note that the uncertainties in T_{cold} and SG pressure are the primary contributors to the fouling factor uncertainty. In view of the uncertainty analysis, the calculated fouling factor may be completely reported for South Texas 1 (in 1996) as

$$R''_{f-STP} = 30 \pm 62\ 10^{-6}\, h - ft^2\ - {}^\circ F / BTU \qquad \text{(eq. 4-13)}$$

Table 4-1
Design Steam Generator Heat-Transfer Parameters

Parameter	Units	Callaway	Sequoyah 1	South Texas 1
T_{hot}	°F	620	609.7	626.1
T_{cold}	°F	557	546.7	559.7
Steam Generator Dome Pressure	psia	1000	857	1100
Steam Generator Average Bundle Pressure	psia	1012	865	1107
Saturation Temp. for Avg. Bundle Pressure	°F	546.1	527.3	557.1
Thermal Power (per SG)	MWt	895	856	954
Thermal Power (per SG)	BTU/h	3.053E+09	2.920E+09	3.256E+09
Heat Transfer Area (OD)	ft^2	55,000	51,500	68,000
Average Heat Flux (Based on OD Area)	BTU/h-ft^2	55,509	56,698	47,882
Design Plugging Margin	–	15%	0%	0%
Number of Tubes (per SG)	–	5626	3388	4864
Feedwater Temperature	°F	446.0	434.5	440.0
Feedwater Pressure	psia	1025	876	1129
Secondary Mass Flow Rate	lb_m/h	3.963E+06	3.749E+06	4.240E+06
Blowdown Flow Rate	lb_m/h	31,250	20,000	NA[†]

[†]Not available; actual average rate was 39,000.

Table 4-2
Plant Measurement Uncertainties

Symbol	Quantity	Tolerance	Source
Callaway (Tight)			
T_{hot}	Hot-Leg Temperature	±1.0°F	Table 3-2 of EPRI NP-5728
T_{cold}	Cold-Leg Temperature	±0.5°F	Table 3-2 of EPRI NP-5728
p_{sat}	SG Steam Pressure	±0.5% FS (±6.5 psi)	Table 3-2 of EPRI NP-5728
m_{FW}	Feedwater Flow Rate	±0.5% FS (±24,000 lb_m/h)	Table 3-2 of EPRI NP-5728 & Utility Calibration Procedure
T_{FW}	Feedwater Temperature	±1.0°F	Estimate
Q_{BD}	Blowdown Flow Rate	±1% (312 lb_m/h)	Estimate
p_{FW}	Feedwater Pressure	±8 psi	Estimate
x	Steam Quality	±0.15%	Estimate
A	Heat-Transfer Area[1]	0.2% (±110 ft^2)	Estimate
Callaway (Loose)			
T_{hot}	Hot-Leg Temperature	±2.0°F	Conservative Estimate
T_{cold}	Cold-Leg Temperature	±1.0°F	Conservative Estimate
p_{sat}	SG Steam Pressure	±1% FS (±13 psi)	Conservative Estimate
m_{FW}	Feedwater Flow Rate	±0.5% FS (±24,000 lb_m/h)	Table 3-2 of EPRI NP-5728 & Utility Calibration Procedure
T_{FW}	Feedwater Temperature	±2.0°F	Estimate
Q_{BD}	Blowdown Flow Rate	±1% (312 lb_m/h)	Estimate
p_{FW}	Feedwater Pressure	±8 psi	Estimate
x	Steam Quality	±0.15%	Estimate
A	Heat-Transfer Area[1]	0.2% (±110 ft^2)	Estimate
Sequoyah 1			
T_{hot}	Hot-Leg Temperature	±1.1°F	Plant Scaling and Set Point Documents
T_{cold}	Cold-Leg Temperature	±1.1°F	Plant Scaling and Set Point Documents
p_{sat}	SG Steam Pressure[1]	±0.4% FS (±4.8 psi)	Plant Scaling and Set Point Documents
m_{FW}	Feedwater Flow Rate[2]	±0.5% FS (±2.25 10^4 lb_m/h)	Utility Personnel
T_{FW}	Feedwater Temperature	±1.5°F	Utility Personnel
Q_{BD}	Blowdown Flow Rate	±10% (2000 lb_m/h)	Utiltity Information
p_{FW}	Feedwater Pressure	±30 psi	Utility Personnel
x	Steam Quality	±0.15%	Estimate
A	Heat-Transfer Area[3]	0.3% (±155 ft^2)	Estimate
South Texas 1			
T_{hot}	Hot-Leg Temperature	±4°F	Utility Personnel (plus allowance for hot-leg streaming)
T_{cold}	Cold-Leg Temperature	±1°F	Utility Personnel
p_{sat}	SG Steam Pressure	±0.5% FS (±7.5 psi)	Best Estimate
m_{FW}	Feedwater Flow Rate	±0.5% FS (±2.12 10^4 lb_m/h)	Best Estimate
T_{FW}	Feedwater Temperature	±1°F	Utility Personnel
Q_{BD}	Blowdown Flow Rate	±10% (3900 lb_m/h)	Bounding Estimate
p_{FW}	Feedwater Pressure	±30 psi	Bounding Estimate
x	Steam Quality	±0.15%	Bounding Estimate
A	Heat-Transfer Area[1]	0.25% (±170 ft^2)	Bounding Estimate

NOTES

1. This tolerance reflects the possibility that plugged tubes may be longer or shorter on average than the average-length tube in the whole bundle.
2. This error is believed to be applicable for operation since 1992. Earlier data may be subject to an error as large as 2.8% (1.8% per utiltity scaling and set point document plus 1% for venturi fouling).
3. This tolerance reflects the possibility that plugged tubes may be longer or shorter on average than the average-length tube in the whole bundle.

Table 4-3a (p. 1 of 2)
Fouling Factor Uncertainty Analysis for Callaway
(Tight Tolerances on Primary Temperatures)

Quantity	Description	Units	Design Value (VWO)	Bilateral Tolerance	Δx
measured quantities					
T_{hot}	hot leg temperature	°F	620.0	1.0	1.0
T_{cold}	cold leg temperature	°F	557.0	0.5	0.5
T_{FW}	feedwater temperature	°F	446.0	1.0	1.0
m_{FW}	feedwater flow rate[1]	lb/h	3.963E+06	0.5% of FS	24,000
Q_{BD}	blowdown volumetric flow rate	gpm	84	1.0%	1
p_{FW}	feedwater pressure	psia	1025	8	8
p_{sat}	steam generator dome pressure[2]	psia	1000	0.5% of FS	6.5
x	steam quality	%	99.75	0.15	0.15
A	heated outside-tube surface area	ft^2	46,750	0.2%	110
intermediate quantities					
$T_{sat,out}$	outlet saturation temperature	°F	544.58		
p_{bundle}	mid-bundle pressure	psia	1011.5		
T_{sat}	bundle saturation temperature	°F	545.97		
ΔT_{lm}	log-mean temperature difference	°F	33.09		
v_f	saturated liquid specific volume	ft^3/lb	0.02163		
m_{BD}	blowdown mass flow rate	lb/h	31,250		
m_{steam}	steam flow rate	lb/h	3.931E+06		
h_f	saturated liquid specific enthalpy	Btu/lb	542.6		
h_g	saturated vapor specific enthalpy	Btu/lb	1192.9		
$h_f(T_{FW})$	feedwater saturated spec. enthalpy	Btu/lb	425.6		
$v_f(T_{FW})$	feedwater saturated spec. volume	ft^3/lb	0.01936		
$p_{sat}(T_{FW})$	saturation pressure at feedwater T	psia	405.7		
h_{FW}	feedwater specific enthalpy	Btu/lb	427.9		
Q	steam generator heat transfer rate	Btu/h	3.005E+09		
R	global resistance to heat transfer	h-°F/Btu	1.101E-08		
U	global heat transfer coefficient	Btu/h-ft^2-°F	1942.8		
calculated quantity					
R"	global area-based resistance	10^{-6} h-ft^2-°F/Btu	514.7		
other quantities required for partial derivatives					
$c_{p,FW}$	feedwater specific heat	Btu/lb-°F	1.109		
v_{FW}	feedwater specific volume	ft^3/lb	0.01936		
h_{fg}	latent heat of vaporization at p_{sat}	Btu/lb	650.4		
v_g	saturated vapor specific volume	ft^3/lb	0.4404		
v_{fg}	specific volume change upon vap.	ft^3/lb	0.41881		
$\partial h_g/\partial p_{sat}$	partial derivative of vapor enthalpy	(Btu/lb)/psi	-0.03659		
$\partial h_f/\partial p_{sat}$	partial derivative of liquid enthalpy	(Btu/lb)/psi	0.1532		
$\partial(h_{fg}/v_f)/\partial p_{sat}$	partial derivative of h_{fg}/v_f ratio	(Btu/ft^3)/psi	-13.856		
$\partial Q/\partial p_{sat}$	partial derivative of thermal power	(Btu/h)/psi	-133,785		

Table 4-3a (p. 2 of 2)
Fouling Factor Uncertainty Analysis for Callaway
(Tight Tolerances on Primary Temperatures)

partial derivatives of area-based resistance		Units for $\partial R''/\partial x$	$\partial R''/\partial x$	$\Delta(x)$	$(\partial R''/\partial x)\Delta(x)$
$\partial R''/\partial T_{hot}$	partial deriv. wrt hot leg temp.	$(10^{-6}$ h-ft^2-°F/Btu)/°F	4.518	1.0	4.52
$\partial R''/\partial T_{cold}$	partial deriv. wrt cold leg temp.	$(10^{-6}$ h-ft^2-°F/Btu)/°F	16.345	0.5	8.17
$\partial R''/\partial T_{FW}$	partial deriv. wrt feedwater temp.	$(10^{-6}$ h-ft^2-°F/Btu)/°F	0.752	1.0	0.75
$\partial R''/\partial m_{FW}$	partial deriv. wrt feedwater flow	$(10^{-6}$ h-ft^2-°F/Btu)/(lb/h)	-1.308E-04	2.400E+04	-3.14
$\partial R''/Q_{BD}$	partial deriv. wrt blowdown flow	$(10^{-6}$ h-ft^2-°F/Btu)/gpm	0.041	1	0.03
$\partial R''/\partial p_{FW}$	partial deriv. wrt feedwater press.	$(10^{-6}$ h-ft^2-°F/Btu)/psi	0.002	8	0.02
$\partial R''/\partial p_{sat}$	partial deriv. wrt steam gen. press.	$(10^{-6}$ h-ft^2-°F/Btu)/psi	-2.477	6.5	-16.10
$\partial R''/\partial x$	partial deriv. wrt outlet quality	$(10^{-6}$ h-ft^2-°F/Btu)/%	-4.380	0.15	-0.66
$\partial R''/A$	partial deriv. wrt heated area	$(10^{-6}$ h-ft^2-°F/Btu)/ft^2	0.011	110	1.21
				$\Sigma\lvert(\partial R''/\partial x)\Delta(x)\rvert$	34.61
				$\Sigma[(\partial R''/\partial x)\Delta(x)]^2$	358.82
				$\{\Sigma[(\partial R''/\partial x)\Delta(x)]^2\}^{1/2}$	18.94
final results of error analysis			**Design**	$\Delta_{worst\ case}(R'')$	$\Delta_{statistical}(R'')$
R''	global area-based resistance	10^{-6} h-ft^2-°F/Btu	514.7	34.6	18.9

Notes

1. The full scale for feedwater flow measurement is 4.8 x 10^6 lb_m/h
2. The full scale for SG pressure measurement is 1300 psi.

Table 4-3b (p. 1 of 2)
Fouling Factor Uncertainty Analysis for Callaway
(Loose Tolerances on Primary Temperatures)

Quantity	Description	Units	Design Value (VWO)	Bilateral Tolerance	Δx
measured quantities					
T_{hot}	hot leg temperature	°F	620.0	2.0	2.0
T_{cold}	cold leg temperature	°F	557.0	1.0	1.0
T_{FW}	feedwater temperature	°F	446.0	2.0	2.0
m_{FW}	feedwater flow rate[1]	lb/h	3.963E+06	0.5% of FS	24,000
Q_{BD}	blowdown volumetric flow rate	gpm	84	1.0%	1
p_{FW}	feedwater pressure	psia	1025	8	8
p_{sat}	steam generator dome pressure[2]	psia	1000	1.0% of FS	13.0
x	steam quality	%	99.75	0.15	0.15
A	heated outside-tube surface area	ft^2	46,750	0.2%	110
intermediate quantities					
$T_{sat,out}$	outlet saturation temperature	°F	544.58		
p_{bundle}	mid-bundle pressure	psia	1011.5		
T_{sat}	bundle saturation temperature	°F	545.97		
ΔT_{lm}	log-mean temperature difference	°F	33.09		
v_f	saturated liquid specific volume	ft^3/lb	0.02163		
m_{BD}	blowdown mass flow rate	lb/h	31,250		
m_{steam}	steam flow rate	lb/h	3.931E+06		
h_f	saturated liquid specific enthalpy	Btu/lb	542.6		
h_g	saturated vapor specific enthalpy	Btu/lb	1192.9		
$h_f(T_{FW})$	feedwater saturated spec. enthalpy	Btu/lb	425.6		
$v_f(T_{FW})$	feedwater saturated spec. volume	ft^3/lb	0.01936		
$p_{sat}(T_{FW})$	saturation pressure at feedwater T	psia	405.7		
h_{FW}	feedwater specific enthalpy	Btu/lb	427.9		
Q	steam generator heat transfer rate	Btu/h	3.005E+09		
R	global resistance to heat transfer	h-°F/Btu	1.101E-08		
U	global heat transfer coefficient	Btu/h-ft^2-°F	1942.8		
calculated quantity					
R"	global area-based resistance	10^{-6} h-ft^2-°F/Btu	514.7		
other quantities required for partial derivatives					
$c_{p,FW}$	feedwater specific heat	Btu/lb-°F	1.109		
v_{FW}	feedwater specific volume	ft^3/lb	0.01936		
h_{fg}	latent heat of vaporization at p_{sat}	Btu/lb	650.4		
v_g	saturated vapor specific volume	ft^3/lb	0.4404		
v_{fg}	specific volume change upon vap.	ft^3/lb	0.41881		
$\partial h_g/\partial p_{sat}$	partial derivative of vapor enthalpy	(Btu/lb)/psi	-0.03659		
$\partial h_f/\partial p_{sat}$	partial derivative of liquid enthalpy	(Btu/lb)/psi	0.1532		
$\partial(h_{fg}/v_f)/\partial p_{sat}$	partial derivative of h_{fg}/v_f ratio	(Btu/ft^3)/psi	-13.856		
$\partial Q/\partial p_{sat}$	partial derivative of thermal power	(Btu/h)/psi	-133,785		

Table 4-3b (p. 2 of 2)
Fouling Factor Uncertainty Analysis for Callaway
(Loose Tolerances on Primary Temperatures)

partial derivatives of area-based resistance		Units for $\partial R''/\partial x$	$\partial R''/\partial x$	$\Delta(x)$	$(\partial R''/\partial x)\Delta(x)$
$\partial R''/\partial T_{hot}$	partial deriv. wrt hot leg temp.	$(10^{-6}$ h-ft^2-°F/Btu)/°F	4.518	2.0	9.04
$\partial R''/\partial T_{cold}$	partial deriv. wrt cold leg temp.	$(10^{-6}$ h-ft^2-°F/Btu)/°F	16.345	1.0	16.35
$\partial R''/\partial T_{FW}$	partial deriv. wrt feedwater temp.	$(10^{-6}$ h-ft^2-°F/Btu)/°F	0.752	2.0	1.50
$\partial R''/\partial m_{FW}$	partial deriv. wrt feedwater flow	$(10^{-6}$ h-ft^2-°F/Btu)/(lb/h)	-1.308E-04	2.400E+04	-3.14
$\partial R''/Q_{BD}$	partial deriv. wrt blowdown flow	$(10^{-6}$ h-ft^2-°F/Btu)/gpm	0.041	1	0.03
$\partial R''/\partial p_{FW}$	partial deriv. wrt feedwater press.	$(10^{-6}$ h-ft^2-°F/Btu)/psi	0.002	8	0.02
$\partial R''/\partial p_{sat}$	partial deriv. wrt steam gen. press.	$(10^{-6}$ h-ft^2-°F/Btu)/psi	-2.477	13.0	-32.21
$\partial R''/\partial x$	partial deriv. wrt outlet quality	$(10^{-6}$ h-ft^2-°F/Btu)/%	-4.380	0.15	-0.66
$\partial R''/A$	partial deriv. wrt heated area	$(10^{-6}$ h-ft^2-°F/Btu)/ft^2	0.011	110	1.21
				$\Sigma \lvert (\partial R''/\partial x)\Delta(x) \rvert$	64.15
				$\Sigma[(\partial R''/\partial x)\Delta(x)]^2$	1400.02
				$\{\Sigma[(\partial R''/\partial x)\Delta(x)]^2\}^{1/2}$	37.42
final results of error analysis			**Design**	$\Delta_{worst\ case}(R'')$	$\Delta_{statistical}(R'')$
R"	global area-based resistance	10^{-6} h-ft^2-°F/Btu	514.7	64.2	37.4

Notes

1. The full scale for feedwater flow measurement is 4.8 x 10^6 lb_m/h
2. The full scale for SG pressure measurement is 1300 psi.

Table 4-4 (p. 1 of 2)
Fouling Factor Uncertainty Analysis for Sequoyah 1

Quantity	Description	Units	Design Value (VWO)	Bilateral Tolerance	Δx
Measured quantities					
T_{hot}	hot leg temperature	°F	609.7	1.1	1.1
T_{cold}	cold leg temperature	°F	546.7	1.1	1.1
T_{FW}	feedwater temperature	°F	434.5	1.5	1.5
m_{FW}	feedwater flow rate	lb/h	3.749E+06	0.5%	2.250E+04
Q_{BD}	blowdown volumetric flow rate	gpm	53	10%	5
p_{FW}	feedwater pressure	psia	876	30	30
p_{sat}	steam generator dome pressure	psia	857	4.8	4.8
x	steam quality	%	99.75	0.15	0.15
A	heated outside-tube surface area	ft^2	51,500	0.3%	155
Intermediate quantities					
$T_{sat,out}$	outlet saturation temperature	°F	526.19		
p_{bundle}	mid-bundle pressure	psia	865		
T_{sat}	bundle saturation temperature	°F	527.27		
ΔT_{lm}	log-mean temperature difference	°F	43.60		
v_f	saturated liquid specific volume	ft^3/lb	0.02111		
m_{BD}	blowdown mass flow rate	lb/h	20,000		
m_{steam}	steam flow rate	lb/h	3.729E+06		
h_f	saturated liquid specific enthalpy	Btu/lb	520.9		
h_g	saturated vapor specific enthalpy	Btu/lb	1197.4		
$h_f(T_{FW})$	feedwater saturated spec. enthalpy	Btu/lb	412.9		
$v_f(T_{FW})$	feedwater saturated spec. volume	ft^3/lb	0.01917		
$p_{sat}(T_{FW})$	saturation pressure at feedwater T	psia	360.4		
h_{FW}	feedwater specific enthalpy	Btu/lb	414.7		
Q	steam generator heat transfer rate	Btu/h	2.915E+09		
R	global resistance to heat transfer	h-°F/Btu	1.496E-08		
U	global heat transfer coefficient	Btu/h-ft^2-°F	1298		
Calculated quantity					
R"	global area-based resistance	10^{-6} h-ft^2-°F/Btu	770.4		
Other quantities required for partial derivatives					
$c_{p,FW}$	feedwater specific heat	Btu/lb-°F	1.098		
v_{FW}	feedwater specific volume	ft^3/lb	0.01917		
h_{fg}	latent heat of vaporization at p_{sat}	Btu/lb	676.5		
v_g	saturated vapor specific volume	ft^3/lb	0.5233		
v_{fg}	specific volume change upon vap.	ft^3/lb	0.5022		
$\partial h_g/\partial p_{sat}$	partial derivative of vapor enthalpy	(Btu/lb)/psi	-0.03106		
$\partial h_f/\partial p_{sat}$	partial derivative of liquid enthalpy	(Btu/lb)/psi	0.1653		
$\partial(h_{fg}/v_f)/\partial p_{sat}$	partial derivative of h_{fg}/v_f ratio	(Btu/ft^3)/psi	-14.74		
$\partial Q/\partial p_{sat}$	partial derivative of thermal power	(Btu/h)/psi	-108,391		

Table 4-4 (p. 2 of 2)
Fouling Factor Uncertainty Analysis for Sequoyah 1

Partial derivatives of area-based resistance		Units for ∂R''/∂x	∂R''/∂x	Δ(x)	(∂R''/∂x)Δ(x)
$\partial R''/\partial T_{hot}$	partial deriv. wrt hot leg temp.	(10-6 h-ft2-°F/Btu)/°F	5.761	1.1	6.57
$\partial R''/\partial T_{cold}$	partial deriv. wrt cold leg temp.	(10-6 h-ft2-°F/Btu)/°F	15.206	1.1	17.33
$\partial R''/\partial T_{FW}$	partial deriv. wrt feedwater temp.	(10-6 h-ft2-°F/Btu)/°F	1.088	1.5	1.63
$\partial R''/\partial m_{FW}$	partial deriv. wrt feedwater flow	(10-6 h-ft2-°F/Btu)/(lb/h)	-2.065E-04	2.250E+04	-4.65
$\partial R''/Q_{BD}$	partial deriv. wrt blowdown flow	(10-6 h-ft2-°F/Btu)/gpm	0.068	5	0.36
$\partial R''/\partial p_{FW}$	partial deriv. wrt feedwater press.	(10-6 h-ft2-°F/Btu)/psi	0.004	30	0.11
$\partial R''/\partial p_{sat}$	partial deriv. wrt steam gen. press.	(10-6 h-ft2-°F/Btu)/psi	-2.814	5	-13.51
∂R''/∂x	partial deriv. wrt outlet quality	(10-6 h-ft2-°F/Btu)/%	-6.668	0.15	-1.00
∂R''/A	partial deriv. wrt heated area	(10-6 h-ft2-°F/Btu)/ft2	0.015	155	2.31
				$\Sigma\lvert(\partial R''/\partial x)\Delta(x)\rvert$	47.46
				$\Sigma[(\partial R''/\partial x)\Delta(x)]^2$	556.74
				$\{\Sigma[(\partial R''/\partial x)\Delta(x)]^2\}^{1/2}$	23.60
Final results of error analysis			Design	$\Delta_{worst\ case}(R'')$	$\Delta_{statistical}(R'')$
R''	global area-based resistance	10^{-6} h-ft^2-°F/Btu	770.4	47.5	23.6

Table 4-5 (p. 1 of 2)
Fouling Factor Uncertainty Analysis for South Texas 1

Quantity	Description	Units	Design Value (VWO)	Bilateral Tolerance	Δx
Measured quantities					
T_{hot}	hot leg temperature	°F	626.1	4.0	4.0
T_{cold}	cold leg temperature	°F	559.7	1.0	1.0
T_{FW}	feedwater temperature	°F	440	1.0	1.0
m_{FW}	feedwater flow rate	lb/h	4.240E+06	0.5%	2.120E+04
Q_{BD}	blowdown volumetric flow rate	gpm	107	10%	11
p_{FW}	feedwater pressure	psia	1129	30	30
p_{sat}	steam generator dome pressure	psia	1100	7.5	7.5
x	steam quality	%	99.75	0.15	0.15
A	heated outside-tube surface area	ft^2	68,000	0.25%	170
Intermediate quantities					
$T_{sat,out}$	outlet saturation temperature	°F	556.27		
p_{bundle}	mid-bundle pressure	psia	1107		
T_{sat}	bundle saturation temperature	°F	557.06		
ΔT_{lm}	log-mean temperature difference	°F	20.34		
v_f	saturated liquid specific volume	ft^3/lb	0.02197		
m_{BD}	blowdown mass flow rate[1]	lb/h	39,000		
m_{steam}	steam flow rate	lb/h	4.201E+06		
h_f	saturated liquid specific enthalpy	Btu/lb	558.6		
h_g	saturated vapor specific enthalpy	Btu/lb	1188.8		
$h_f(T_{FW})$	feedwater saturated spec. enthalpy	Btu/lb	419.0		
$v_f(T_{FW})$	feedwater saturated spec. volume	ft^3/lb	0.01926		
$p_{sat}(T_{FW})$	saturation pressure at feedwater T	psia	381.54		
h_{FW}	feedwater specific enthalpy	Btu/lb	421.6		
Q	steam generator heat transfer rate	Btu/h	3.222E+09		
R	global resistance to heat transfer	h-°F/Btu	6.313E-09		
U	global heat transfer coefficient	Btu/h-ft^2-°F	2330		
Calculated quantity					
R"	global area-based resistance	10^{-6} h-ft^2-°F/Btu	429.3		
Other quantities required for partial derivatives					
$c_{p,FW}$	feedwater specific heat	Btu/lb-°F	1.103		
v_{FW}	feedwater specific volume	ft^3/lb	0.01926		
h_{fg}	latent heat of vaporization at p_{sat}	Btu/lb	630.3		
v_g	saturated vapor specific volume	ft^3/lb	0.3978		
v_{fg}	specific volume change upon vap.	ft^3/lb	0.3758		
$\partial h_g/\partial p_{sat}$	partial derivative of vapor enthalpy	(Btu/lb)/psi	-0.03818		
$\partial h_f/\partial p_{sat}$	partial derivative of liquid enthalpy	(Btu/lb)/psi	0.1448		
$\partial(h_{fg}/v_f)/\partial p_{sat}$	partial derivative of h_{fg}/v_f ratio	(Btu/ft^3)/psi	-13.36		
$\partial Q/\partial p_{sat}$	partial derivative of thermal power	(Btu/h)/psi	-148,516		

Table 4-5 (p. 2 of 2)
Fouling Factor Uncertainty Analysis for South Texas 1

Partial derivatives of area-based resistance		Units for ∂R''/∂x	∂R''/∂x	Δ(x)	(∂R''/∂x)Δ(x)
$\partial R''/\partial T_{hot}$	partial deriv. wrt hot leg temp.	$(10^{-6}$ h-ft^2-°F/Btu)/°F	4.560	4.0	18.24
$\partial R''/\partial T_{cold}$	partial deriv. wrt cold leg temp.	$(10^{-6}$ h-ft^2-°F/Btu)/°F	43.386	1.0	43.39
$\partial R''/\partial T_{FW}$	partial deriv. wrt feedwater temp.	$(10^{-6}$ h-ft^2-°F/Btu)/°F	0.623	1.0	0.62
$\partial R''/\partial m_{FW}$	partial deriv. wrt feedwater flow	$(10^{-6}$ h-ft^2-°F/Btu)/(lb/h)	-1.020E-04	2.120E+04	-2.16
$\partial R''/Q_{BD}$	partial deriv. wrt blowdown flow	$(10^{-6}$ h-ft^2-°F/Btu)/gpm	0.031	11	0.33
$\partial R''/\partial p_{FW}$	partial deriv. wrt feedwater press.	$(10^{-6}$ h-ft^2-°F/Btu)/psi	0.002	30	0.06
$\partial R''/\partial p_{sat}$	partial deriv. wrt steam gen. press.	$(10^{-6}$ h-ft^2-°F/Btu)/psi	-5.359	8	-40.19
∂R''/∂x	partial deriv. wrt outlet quality	$(10^{-6}$ h-ft^2-°F/Btu)/%	-3.528	0.15	-0.53
∂R''/A	partial deriv. wrt heated area	$(10^{-6}$ h-ft^2-°F/Btu)/ft^2	0.006	170	1.07
				$\Sigma\lvert(\partial R''/\partial x)\Delta(x)\rvert$	106.59
				$\Sigma[(\partial R''/\partial x)\Delta(x)]^2$	3837.05
				$\{\Sigma[(\partial R''/\partial x)\Delta(x)]^2\}^{1/2}$	61.94
Final results of error analysis			**Design**	$\Delta_{worst\ case}(R'')$	$\Delta_{statistical}(R'')$
R''	global area-based resistance	10^{-6} h-ft^2-°F/Btu	429.3	106.6	61.9

Notes
1. The average reported blowdown flow rate is used in the absence of a design value.

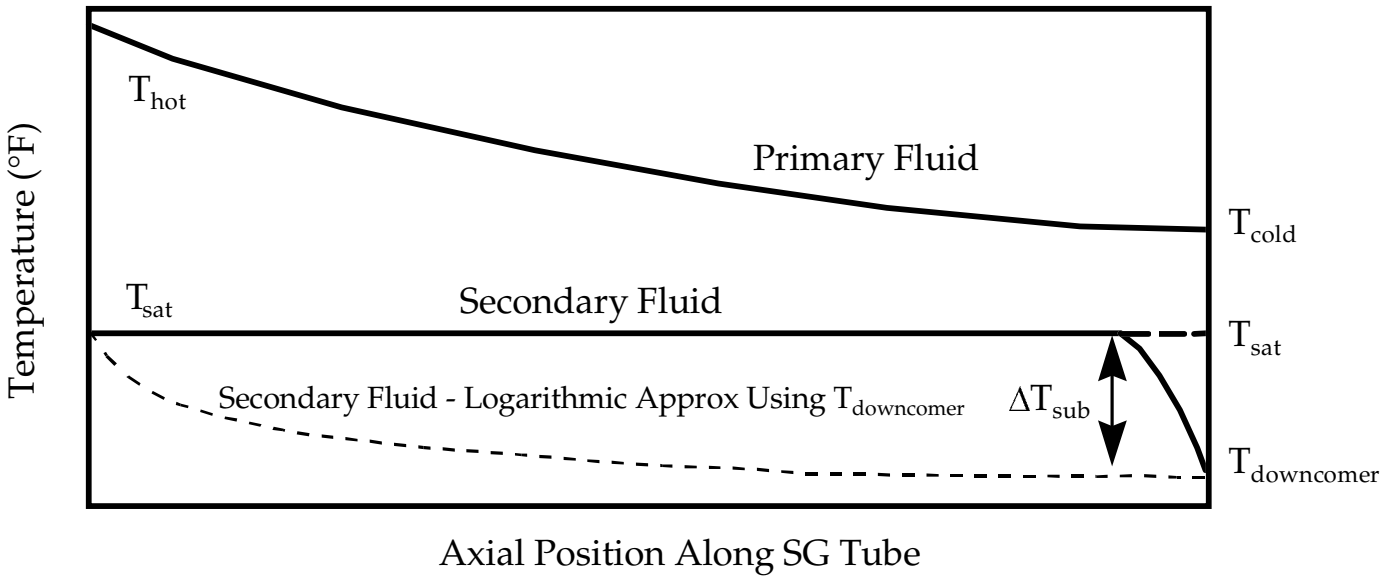

Figure 4-1
Temperature Variation Along RSG Tubes (To Scale for a Sample Plant)

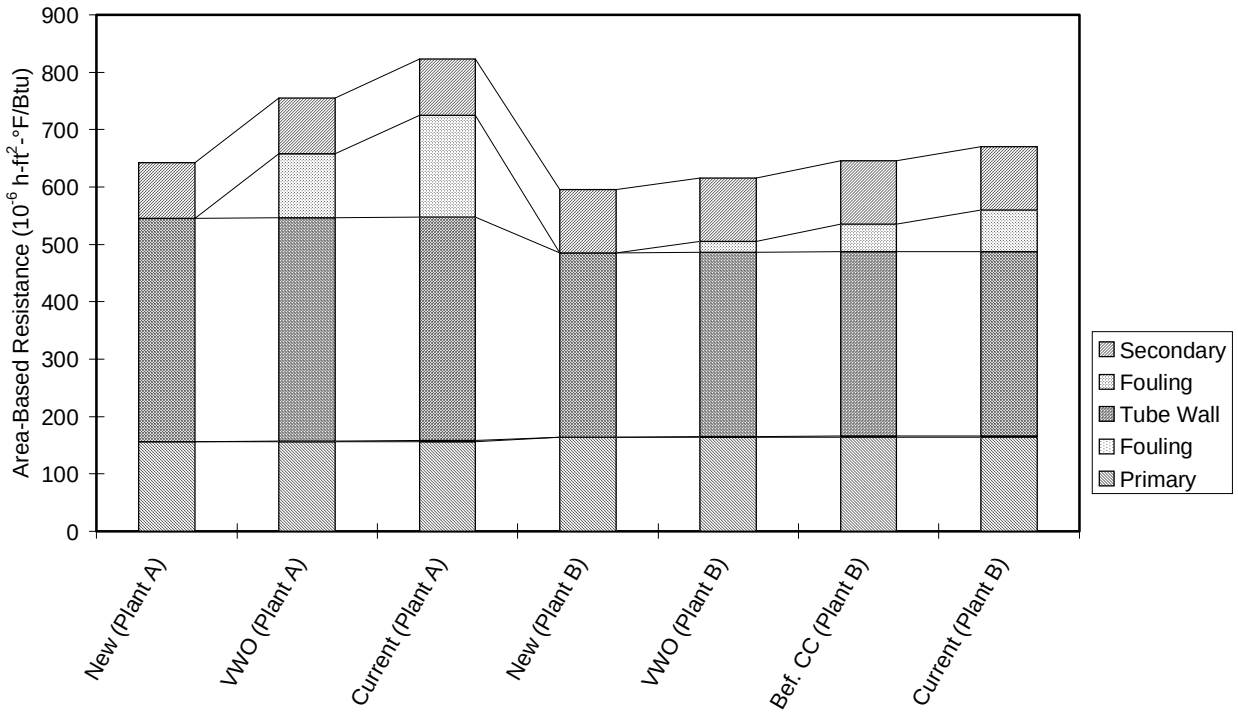

Figure 4-2
Theoretical Components of Heat Transfer Resistance

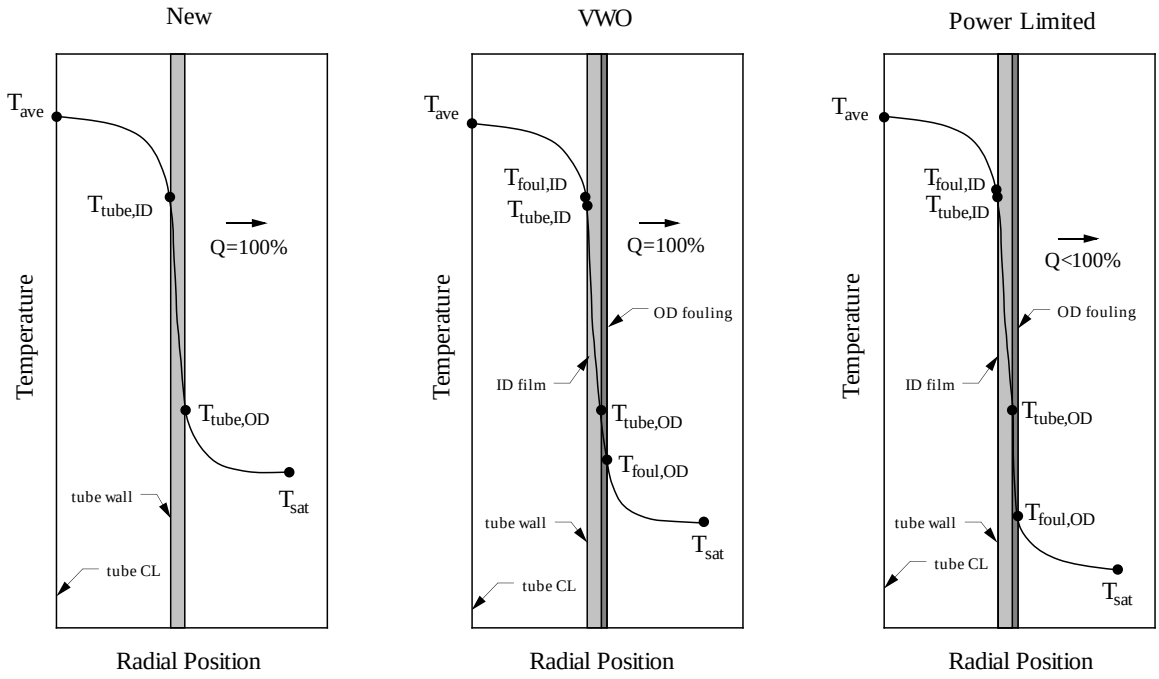

Figure 4-3
Change in Temperature Profile from Primary to Secondary Fluids Due to Fouling

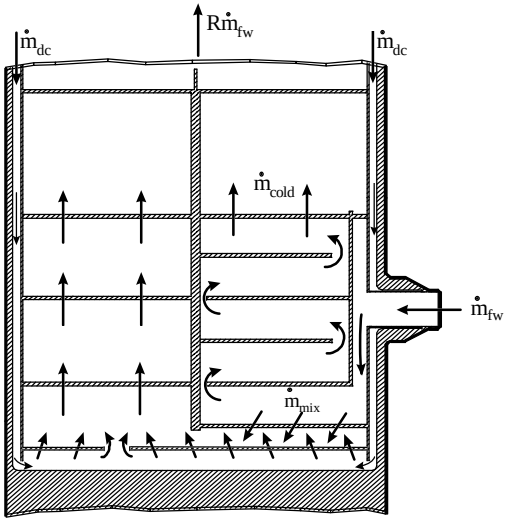

Figure 4-4
Schematic of Westinghouse Model E2 Steam Generator Preheater

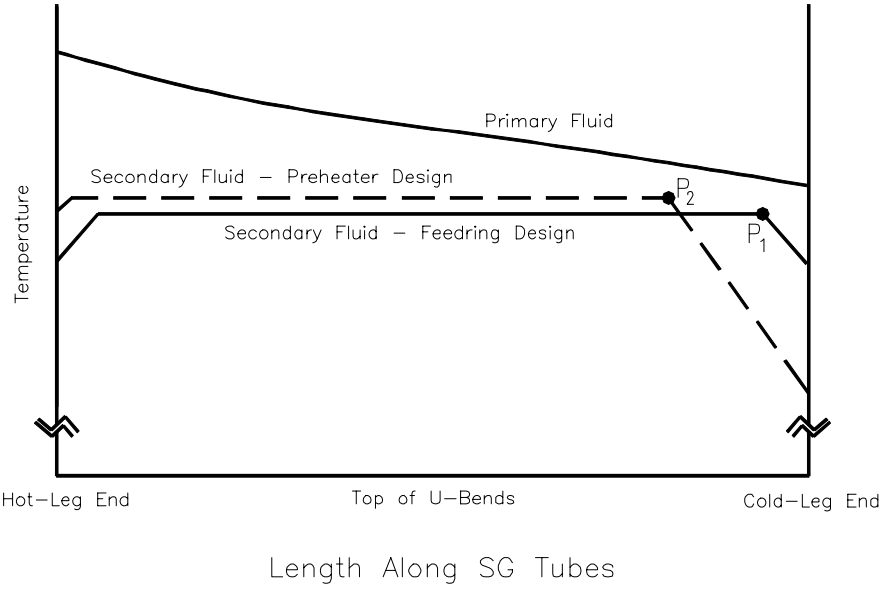

Figure 4-5
Fluid Temperature vs. Tube Position for Preheater and Feedring SGs

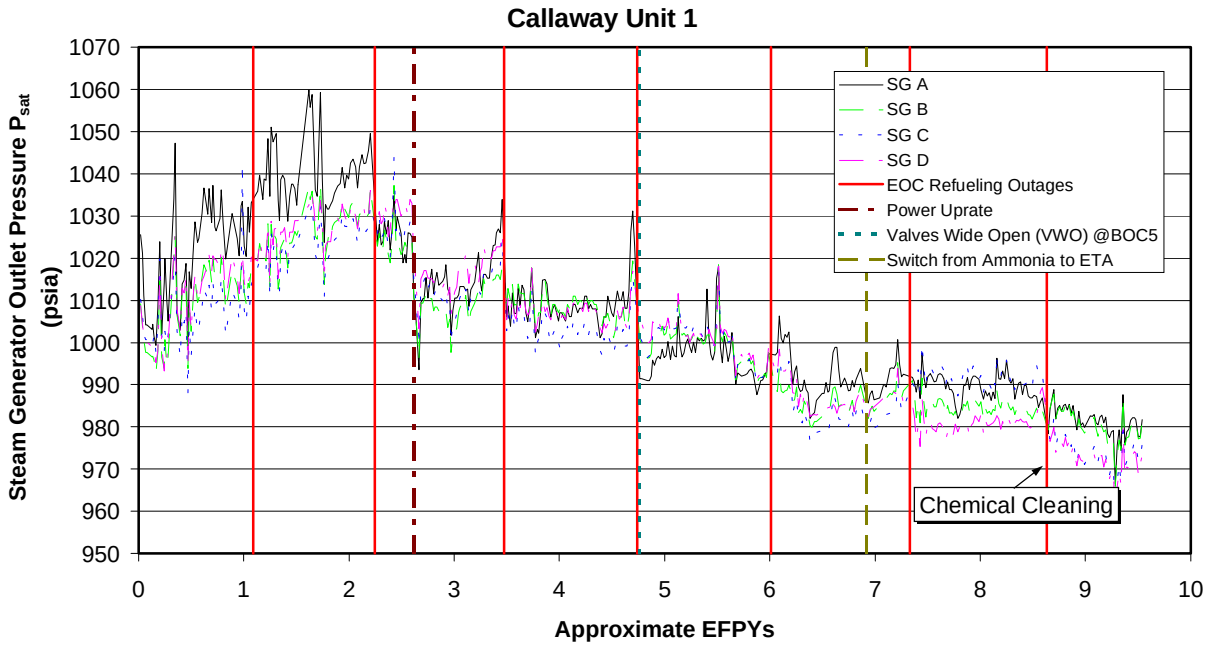

Figure 4-6
Historical Steam Generator Outlet Steam Pressure for Callaway

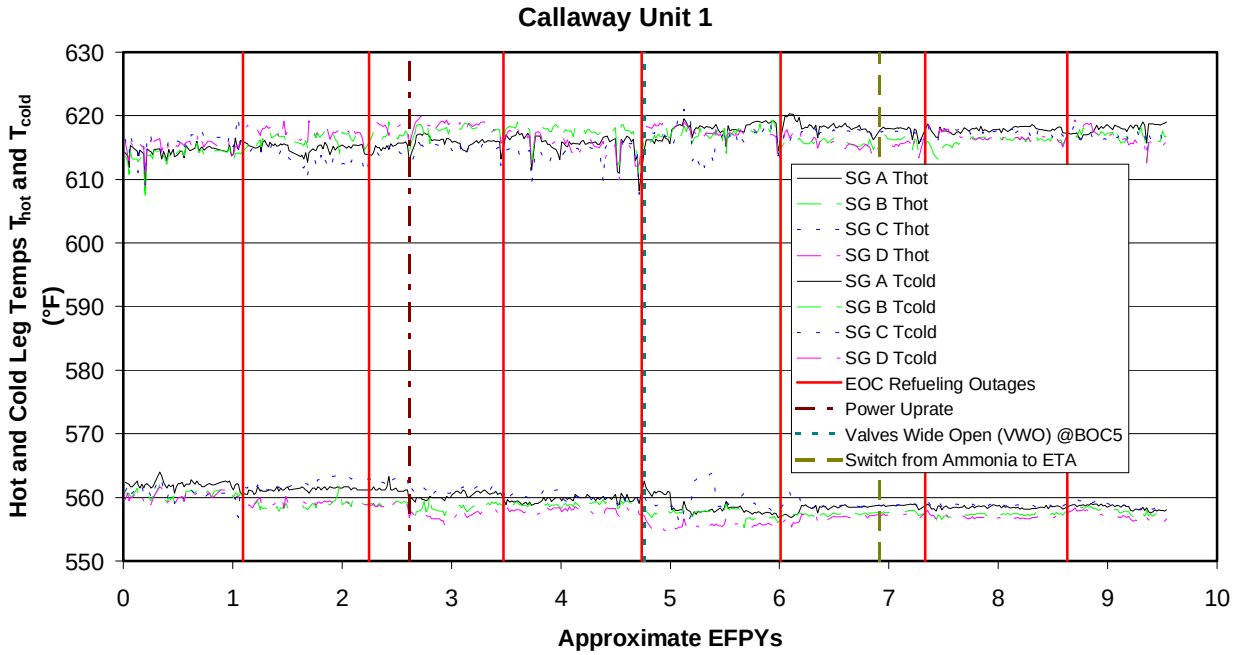

Figure 4-7a
Historical Hot and Cold Leg Temperatures at Callaway

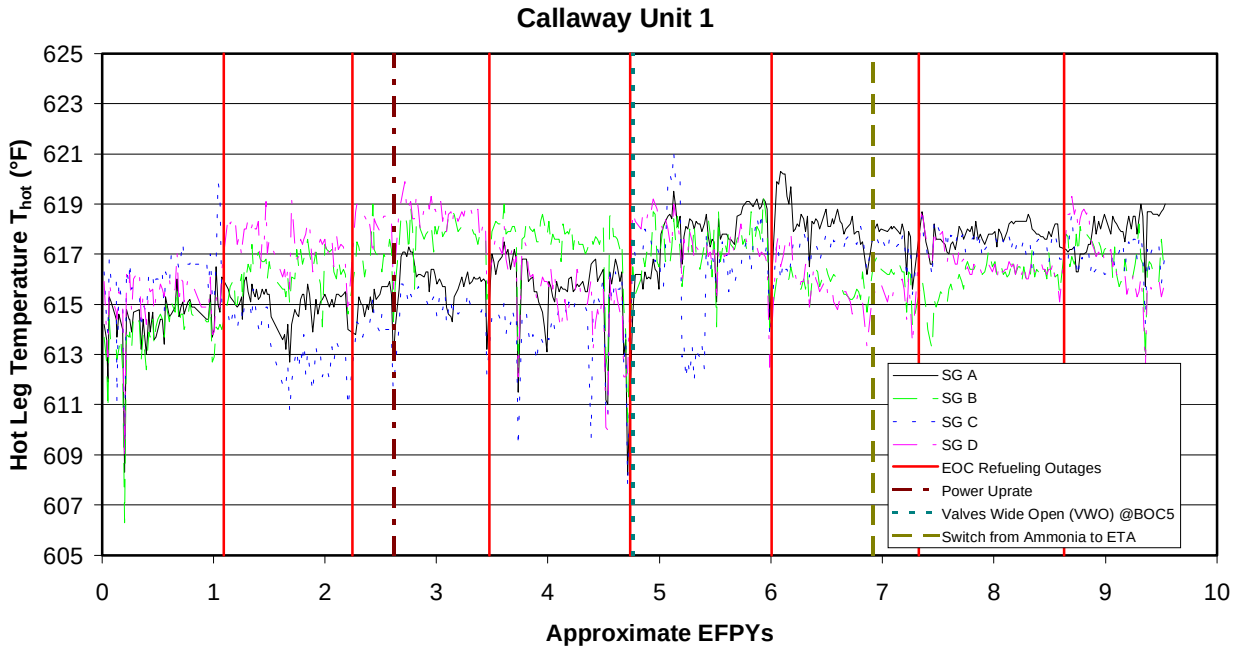

Figure 4-7b
Historical Hot Leg Temperature at Callaway

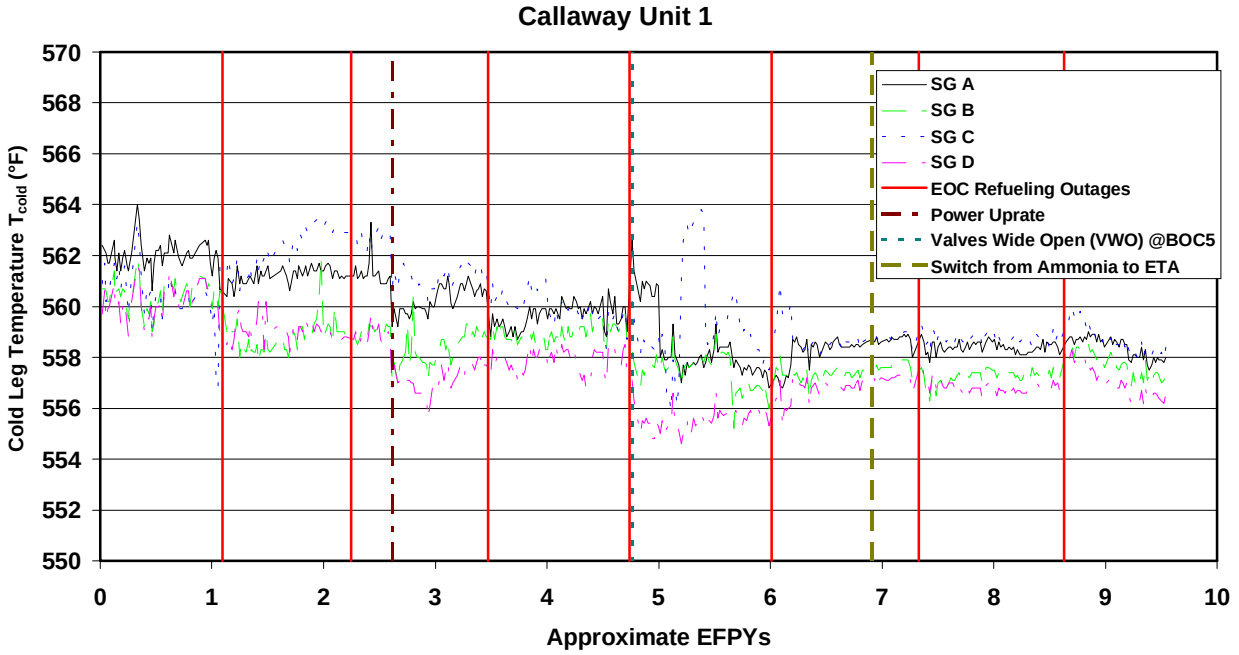

Figure 4-7c
Historical Cold Leg Temperature at Callaway

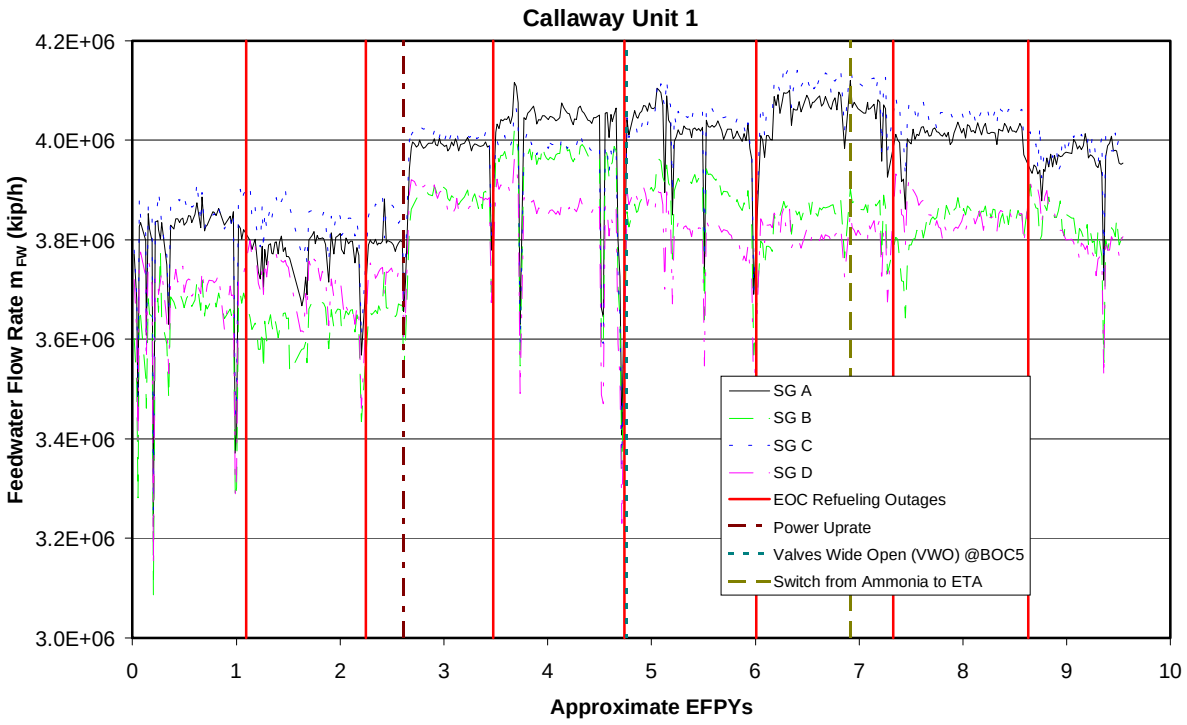

Figure 4-8a
Historical Feedwater Mass Flow Rate at Callaway

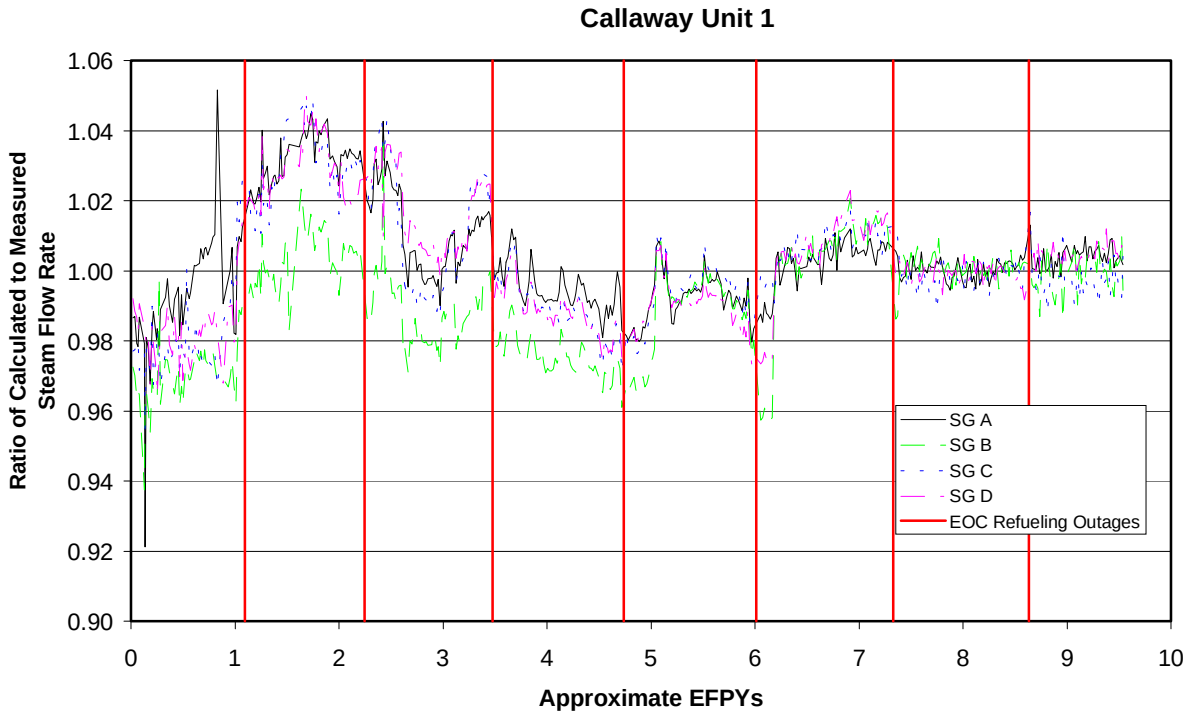

Figure 4-8b
Historical Ratio of Calculated to Measured Steam Flow Rate at Callaway

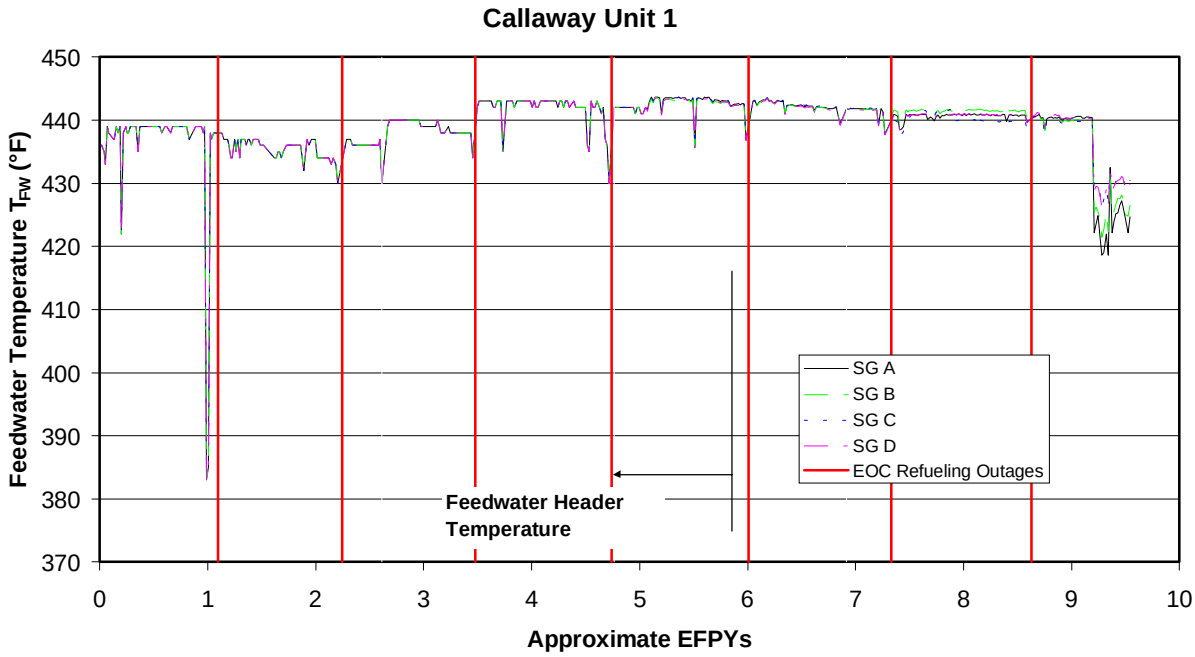

Figure 4-9
Historical Feedwater Temperature at Callaway

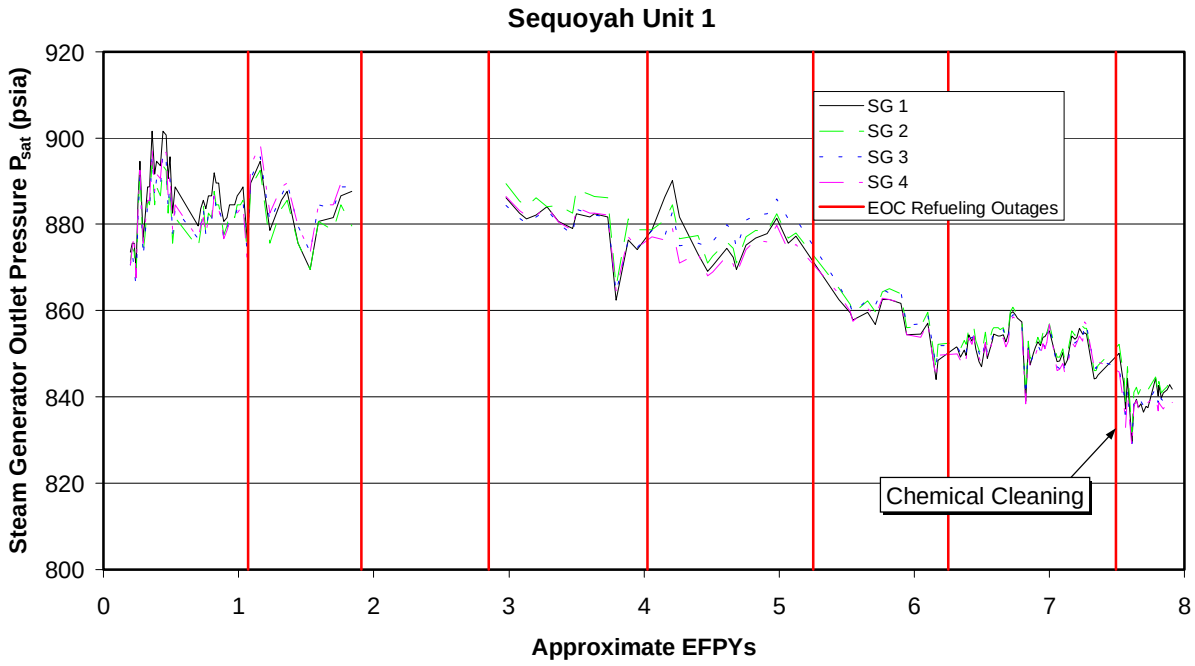

Figure 4-10
Historical Steam Generator Outlet Steam Pressure at Sequoyah 1

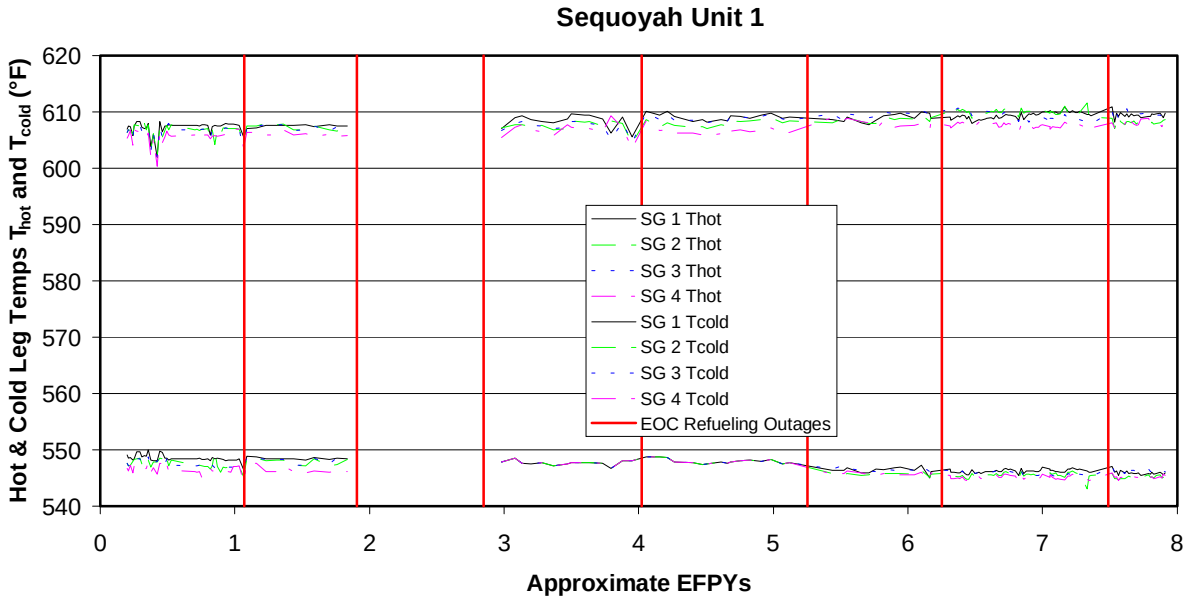

Figure 4-11a
Historical Hot and Cold Leg Temperatures at Sequoyah 1

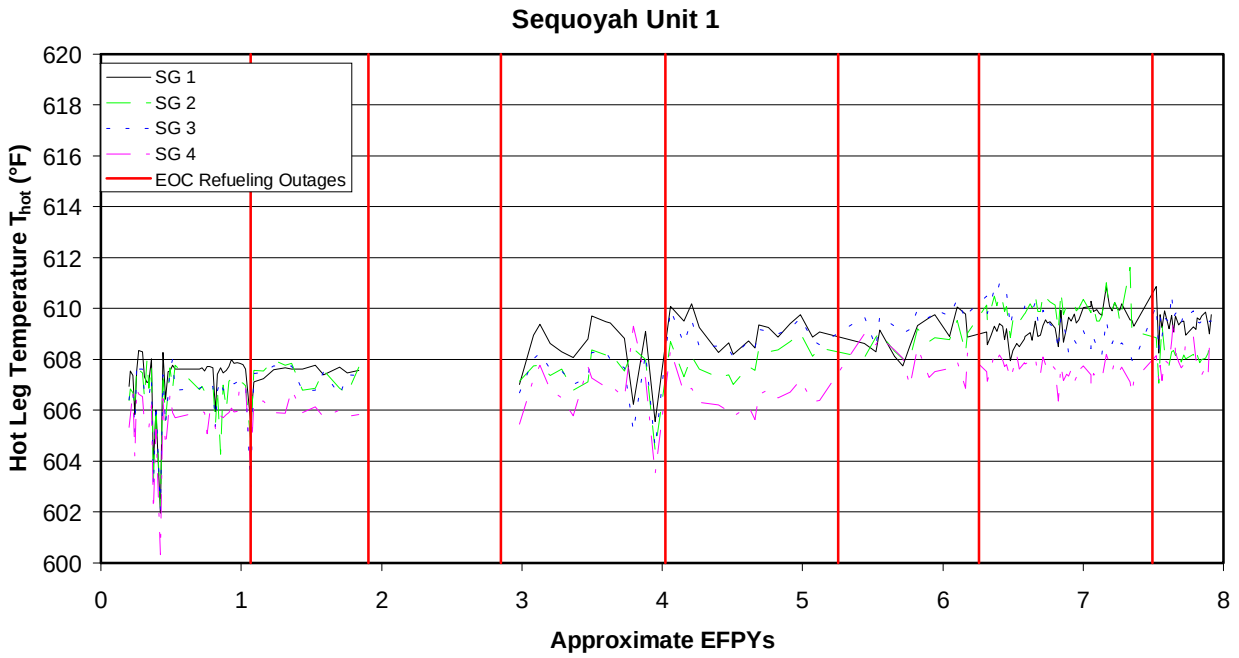

Figure 4-11b
Historical Hot Leg Temperature at Sequoyah 1 (As Measured)

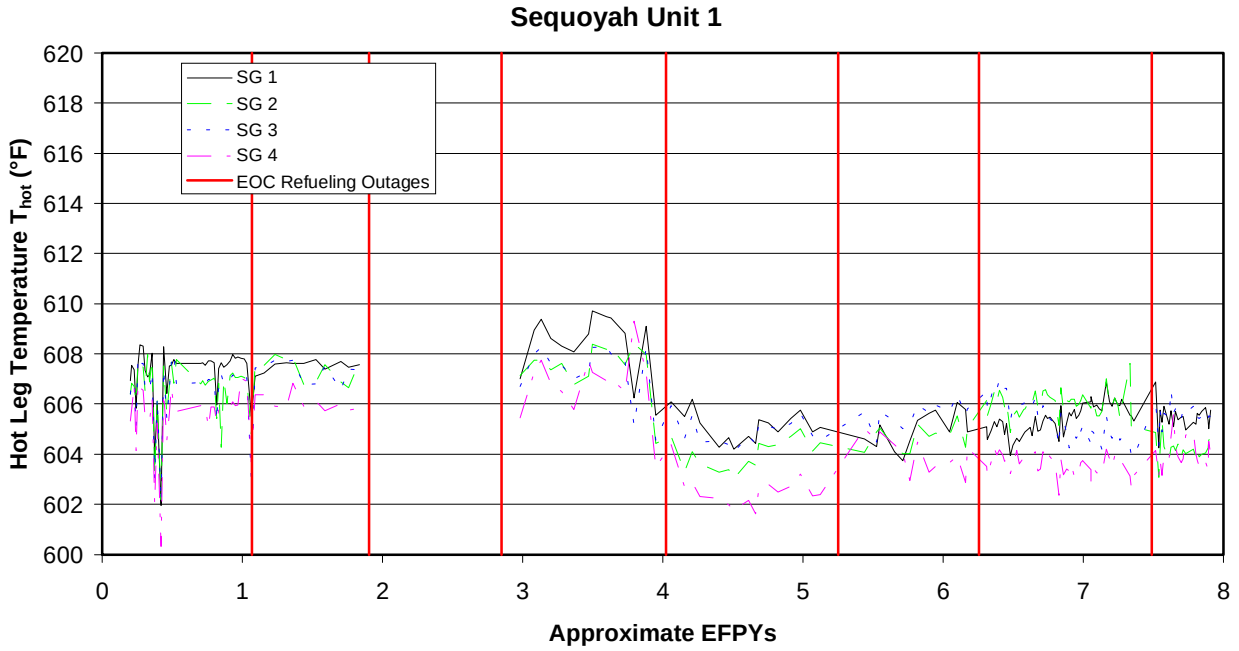

Figure 4-11c
Historical Hot Leg Temperature at Sequoyah 1 (Corrected for HL Streaming)

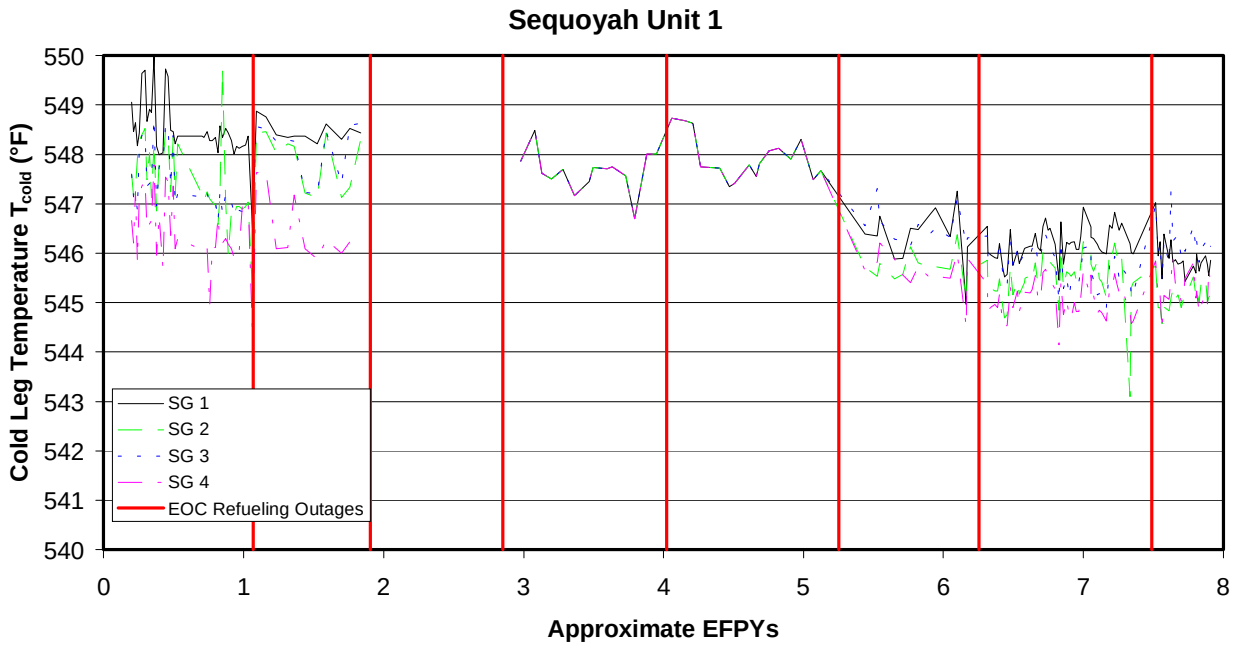

Figure 4-11d
Historical Cold Leg Temperature at Sequoyah 1

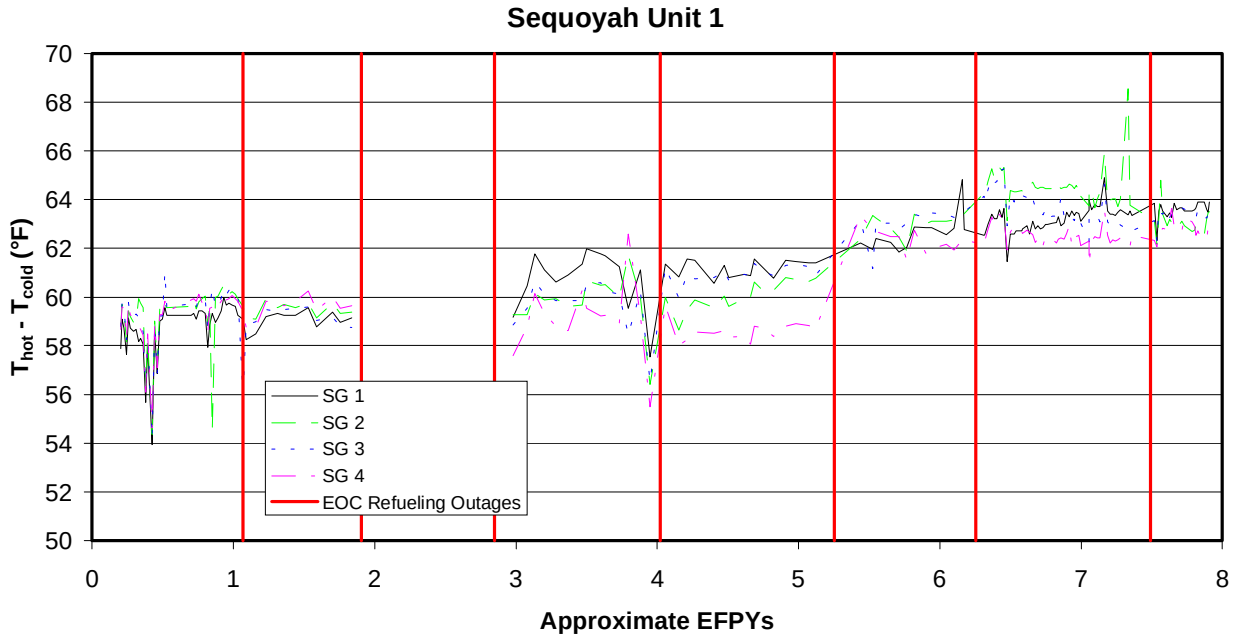

Figure 4-11e
Historical Primary Temperature Difference at Sequoyah 1

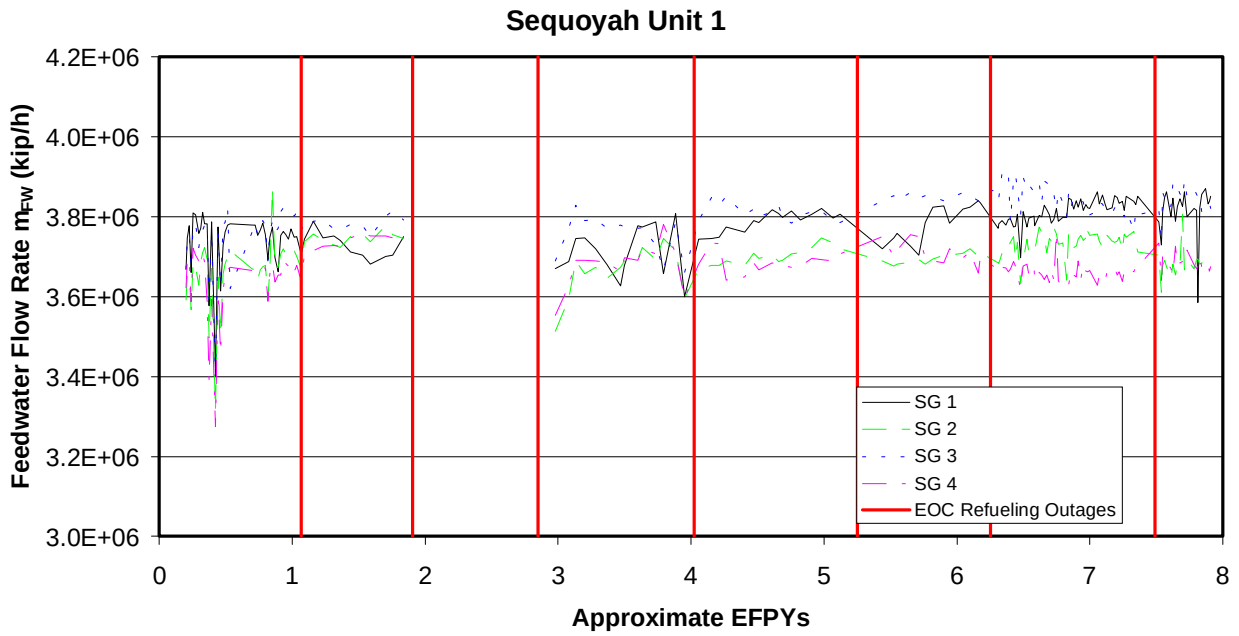

Figure 4-12a
Historical Feedwater Mass Flow Rate at Sequoyah 1

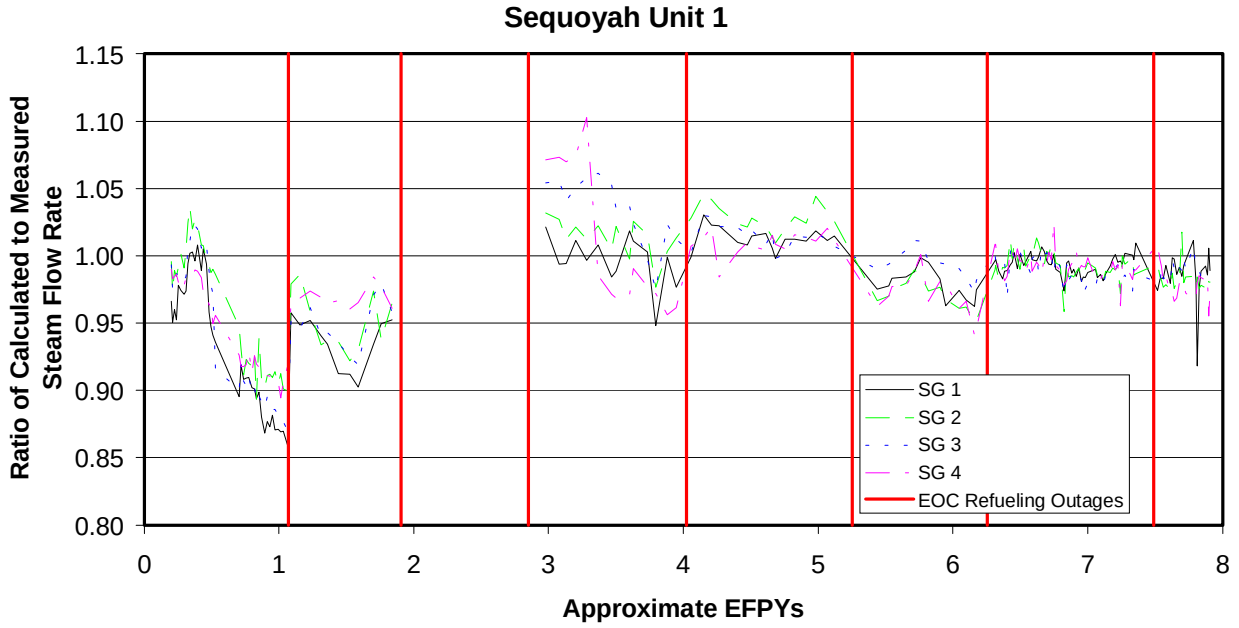

Figure 4-12b
Historical Ratio of Calculated to Measured Steam Flow Rate at Sequoyah 1

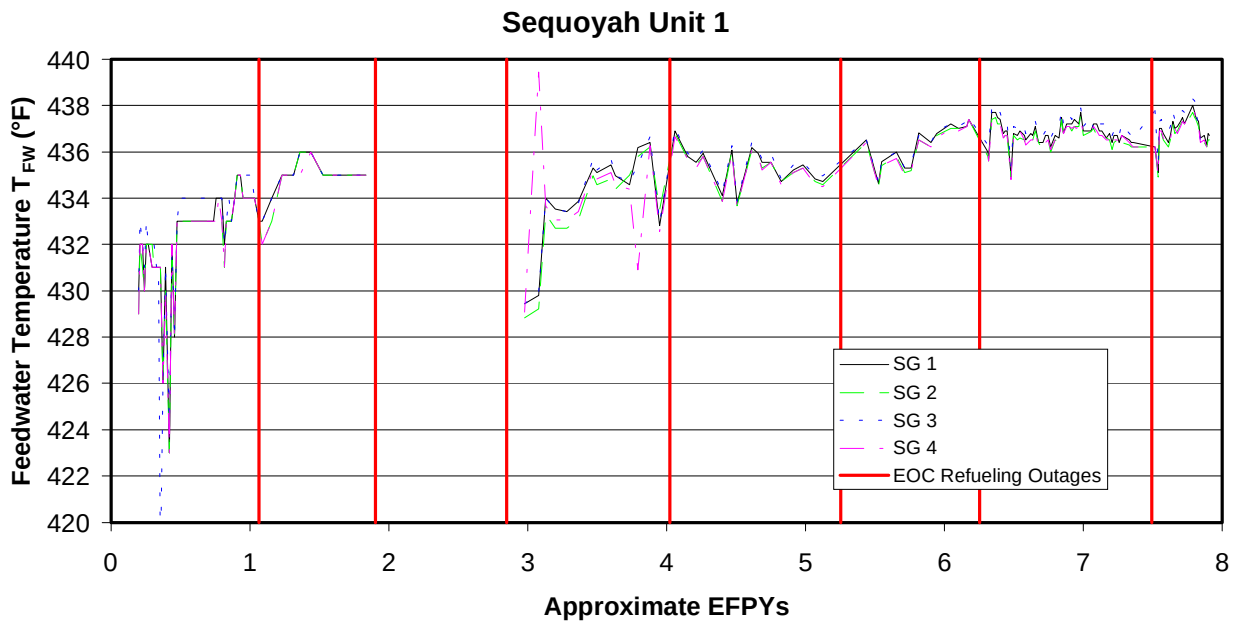

Figure 4-13
Historical Feedwater Temperature at Sequoyah 1

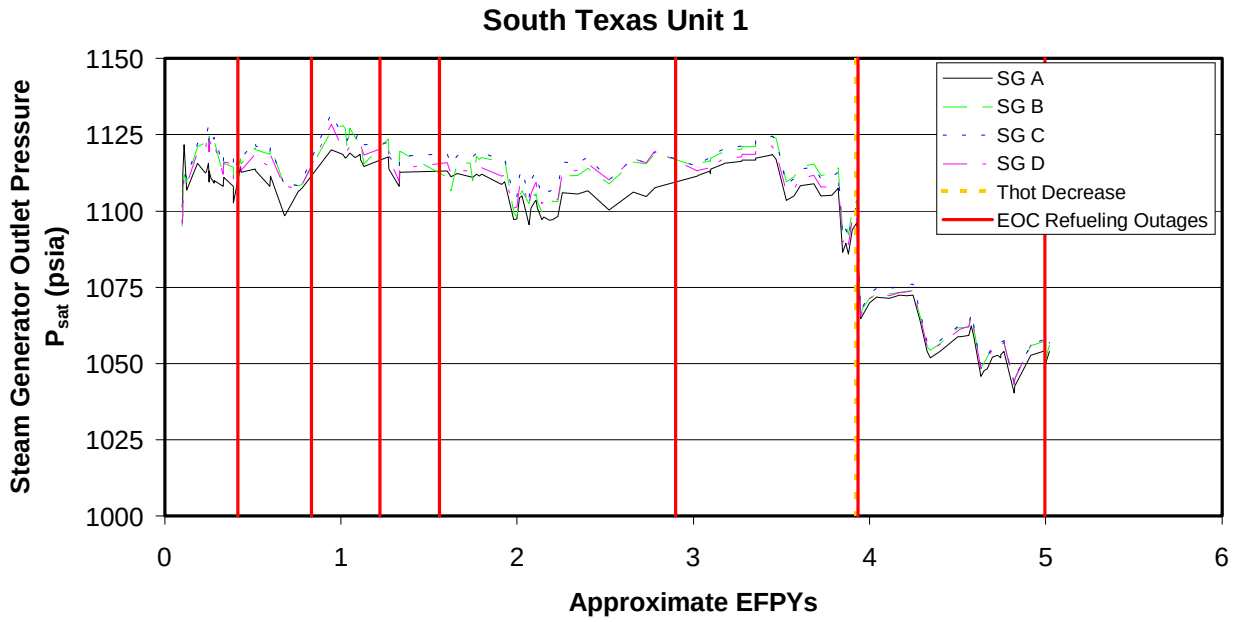

Figure 4-14
Historical Steam Generator Outlet Steam Pressure for South Texas 1

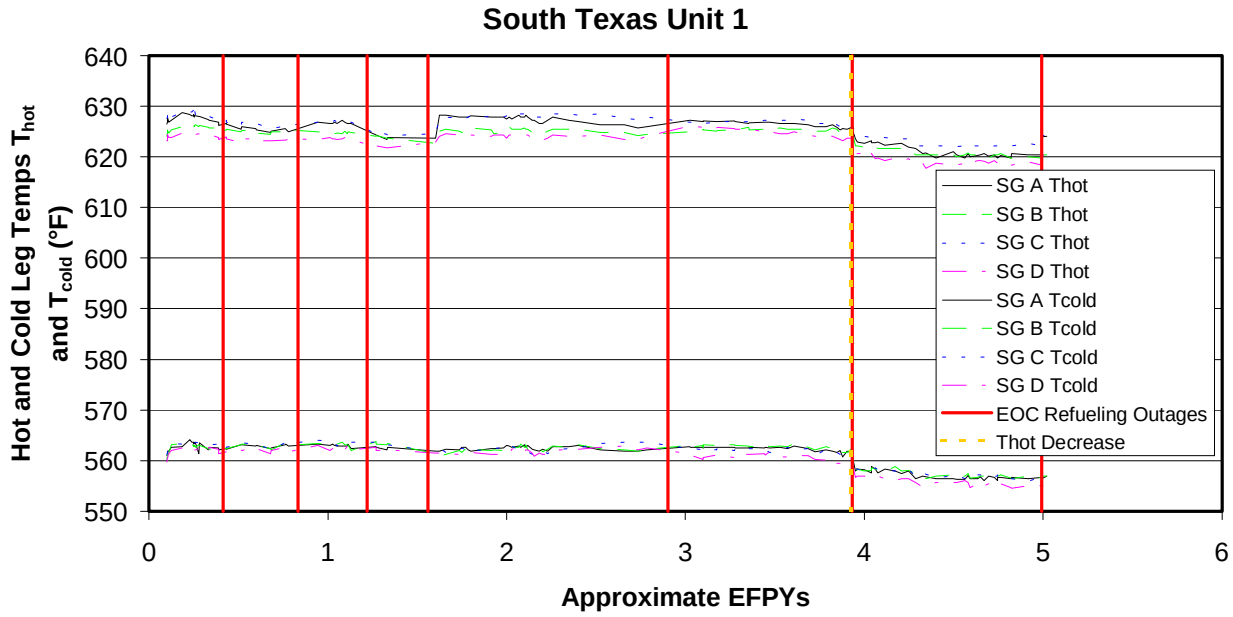

Figure 4-15a
Historical Hot and Cold Leg Temperatures at South Texas 1

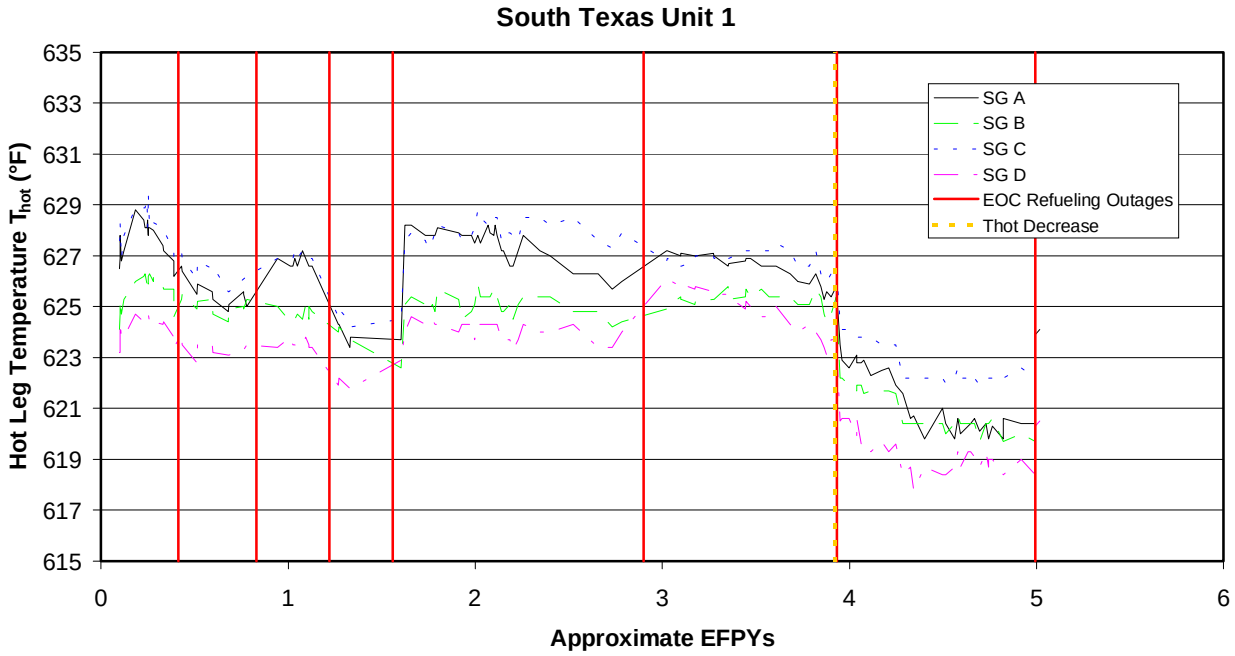

Figure 4-15b
Historical Hot Leg Temperature at South Texas 1

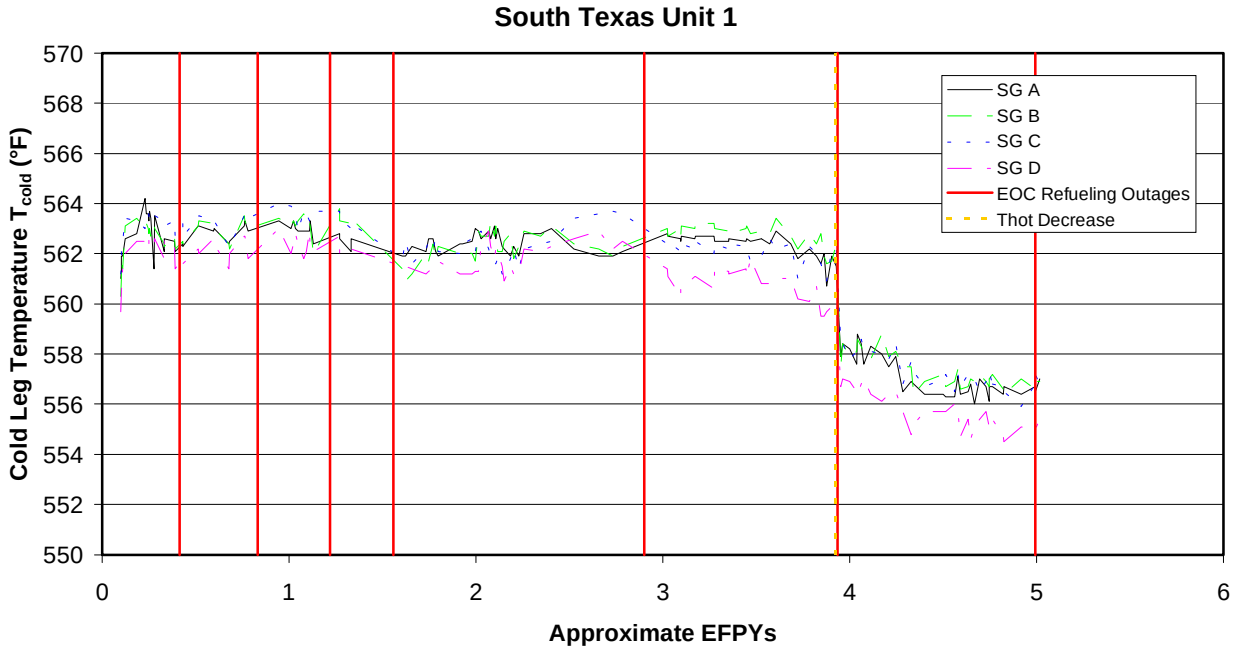

Figure 4-15c
Historical Cold Leg Temperature at South Texas 1

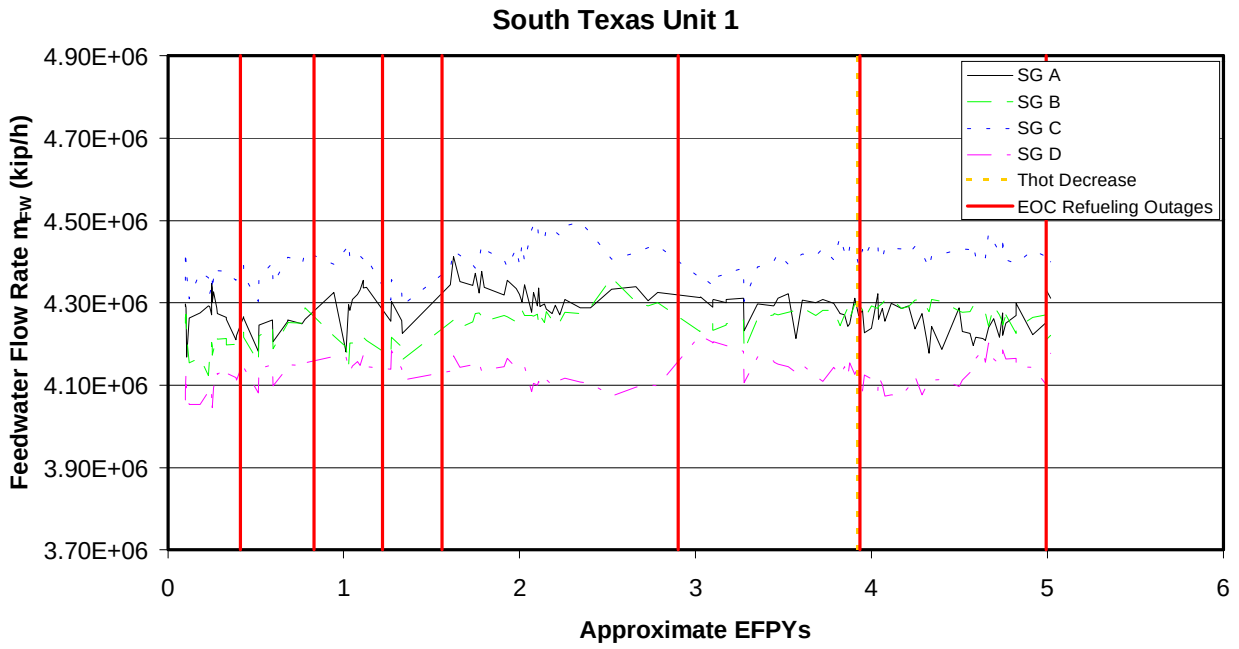

Figure 4-16a
Historical Feedwater Mass Flow Rate at South Texas 1

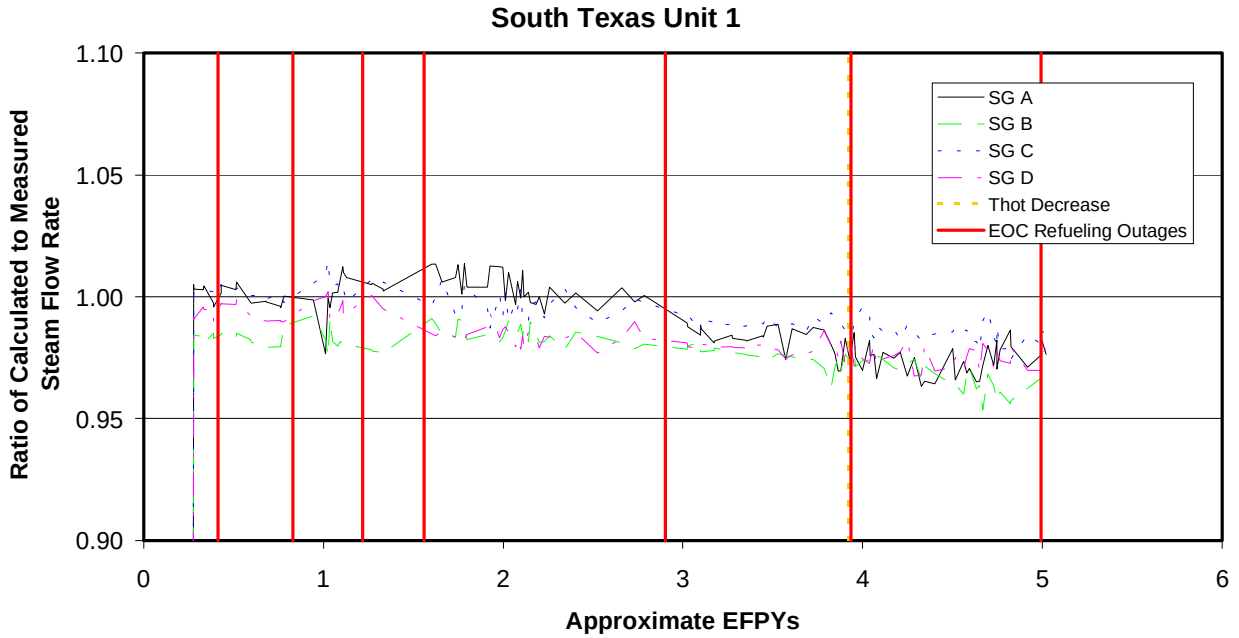

Figure 4-16b
Historical Ratio of Calculated to Measured Steam Flow Rate at South Texas 1

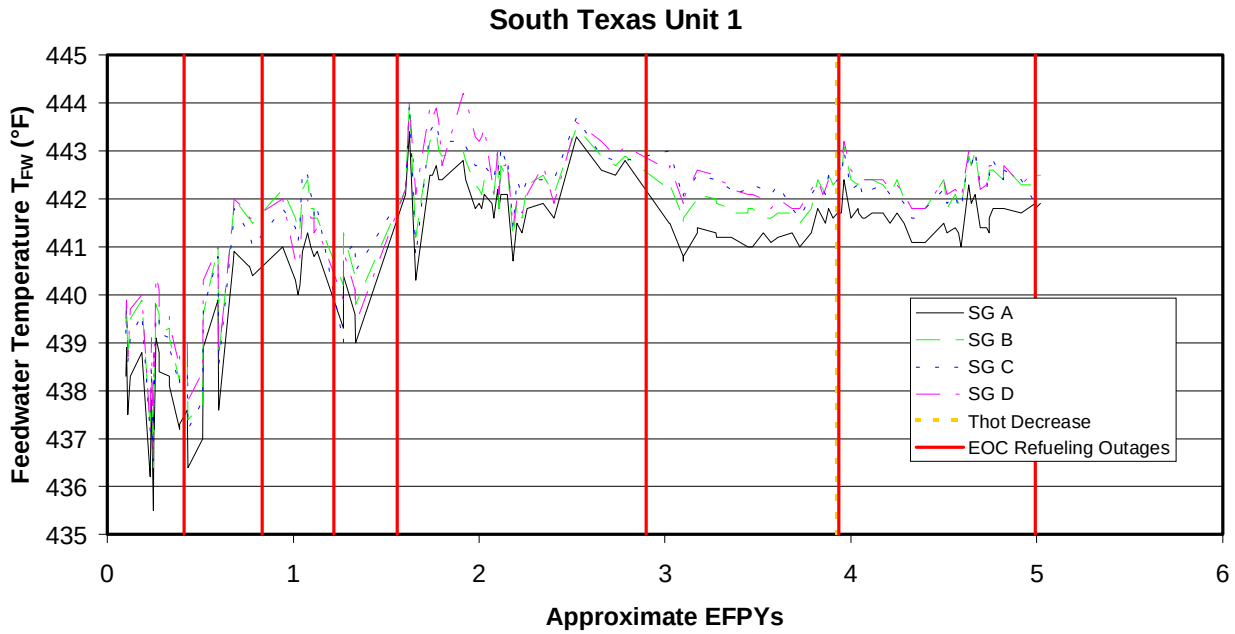

Figure 4-17
Historical Feedwater Temperatures at South Texas 1

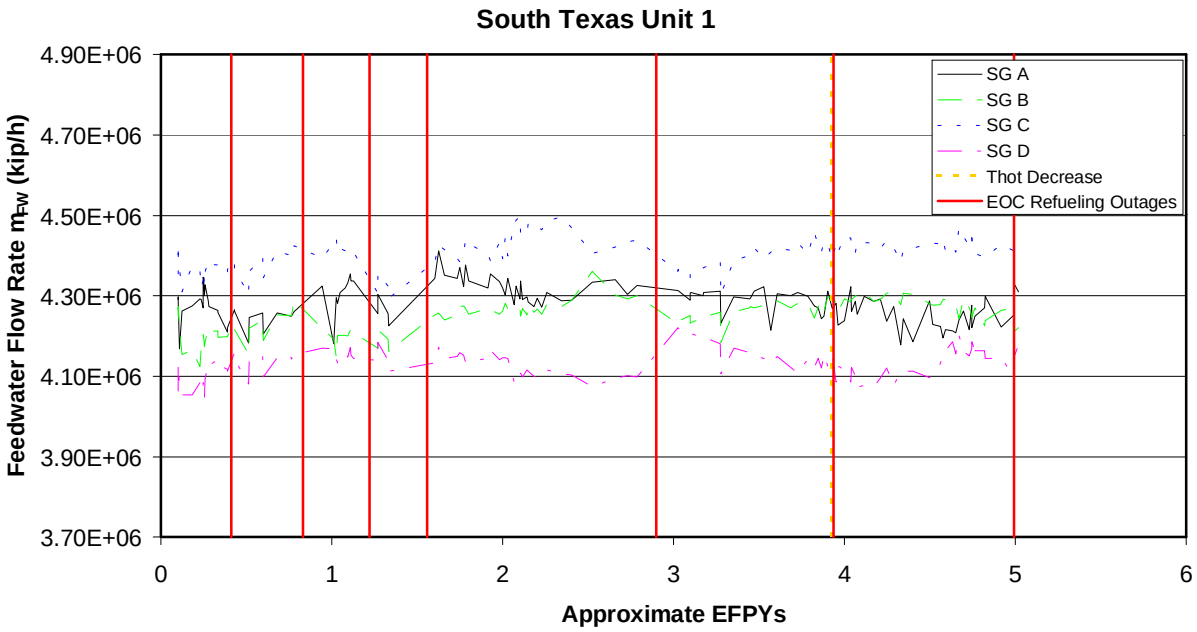

Figure 4-18a
Historical Fouling Factor for Callaway (Using FW Flow Measurements)

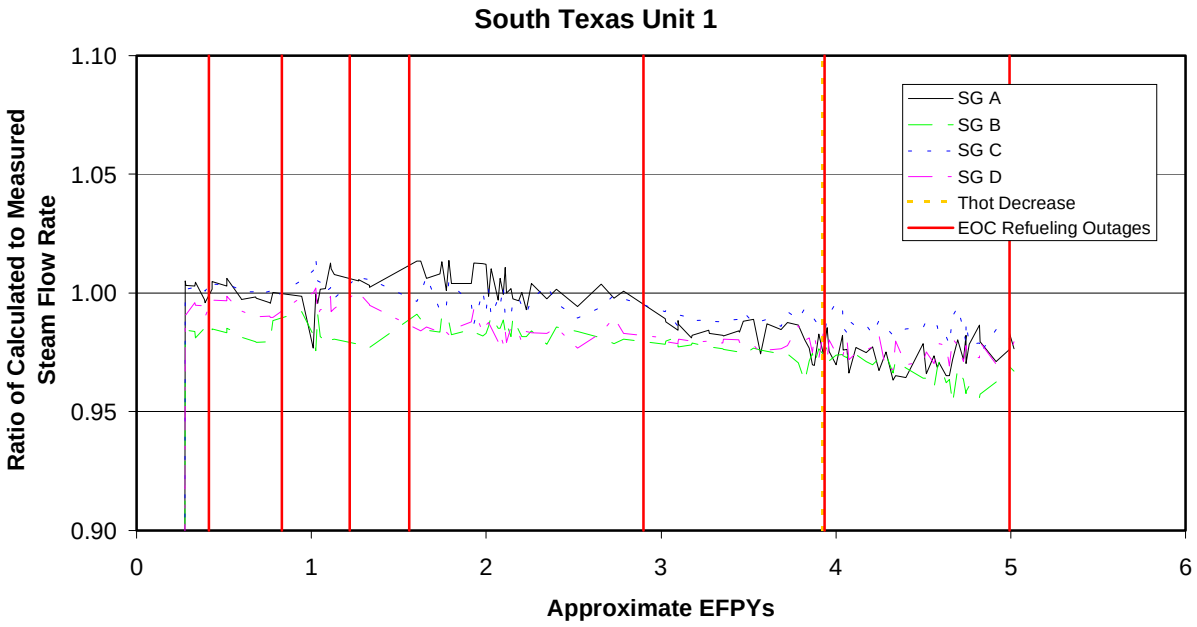

Figure 4-18b
Historical Fouling Factor for Callaway (Using Steam Flow Measurements)

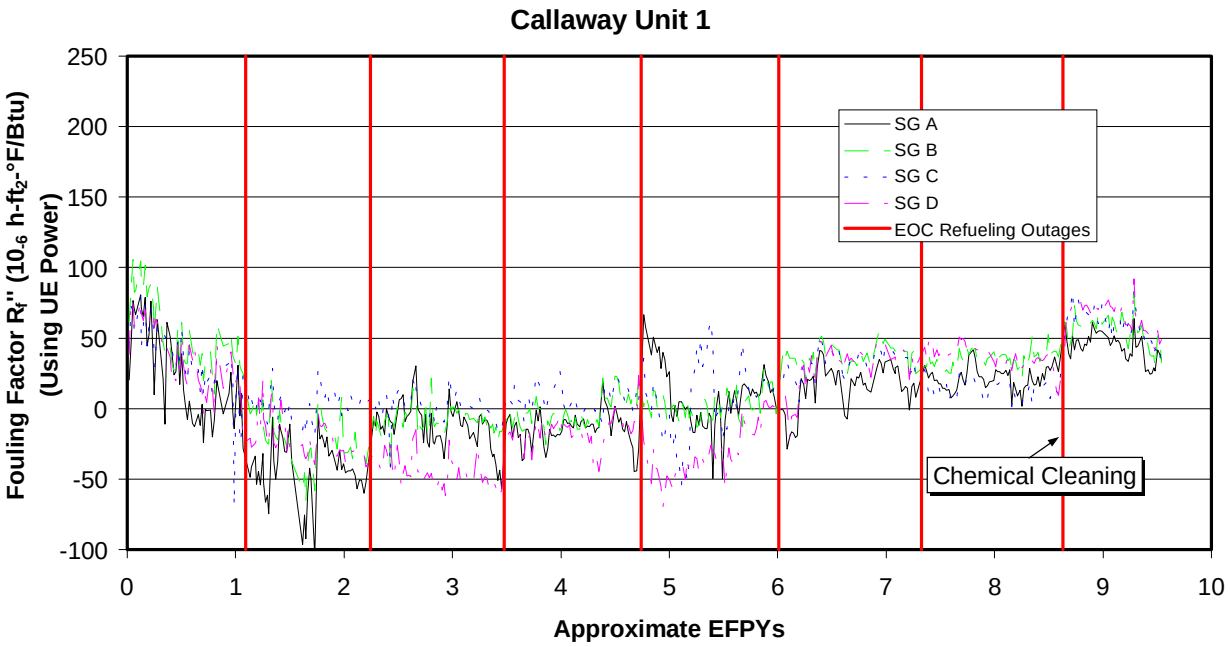

Figure 4-18c
Historical Fouling Factor for Callaway (Using UE-Supplied Power)

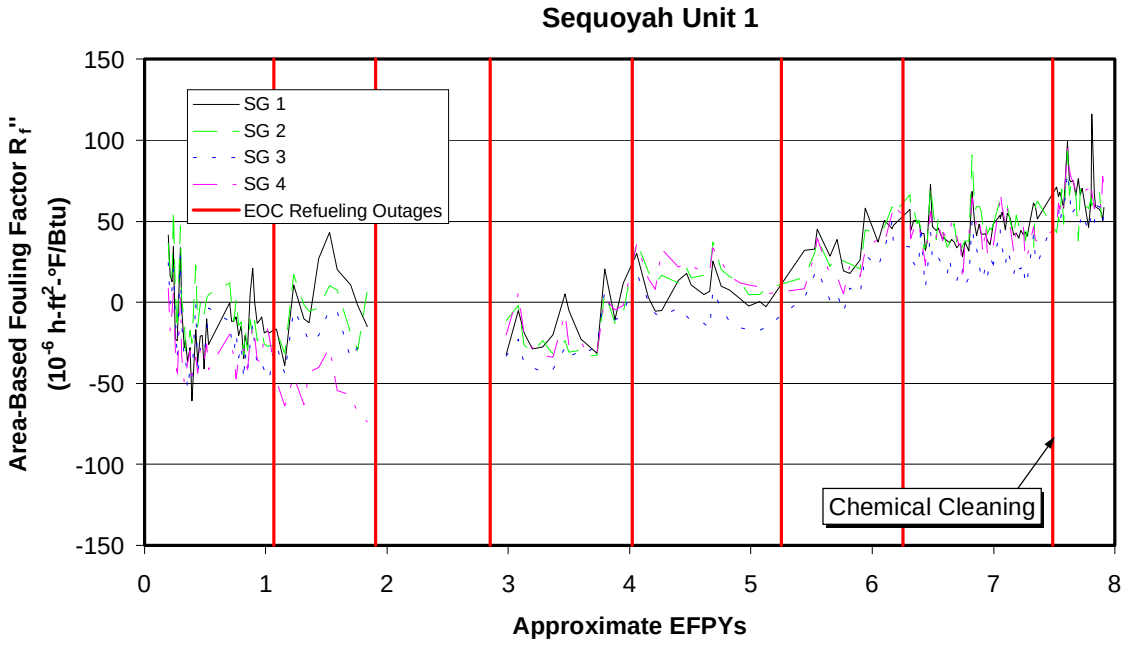

Figure 4-19a
Historical Fouling Factor for Sequoyah 1 (Using Feedwater Flow Measurements)

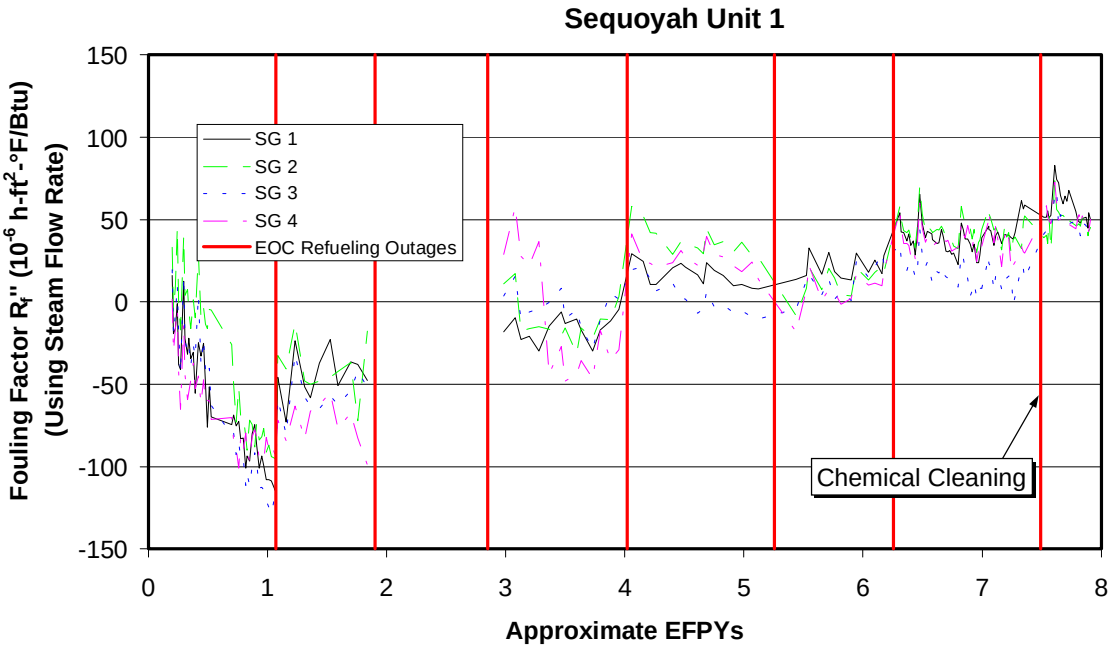

Figure 4-19b
Historical Fouling Factor for Sequoyah 1 (Using Steam Flow Measurements)

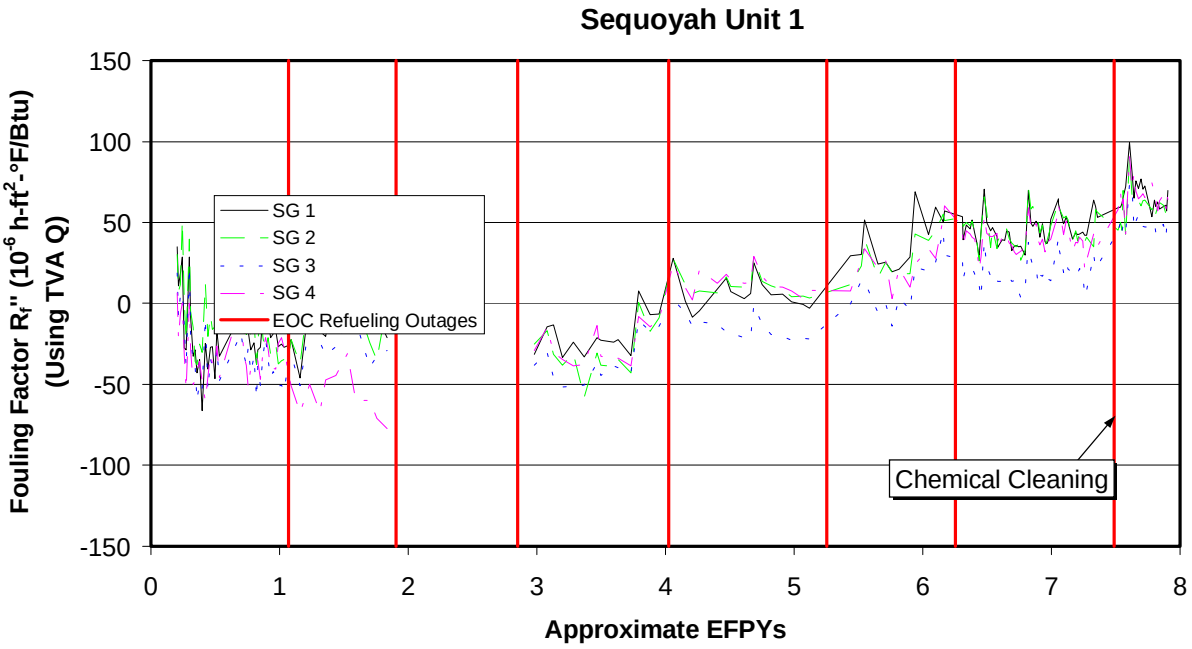

Figure 4-19c
Historical Fouling Factor for Sequoyah 1 (Using TVA-Supplied Thermal Power)

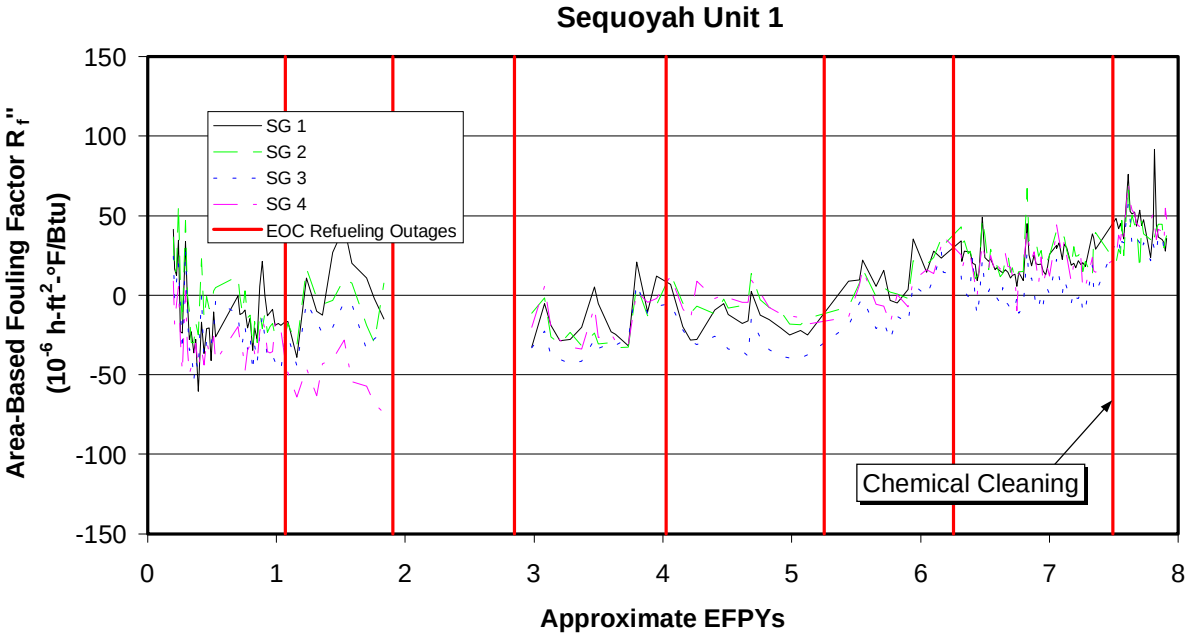

Figure 4-19d
Historical Fouling Factor for Sequoyah 1 (Using Feedwater Flow and Corrected T_{hot})

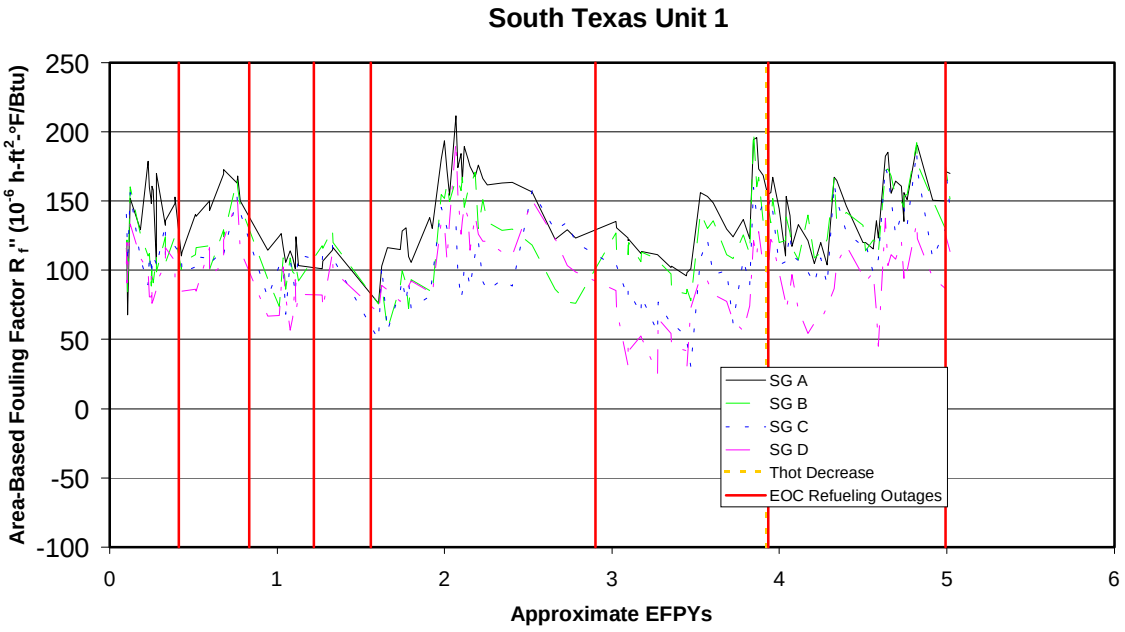

Figure 4-20a
Historical Fouling Factor for South Texas 1 (Using FW Flow Measurements)

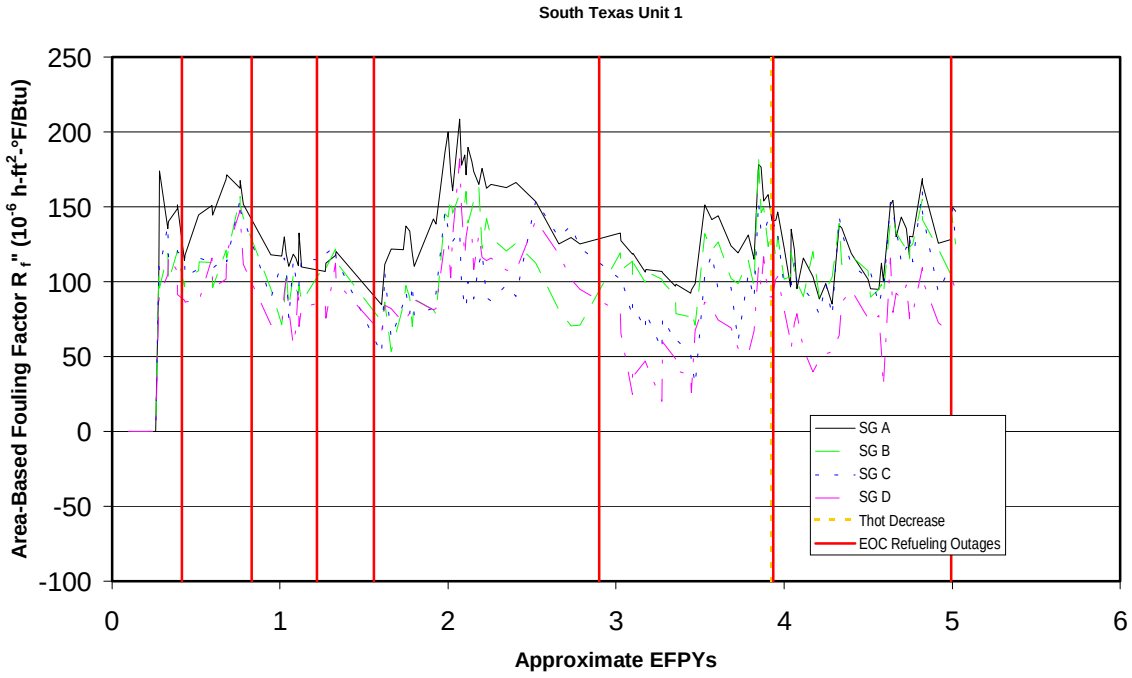

Figure 4-20b
Historical Fouling Factor for South Texas 1 (Using Steam Flow Measurements)

5

TUBE DEPOSIT THERMAL PROPERTIES

As is discussed in greater detail in Chapter 6, calculated global fouling factors can reflect increased resistance to heat transfer from a number of sources, including corrosion deposits on the ID and OD heat-transfer surfaces of the SG tubes. Before any calculated fouling factor can be attributed (either wholly or in part) to such deposit layers with high confidence, it is necessary to analyze the heat-transfer properties of the deposit layers.

In a PWR SG, the net heat flux between the primary coolant and the secondary-side fluid is directly dependent on the total "thermal resistance" to heat transfer in the system. Under clean design conditions, this total resistance includes boundary-layer resistances in both the primary and secondary fluids at the heat exchanger surfaces (i.e., the ID and OD surfaces of the SG tubes) plus the resistance of the tube wall, which depends on the thermal conductivity of the tube material and the wall thickness. After sufficient operating time, both the ID and the OD surfaces of the tubes can become covered with layers of corrosion products (i.e., become fouled). This process introduces two additional thermal resistances which depend on the thicknesses and effective thermal conductivities of the corrosion layers. If these resistances are large enough, they can have a significant effect on the overall heat-transfer performance of SGs. This chapter explores the potential impact of both primary-side and secondary-side corrosion layers on the SGs at Callaway, Sequoyah 1, and South Texas 1.

Expected Influence of Primary-Side Deposits Based on Industry Data

Because the secondary-side fluid in SGs boils, relatively concentrated solutions are possible, which can accelerate and exacerbate corrosion. Hence, much effort has been spent examining secondary corrosion (e.g., numerous detailed tube-pull examinations have been documented in other EPRI reports). On the other hand, the primary fluid remains subcooled, meaning that the concentrations of potentially corrosive species remain at the low levels of the original primary coolant. As a consequence, much less work has been focused on potential primary-side (i.e., ID) corrosion films. Nevertheless, until the physical characteristics of the primary-side film are investigated, the potential contribution of an ID corrosion layer to an observed degradation in SG heat transfer capability cannot be ruled out.

In order to evaluate the heat-transfer role of primary films, the following characteristics must be considered:

- composition
- effective thermal conductivity (reflects both composition and morphology)
- deposit thickness

These properties have an impact on the potential for a particular corrosion layer to cause significant heat-transfer degradation. Based on a survey of EPRI tube pull reports, it seems that none of these variables has been measured consistently or frequently on actual pulled SG tubes in the US.* Pulled tubes have been examined most often on the secondary side where thicker deposit layers have been observed.

Composition

Like the secondary side, where corrosion layers are most often composed predominantly of iron oxides, primary-side layers are thought to contain primarily metal oxides. This conclusion is supported by tube examinations performed on SG tubes from several Electricité de France (EdF) plants (i.e., Dampierre, Gravelines, and Tricastin). These are plants which had been in operation for approximately 8–10 years at the time of the tube pulls. For over 40 tubes, the primary film constituents were the following, with average weight percents indicated (21):

Cr_2O_3	47%
Fe_3O_4	29%
NiO	23%

A literature survey of tube-pull reports for US plants did not reveal any similar detailed analyses of the ID surface film. A few tube exams have included reports of the ID layer components by element (References (22) through (26)). In addition to the main constituents of Alloy 600 and 690 (the typical tube materials), the following other elements were found in measurable quantities (not all were found in each test): Si, Ti, Al, Ca, P, S, O, Mn, Na, Cl, Zn, Zr.

No plant-specific information on the ID corrosion layers at Callaway, Sequoyah 1, and South Texas 1 was available. However, the ages of these plants at the time of the fouling factor calculations (9.5, 7.9, and 5.0 EFPY, respectively) are comparable to the

* As discussed later, some data have been taken on tubes pulled from overseas plants.

ages of the plants examined by EdF. In addition, primary-side water chemistry generally does not experience the plant-to-plant variation that is typical of secondary-side environments. As a result, it is assumed for the purposes of this study that the primary film composition at Callaway, Sequoyah 1, and South Texas 1 is characterized primarily by the three oxides reported in Reference (21).

Morphology

Based on discussions with three independent researchers (see Appendix E), the following is noted regarding the structure of primary-side corrosion layers:

- The thickness is very uniform.
- Intergranular attack (IGA) penetrated the tube surface beneath the corrosion layer. The voids created by the IGA are believed to be oxide filled (as opposed to steam filled).
- No spalling of these films has been observed.

As with composition, these features are presumed to be representative of the primary-side layers present at Callaway, Sequoyah 1, and South Texas 1.

Effective Thermal Conductivity

In order to ascertain the effect of primary-side layers on heat transfer, the effective thermal conductivity of the layer must be determined, either by measurement or by calculation. No heat-transfer measurements for corrosion layers typical of PWR SG primary tubing are known to be available. It is believed that few if any experiments have been performed for this purpose due to the fact that secondary-side corrosion layers tend to be thicker than their primary-side counterparts and hence receive most of the attention. Consequently, calculation and/or estimation of the effective thermal conductivity must be performed.*

As a first step, thermal conductivity values for some solid metal oxides were compiled. This list is presented in Table 5-1. As noted earlier, the bulk of primary films most likely comprise Cr_2O_3, Fe_3O_4, and NiO. However, a number of other oxides are included in the table to indicate a wide range of thermal conductivity values. All SI values are taken from Reference (27),† except for hematite (Fe_2O_3) and magnetite (Fe_3O_4),

---

* However, note that primary-side deposits are a major concern for SGs in PHWR plants (e.g., CANDU design) because of their use of carbon steel piping. Deposits in these SGs have been subjected to heat-transfer measurements.

† In some cases, averages of the values presented in Reference (27) are reported in Table 5-1.

which are curve-fit values for 573 K taken from Reference (28). Conversion to English units is made based on standard conversion factors. The compounds are listed in order of increasing thermal conductivity. When possible, values were selected for temperatures close to typical primary-side SG temperatures (i.e., near 600°F). Comments regarding the characteristics of the samples used in the measurements are provided in the right-most column (e.g., some samples were single crystals while others consisted of pressed powder). Note that the data in the table span the range from 0.2 to 53 BTU/hr-ft-°F.* In addition to magnetite and hematite (with thermal conductivities of 2.0 and 2.8 at 572°F), potentially relevant compounds include SiO_2 (1.0 at 578°F) and NiO (3.1–5.7 depending on temperature and porosity). Except for beryllium oxide, thermal conductivity values fall for the most part between 1.0 and 10, including the iron oxide, nickel oxide, and silica values. Based on this range and also the values for relevant compounds (i.e., Cr_2O_3, Fe_3O_4, NiO), the constituents of typical primary-side films (including those at Callaway, Sequoyah 1, and South Texas 1) are assumed to have thermal conductivity values somewhere between 1.0 and 10.

The second step in computing effective thermal conductivity is accounting for possible porosity in the primary-side surface layer. If we assume a certain percentage of the film comprises pores that are filled with stagnant water, we can then compute the effective thermal conductivity from an equation developed by Bruggeman (29) for two-phase dispersions of one material within a matrix of another material:

$$\left(\frac{k_{eff} - k_d}{k_c - k_d}\right)\left(\frac{k_c}{k_{eff}}\right)^{1/3} = 1 - v_d \qquad \text{(eq. 5-1)}$$

In Eq. [5-1], k_c is the thermal conductivity of the matrix (in this case, the oxide components), k_d is the thermal conductivity of the dispersed material (in this case, water), and v_d is the volume fraction of the dispersed material. The results of best-estimate and bounding calculations for k_{eff} are shown in the bottom portion of Table 5-2.

Film Thickness

Because most of the attention on heat transfer loss has been focused on the secondary-side deposits, relatively few detailed examinations of primary-side oxide thickness have been recorded. However, several researchers have documented this thickness. Per Reference (21) and Appendix E, three independent researchers who have examined numerous SG tubes all indicate that the primary-side oxide thickness after substantial operating times (i.e., approximately 5–10 EFPY) averages nearly 1 micron (0.04 mils), with possible maximum values near 5 microns (0.2 mils). The average thickness did

* All subsequent references to thermal conductivity values are in BTU/hr-ft-°F unless otherwise indicated.

not vary significantly among the plants involved (Doel 3 and 4 in Belgium; Dampierre, Gravelines, and Tricastin in France; and Ringhals 3 and 4 in Sweden). Nor was there substantial variation based on tube manufacturer: oxide thicknesses for Vallourec/Inphy tubing, Westinghouse/Huntington tubing, and Vallourec/Huntington tubing all averaged between 1 and 1.5 microns. None of this data conclusively proves that primary-side oxides in the Callaway, Sequoyah 1, and South Texas 1 SGs are the same thickness. It is possible, for example, that variations in primary-side chemistry could result in thicker films. However, since there is no boiling on the primary side, minor differences in water chemistry will have a much smaller potential impact on the primary side than on the secondary side. It is judged unlikely that the Callaway, Sequoyah 1, and South Texas 1 films (which are all the product of less than 10 EFPY) are thicker than the thickest samples described in Reference (21). Thus, 5 microns, or 0.2 mils, is taken as a reasonable upper bound for the primary oxide thickness, 1 micron is taken as the best-estimate thickness, and 0.5 microns is taken as the lower-bound thickness.

Based on the best-estimate and bounding values for thickness and effective thermal conductivity developed above, the associated best-estimate and bounding fouling factors attributable to primary deposits are calculated and reported in Table 5-2. For all plants, the best estimate value is 2 10^{-6} h-ft^2-°F/BTU and the conservative upper bound is about 30 10^{-6}.

Expected Influence of Callaway, Sequoyah 1, and South Texas 1 Secondary-Side Deposits

The characterization data available for the secondary deposits at Callaway, Sequoyah 1, and South Texas 1 can be used to estimate the impact these deposits have had on steam generator performance. This evaluation is independent of the global fouling factor calculations and is highly plant-specific due to the wide range of known secondary deposit characteristics. Available information for each plant is briefly discussed below.

Callaway

The following have been measured or estimated regarding the secondary tube scale at Callaway prior to the chemical cleaning in 1995:

- Composed almost entirely of magnetite.
- Average layer thickness of approximately 4 mils based on the amount of material removed from the SGs during chemical cleaning and on Callaway's feedwater iron concentration history. Scale samples from the Callaway SGs prior to the cleaning were measured to be between 0.9 and 6 mils.

- Total porosity of about 35%.
- Thin (0.1 mil) non-porous inner layer of 3% copper metal and 97% magnetite adjacent to the tube OD surface.
- Specific surface area of 0.68 m^2/g.
- Skeletal density of 5.38 g/cm^3.

Sequoyah 1

Based on research conducted on Sequoyah tube deposits in 1990–91 (31) and also on information provided by TVA, a number of key properties are available for characterizing Sequoyah tube flake samples. These can be summarized as follows:

- The composition of 1990 samples was approximately 70% magnetite (Fe_3O_4) and 30% copper, with small amounts of nickel. Samples tested in 1992 were approximately 80% magnetite and 10% copper.
- The bulk density as of 1990 (i.e., including porosity) was 2.44 g/cm^3, and the skeletal density (i.e., excluding porosity) was 5.41 g/cm^3. The values indicate an apparent porosity of 55%.
- The specific surface area, also as of 1990, was 1.24 m^2/g.
- 94% of the 1990 sample weight comprised particles of 150 microns (μm) or bigger. The predominant particle size was 20–40 μm.
- The average pore diameter was as of 1990 was 0.45 μm (including a maximum of 4 μm and a minimum of 0.04 μm).
- Based on direct sample measurements and the feedwater iron concentration history, the average scale thickness as of 1990 was approximately 2.5 mils.
- Based on the chemical cleaning mass removal in 1995 and on feedwater iron transport data, the average scale thickness just prior to the chemical cleaning was between 5 and 6 mils.

South Texas 1

Limited information on tube OD deposits at South Texas 1 was provided by HL&P for tubes pulled from the lower hot-leg side of two out of the four SGs in 1993. Measurements made by examining 630X micrographs of metallographic mounts indicate that the average deposit thickness for the four tubes was about 0.3 mils, with a

maximum of 1.1 mils. X-ray diffraction (XRD) analyses of the deposits revealed that in the free span region, the tube scale was composed primarily of Fe_3O_4, with minor amounts of NiO.

SONGS 2

Shown in Figure 5-1 is a schematic of the cross section of a typical tube scale flake collected from SONGS 2 in 1995 based on metallography results. Also included in the figure are some of the relevant thermal properties (e.g., composition, porosity, etc.).

Secondary Deposit Thermal Resistance

Table 5-2 summarizes the secondary tube scale characterization data for Callaway, Sequoyah 1, and South Texas 1, including best-estimate and bounding values.* Note that the tube scale samples from the subject plants have different structures:

- Callaway scale is believed to contain two sub-layers: a thin (0.1 mil) non-porous inner layer and a moderately thick (3.5–4 mil) porous outer layer.
- Photomicrographs of 1995 Sequoyah scale cross sections suggest a variable thickness of between 2.5 and 5.5 mils. The thinner samples exhibit a single, fairly dense layer while the thicker samples revealed a very porous outer layer of 1–2 mils and a relatively nonporous inner layer.
- Thickness data for South Texas 1 scale (0.5-mil best estimate) suggest a single-layer structure is most likely.
- Deposit characterization work on the SONGS 2 tube scale indicates three distinct sub-layers: an inner layer composed of magnetite and copper (an average of about 4 mils), a void-filled middle layer (about 1.5 mils), and a porous outer layer (5 mils). Note that the total thickness (about 11 mils) is much greater than any of the other plants.

The thermal resistances of the inner Callaway and Sequoyah 1 layer and the inner and middle layers at SONGS 2 are calculated using Bruggeman's equation [5-1]. For the outer layers at Callaway, Sequoyah 1, and SONGS 2, the presence of significant porosity means that boiling processes affect the heat transfer through the layers, invalidating Bruggeman's equation. Instead, the results of an implementation of Pan's model of wick boiling (see, for example, Reference (32)) are listed in Table 5-2 for Callaway and SONGS 2. See Appendix C for a brief description of this model, which

* SONGS 2 results are also included in this table from a prior analysis.

was developed at the University of Illinois (Urbana-Champaign) in the mid-1980s with support from EPRI.

Bruggeman's equation suggests that the nonporous inner and void-filled middle layers of SONGS 2 are quite thermally resistant with a best estimate fouling factor sum of 175 10^{-6} h-ft^2-°F/BTU for the two layers. The relatively small temperature differences predicted by the Pan model through the outer Callaway and SONGS 2 layers, as well as experience in fouling factor heat transfer experimental measurements and published fouling factor values, suggest that these outer layers are either marginally augmenting or marginally insulating to heat transfer. Our best estimate is that the pre-chemical cleaning Callaway outer layer was slightly augmenting (fouling factor of –15 10^{-6} h-ft^2-°F/BTU) while the pre-chemical cleaning SONGS 2 outer layer was slightly insulating (fouling factor of +10 10^{-6} h-ft^2-°F/BTU). This is based on the smaller temperature drop predicted by the Pan model.

For Sequoyah 1, insufficient information is currently available to use the Pan model. However, the best-estimate average thickness in 1995 (5–6 mils) and presence of two layers—an inner, relatively nonporous layer and an outer, very porous layer—suggest a slightly resistive to slightly enhancing net effect on heat transfer. Our best estimate is that the Sequoyah 1 scale (prior to chemical cleaning) was slightly resistive with an associated fouling factor of +29 10^{-6} h-ft^2-°F/BTU.

For South Texas 1, the very small measured deposit thicknesses are believed to have little impact on heat transfer (either positive or negative). While some thermal resistance (or enhancement) is possible for such thin layers, the best estimate fouling factor attributable to STP 1 deposits is zero.

Table 5-2 also lists fouling factor predictions for Callaway and Sequoyah 1 following chemical cleaning based on an estimate of what type of layer may have deposited onto the tube surfaces immediately following the cleaning. The insulating properties of such a new layer have been proposed at industry meetings as a possible explanation of the lack of performance improvement following the Callaway cleaning (33). Our best estimate is that 75 pounds of silicates may have deposited in each SG, forming a nonporous layer 0.09 mils thick with a thermal conductivity of 0.75 BTU/h-ft-°F, resulting in a fouling factor of only about 10 10^{-6} h-ft^2-°F/BTU. However, the upper bound calculation yields a fouling factor of about 29 10^{-6} h-ft^2-°F/BTU. Therefore, it is possible that the fouling factor increase observed at Callaway following chemical cleaning is due to slightly heat-transfer-augmenting deposits being removed and replaced by slightly insulating deposits.

Table 5-1
Thermal Conductivities of Selected Solid Oxides[1]

Oxide	Temperature		Thermal Conductivity		Comments
	K	°F	W/m-K	BTU/h-ft-°F	
Co_2O_3	322	121	0.4	0.2	pressed powder
ZnO	323	122	0.6	0.3	pressed powder
CdO	320	117	0.7	0.4	pressed powder
Ni_2O_3	319	115	0.9	0.5	pressed powder
CuO	319	115	1.0	0.6	pressed powder
SiO_2	576	578	1.7	1.0	pure fused quartz
V_2O_5	673	752	1.8	1.0	
Zr_2O_3	673	752	2.1	1.2	
V_2O_5	473	392	2.6	1.5	
Ti_3O	575	576	2.9	1.7	
BaO	600	621	3.0	1.7	single crystal in argon
TiO	575	576	3.2	1.8	
Y_2O_3	673	752	3.3	1.9	single crystal; ±20%
Fe_3O_4	**573**	**572**	**3.4**	**2.0**	**crystalline wafers[2]**
Ti_5O	575	576	4.0	2.3	
Ti_6O	575	576	4.4	2.5	
Cr_2O_3	**333**	**140**	**4.5**	**2.6**	**pressed powder[3]**
Fe_2O_3	573	572	4.9	2.8	crystalline wafers
TiO_2	473	392	5.0	2.9	polycrystalline
Sc_2O_3	573	572	5.0	2.9	sintered with zero open porosity
NiO	**673**	**752**	**5.3**	**3.1**	**25.7% porosity**
SrO	600	621	5.5	3.2	single crystal in argon
NiO	**673**	**752**	**7.2**	**4.2**	**polycrystalline, nonporous**
NiO	**473**	**392**	**7.4**	**4.3**	**25.7% porosity**
CeO_2	500	441	8.6	5.0	porous specimen
VO_2	373	212	9.8	5.7	
NiO	**473**	**392**	**9.9**	**5.7**	**polycrystalline, nonporous**
ZnO	673	752	11.0	6.4	polycrystalline
Ti_2O	575	576	11.5	6.6	
Al_2O_3	673	752	13.0	7.5	little or no porosity
CaO	600	621	14.0	8.1	single crystal in argon
ZnO	473	392	17.0	9.8	polycrystalline
MgO	575	576	17.5	10.1	
SnO_2	423	302	22.4	12.9	2% impurities
Al_2O_3	373	212	29.0	16.8	little or no porosity
BeO	673	752	91.0	52.6	nonporous

Notes

1. All values taken from Reference (27) except as noted below.
2. Values are based on a curve fit to actual data taken from Reference (28).
3. Values calculated from information taken from References (29) and (30).
4. Entries in bold describe oxides found in primary-side films.

Table 5-2

Secondary and Primary Deposit Local Foulding Factor Predictions Based on Deposit Characterization

		Callaway Just Before Chem Clean			Callaway Now (1/96-4/96)			Sequoyah 1 Just Before Chem Clean			Sequoyah 1 Now (3/96-5/96)			South Texas 1 Now (2/96-6/96)			SONGS 2		
Nominal tube outside diameter (in)		0.688			0.688			0.875			0.875			0.750			0.750		
Nominal tube thickness (in)		0.040			0.040			0.050			0.050			0.043			0.048		
Tube inside diameter (in)		0.608			0.608			0.775			0.775			0.664			0.654		
Ratio of outside to inside surface areas		1.132			1.132			1.129			1.129			1.130			1.147		
Total outside surface area (ft^2)		55,000			55,000			51,500			51,500			68,000			104,130		
Secondary Fouling Factor Calculation (10^{-6} h-ft^2-°F/Btu)		Lower Bound	Best Estimate	Upper Bound	Lower Bound	Best Estimate	Upper Bound	Lower Bound	Best Estimate	Upper Bound	Lower Bound	Best Estimate	Upper Bound	Lower Bound	Best Estimate	Upper Bound	Lower Bound	Best Estimate	Upper Bound
Inner Nonporous Layer	Thickness (mils)	0.1	0.1	0.1				1.0	2.0	3.0							2.5	3.9	5.3
	Continuous/dispersed phases	Cu (no dispersed)						Fe_3O_4/Cu									Fe_3O_4/Cu		
	Dispersed phase volume fraction	0.00	0.00	0.00				0.30	0.20	0.10							0.30	0.25	0.20
	Cont. thermal cond (Btu/h-ft-°F)	219	219	219				2.0	2.0	2.0							2.0	2.0	2.0
	Disp. thermal cond (Btu/h-ft-°F)							219	219	219							219	219	219
	Effective thermal cond (Btu/h-ft-°F) (1)	219	219	219				5.53	3.80	2.71							5.53	4.56	3.80
	Fouling factor	0.04	0.04	0.04				15.0	43.8	92.0							37.5	70.9	115.4
Middle Layer	Thickness (mils)																1.0	1.5	2.0
	Continuous/dispersed phases																Fe_3O_4/H_20(l) voids		
	Dispersed phase volume fraction																0.20	0.38	0.56
	Cont. thermal cond (Btu/h-ft-°F)																2.0	2.0	2.0
	Disp. thermal cond (Btu/h-ft-°F)																0.32	0.32	0.32
	Effective thermal cond (Btu/h-ft-°F) (1)																1.55	1.20	0.88
	Fouling factor																53.6	104.2	188.2
Outer Porous Layer	Thickness (mils)	2.2	3.6	5.0				2.7	3.7	4.7				0.1	0.5	2.1	3.5	4.9	6.3
	Porous matrix phase	Fe_3O_4						Fe_3O_4 + 20% Cu						Fe_3O_4			Fe_3O_4		
	Fe_3O_4 thermal cond (Btu/h-ft-°F)	2.0	2.0	2.0				5.6	3.8	2.7				2.0	2.0	2.0	2.0	2.0	2.0
	Total porosity fraction all layers	0.350	0.350	0.350				0.550	0.550	0.550				NA	NA	NA	0.224	0.224	0.224
	Total porosity fraction outer layer	0.366	0.360	0.357				0.550	0.550	0.550				NA	NA	NA	0.391	0.355	0.306
	Chimney diameter (mm)	10.0	10.0	10.0				NA	NA	NA				NA	NA	NA	2.5	2.5	2.5
	Fraction of porosity in chimneys	0.54	0.38	0.22				NA	NA	NA				NA	NA	NA	0.12	0.12	0.12
	Chimney density (mm^{-2})	2500	1750	1000				NA	NA	NA				NA	NA	NA	9555	8667	7475
	Porous shell porosity fraction	0.211	0.258	0.302				NA	NA	NA				NA	NA	NA	0.361	0.326	0.279
	Bulk Na concentration (ppb) (2)	0.01	0.02	0.04				NA	NA	NA				NA	NA	NA	0.05	0.09	0.18
	Bulk NaOH concentration (ppb)	0.017	0.035	0.070				NA	NA	NA				NA	NA	NA	0.078	0.157	0.313
	Nominal system pressure (psia)	1000	1000	1000				857	857	857				1100	1100	1100	900	900	900
	Nominal heat flux (Btu/h-ft^2)	55,509	55,509	55,509				56,698	56,698	56,698				47,883	47,883	47,883	55,863	55,863	55,863
	Concentration factor Pan model	35	89	149				NA	NA	NA				NA	NA	NA	15	72	623
	DT predicted by Pan model (°F)	0.85	1.12	1.67				NA	NA	NA				NA	NA	NA	1.30	1.30	1.33
	DT predicted by Thom corr. (°F)	7.7	7.7	7.7													8.3	8.3	8.3
	DT_{Pan} - DT_{Thom} (°F)	-6.8	-6.6	-6.0													-7.0	-7.0	-7.0
	Fouling factor from Pan model	-122.9	-118.1	-108.0													-125.9	-125.9	-125.3
	Fouling factor engineering judgment (3)	-30.0	-15.0	0.0				-30.0	-15.0	15.0				-15.0	0.0	5.0	-40.0	10.0	60.0
	Effective thermal cond (Btu/h-ft-°F)	-6.1	-19.9	∞				-7.5	-20.5	26.0				-0.6	∞	34.9	-7.3	40.6	8.7
Mass of silicates deposited after cleaning (lb)					25	75	150				25	75	150						
Assumed density of silicates (g/cm^3)					3.0	3.0	3.0				3.0	3.0	3.0						
Calculated silicate volume (ft^3)					0.133	0.400	0.801				0.133	0.400	0.801						
Calculated silicate thickness (mils)					0.029	0.087	0.175				0.029	0.087	0.175						
Silicate thermal conductivity (Btu/h-ft-°F)					1.00	0.75	0.50				1.00	0.75	0.50						
Secondary deposit fouling factor		-30.0	-15.0	0.0	2.4	9.7	29.1	-15.0	28.8	107.0	2.4	9.7	29.1	-15.0	0.0	5.0	51.1	185.1	363.6
Primary Fouling Factor Calculation (10^{-6} h-ft^2-°F/Btu)		Lower Bound	Best Estimate	Upper Bound	Lower Bound	Best Estimate	Upper Bound	Lower Bound	Best Estimate	Upper Bound	Lower Bound	Best Estimate	Upper Bound	Lower Bound	Best Estimate	Upper Bound	Lower Bound	Best Estimate	Upper Bound
Primary deposit layer thickness (mm)		0.5	1.0	5.0	0.5	1.0	5.0	0.5	1.0	5.0	0.5	1.0	5.0	0.5	1.0	5.0	0.5	1.0	5.0
Primary deposit layer thickness (mils)		0.020	0.039	0.197	0.020	0.039	0.197	0.020	0.039	0.197	0.020	0.039	0.197	0.020	0.039	0.197	0.020	0.039	0.197
Primary layer thermal cond. (Btu/h-ft-°F)		4.6	1.8	0.6	4.6	1.8	0.6	4.6	1.8	0.6	4.6	1.8	0.6	4.6	1.8	0.6	4.6	1.8	0.6
Primary fouling factor (based on inside area)		0.4	1.8	27.3	0.4	1.8	27.3	0.4	1.8	27.3	0.4	1.8	27.3	0.4	1.8	27.3	0.4	1.8	27.3
Primary fouling factor (based on outside area)		0.4	2.1	30.9	0.4	2.1	30.9	0.4	2.1	30.9	0.4	2.1	30.9	0.4	2.1	30.9	0.4	2.1	31.4

(1) Effective thermal conductivity as given by Bruggeman's equation.

(2) Nominal SONGS values given by "Unit 2/3 Chemistry Status Report" dated October 3, 1994 by John A. Mundis.

(3) Fouling factor based on engineering judgment using DEI experience in fouling factor heat transfer experiments and literature values.

(4) "NA" indicates that this information is not yet available.

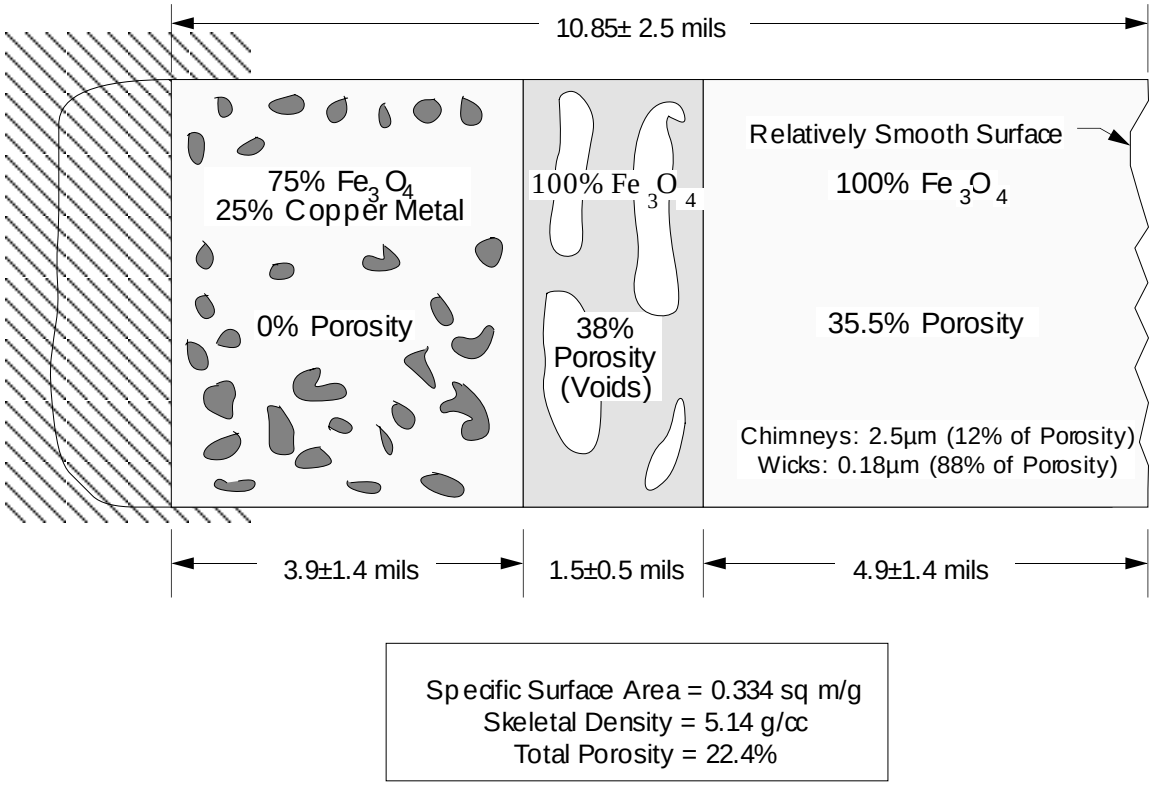

Figure 5-1
Morphology and Properties of SONGS 2 Secondary Tube Scale Flakes

6

CAUSES OF SG STEAM PRESSURE LOSS

The fouling factor methodology detailed in the Chapter 4 adjusts for changes in primary temperatures, thermal power, and heat-transfer area (e.g., plugged tubes). In other words, changes in these variables, if they are known, will not contribute to an increasing fouling factor. However, there are numerous other possible causes of SG pressure loss which are not accounted for by the fouling factor. These other causes need to be evaluated before any calculated level of fouling can be attributed to secondary deposits.

Effects of Fouling Factor Variables on SG Steam Pressure

As indicated above, the fouling factor adjusts for changes in T_{hot}, T_{cold}, A, and Q. Nevertheless, such changes can adversely affect the SG pressure. The sensitivity of SG pressure to each of these variables may be examined in the context of the overall heat transfer equation, introduced in the last chapter and repeated here for convenience:

$$Q = UA\frac{T_{hot} - T_{cold}}{\ln\left(\frac{T_{hot} - T_{sat}(p_{sat})}{T_{cold} - T_{sat}(p_{sat})}\right)} \qquad \text{(eq. 6-1)}$$

The equation also allows predicted fouling factors calculated with the methods described in the last chapter to be translated into predicted pressure losses. Because thermal power (Q) and primary temperatures (T_{hot} and T_{cold}) appear explicitly in Eq. [6-1], their individual effects on SG steam pressure can be calculated with the proper partial derivatives. This separation allows the effects of variations or errors in heat-transfer area, reactor thermal power, and primary control temperature (T_{ave} for Callaway, Sequoyah 1, and South Texas 1) to be individually quantified.

Results of this sensitivity analysis are presented in Tables 6-1, 6-2, and 6-3 for each of the plants examined in this study. Note that there are three separate cases analyzed: (1) design values, (2) values that reflect early operation, and (3) values that reflect

recent operation.* Using the values for most recent operation, the pressure loss that can be attributed to each cause may be calculated using the following equation:

$$\Delta p_{sat} = \frac{\partial p_{sat}}{\partial X} \Delta X \qquad \text{(eq. 6-2)}$$

where X represents A, T_{ave}, or Q. (Note that this calculation is an approximation, since the partial derivative is not necessarily constant during the pressure decrease. However, as is clear from Tables 6-1 through 6-3, the values do not vary widely.) The results of this calculation for each variable are shown at the bottom of Table 6-4 under the heading "Sources That are Accounted for by the Fouling Factor Calculation." Best-estimate, lower-bound, and upper-bound results are included for Callaway (both just prior to chemical cleaning and afterwards), Sequoyah 1 (also before and after chemical cleaning), and South Texas 1. In addition, the results for SONGS 2, examined in a previous study, are also shown.† Noteworthy results in the lower part of Table 6-4 include

- Tube plugging has played a relatively minor role in reducing steam pressure at Callaway (1.6 psi) and South Texas (1.5 psi). The effect at Sequoyah 1 is more significant (3.6 psi before chemical cleaning and 6.9 psi afterwards).

- The effect on steam pressure of primary temperature variations are shown compared to the design primary temperatures and also compared to the initial primary temperatures characteristic of early operation. Note that all plants have experienced steam pressure differences due to this variable versus design: Callaway experienced a decrease of about 12 psi, Sequoyah 1 a decrease of 7 psi, South Texas 1 a decrease of 38 psi (due mainly to a T_{hot} reduction of 4°F), and SONGS 2 an increase of 6 psi. Compared to early operation, Callaway has seen a modest decrease of 3.3 psi, Sequoyah 1 almost no change, South Texas 1 a decrease of 52 psi, and SONGS 2 an increase of 5 psi. It is clear that this factor must be accounted for when discussing the size of steam pressure losses, as its effects are potentially large.

- Thermal power levels below 100% have slightly increased steam pressure at all 3 plants. However, the effect is relatively small (4 psi or less).

- Callaway's power uprate of 4.5% (154 MWt) in 1988 caused a 15-psi drop in steam pressure.

---

* Early operation values are based on the first 2–4 months of operating data available. Recent operating values are based on the most recent 2–4 months of data.

† Detailed comparisons of steam pressure degradation at the subject plants, including SONGS 2, are provided in Chapter 7.

Effects of Other Major Variables

Other potential sources of SG pressure loss include the following categories:

SOURCES THAT AFFECT INITIAL PERFORMANCE VS. IDEAL DESIGN PERFORMANCE. These factors can cause a steam generator to perform more poorly than expected, but they cannot account for an observed pressure loss over life. They can, however, decrease the performance margin available for accommodating fouling and plugging. Included are the following:

1. Pre-service tube plugging.
2. Initial primary temperatures different from the design values.
3. Initial primary tube velocity different from the design value.
4. Variation in tube wall thickness from the nominal value.
5. Variation in tube material thermal conductivity from the nominal value.

The effects of the first two on steam pressure are calculated using Eq. [6-2]. The effect of changes in primary-side velocity is calculated using the Dittus-Boelter correlation for internal flow through circular pipes (see, for example, p. 394 of Reference (34)):

$$R'' = \frac{1}{h}\left(\frac{d_o}{d_i}\right) = \left(\frac{1}{\frac{k}{d_i}\left(0.023 Re^{0.8} Pr^{0.3}\right)}\right) \times \left(\frac{d_o}{d_i}\right) \qquad \text{(eq. 6-3)}$$

where *Re* is the Reynolds number and *Pr* is the Prandtl number. Note that the calculations compare the resistance corresponding to the design value of primary flow rate with the resistances corresponding to a range of flow rates calculated from measured values of T_{hot}, T_{cold}, and thermal power.

The effects of wall thickness and material thermal conductivity variations are computed using the expression for thermal resistance through a cylindrical wall:

$$R'' = \frac{d_o}{2k} \ln\left(\frac{d_o}{d_i}\right) \qquad \text{(eq. 6-4)}$$

The change in this resistance is calculated for wall thicknesses of ±10% relative to the nominal thickness and for thermal conductivities of ±5% relative to the nominal value.

The effect of each of these causes is listed in the appropriately titled portions of Table 6-4 for each plant. In each case, pre-service plugging had a negligible effect on steam pressure. Initial primary temperatures, on the other hand, varied significantly from the originally specified design values. Callaway and Sequoyah 1 started up with T_{ave}'s that decreased the steam pressure about 9 psi and 7 psi, respectively, relative to what it would have been at the design temperatures. In contrast, South Texas 1 experienced an initial steam pressure increase of about 14 psi due to an above-design T_{ave} during early operation.* Best-estimate predictions of steam pressure changes due to primary velocity differences from the design value range from –1 psi up to +4 psi (i.e., a relatively minor effect although potentially significant). No dimensional information was available to indicate that the tube wall thickness or conductivity deviated from nominal values; hence, the best-estimate changes in pressure due to these causes is zero for all plants. However, the bounding calculations shown in Table 6-4 reveal that a wall thickness variation of 10% can cause steam pressure to be 9 psi to 16 psi higher (or lower) than design. Similarly, a 5% thermal conductivity variation can induce a 4 psi to 8 psi change in steam pressure.

SOURCES THAT ARE DUE TO DEPOSITS WITHIN THE TUBE BUNDLE. Such deposits may be primary or secondary in nature. Best-estimate and bounding calculations of the fouling factors (and associated SG steam pressure losses) are listed in Table 6-4. Descriptions of the bases for the calculations are provided in Chapter 5 of this report. Note that the tube scale layer at Callaway (prior to chemical cleaning) is predicted to have been slightly heat-transfer enhancing ($-15\ 10^{-6}$ h-ft^2-°F/BTU), thereby tending to raise the steam pressure a modest amount (5 psi). The Sequoyah 1 scale before chemical cleaning is predicted to have been slightly resistive ($+29\ 10^{-6}$ h-ft^2-°F/BTU), lowering steam pressure by an estimated 10 psi.† The very thin scale at South Texas 1 is estimated to have no effect at all on heat transfer. In contrast, the tube scale at SONGS 2 is estimated to have a substantial thermal resistance ($185\ 10^{-6}$ h-ft^2-°F/BTU), resulting in a large pressure loss (72 psi).

It is important to note that the above estimates of deposit thermal resistance are based on: 1) the scale properties (e.g., composition, porosity, morphology, thickness), as is described in greater detail in Chapter 5, and 2) experimental correlations between scale thickness and thermal resistance (see References (4) and (9)). As a result, the estimates are independent of the observed pressure loss and can thus act as confirmation of the role of deposits in causing thermal performance degradation.

---

* It is important to note that the higher T_{ave} for South Texas 1 reflected a higher-than-design thermal resistance of the STP 1 SGs. Although the initial T_{hot} was about equal to the design value, T_{cold} was about 3°F higher than design, suggesting that the SGs were less effective at removing heat than the design values would indicate.

† Note, however, that the evidence on the effects of Sequoyah 1 scale is ambiguous. The scale may have had no effect or even enhanced heat transfer slightly.

SOURCES THAT ARE NOT DUE TO DEPOSITS WITHIN THE BUNDLE BUT WHICH ARE CAPTURED IN THE FOULING FACTOR CALCULATION. These sources of pressure loss can also be expected to result in uncertainty in the fouling factor calculation. They include the following, all of which are summarized in Table 6-4 under the above heading.

1. Uncertainty in SG pressure measurements. As indicated in Table 4-2, this tolerance is estimated to be about ±5 to ±8 psi for each plant. This uncertainty is somewhat difficult to evaluate accurately because the maximum allowable tolerance on steam pressure measurement can be significantly larger than the actual tolerance achieved by the plant.

2. Additional pressure drop across the dryers and moisture separators (i.e., above the design value). Although this cause does not reflect fouling of the tube bundle, it nevertheless causes lower-than-expected pressure at the HP turbine. Tests at Callaway in February 1996 indicated that this pressure drop was about 4 psi larger than the design value. Sequoyah 1 tracks the pressure drop between the top of the bundle and the main steam measurement location; this measurement has shown little net change since 1991, suggesting that the moisture separators are not actively fouling. South Texas 1 did not report any information on this subject.*

3. Error in applied primary temperature. This can be caused by at least four separate problems:

   a. T_{AVE} MEASUREMENT ERROR. As with steam pressure measurement, determining the actual tolerances achieved by each plant (as opposed to the allowable limits) is difficult. The best estimates for each tolerance were reported in Table 4-2, and the resulting calculated effect on steam pressure is shown in the upper- and lower-bound columns of Table 6-4. These values range from 5 psi to 22 psi.

   b. HOT-LEG TEMPERATURE STREAMING. Reported calculations by one NSSS vendor indicate that a pressure loss of 10 psi is possible due to streaming. This phenomenon is caused by a nonuniform temperature through the pipe cross section where hot-leg temperature is measured. If the measured temperature is significantly higher than the bulk fluid temperature (e.g., even 0.5°F), then T_{ave} can be incorrectly decreased. Plants which control the average primary temperature (T_{ave}) rather than T_{cold} are potentially susceptible to this phenomenon. (Callaway, Sequoyah 1, and South Texas 1 all control T_{ave}.) An additional risk factor is the usage of low-neutron-leakage fuel assemblies in the reactor core (or the arrangement of existing fuel to minimize neutron leakage). Often the result

* Note that another US utility has recently observed severe fouling of the moisture separators at one of its plants possessing Combustion Engineering Model 67 SGs. The estimated pressure recovery following a cleaning of these separators (13 psi) is considered to be a reasonable upper bound on the expected pressure loss due to separator fouling at a typical plant.

is less thermal mixing, increasing the chance that the RTDs used to measure T_{hot} will be in error.

In order to understand the effect of hot-leg streaming on primary temperature, consider Table 6-5. When no streaming is taking place, the actual temperatures match the measurements (top line of each part of the table). Now suppose the hot-leg RTDs measure temperatures which average 4° greater than the actual temperature. This situation is reflected by the middle lines in Table 6-5. Now the plant computer attempts to restore T_{ave} to the desired value by decreasing T_{hot} and T_{cold} by 2° (bottom lines in Table 6-5). It is clear from the table that a hot-leg streaming effect of a certain magnitude (e.g., 4°) causes the reported T_{hot} and T_{cold} values to diverge by half that amount (i.e., T_{hot} increases by 2° and T_{cold} decreases by 2°). Meanwhile, the actual primary temperatures in this situation both decrease by 2°, or half the amount of the original streaming error. The potential effects of hot-leg streaming are explored for each plant below.

Callaway: Hot-leg streaming at Callaway during recent operation has been documented by Union Electric. Through the use of a reverse calorimetric procedure to back calculate hot-leg temperature, the error associated with hot-leg streaming was calculated to be 0.91°F at the beginning of Cycle 7 and 1.01°F at the beginning of Cycle 8. The average of these 2 values (0.96°F) is used in Table 6-4 to calculate a corresponding best-estimate pressure loss of about 4 psi.

Sequoyah 1: According to TVA, low-leakage fuel was introduced at Sequoyah 1 in either 1988 or 1990. Examination of Figures 4-11a, 4-11b, and 4-11c indicates that the hot-leg and cold-leg temperatures begin to diverge at least as early as Cycle 6 (1992). Analysis of these values reveals that in fact T_{hot} increased about 2°F compared to initial operation while T_{cold} decreased by almost the same amount. The effect of this error on steam pressure is indicated in Table 6-4; the best estimate is a 15 psi decrease.

South Texas 1: Like Sequoyah 1, South Texas 1 has also attempted to minimize neutron leakage during the last few operating cycles by rearranging fuel in order to place lower-reactivity assemblies at the periphery of the reactor, a practice which increases the potential for significant hot-leg streaming effects. No definitive data or analyses have been provided by the utility regarding hot-leg streaming. However, the utility did report that RTD readings on a single pipe have varied as much as 7–8°F, indicating that streaming is taking place. In addition, calculated primary flow rates (which are based on primary temperature readings) have decreased substantially although no significant decrease was expected. These two signs suggest that hot-leg streaming is taking place. The current best estimate, reflected in Table 6-4, is 3°F of streaming (corresponding to a 1.5°F primary temperature error), which would lower steam pressure by about 13 psi.

Note that the primary temperatures at South Texas 1 were intentionally lowered 4°F beginning in Cycle 6, and subsequently fell at least another 1°F, most likely due to temperature asymmetry among the four loops (see p. 8-4 for a description of the change in control scheme that led to this decrease). These temperature changes are unrelated to hot-leg streaming occurring within the pipe cross sections.

General Conclusions: Accurate quantitative estimates of hot-leg streaming require one or more of the following: a) detailed measurements of the temperature profile through the hot-leg pipe cross sections, b) a primary-side calorimetric enthalpy balance calculation to check for consistency in the temperature measurements (as was performed by Callaway), or c) more accurate temperature instrumentation not subject to streaming (e.g., ultrasonic techniques—see Reference (35) for further details on a specific application at one US plant). It may also be possible to analytically calculate the magnitude of hot-leg streaming by modeling the thermal hydraulics in the reactor and its outlet piping.

c. LOOP TEMPERATURE ASYMMETRY. Due to asymmetries in reactor flow patterns and/or differences in heat-transfer coefficients among SGs, the observed primary temperatures in one or more loops may exceed those observed in the others. If the plant uses a maximum (auctioneer) T_{ave} control scheme, such asymmetries can reduce the average T_{ave} below the desired value, causing a decrease in steam pressure and a slight reduction in thermal power. As discussed in Chapter 8, this phenomenon has affected Callaway and may be affecting South Texas 1. Note that the SG thermal performance at plants which control the average T_{ave} will be largely unaffected by loop asymmetries.

d. DIVIDER PLATE LEAKAGE. Leaks from the hot to the cold side of the primary channel head can cause three distinct effects that can lead to pressure loss: a) an inaccurate reading of the actual cold-leg temperature leaving the SG bundle, b) lower primary-side mass flow rate through the tube bundle and hence a lower primary-side velocity, which increases the primary boundary-layer thermal resistance, and c) an actual T_{cold} decrease due to the smaller primary mass flow rate through the tube bundle. All of these effects tend to cause the SG pressure to decrease. Note, however, that this problem has been primarily associated with the bolted connections typical of the CANDU SG design.

None of the plants involved in this study reported any knowledge of this phenomenon, and it is considered very unlikely that a significant leak could develop through the welded divider plates in US PWR SGs. As a result, it is postulated that the induced primary temperature error is equal to an undetectable 10^{-4} times the primary temperature difference. As indicated in Table 6-4, the effect on steam pressure is nearly zero. The upper-bound values (about 2 psi) are based on a 1% error in primary temperature caused by divider plate leakage.

Effects of Minor Contributors

Degradation of steam generator pressure could potentially be due in part to performance degradation of secondary cycle equipment, such as turbines, condensers, moisture separator reheaters, and feedwater heaters. The potential effect of changes in the secondary cycle can be empirically evaluated through the observed changes in feedwater temperature. Examining Figures 4-9, 4-13, and 4-17, we note that Callaway feedwater temperature has varied by up to 20°F, while Sequoyah 1 and South Texas 1 have seen smaller changes (10°F and 5°F, respectively). The pressure losses attributed to this cause for Callaway and SONGS 2 in Table 6-4 were evaluated using a preliminary one-dimensional model of the SG based on the Dittus-Boelter and Chen correlations for single-phase cooling of the primary coolant and subcooled and saturated forced convection boiling in the tube bundle, respectively. The values for Sequoyah 1 and South Texas 1 are estimates based on the SONGS 2 and Callaway results and engineering judgment.*

A second mechanism through which the secondary cycle performance may affect the steam generator pressure is the turbine back-pressure. This mechanism can only be active once steam generator pressure control is lost (i.e., the turbine throttle valves are wide open (VWO)). When the turbine throttle valves are being actively controlled, variations in the turbine back-pressure are essentially canceled out. This is the case for both Sequoyah 1 and South Texas 1. However, at Callaway, the throttle valves have frequently been wide open since the beginning of Cycle 5. Also, both SONGS 2 and 3 operated in the VWO condition until recent chemical cleanings in 1996–97.

Figure 6-1 illustrates graphically how changes in the secondary cycle and SG fouling affect thermal power and SG pressure once the turbine throttle valves are wide open. The figure is based on data from SONGS 3 and is to scale. The flatter line represents the overall heat-transfer equation [4-4] at a given value of T_{cold} (since SONGS 3 is T_{cold} controlled). The steeper line represents the approximate proportionality of thermal power and SG steam pressure. For a constant turbine speed, which means a smaller mass flow rate approximately in proportion to any steam pressure decreases, this relationship is essentially a straight line as shown. As indicated on the figure, the plant will operate at the intersection of these two curves once the throttle valves are wide open. For decreases in primary temperature or SG fouling, the flatter curve moves down, lowering both pressure and thermal power. On the other hand, changes in the secondary cycle (e.g., changes in moisture carryover) can move the steeper curve in either direction as indicated on the figure. In one case, SG pressure is raised slightly but thermal power decreases. In the other case (e.g., changes to the HP turbine configuration), SG pressure decreases slightly but thermal power increases.

---

* Note that the effect of feedwater temperature (i.e., degree of subcooling) is best investigated using a detailed thermal-hydraulics code such as ATHOS (5, 6). Such calculations are beyond the scope of this project.

Summary of Pressure Losses

Using the results in Table 6-4, Table 6-6 summarizes the best-estimate pressure losses in psi (relative to the initial performance) by cause for each plant in this study. The most striking thing about this table is that the observed pressure loss does not necessarily correlate well with secondary fouling. Callaway's pressure loss can largely be attributed to the 1988 power uprate. The loss at Sequoyah 1, meanwhile, is caused mainly by tube plugging and hot-leg streaming (22 of 36 psi) while deposits are likely having a smaller effect (10 psi). South Texas 1 has seen a pressure drop in excess of 60 psi, but this is mainly the result of reduced primary temperatures. SONGS 2, on the other hand, is the only plant for which secondary deposits are believed to be causing a major pressure loss. This subject is discussed further in Chapter 7.

Thermal Power Degradation

Although steam pressure loss is one symptom of performance degradation, it should also be noted that thermal power can degrade, leading to the same loss in electrical power generation that can be caused by SG performance loss. For the secondary system to properly do its job, it must receive sufficient steam pressure and the full level of thermal power input. Potential sources of thermal power loss include the following, each of which is evaluated in Table 6-4.

1. FEEDWATER FLOW MEASUREMENT ERROR. This can be caused either by inaccuracies inherent in the measurement device, or a by a systematic error such as venturi fouling. Venturi meters are typically used to measure feedwater flow rate. They do so by converting the pressure drop across a known geometry to an average flow rate. If a layer of corrosion products accumulates on the surface of the venturi, then less flow will be passing through the meter for a given velocity, meaning that the meter measurement will be higher than the actual flow rate.* The result is an actual thermal-power level below the "measured" level based on a secondary calorimetric calculation.

   Callaway probably experienced significant venturi fouling during early cycles, as is evident from the mismatch between measured steam flow and calculated steam flow based on feedwater flow measurements (Figure 4-8b). However, during the last 2 cycles, feedwater and steam flow measurements agree closely, indicating that venturi fouling is absent or minimal. As a consequence, the best-estimate for feedwater flow error in Table 6-4 is zero. The upper-bound estimate

* It is also possible for the meter to underreport the actual flow rate. This can happen if the venturi is calibrated while it is fouled, and then subsequently cleaned without being re-calibrated.

incorporates a 0.5% venturi fouling error, plus the measurement uncertainty indicated in Table 4-2.

Sequoyah 1 has also reported venturi fouling of up to 1%. However, recent operation (since 1992) is believed to reflect a total tolerance of ±0.5%, in large part because the venturis are cleaned during each refueling outage. As a result, the best-estimate for this error is zero, while the upper-bound estimate includes a 0.5% venturi fouling error (like Callaway).

HL&P has not reported any venturi fouling. Although Figure 4-16b shows a rather large systematic disagreement of 2-3% during the last cycle, the direction of the discrepancy is opposite of that expected for venturi fouling. Without further clarification, the same assumption is used as for Callaway and Sequoyah 1 (i.e., zero best-estimate error and 0.5% venturi fouling in the upper-bound case).

2. FEEDWATER TEMPERATURE VARIATIONS FROM THE DESIGN VALUE.

3. OUTLET STEAM QUALITY VARIATIONS FROM THE DESIGN VALUE.

4. BLOWDOWN FLOW RATE VARIATIONS FROM THE DESIGN VALUE.

The effects of the last three items are minor (less than 1 psi) as shown in Table 6-4.

Table 6-1
Sensitivity of Callaway Steam Generator Pressure to Other Parameters in Overall Heat Transfer Equation

Quantity	Description	Units	Design VWO	Early Operation	Recent Oper. (Cycle 8)
nominal values of parameters in overall heat transfer coefficient equation (inputs)					
T_{hot}	hot leg temperature	°F	620.0	616.8	616.9
T_{cold}	cold leg temperature	°F	557.0	557.4	557.8
p_{sat}	steam generator dome pressure	psia	1000.0	974.7	986.1
A	total outside-tube surface area	ft^2	55,000	54,939	54,558
N_{tot}	total number tubes	--	5626	5620	5581
Q	steam generator thermal power	MWt	895	835	883
nominal values of parameters in overall heat transfer coefficient equation (calculated)					
p_{bundle}	mid-bundle pressure	psia	1011.5	986.2	997.6
T_{sat}	bundle saturation temperature	°F	545.97	542.90	544.30
Q	steam generator thermal power	Btu/h	3.053E+09	2.850E+09	3.013E+09
ΔT_{lm}	log-mean temperature difference	°F	33.09	36.54	35.16
R	global resistance to heat transfer	h-°F/Btu	1.084E-08	1.282E-08	1.167E-08
U	global heat transfer coefficient	Btu/h-ft^2-°F	1678	1420	1571
R"	global area-based resistance	10^{-6} h-ft^2-°F/Btu	596.0	704.4	636.6
calculation of dp_{sat}/dT_{sat} using Clapeyron relation: $dp_{sat}/dT_{sat} = h_{fg}/(Tv_{fg})$					
h_f	saturated liquid specific enthalpy	Btu/lb	544.3	540.4	542.2
h_g	saturated vapor specific enthalpy	Btu/lb	1192.5	1193.5	1193.0
h_{fg}	latent heat of vaporization at p_{sat}	Btu/lb	648.2	653.0	650.8
T	absolute bundle saturation temp.	°R	1005.6	1002.6	1004.0
v_f	saturated liquid specific volume	ft^3/lb	0.0216	0.0215	0.0216
v_g	saturated vapor specific volume	ft^3/lb	0.4404	0.4531	0.4473
v_{fg}	specific volume change upon vap.	ft^3/lb	0.4188	0.4315	0.4257
$\partial p_{sat}/\partial T_{sat}$	partial deriv. of sat. press. with T	psi/°F	8.32	8.16	8.23
partial derivatives of steam generator pressure					
effect of variations in reactor coolant loop temperature					
$\partial p_{sat}/\partial T_{cold/ave}$	partial deriv. wrt RCL temperature	psi/°F	8.32	8.16	8.23
effect of tube plugging					
$\partial p_{sat}/\partial A$	partial deriv. wrt heated area	psi/ft2	0.00373	0.00437	0.00421
$\partial p_{sat}/\partial N_{plug}$	partial deriv. wrt no. tubes plugged	psi/tube plugged	-0.036	-0.043	-0.041
$\partial p_{sat}/\partial \%_{plug}$	partial deriv. wrt % tubes plugged	psi/1% plugged	-2.05	-2.40	-2.30
effect of variations in steam generator thermal power					
$\partial p_{sat}/\partial Q$	partial deriv. wrt thermal power	psi/(Btu/h)	-1.16E-07	-1.27E-07	-1.18E-07
$\partial p_{sat}/\partial Q$	partial deriv. wrt thermal power	psi/MWt	-0.395	-0.432	-0.401
effect of variations in overall heat transfer coefficient (fouling factor)					
$\partial p_{sat}/\partial U$	partial deriv. wrt overall HT coeff.	psi/(Btu/h-ft^2-°F)	0.122	0.169	0.146
$\partial p_{sat}/\partial R_f$"	partial deriv. wrt fouling factor	psi/(10^{-6} h-ft^2-°F/Btu)	-0.344	-0.341	-0.361

Table 6-2
Sensitivity of Sequoyah 1 Steam Generator Pressure to Other Parameters in Overall Heat Transfer Equation

Quantity	Description	Units	Design VWO	Early Operation	Recent Operation (Cycle 8)
nominal values of parameters in overall heat transfer coefficient equation (inputs)					
T_{hot}	hot leg temperature	°F	609.7	608.8	608.9
T_{cold}	cold leg temperature	°F	546.7	545.6	545.7
p_{sat}	steam generator dome pressure	psia	857	841	852
A	total outside-tube surface area	ft^2	51,500	51,500	50,197
N_{tot}	total number tubes	--	3388	3388	3302
Q	steam generator thermal power	MWt	856	838	852
nominal values of parameters in overall heat transfer coefficient equation (calculated)					
p_{bundle}	mid-bundle pressure	psia	865	849	860
T_{sat}	bundle saturation temperature	°F	527.27	525.09	526.60
Q	steam generator thermal power	Btu/h	2.920E+09	2.859E+09	2.908E+09
ΔT_{lm}	log-mean temperature difference	°F	43.60	44.92	43.24
R	global resistance to heat transfer	h-°F/Btu	1.493E-08	1.571E-08	1.487E-08
U	global heat transfer coefficient	Btu/h-ft^2-°F	1300	1236 (1)	1340
R"	global area-based resistance	10^{-6} h-ft^2-°F/Btu	769.0	809.2	746.3
calculation of dp_{sat}/dT_{sat} using Clapeyron relation: $dp_{sat}/dT_{sat} = h_{fg}/(Tv_{fg})$					
h_f	saturated liquid specific enthalpy	Btu/lb	520.9	518.2	520.1
h_g	saturated vapor specific enthalpy	Btu/lb	1197.4	1197.9	1197.6
h_{fg}	latent heat of vaporization at p_{sat}	Btu/lb	676.5	679.7	677.5
T	absolute bundle saturation temp.	°R	986.9	984.8	986.3
v_f	saturated liquid specific volume	ft^3/lb	0.0211	0.0210	0.0211
v_g	saturated vapor specific volume	ft^3/lb	0.5233	0.5340	0.5266
v_{fg}	specific volume change upon vap.	ft^3/lb	0.5022	0.5130	0.5055
$\partial p_{sat}/\partial T_{sat}$	partial deriv. of sat. press. with T	psi/°F	7.38	7.27	7.34
partial derivatives of steam generator pressure					
effect of variations in reactor coolant loop temperature					
$\partial p_{sat}/\partial T_{cold/ave}$	partial deriv. wrt RCL temperature	psi/°F	7.38	7.27	7.34
effect of tube plugging					
$\partial p_{sat}/\partial A$	partial deriv. wrt heated area	psi/ft^2	0.00526	0.00539	0.00531
$\partial p_{sat}/\partial N_{plug}$	partial deriv. wrt no. tubes plugged	psi/tube plugged	-0.080	-0.082	-0.081
$\partial p_{sat}/\partial \%_{plug}$	partial deriv. wrt % tubes plugged	psi/1% plugged	-2.71	-2.78	-2.66
effect of variations in steam generator thermal power					
$\partial p_{sat}/\partial Q$	partial deriv. wrt thermal power	psi/(Btu/h)	-1.29E-07	-1.32E-07	-1.28E-07
$\partial p_{sat}/\partial Q$	partial deriv. wrt thermal power	psi/MWt	-0.439	-0.452	-0.437
effect of variations in overall heat transfer coefficient (fouling factor)					
$\partial p_{sat}/\partial U$	partial deriv. wrt overall HT coeff.	psi/(Btu/h-ft^2-°F)	0.208	0.225	0.199
$\partial p_{sat}/\partial R_f$"	partial deriv. wrt fouling factor	psi/(10^{-6} h-ft^2-°F/Btu)	-0.352	-0.343	-0.357

NOTES
1. The corresponding heat-transfer coefficient calculated for clean conditions is 1420.

Table 6-3
Sensitivity of South Texas 1 Steam Generator Pressure to Other Parameters in Overall Heat Transfer Equation

Quantity	Description	Units	Design VWO	Early Operation	Recent Operation (Cycle 6)
nominal values of parameters in overall heat transfer coefficient equation (inputs)					
T_{hot}	hot leg temperature	°F	626.1	626.5	620.7
T_{cold}	cold leg temperature	°F	559.7	562.5	556.3
p_{sat}	steam generator dome pressure	psia	1100	1115	1052
A	total outside-tube surface area	ft^2	68,000	67,951	67,441
N_{tot}	total number tubes	--	4864	4861	4824
Q	steam generator thermal power	MWt	954	942	954
nominal values of parameters in overall heat transfer coefficient equation (calculated)					
p_{bundle}	mid-bundle pressure	psia	1107	1122	1059
T_{sat}	bundle saturation temperature	°F	557.06	558.71	551.62
Q	steam generator thermal power	Btu/h	3.256E+09	3.215E+09	3.257E+09
DT_{lm}	log-mean temperature difference	°F	20.34	22.17	23.94
R	global resistance to heat transfer	h-°F/Btu	6.246E-09	6.896E-09	7.352E-09
U	global heat transfer coefficient	Btu/h-ft^2-°F	2354	2134 (1)	2017
R''	global area-based resistance	10^{-6} h-ft^2-°F/Btu	424.7	468.6	495.8
calculation of dp_{sat}/dT_{sat} using Clapeyron relation: $dp_{sat}/dT_{sat} = h_{fg}/(Tv_{fg})$					
h_f	saturated liquid specific enthalpy	Btu/lb	558.6	560.7	551.6
h_g	saturated vapor specific enthalpy	Btu/lb	1188.8	1188.2	1190.7
h_{fg}	latent heat of vaporization at p_{sat}	Btu/lb	630.3	627.5	639.2
T	absolute bundle saturation temp.	°R	1016.7	1018.4	1011.3
v_f	saturated liquid specific volume	ft^3/lb	0.0220	0.0220	0.0218
v_g	saturated vapor specific volume	ft^3/lb	0.3978	0.3918	0.4181
v_{fg}	specific volume change upon vap.	ft^3/lb	0.3758	0.3698	0.3963
$\partial p_{sat}/\partial T_{sat}$	partial deriv. of sat. press. with T	psi/°F	8.91	9.01	8.62
partial derivatives of steam generator pressure					
effect of variations in reactor coolant loop temperature					
$\partial p_{sat}/\partial T_{cold/ave}$	partial deriv. wrt RCL temperature	psi/°F	8.91	9.01	8.62
effect of tube plugging					
$\partial p_{sat}/\partial A$	partial deriv. wrt heated area	psi/ft^2	0.00117	0.00153	0.00173
$\partial p_{sat}/\partial N_{plug}$	partial deriv. wrt no. tubes plugged	psi/tube plugged	-0.016	-0.021	-0.024
$\partial p_{sat}/\partial \%_{plug}$	partial deriv. wrt % tubes plugged	psi/1% plugged	-0.80	-1.04	-1.17
effect of variations in steam generator thermal power					
$\partial p_{sat}/\partial Q$	partial deriv. wrt thermal power	psi/(Btu/h)	-9.81E-08	-1.00E-07	-9.76E-08
$\partial p_{sat}/\partial Q$	partial deriv. wrt thermal power	psi/MWt	-0.335	-0.342	-0.333
effect of variations in overall heat transfer coefficient (fouling factor)					
$\partial p_{sat}/\partial U$	partial deriv. wrt overall HT coeff.	psi/(Btu/h-ft^2-°F)	0.034	0.049	0.058
$\partial p_{sat}/\partial R_f$''	partial deriv. wrt fouling factor	psi/(10^{-6} h-ft^2-°F/Btu)	-0.188	-0.222	-0.235

NOTES
1. The corresponding heat-transfer coefficient calculated for clean conditions is 2715.

Table 6-4
Sources of Steam Generator Pressure Degradation

		Callaway Just Before Chem Clean			Callaway After CC (1/96-4/96)			Sequoyah 1 Just Before Chem Clean			Sequoyah 1 After CC (3/96-5/96)			South Texas 1 (2/96-6/96)			SONGS 2 Just Before CC		
Steam generator type		Westinghouse Model F						Westinghouse Model 51						W Model E2			CE Model 3410		
Current EFPYs		8.63			9.54			7.49			7.91			5.02			10.02		
Design plugging margin for heat transfer		0%						0%						0%			10%		
Current plugging level		0.63%			0.80%			1.32%			2.53%			1.32%			3.70% (EOC 8)		
Current fouling factor (10^{-6} h-ft^2-°F/Btu)		-28 ± 19			-5 ± 19 (1)			21 ± 24			42 ± 24 (1)			30 ± 62			172 ± 48		
Nominal design dome pressure (psia)		1000						857						1100			900		
Design start-up dome pressure (psia)		1009						878						1106			941		
Actual start-up dome pressure (psia)		1003						877						1115			933		
Current dome pressure (psia)		986			975			852			841			1052			855		
Current total pressure loss vs. Initial Perf. (psi)		17			28			25			36			63			77		
Deposit Fouling Factors from Local Heat Transfer Analyses (10^{-6} h-ft^2-°F/Btu)		Lower Bound	Best Estimate	Upper Bound	Lower Bound	Best Estimate	Upper Bound	Lower Bound	Best Estimate	Upper Bound	Lower Bound	Best Estimate	Upper Bound	Lower Bound	Best Estimate	Upper Bound	Lower Bound	Best Estimate	Upper Bound
Secondary freespan deposits		-30.0	-15.0	0.0	2.4	9.7	29.1	-15.0	28.8	107.0	2.4	9.7	29.1	-15.0	0.0	5.0	51.1	185.1	363.6
Secondary flow blockage and extra friction	lower recirc ratio (2)	-5.8	5.3	17.8	flow paths open & little extra friction			-11.2	0.0	11.2	flow paths open & little extra friction			-4.3	0.0	4.3	-4.5	6.0	19.5
	greater Δp in bundle	(3)						(3)						(3)			(3)		
Primary deposits		0.4	2.1	30.9	0.4	2.1	30.9	0.4	2.1	30.9	0.4	2.1	30.9	0.4	2.1	30.9	0.4	2.1	31.4
Total (10^{-6} h-ft^2-°F/Btu)		*-35.4*	*-7.6*	*48.8*	*2.8*	*11.8*	*60.1*	*-25.8*	*30.8*	*149.1*	*2.8*	*11.8*	*60.0*	*-18.8*	*2.1*	*40.1*	*47.0*	*193.2*	*414.5*
SOURCES OF PRESSURE LOSS (psi)		Lower Bound	Best Estimate	Upper Bound	Lower Bound	Best Estimate	Upper Bound	Lower Bound	Best Estimate	Upper Bound	Lower Bound	Best Estimate	Upper Bound	Lower Bound	Best Estimate	Upper Bound	Lower Bound	Best Estimate	Upper Bound
Sources That Affect Initial Performance vs. Ideal Design Performance (But Not Pressure Loss Since Start-Up)																			
Pre-service tube plugging		0.3	0.3	0.3	0.3	0.3	0.3	0.0	0.0	0.0	0.0	0.0	0.0	0.1	0.1	0.1	0.4	0.4	0.4
Initial RCL temps. different than design		-0.6	8.6	17.8	-0.6	8.6	17.8	-5.1	6.8	18.6	-5.1	6.8	18.6	-49.3	-13.8	21.7	-23.8	-1.5	20.8
Primary tube velocity different than design		-4.0	-3.1	-1.7	-5.2	-2.9	-0.5	-0.4	1.1	2.7	-0.4	1.1	6.9	-3.4	-2.2	-0.3	-5.8	-3.5	-2.9
Tube thickness variation from nominal		-12.3	0.0	12.5	-12.3	0.0	12.5	-15.2	0.0	15.4	-15.2	0.0	15.4	-8.6	0.0	8.7	-16.1	0.0	16.3
Tube thermal cond. variation from nominal		-5.5	0.0	6.1	-5.5	0.0	6.1	-6.8	0.0	7.6	-6.8	0.0	7.6	-3.9	0.0	4.3	-7.2	0.0	8.0
Subtotal (psi) (not included in Total below)		*-22.2*	*5.8*	*35.0*	*-23.3*	*6.0*	*36.2*	*-27.5*	*7.9*	*44.3*	*-27.5*	*7.9*	*48.4*	*-65.2*	*-15.9*	*34.5*	*-52.5*	*-4.6*	*42.5*
Sources That are Due to Deposits within the Tube Bundle																			
Secondary freespan deposits		-10.8	-5.4	0.0	0.9	3.5	10.5	-5.3	10.3	38.2	0.9	3.5	10.4	-3.5	0.0	1.2	19.8	71.9	141.2
Secondary flow blockage and extra friction	lower recirc ratio (2)	-2.1	1.9	6.4	flow paths open & little extra friction			-4.0	0.0	4.0	flow paths open & little extra friction			-1.0	0.0	1.0	-1.7	2.3	7.5
	greater Δp in bundle	(3)						(3)						(3)			(3)		
Primary deposits		0.1	0.7	11.2	0.1	0.7	11.2	0.1	0.7	11.0	0.1	0.7	11.0	0.1	0.5	7.3	0.2	0.8	12.2
Subtotal (psi)		*-12.8*	*-2.7*	*17.6*	*1.0*	*4.3*	*21.7*	*-9.2*	*11.0*	*53.2*	*1.0*	*4.2*	*21.4*	*-4.4*	*0.5*	*9.4*	*18.3*	*75.0*	*160.8*
Sources That are NOT Due to Deposits within the Tube Bundle which are Captured in the Fouling Factor Calculation																			
Uncertainty in steam generator press. meas.		-6.5	0.0	6.5	-6.5	0.0	6.5	-4.8	0.0	4.8	-4.8	0.0	4.8	-7.5	0.0	7.5	-6.0	0.0	6.0
Extra separator/dryer pressure drop		3.5	4.0	4.4	3.5	4.0	4.4	0.0	0.0	4.0	0.0	0.0	4.0	0.0	0.0	13.0	0.0	4.0	13.0
Error in applied primary temperature due to	$T_{cold/ave}$ meas. error	-4.6	0.0	4.6	-4.6	0.0	4.6	-5.9	0.0	5.9	-5.9	0.0	5.9	-17.8	0.0	17.8	-22.3	0.0	22.3
	Hot leg streaming	0.0	4.0	5.9	0.0	4.0	5.9	0.0	14.7	22.0	0.0	14.7	22.0	0.0	12.9	25.9	T_{cold} control plant		
	Divider plate leakage	0.00	0.02	2.4	0.00	0.02	2.4	0.00	0.02	2.3	0.00	0.02	2.3	0.00	0.03	2.8	0.00	0.04	3.9
Error in reactor power calibration due to uncertainty in	FW flow including venturi fouling	-2.2	0.0	3.9	-2.2	0.0	3.9	-2.2	0.0	4.1	-2.2	0.0	4.1	-1.6	0.0	3.2	-1.9	0.5	3.8
	FW temperature	-0.5	0.0	0.5	-0.5	0.0	0.5	-0.8	0.0	0.8	-0.8	0.0	0.8	-0.5	0.0	0.5	-0.8	0.0	0.8
	Outlet steam quality	-0.5	0.0	0.5	-0.5	0.0	0.5	-0.5	0.0	0.5	-0.5	0.0	0.5	-0.4	0.0	0.4	-0.3	0.0	0.3
	Blowdown flow	-0.02	0.0	0.02	-0.02	0.0	0.02	-0.2	0.0	0.2	-0.2	0.0	0.2	-0.2	0.0	0.2	-0.01	0.0	0.0
Subcooling (feedwater temp. variations) (2)		-2.1	-0.7	0.0	-10.1	-3.4	0.0	-2.0	0.0	2.0	-1.0	0.0	1.0	-1.0	0.0	1.0	-4.3	-1.4	0.0
Flow maldistribution in preheater														0.0	3.0	15.0			
Subtotal (psi)		*-12.9*	*7.2*	*28.8*	*-20.9*	*4.5*	*28.8*	*-16.4*	*14.7*	*46.6*	*-15.4*	*14.7*	*45.6*	*-28.9*	*16.0*	*87.2*	*-35.6*	*3.1*	*50.1*
Apparent fouling factor corresponding to this pressure loss (10^{-6} h-ft^2-°F/Btu)		*-36*	*20*	*80*	*-58*	*13*	*80*	*-46*	*41*	*131*	*-43*	*41*	*128*	*-123*	*68*	*371*	*-92*	*8*	*129*
Net fouling factor after subtracting this component (10^{-6} h-ft^2-°F/Btu)		*8*	*-48*	*-108*	*53*	*-18*	*-85*	*66*	*-21*	*-110*	*85*	*1*	*-86*	*153*	*-38*	*-341*	*264*	*164*	*43*
Sources That are Accounted for by the Fouling Factor Calculation																			
Tube plugging since start-up		1.2	1.2	1.2	1.6	1.6	1.6	3.6	3.6	3.6	6.9	6.9	7.0	1.5	1.5	1.5	11.6	11.7	11.8
T_{cold}/T_{ave} variations vs. design temperatures		4.5	9.1	13.7	6.9	11.5	16.1	0.7	6.6	12.5	1.4	7.3	13.3	20.2	37.9	55.7	-28.2	-5.9	16.3
T_{cold}/T_{ave} variations vs. initial temperatures		-3.8	0.8	5.4	-1.3	3.3	7.9	-5.9	0.0	5.9	-5.2	0.7	6.7	33.9	51.7	69.5	-26.7	-4.5	17.8
Variations in thermal power		-4.5	-3.6	-2.7	-3.6	-2.7	-1.8	-3.7	-2.8	-1.9	-2.8	-1.9	-0.9	-1.6	-0.8	0.0	-1.3	-0.7	0.0
Power uprate		13.9	15.4	17.0	13.9	15.4	17.0	No Uprate			No Uprate			No Uprate			No Uprate		
Subtotal vs. Design (psi)		*15.1*	*22.1*	*29.2*	*18.8*	*25.9*	*32.9*	*0.5*	*7.4*	*14.3*	*5.5*	*12.4*	*19.3*	*20.0*	*38.6*	*57.2*	*-17.9*	*5.1*	*28.2*
Subtotal vs. Initial Perf. (psi)		*6.8*	*13.9*	*20.9*	*10.6*	*17.7*	*24.7*	*-6.1*	*0.8*	*7.7*	*-1.1*	*5.8*	*12.7*	*33.8*	*52.4*	*70.9*	*-16.4*	*6.6*	*29.7*
Summary																			
Best-Est. Total Loss vs. Design New (psi) (4)		***27***			***35***			***33***			***31***			***55***			***83***		
Actual Total Loss vs. Design New (psi)		***23***			***34***			***26***			***37***			***54***			***85***		
Best-Est. Total Loss vs. Initial Perf. (psi) (4)		***18***			***26***			***27***			***25***			***69***			***85***		
Actual Total Loss vs. Initial Perf. (psi)		***17***			***28***			***25***			***36***			***63***			***77***		

(1) The fouling factor has been decreasing at Callaway and Sequoyah 1 since just after chemical cleaning. Callaway's has decreased about 11 10^{-6} and Sequoyah's has decreased about 4 10^{-6}.
(2) The values for Callaway and SONGS 2 are preliminary results of a one-dimensional heat transfer model of the steam generator using the Chen correlation for secondary resistance. The values for Sequoyah 1 and South Texas 1 are estimates based on engineering judgment.
(3) This effect may be evaluated using ATHOS modeling.
(4) These estimates include calculated pressure losses due to secondary deposits based on available tube scale characterization data.

Table 6-5
Example Hot-Leg Streaming Calculation

Instrument Readings	T_{hot}	T_{ave}	T_{cold}
No HL Streaming	600	570	540
HL Streaming (Transient)	604	572	540
HL Streaming (Steady-State)	602	570	538
Net Change	2	0	-2

Actual Temperatures			
No HL Streaming	600	570	540
HL Streaming (Transient)	600	570	540
HL Streaming (Steady-State)	598	568	538
Net Change	-2	-2	-2

Table 6-6
Summary of Pressure Loss Breakdowns

Cause	Callaway		Sequoyah 1		South Texas 1	SONGS 2
	Before CC	After CC	Before CC	After CC	Mid-1996	Before CC
Tube Plugging	1.2	1.6	3.6	6.9	1.5	11.7
Power Uprate	15.4	15.4	0.0	0.0	0.0	0.0
Primary Temp. Variation	0.8	3.3	0.0	0.7	51.7	-4.5
Secondary Tube Fouling	-5.4	3.5	10.3	3.5	0.0	71.9
Hot-Leg Streaming	4.0	4.0	14.7	14.7	12.9	0.0
Addit'l Separator/Dryer ΔP	4.0	4.0	0.0	0.0	0.0	4.0
Balance[1]	-3.0	-3.4	-3.4	10.5	-3.6	-6.0
Total Loss (psi)	17.0	28.4	25.2	36.3	62.5	77.1

[1] This category represents the pressure loss (or gain, if negative) required to make the total agree with the actual observed loss. It includes the sum of other minor causes shown in Table 6-4 that are not explicitly listed here. It also includes the error associated with any of the attributed causes (e.g., based on the restart pressure after chemical cleaning, the SONGS 2 tube scale was likely only responsible for about 57 psi of pressure loss rather than the estimated 72).

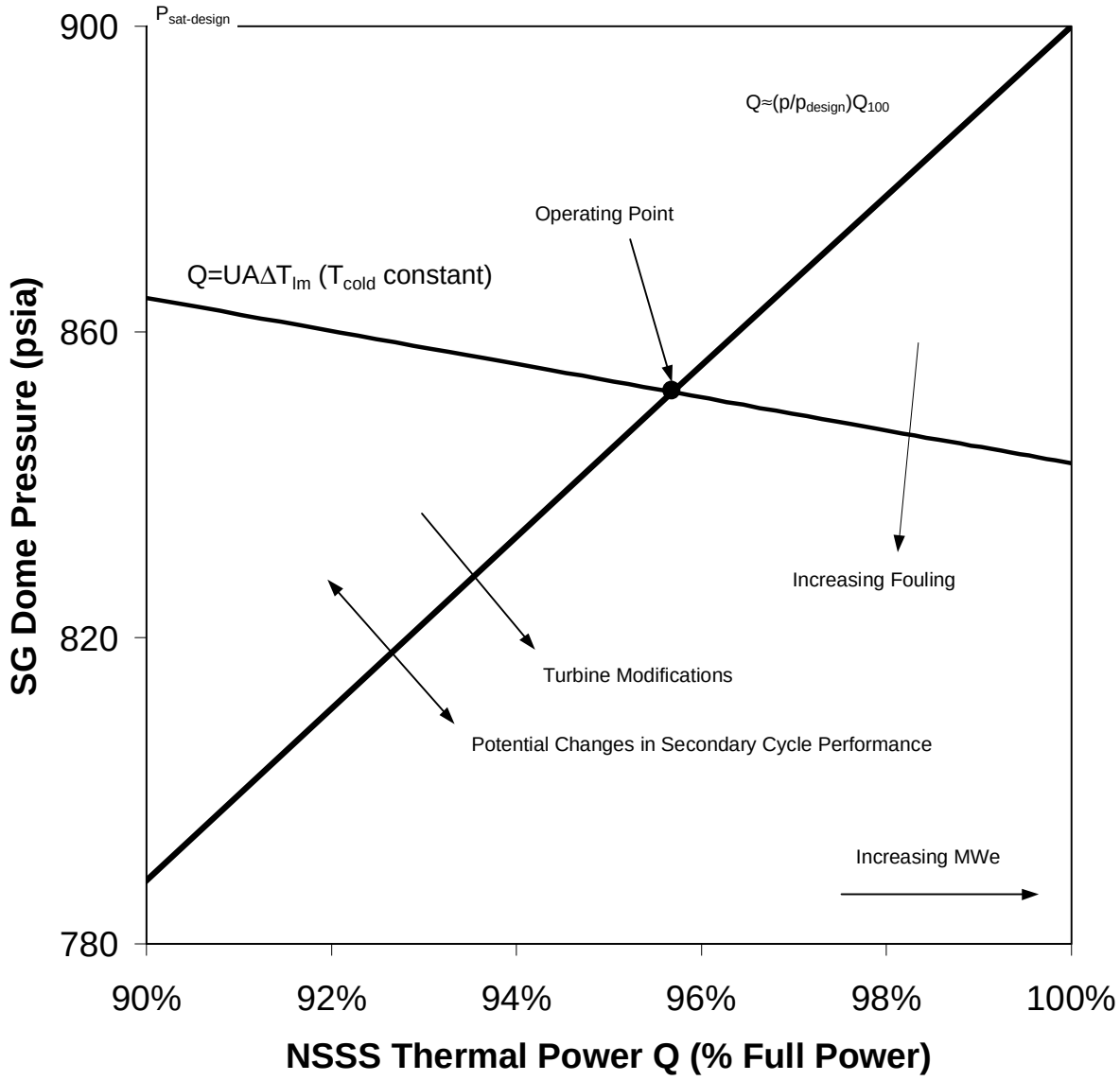

Figure 6-1
Relationship Between SG Pressure and Thermal Power at SONGS 3

7

PLANT COMPARISONS

The purpose of this chapter is to compare the key results presented in the preceding chapters on a plant-by-plant basis. The most noteworthy similarities and differences are discussed.

Callaway (Westinghouse Model F)

The fouling factor analysis described in Chapter 4 indicated that Callaway actually experienced a slight decrease in the fouling factor since the beginning of plant life. The computed values were

- Just Before Chemical Cleaning: $-28 \pm 19\ 10^{-6}$ h-ft^2-°F/BTU
- After Chemical Cleaning (April 1996): $-5 \pm 19\ 10^{-6}$ h-ft^2-°F/BTU

These values are suggestive of heat-transfer enhancing secondary deposits. However, over the same time periods, Callaway recorded respective pressure decreases of 17 psi (before chemical cleaning) and 28 psi (after cleaning). These two seemingly contradictory behaviors may be rectified by examining Figure 7-1, which displays the time histories of both steam pressure and fouling factor.* Note that the gradual decrease in fouling factor over the first two cycles is matched by an increase in steam pressure of nearly 30 psi over the same time span. Both of these changes are consistent with heat-transfer-enhancing tube scale. The 15-psi drop coincident with Callaway's power uprate is not matched by any step changes in the fouling factor, as would be expected. Much of the subsequent decrease in steam pressure during Cycles 5 and 6 correlates with an increase in the fouling factor over the same time period, which may reflect thicker and/or more resistive tube scale. The step increase in the fouling factor that occurred following the chemical cleaning is consistent with the calculated net fouling factor at that point (i.e., $-28\ 10^{-6}$). One other noteworthy feature of the Callaway fouling history is the reduction in fouling rate that occurs at about 6.3 EFPY, coincident with the introduction of ETA as a feedwater additive and the implementation of PPC in

* The dark lines in Figures 7-1, 7-4, 7-5, and 7-7 are "eyeball" curve fits used to more clearly show the trends of pressure and fouling factor. The curve fits remove the substantial scatter from the actual data, making it easier to interpret.

1992. As shown in Figure 7-2, ETA reduced the average iron feedwater concentration from about 10 ppb to 3 or 4 ppb. It is unclear whether ETA (or PPC performed during the same outage) caused the reduction in fouling rate, although the available data suggest this as a possibility.

Note in Figure 7-1 that there is not a marked step decrease in steam pressure following chemical cleaning as might be expected if heat-transfer-enhancing deposits were removed.* However, variations of primary temperature may provide an explanation for this behavior. In Figure 7-3, which shows the history of primary temperature at Callaway, it is apparent that greater disparities exist among the four loops just prior to the chemical cleaning compared to immediately afterwards. As discussed on p. 8-4, disparities in temperature among the loops will cause a reduction in steam pressure if an auctioneer control system (i.e., a system controlling the maximum T_{ave}) is used. Recovery of such a loss at Callaway following chemical cleaning may explain why a more obvious step decrease in steam pressure was not observed.

Further confirmation that secondary deposits were not responsible for steam pressure loss at Callaway is provided by adding up the pressure decreases due to other well-known factors. Per Table 6-6, well-known sources of pressure loss can fully account for the observed pressure decrease over the life of the plant:

Power Uprate	15 psi
Hot-Leg Streaming	4 psi
Additional Separator/Dryer Pressure Drop	4 psi
Tube Plugging (Pre-CC/Post-CC)	1/2 psi
Reported Primary Temperature Variation (Pre-CC/Post-CC)	1/3 psi
Total - Well-Known Causes (Pre-CC/Post-CC)	**25/28 psi**
Actual Observed Loss (Pre-CC/Post-CC)	**17/28 psi**

The total prior to chemical cleaning (25 psi) is 8 psi *greater* than the actual loss observed between initial start-up and chemical cleaning. The total for recent operation (28 psi) is equal to the actual loss (28 psi), suggesting that tube scale at Callaway currently does not have a significant impact on heat transfer. Clearly, Callaway's small margin for performance loss, made smaller by the power uprate, makes recovery of the relatively small amounts of pressure loss listed above critical for maintaining 100% reactor power.

* Although not easily discernible from Figure 7-1, SGs C and D do exhibit steam pressure decreases following chemical cleaning. See Chapter 8 under the heading "Pressure and Fouling Factor Transients."

Sequoyah 1 (Westinghouse Model 51)

At first glance, the behavior of the Sequoyah 1 SGs would appear to differ from that at Callaway. Unlike Callaway, the Sequoyah 1 net fouling factor was positive, both just prior to chemical cleaning and recently:

- Just Before Chemical Cleaning: $21 \pm 24\ 10^{-6}$ h-ft^2-°F/BTU
- After Chemical Cleaning (May 1996): $42 \pm 24\ 10^{-6}$ h-ft^2-°F/BTU

Although Sequoyah 1 has experienced a net increase in fouling factor, inspection of the steam pressure and fouling factor histories in Figure 7-4* shows a trend similar to Callaway, although not as pronounced. Note the slight decrease in fouling factor during the first cycle which corresponds to a slight increase in SG steam pressure. Until Cycle 6, the fouling factor remained negative (and nearly constant), while steam pressure remained nearly constant at a level slightly above the design pressure. These trends are both consistent with heat-transfer enhancing tube scale similar to that believed to have been present at Callaway. However, the decrease in fouling factor (about $30\ 10^{-6}$ vs. over $60\ 10^{-6}$ at Callaway) and increase in pressure (10–15 psi compared to 30 psi at Callaway) suggest that the Sequoyah 1 scale did not enhance heat transfer as dramatically as the Callaway scale. Starting in Cycle 5 and continuing until the present, the fouling factor began to increase and the steam pressure decrease. Upon chemical cleaning at EOC 7, there is perhaps a slight step increase in the fouling factor (Callaway also experienced a step increase in the fouling factor, albeit a larger one). Although this increase is suggestive of tube scale deposits that are slightly heat-transfer enhancing, the amount of the increase is small, making this conclusion uncertain.

To see if the sum of pressure decreases due to other causes supports the idea of heat-transfer enhancing deposits, we consult Table 6-6. For Sequoyah 1, the only significant well-known causes of pressure loss are hot-leg streaming and tube plugging, with a reported primary temperature decrease playing a small role during recent operation. Per Table 6-6, we have the following balance sheet:

Hot-Leg Streaming	15 psi
Tube Plugging (Pre-CC/Post-CC)	4/7 psi
Reported Primary Temperature Variation (Pre-CC/Post-CC)	0/1 psi
Total - Well-Known Causes (Pre-CC/Post-CC)	**19/23 psi**
Actual Observed Loss (Pre-CC/Post-CC)	**25/36 psi**

* The fouling factor plot in Figure 7-4 is identical to Figure 4-19d; operation since the beginning of Cycle 5 reflects a 2°F correction to T_{ave} for hot-leg streaming.

In this case, the total prior to chemical cleaning (19 psi) is 6 psi smaller than the actual observed loss (25 psi). During recent operation, the gap is even larger (13 psi). Coupled with the deposit characterization data in Chapter 5—which indicate a fairly dense inner layer of 2–3 mils covering some portion of the bundle—this unexplained pressure loss suggests that slightly to moderately resistive, rather than enhancing, deposits were present prior to the chemical cleaning (best estimate of +29 10^{-6} as indicated in Chapter 5).

However, if resistive deposits were present prior to the cleaning, then the increase in fouling factor after the cleaning remains unexplained. One possible reason for this increase is a cyclic change in the degree of hot-leg streaming. That is, core changes during the chemical cleaning outage may have worsened the hot-leg temperature error, causing a temporary increase in the apparent fouling factor that offset any decrease due to removal of slightly resistive deposits.*

Although this scenario is plausible, it should be noted that the uncertainties inherent in both the fouling factor calculation and the assignment of pressure loss values to each possible cause (reflected by the bounding values in Table 6-4) make it impossible to be sure whether the tube scale at Sequoyah 1 before chemical cleaning (and even afterwards) was slightly thermally resistive or had essentially no effect. However, all available fouling factor data indicate that these deposits were not highly thermally resistive.

South Texas 1 (Westinghouse Model E2)

The performance of the SGs at South Texas 1 is markedly different from that observed at both Callaway and Sequoyah 1. As shown in Figure 7-5, steam pressure has remained relatively constant except for two transients associated with primary temperature control and several other short-lived transients. Beginning in Cycle 6, the average primary temperature was reduced a nominal 4°F in order to slow the rates of incipient tube degradation that had begun to be observed. As discussed in Chapter 6, this resulted in a large steam pressure decrease (over 50 psi). As expected, the fouling factor exhibited no step change with the reduction in T_{ave}. In August 1995 (about 4.2 EFPY), a second, smaller primary temperature decrease resulted from a change in the control scheme. Prior to this time, HL&P used an algorithm that controlled the average value of T_{ave} across all four loops to be within the desired temperature range. Since the change to "auto-rod control," the maximum (or auctioneer) T_{ave} is controlled to be within the desired range. As is evident from Figure 7-6, there is a significant difference between the maximum T_{ave} and the other three loops. This asymmetry, combined with

* Although the long-term effect of streaming is believed to have been 15 psi, short-term variations are probable based on cyclic changes to the core.

the new control scheme, causes the overall average primary temperature to decrease (in this case by at least 1°F), resulting in a further steam pressure decrease, which is evident in Figure 7-5. Again as expected, the fouling factor does not reflect any step change associated with the adjustment in primary temperatures.

While not affected by primary temperature changes, the fouling factor at South Texas 1 does exhibit several noteworthy features, discussed in more detail below:

1. Unlike Callaway and Sequoyah 1, it does not show a noticeable decrease during the first one or two cycles.*

2. The initial value is over 100 10^{-6} h-ft^2-°F/BTU.

3. There is a modest net increase of about 30 ± 62 10^{-6} between early and recent operation.

4. There are significant transient swings (particularly noticeable in Cycle 4 and at the end of Cycle 5). Corresponding steam pressure transients also seem to be present.

NO FOULING FACTOR DECREASE. The lack of a decrease in the early fouling factor suggests that heat-transfer enhancing deposits were not present at South Texas 1. This is corroborated by tube scale thickness measurements made in 1993; with an average thickness of less than 0.5 mils, the South Texas 1 deposits probably had little long-term effect on heat transfer prior to 1993.

LARGE POSITIVE INITIAL FOULING FACTOR. The initial value of the fouling factor suggests that the initial thermal resistance of the SGs was larger than predicted by the Westinghouse design values. This conclusion is supported by early primary temperature measurements, which indicate early T_{hot} values of 626°F (equal to design) and early T_{cold} values of 562.5°F (almost 3°F higher than the design value). Coupled with the fact that the actual average SG pressure, and hence the secondary fluid temperature, were close to the design values, the higher-than-design T_{cold} value indicates that the SGs were less efficient at removing heat from the primary coolant than the design value suggests it should have been.

SLIGHT RECENT INCREASE IN FOULING FACTOR. The slight increase in fouling factor since startup has taken place mostly over the past cycle or two. To see if this increase can be attributed to secondary deposits, let us make a summary of well-known causes of pressure decrease at STP 1 (based on Table 6-6):

---

* Note, however, that there are significant periods of missing data, including more than half of Cycle 1 and all of the short Cycle 3.

Reported Primary Temperature Variation	52 psi
Tube Plugging	2 psi
Total - Well-Known Causes	**54 psi**
Actual Observed Loss	**63 psi**

The shortfall of 9 psi is most likely due chiefly to hot-leg streaming (best-estimate of 13 psi loss), although it could be caused in part by some combination of the sources discussed in Chapter 6, including secondary deposits. (Since tube scale measurements were taken in 1993, it is possible that in the interim the deposits have thickened and/or changed structure in order to become thermally resistive.)

FOULING FACTOR AND PRESSURE TRANSIENTS. From Figure 7-5, there appear to be at least two noticeable transients in the fouling factor behavior which are mirrored by the steam pressure. At about 2.2 EFPY and again at about 3.9 EFPY, the fouling factor exhibits an increase of about 50 10^{-6} h-ft^2-°F/BTU and a subsequent decrease of nearly the same magnitude. In each case, the steam pressure exhibits a transitory decrease of 15-20 psi.* The cause of these transients (and others that may not be discernible in the figure due to data scatter, missing data, or the frequency of reported data) is not known.

Perhaps the most likely explanation is cyclic changes in hot-leg streaming (and thus in the apparent fouling factor) due to changes in core flow patterns following refueling or a reactor trip. Refueling introduces significant changes to the core which may have a significant effect on the amount of hot-leg streaming experienced at any particular time. While reactor trips do not coincide with intentional changes to the fuel assemblies, the cool-down and heat-up transients may alter (or result in the removal of) the oxide layers present on the fuel cladding. Such changes may also cause a difference in the degree of hot-leg streaming.

A second possible explanation for such transients that often occur immediately following an outage or even a reduction in power that has been proposed at industry conferences is partial secondary deposit exfoliation (33). During a plant restart (or power increase), it is possible that some portion of the secondary deposits become partially detached from the tube surfaces but do not fall off. The resulting space between the tube and the deposit can then become steam filled. If this steam is stagnant, the associated thermal resistance can be quite large. As shown in Appendix B, a 1-mil annular gap filled with stagnant steam covering only 4% of the tube OD surface area is sufficient to cause a 20 psi pressure decrease at South Texas 1. While there is no direct evidence that this phenomenon is taking place, the values indicate that it is plausible. (Note that there were significant power reductions just prior to both

* Note that the pressure "recovery" associated with the second transient is difficult to see from Figure 7-5 due to the effects of the primary temperature decrease in Cycle 6.

of the noticeable transients in Figure 7-5. A more complete set of fouling factor data for STP 1 would be required in order to strengthen any such correlation between fouling transients and plant transients.)

PREHEATER ISSUES. No information was available regarding the specific performance of the South Texas 1 preheaters. It is possible that the transients discussed above are in part caused by tube surface fouling and/or baffle plate clogging (and partial or complete unfouling/unclogging) in the preheater area. Because the performance of preheater SGs is sensitive to changes in the distribution of flow within the preheater, even modest amounts of fouling or clogging in that area might cause significant changes in the overall heat-transfer coefficient (and hence in the steam pressure).

SONGS 2 (CE Model 3410)

For the purpose of comparing the fouling and pressure loss behavior at different plants, the results for SONGS 2 are also discussed in this chapter. Note that a similar analysis was also performed for SONGS 3. Because the results were so similar at the two plants, only SONGS 2 is discussed here for the sake of brevity. As was indicated in Table 6-4, the calculated fouling factor over the life of SONGS 2 prior to chemical cleaning was $172 \pm 48\ 10^{-6}$ h-ft^2-°F/BTU. In contrast to the situation with the other plants in this study, the computed fouling factor for SONGS 2 is significantly larger than the uncertainty band. The steam pressure and fouling factor histories for SONGS 2 are shown in Figure 7-7. Like Callaway and Sequoyah 1, there is a significant decrease in the fouling factor and a concomitant increase in steam pressure evident in Cycle 1. Unlike those plants, however, the fouling factor then increases far beyond the initial decrease, accompanied by a corresponding decrease in steam pressure. Both of these trends are steady over the length of at least five cycles of operation. Absent any other information, the data in Figure 7-7 are strongly suggestive of thermally resistive secondary tube deposits.

To confirm that secondary deposits are likely to have been the primary cause of the steam pressure decrease at SONGS prior to the 1996–97 chemical cleaning, we tabulate the well-known causes of pressure loss from Table 6-6:

Tube Plugging	12 psi
Reported Primary Temperature Variation	-5 psi
Total - Well-Known Causes	**7 psi**
Actual Observed Loss	**77 psi**

Clearly, this situation is far different from Callaway, Sequoyah 1, and South Texas 1. In this case, about 70 psi cannot be readily accounted for unless secondary tube deposits are largely responsible. In fact, tube characterization studies on SONGS 2 tube scale

flakes are wholly consistent with this conclusion. SONGS 2 tube scale averaged 11 mils thick (compared to 3.5 mils at Callaway, 5–6 mils at Sequoyah 1 (1995), and <0.5 mils at South Texas 1 (1993)). In addition, the SONGS 2 scale exhibited three distinct sub-layers:

- An inner copper-rich layer with almost no porosity.
- A middle porous layer with enclosed voids.
- An outer porous layer subject to the wick boiling mechanism.

This evidence suggests that the two inner layers are quite thermally resistive and therefore responsible for the bulk of the unaccounted-for 70 psi listed above. Confirmation of this conclusion came in early 1997 upon the SONGS 2 restart after chemical cleaning of the SGs. After this outage, the average steam pressure increased by 51 psi compared to August 1996 (see Reference (2) for additional details).* This increase is the largest recorded for a US PWR after chemical cleaning and verifies that in some cases, secondary deposits can cause substantial SG thermal performance degradation.

* After correcting for approximately 6 psi of steam pressure loss due to tube plugging during this outage, the actual pressure increase due to deposit removal was closer to 57 psi.

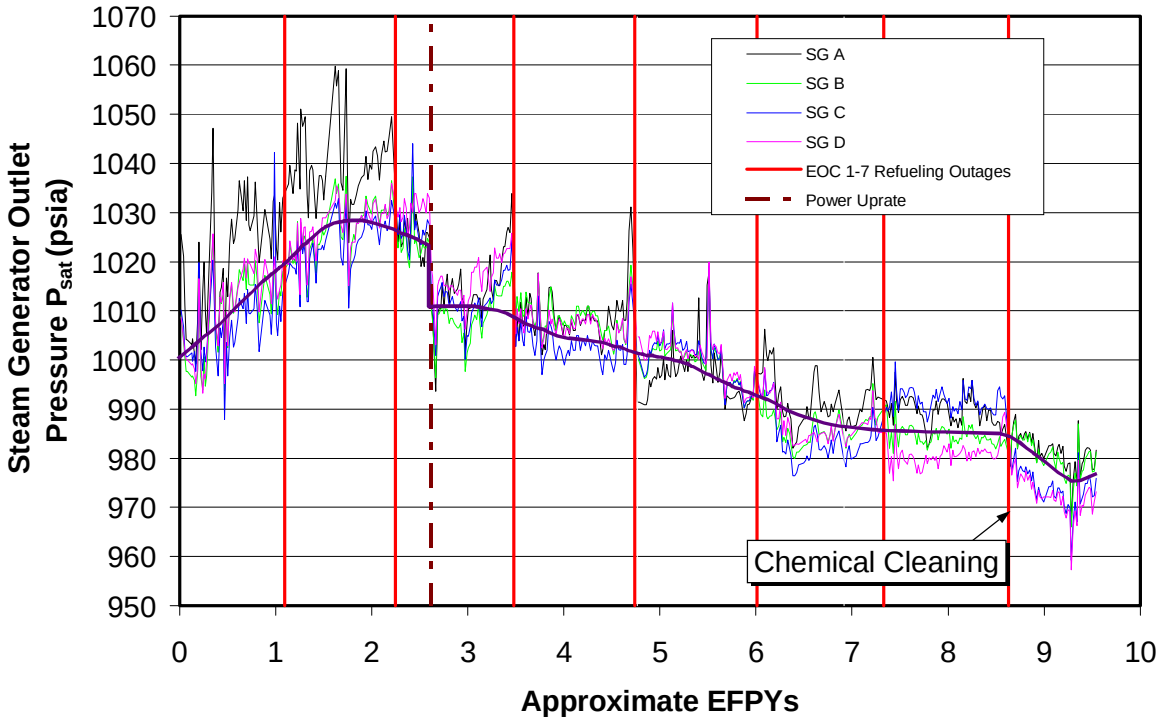

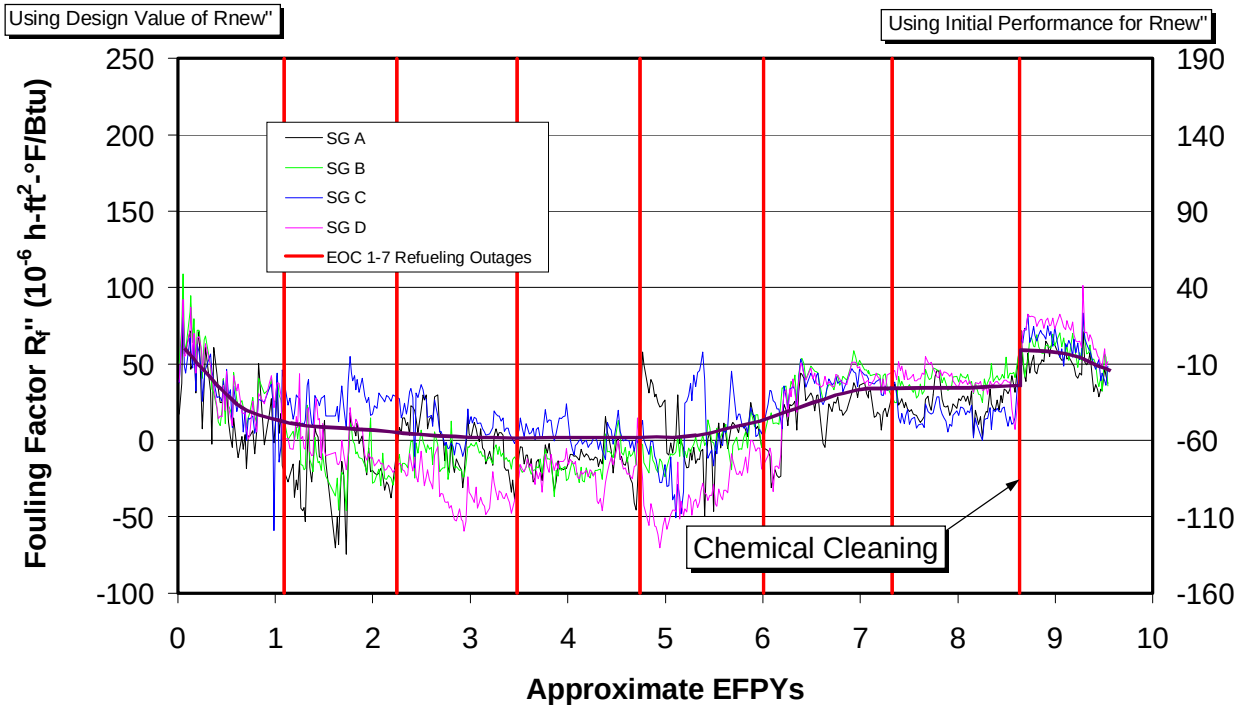

Figure 7-1
Steam Pressure and Fouling Trends at Callaway

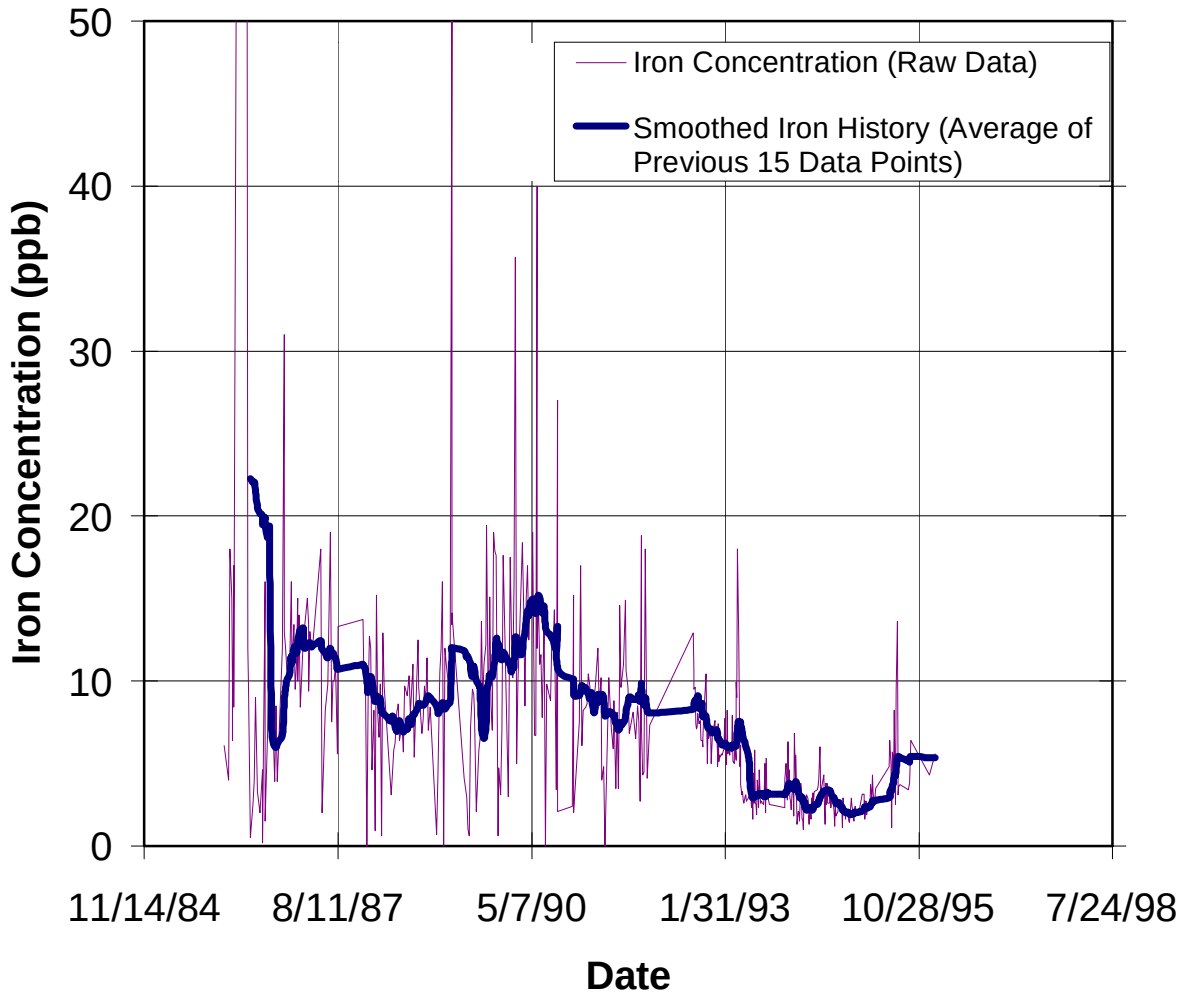

Figure 7-2
Historical Feedwater Iron Transport at Callaway

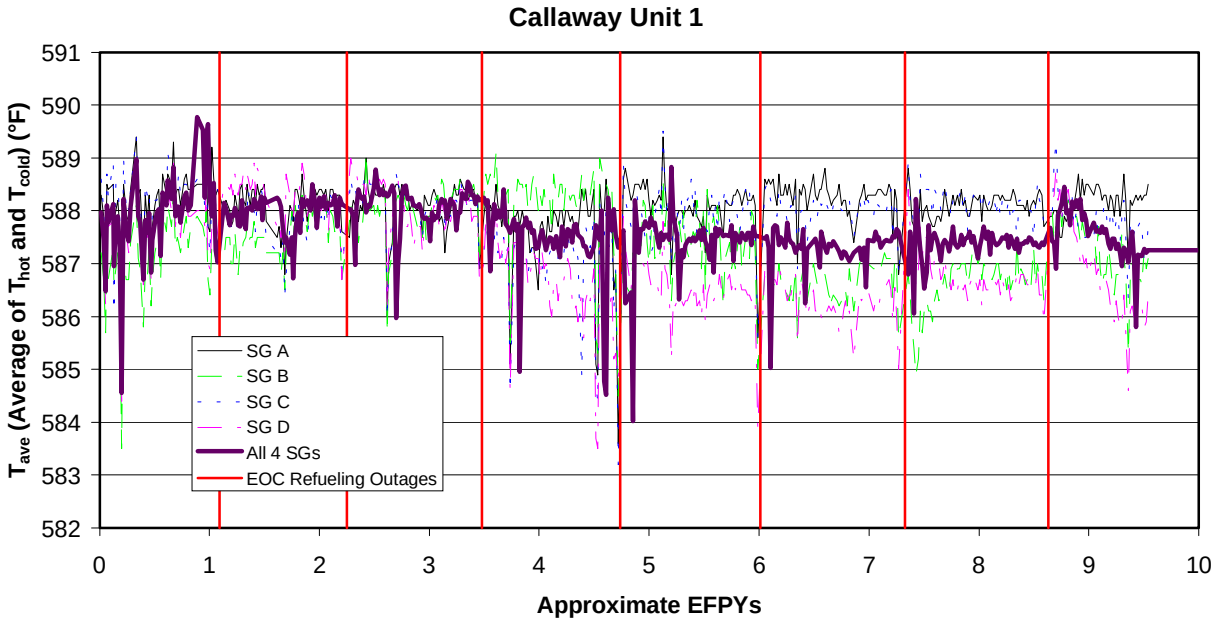

Figure 7-3
Historical Average of Hot and Cold Leg Temperatures at Callaway

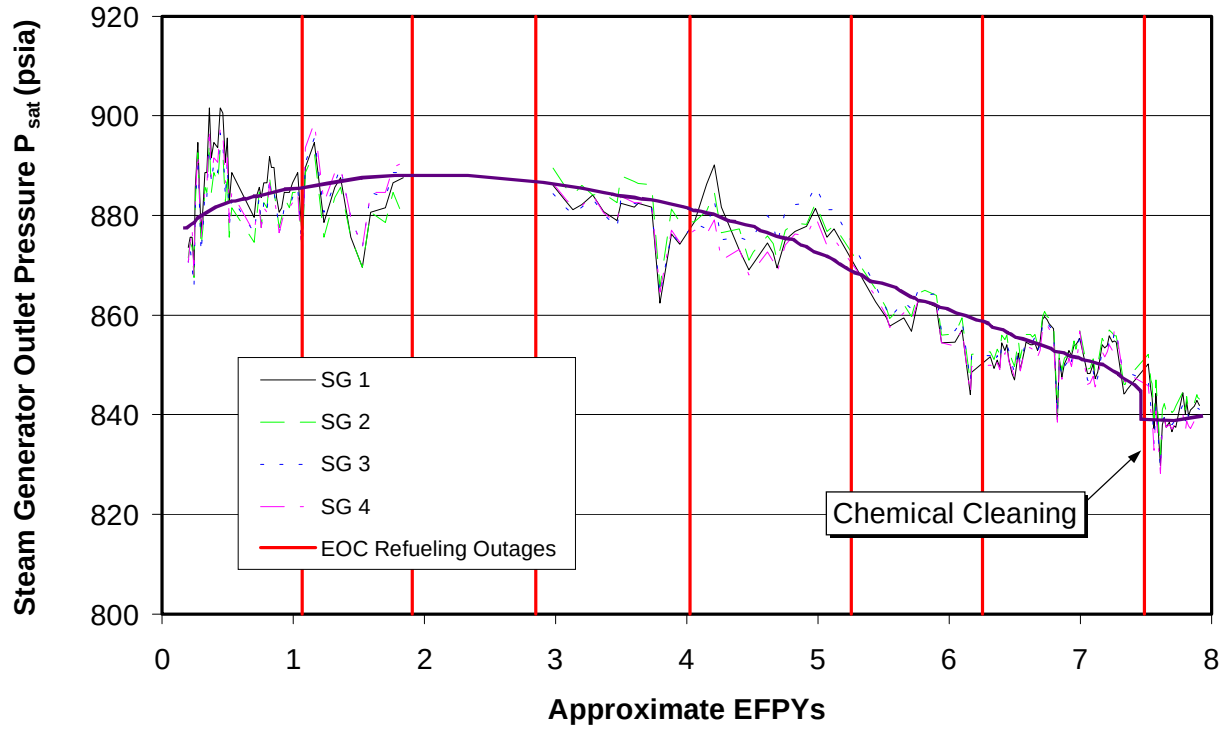

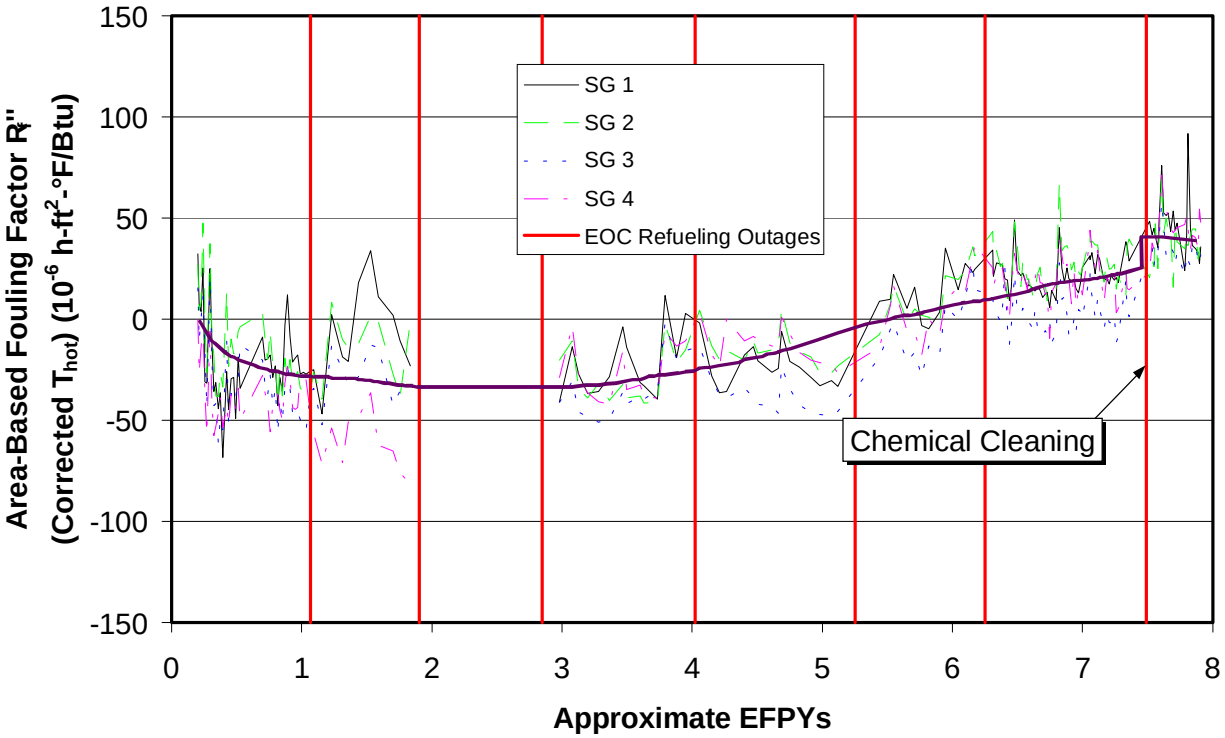

Figure 7-4
Steam Pressure and Fouling Trends at Sequoyah 1

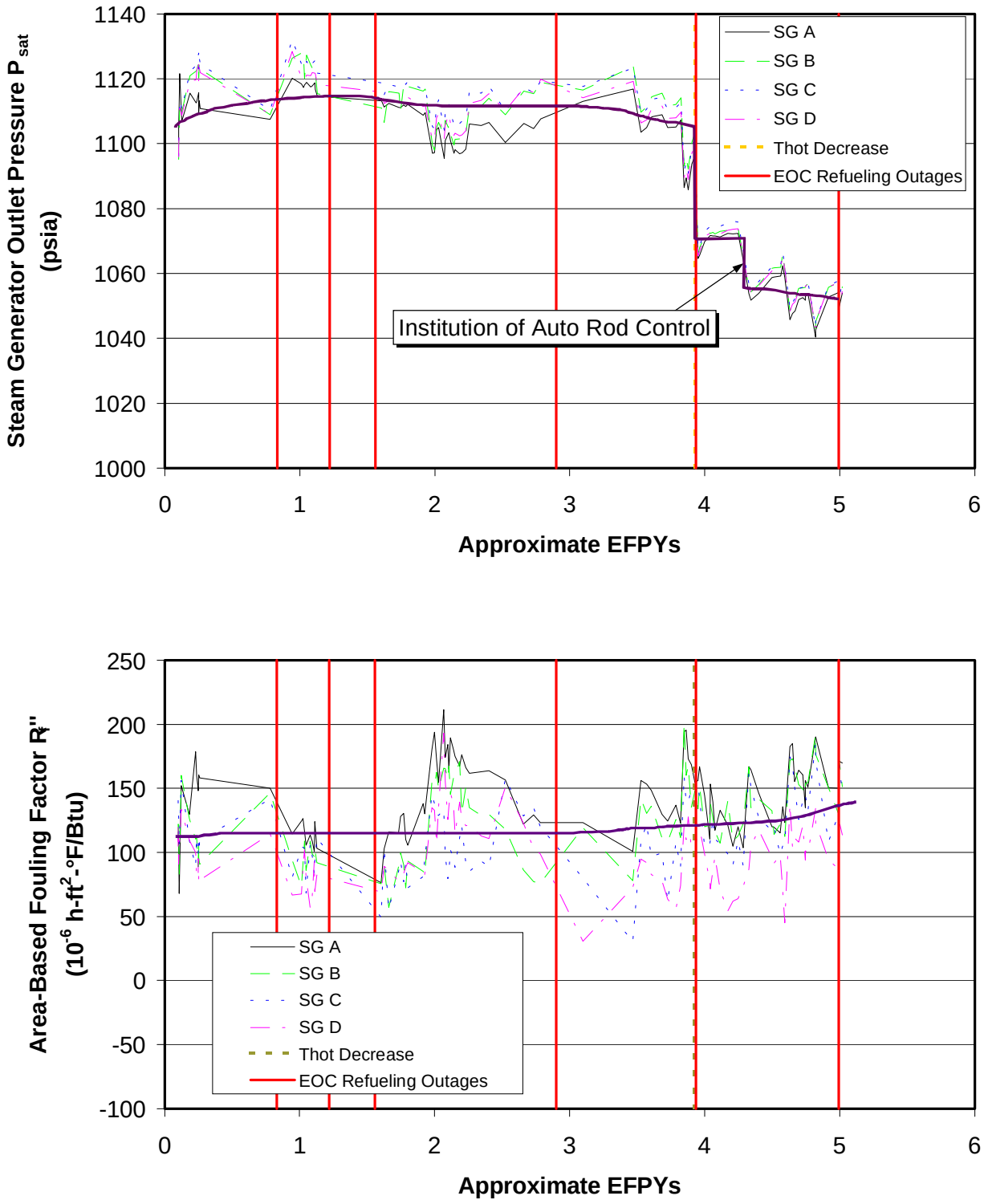

Figure 7-5
Steam Pressure and Fouling Trends at South Texas 1

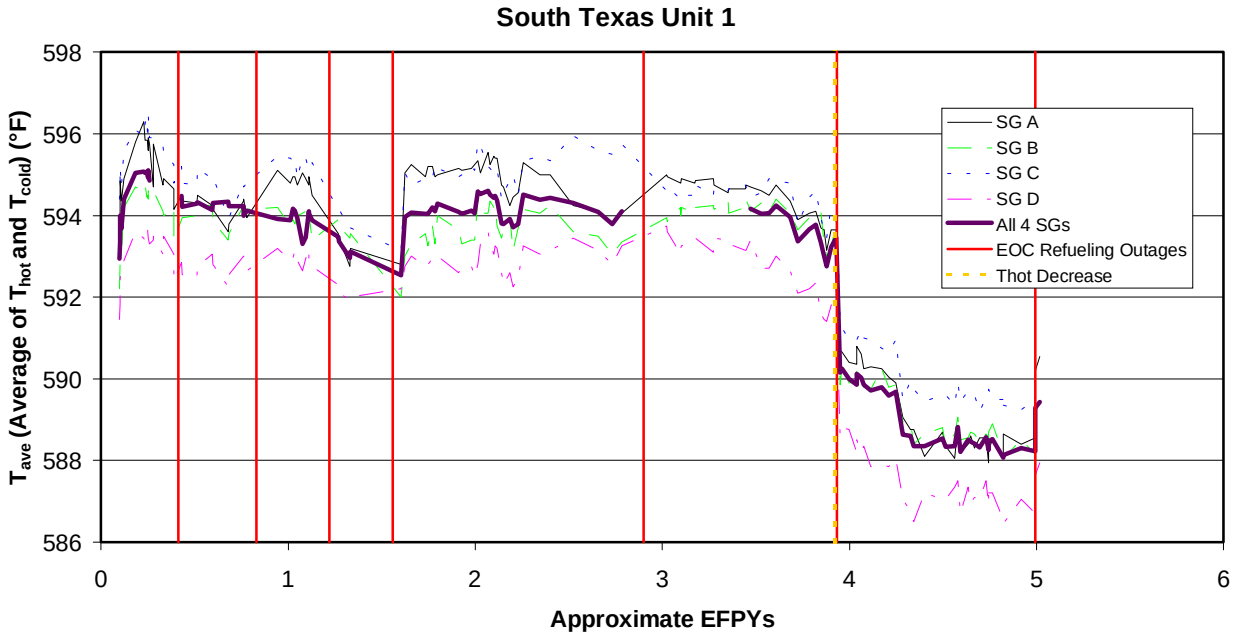

Figure 7-6
Historical Average of Hot and Cold Temperatures (T_{ave}) at South Texas 1

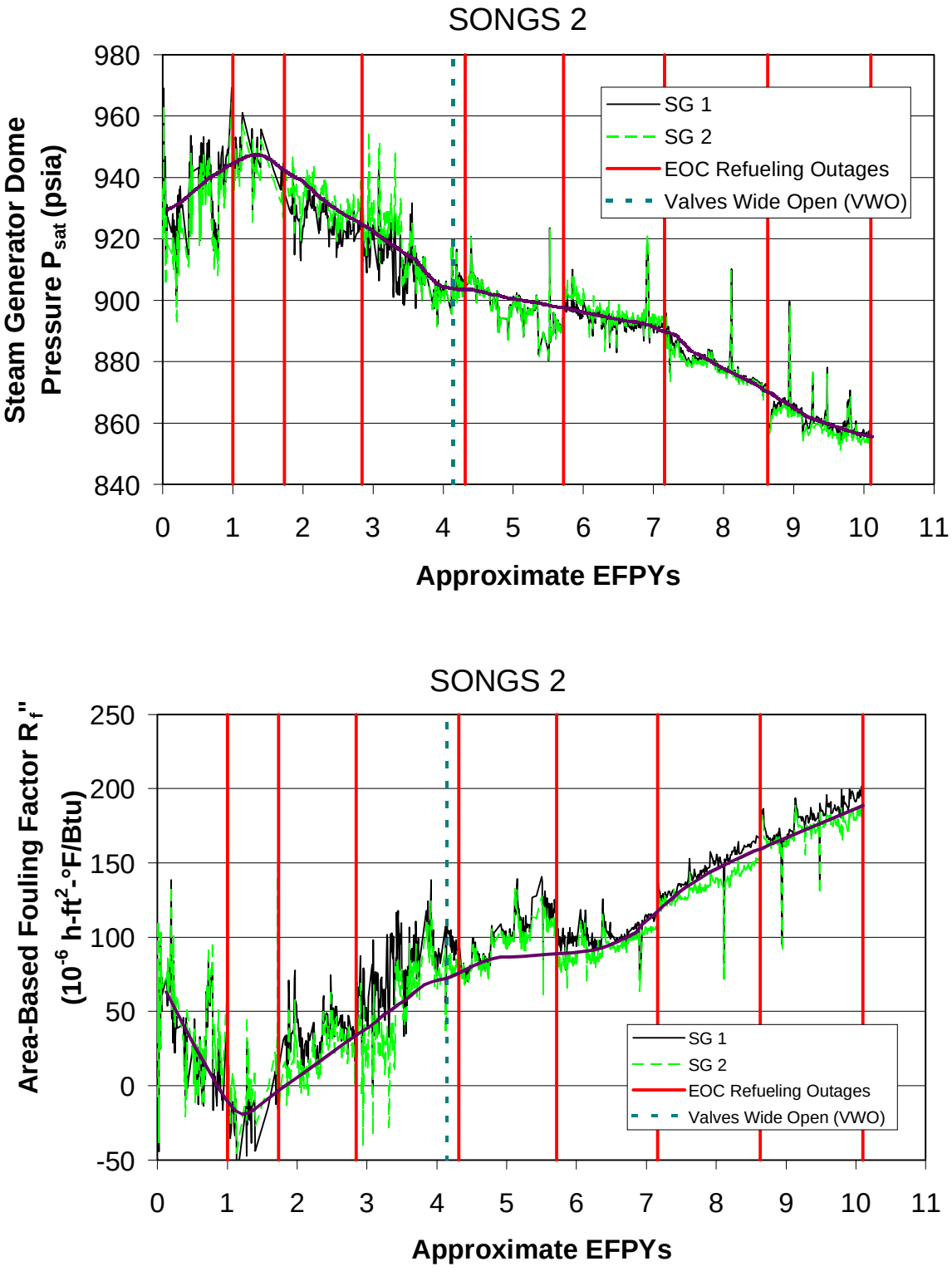

Figure 7-7
Steam Pressure and Fouling Trends at SONGS 2

8

PLANT THERMAL PERFORMANCE MEASUREMENTS

As was clear from the fouling factor uncertainty analyses in Chapter 4, the uncertainty of actual plant measurements can result in significant uncertainties in the calculated fouling factor. In particular, the global fouling factor is sensitive to uncertainties in measured SG steam pressure, primary temperatures (especially T_{cold}), and feedwater flow rate. Thus, examining how these measurements are performed at each plant is likely to be instructive.

SG Steam Pressure

As indicated in Chapter 4, a global fouling factor analysis requires as an input the average steam pressure throughout the tube bundle. The actual pressure just upstream of the SG outlet nozzle (i.e., the "dome" pressure) can also be useful for evaluating potential increases in separator/dryer pressure drop. However, steam pressure measurements are often not made inside the SG, but rather at some point in the downstream piping leading to the HP turbine.* This can sometimes lead to confusion, as reported "SG pressures" may in fact represent the uncorrected measurements made downstream of the SGs.

Callaway

Secondary steam pressure is measured in the main steam piping downstream of the SGs. For each loop, the piping exiting the SG is 32" diameter, which is reduced immediately to 28" pipe. The pressure transducers (one per loop) measure the pressure in the 28" pipe, downstream approximately 150 feet from the SG outlets (past 5 to 8 bends). Based on Reference (12), the applicable tolerance for the pressure indicated by this measurement is ±6.5 psi. As discussed in Chapter 4, the pressure measurements recorded by the instruments are lower than the actual pressure at the SG outlet due to frictional losses in the outlet nozzle and piping. Union Electric makes an adjustment for the frictional losses in order to calculate the pressure at the SG outlet. (The equation used to compute the adjustment depends on the mass flow rate and density of the

* Note that the CE 3410 SGs at SONGS 2 and 3 are exceptions; each has four pressure transducers located in the SG dome.

steam in the pipe; see Appendix A for more detail.) The magnitude of the adjustment ranged from 6 to 11 psi for the Callaway measured data, depending on the time and the SG. In addition to the pipe loss correction, a separate adjustment was made to determine the average bundle pressure from the outlet pressure for use in the fouling factor calculations. For Callaway, this adjustment is based on two factors: 1) additional pressure drop of about 4 psi across the separators and dryers per Union Electric measurements, and 2) an estimated 11.5 psi drop between the average bundle pressure and the outlet pressure (per References (12) and (13) as discussed in Chapter 4).

Sequoyah 1

Secondary steam pressure is measured for each loop by three transducers located approximately 40 feet downstream of the SG outlet nozzle. The instruments measure the pressure in the 32" diameter piping immediately upstream of the main steam isolation valves. Note that the length of pipe between the SG outlets and the pressure transducers is considerably smaller (with fewer bends) than that present at Callaway. The tolerance associated with steam pressure measurement at Sequoyah 1 is estimated by TVA from actual data to be ±5 psi. This value is much smaller than the administrative limit imposed on pressure measurement (±41 psi). As with Callaway, the pressure measurements recorded by the instruments are lower than the actual pressure within the SG due to frictional losses. TVA has indicated that the pressure drop between the SG outlet and the measurement location is about 5 psi.* Also per TVA information, the approximate decrease between the average tube bundle pressure and the dome pressure is 8 psi. Both of these values were used in Chapter 4 to compute average tube bundle pressures at Sequoyah 1. Measurements of the pressure drop from the top of the bundle to a location on the main steam piping (i.e., across the separators) have varied little over the past several cycles, suggesting little or no added pressure loss due to separator fouling.

South Texas 1

Similar to Callaway and Sequoyah, steam pressure at South Texas is also measured in the main steam piping downstream of the SGs. In this case, the distances between the SG outlets and the transducers were not provided, but all instruments (three per loop) are known to be located on 30" diameter pipe located just outside the containment building. No plant-specific information regarding the accuracy of the instrumentation was provided.† Approximate values for the pressure drop due to frictional loss in the

---

* Note that a constant correction was used. However, as indicated for Callaway, this pressure drop does vary with mass flow rate and fluid density. A more accurate correction would include these variations.

† A best-estimate value based on engineering judgment (±8 psi) was used in the Chapter 4 uncertainty analysis. However, the actual tolerance could be higher or lower.

main steam piping (10 psi) and the pressure drop between the middle of the tube bundle and the outlet (7 psi) were provided by HL&P and were used in the fouling factor calculations. No information on the actual pressure drop across the separators and dryers was provided.

The primary conclusions suggested by the above discussion are:

1. The tolerance associated with the measurement instrumentation does not include the uncertainty of calculated corrections necessary to convert main steam pressure (where the instruments are located) to SG outlet, dome, or bundle pressure. Included in this uncertainty is potentially higher-than-design pressure drop across the separators and dryers in the SGs.

2. The experience at Sequoyah indicates that the administrative limit placed on SG pressure measurement (e.g., by calibration procedures) may be much larger than the actual accuracy achieved by the instruments. Knowing about such discrepancies is crucial to assigning a realistic uncertainty band to the measurements.

Primary Temperatures

The primary coolant temperatures (i.e., T_{hot} and T_{cold}) are also key inputs to a global fouling factor analysis. As demonstrated in Chapter 4, uncertainties in T_{cold} have a greater impact on the overall fouling factor uncertainty than uncertainties in T_{hot} do. This is mainly because T_{cold} is closer in magnitude to the secondary steam temperature, meaning variations in T_{cold} have a greater impact on the log-mean temperature difference than changes in T_{hot}. Differences in plant-specific measurement techniques are discussed below.

Callaway

Callaway has three equally-spaced RTDs that indicate the narrow-range hot-leg temperature for each loop. The instruments are mounted on a horizontal stretch of pipe, with one at the top of the pipe and the other two at 120° intervals around the circumference of the pipe. Each is located about 11 feet from the outlet nozzle on the reactor, or 21 feet from the reactor centerline. Based on Reference (12), the tolerance on each T_{hot} measurement is ±1.0°F. Callaway has a single cold-leg RTD for each loop, located at the top of the horizontal piping entering the reactor. Each is located about 15 feet from the reactor inlet nozzle, or 25 feet from the reactor centerline. Based on Reference (12), the tolerance applicable to T_{cold} is ±0.5°F.

The Callaway temperature control scheme is based on T_{ave}, which in this case is calculated using the following equation:

$$T_{ave} = \frac{\frac{1}{3}\left(T_{hot-1} + T_{hot-2} + T_{hot-3}\right) + T_{cold}}{2} \qquad \text{(eq. 8-1)}$$

There are two phenomena that have caused problems in regulating primary temperature at Callaway, independent of any instrument measurement errors:

- HOT-LEG TEMPERATURE STREAMING. As described in Chapter 6, hot-leg streaming is the result of a nonuniform temperature across the pipe cross section where T_{hot} is measured. Back-calculated values of T_{hot} and T_{cold} based on primary flow-rate measurements and thermal power output have suggested that Callaway is experiencing roughly 1°F of streaming (i.e., a 0.5°F primary temperature error) due to this phenomenon.

- UPPER PLENUM FLOW CROSSOVER (UPFC). This phenomenon is believed to result in nonuniformities in the flow leaving the reactor. In other words, the "A" hot leg may, for example, receive fluid which is 1°F hotter (on average) than the fluid entering the other hot legs. While this does not cause any incorrect temperature measurements by itself, it can cause the calculated T_{ave} (Eq. [8-1]) for one loop to be significantly higher than the other loops. If the reactor control scheme is based on the maximum T_{ave} (as is the case at Callaway), then the other loops will operate at lower-than-design temperatures, thereby reducing the average SG steam pressure. (Note that thermal power for each SG changes slightly, which also has an effect on the steam pressure in each SG.)

Sequoyah 1

The physical layout of primary-temperature RTDs at Sequoyah 1 is very similar to Callaway. There are three hot-leg RTDs for each loop arranged in the same configuration. All of the hot-leg instruments are located about 10–12 feet from the reactor outlet nozzles (or about 20–22 feet from the reactor centerline). Based on utility calibration procedures (17), the hot-leg temperature measurements are accurate to about ±0.6°F following calibration (±1.6°F during operation). Sequoyah 1 also has two cold-leg RTDs per loop; one located at the top of the pipe cross section (like Callaway) and a second one at a 45° angle to the first. Based on Reference (17), the accuracy of the cold-leg measurements is also ±0.6°F after calibration, or ±1.6°F during operation.

The primary temperature history at Sequoyah 1 (see Figures 4-11a, 4-11b, and 4-11c) suggests that, like Callaway, it has also been subject to hot-leg streaming. The average hot-leg temperature (as recorded) increased from an average of 606.8°F during early Cycle 1 operation to an average of 608.8°F over the most recent months for which data were available (March to May 1996). Over the same span, the average cold-leg temperature dropped from 547.8°F to 545.7°F. This divergence of T_{hot} and T_{cold} is a characteristic of hot-leg streaming. Using Table 6-5, we note that the corresponding

error in T_{hot} is close to 4°F. Examination of Sequoyah 1 data indicates that this change most likely occurred during a relatively short time period near the end of Cycle 4, which corresponds roughly to the introduction of low-neutron-leakage fuel in the reactor core. This is the most probable cause of the streaming effect.

South Texas 1

Although detailed piping drawings were not provided, the reactor coolant P&ID indicates that each hot leg has three narrow-range RTDs, like both Callaway and Sequoyah 1. Like Callaway, a single cold-leg RTD is responsible for measuring T_{cold}. According to HL&P personnel, the measurement tolerances for T_{hot} and T_{cold} both are ±0.5°F.* According to HL&P, the three hot-leg RTDs for a given loop often disagree by as much as 7–8°F, suggesting that hot-leg streaming may be taking place at STP 1. Also, calculated primary flow rates have been decreasing unexpectedly, further indicating hot-leg streaming. In addition to potential streaming in each loop, note in Figures 4-15a, -15b, and -15c that the four loops have a significant temperature disparity. Prior to August 1995 (about 4.3 EFPY), the South Texas control scheme used the average value of T_{ave} to regulate primary temperatures (using Eq. [8-1] like Callaway), meaning that the disparity had little or no effect. However, after August 1995, the control scheme was changed to an "auto-rod" system, meaning that the maximum loop (or auctioneer) value of T_{ave} is used to regulate primary temperature. As is evident from the plots, this change caused a primary temperature decrease of at least 1°F. It is unknown whether the cause responsible for the temperature asymmetry at South Texas 1 is the same as that identified at Callaway (UPFC).

In conclusion, utilities should watch for the following potential problems regarding interpretation of primary temperature measurements: 1) hot-leg streaming, 2) loop asymmetry (caused, e.g., by UPFC), 3) actual accuracy versus administrative limits (i.e., calibration procedures), and 4) wide-range versus narrow-range measurements. This last item is potentially a source of confusion, as wide-range values (which are less accurate than narrow-range values) may be inadvertently reported, potentially increasing the uncertainty of fouling factor calculations based on such measurements.

Feedwater Mass Flow Rate

Because the bulk of the heat transferred in a steam generator is used to boil the secondary fluid, the effects of small (or even moderate) errors or uncertainties in feedwater temperature and pressure do not have a major effect on the overall fouling

---

* Although drift up to an additional ±0.7°F is permissible, virtually none has been observed. It should be noted that these tolerances are believed to reflect narrow-range measurements rather than the reported wide-range measurements. Tolerances for the latter values are estimated at ±4.0°F for T_{hot} and ±1.0°F for T_{cold}.

factor uncertainty, as is documented in Chapter 4. However, uncertainties in the feedwater flow rate can have a significant or even dominant effect on the overall fouling factor uncertainty. Although all three plants use venturi meters to measure feedwater flow rate, there are a couple of plant-specific issues that are addressed below. Note that feedwater flow uncertainty is an important input to the reactor power limit because of its role in secondary calorimetric calculations.

Callaway

The venturis that measure feedwater flow rate in each loop are believed to have a tolerance of ±0.5% of full scale, or 24,000 lb_m/h, based on Reference (12). In past cycles, this tolerance may have been too small due to venturi fouling observed at Callaway. However, recent operation has been characterized by minimal amounts of venturi fouling.

Sequoyah 1

As with SG pressure measurement, the administrative limits on feedwater flow measurement are significantly larger than the actual performance during recent cycles. According to Reference (18), the acceptable tolerance on this measurement is ±1.8%. However, conversations with TVA personnel revealed that the actual variation was limited to about ±0.5%. Like Callaway, Sequoyah 1 also experienced appreciable venturi fouling during early operation (as much as 2–3%) that has largely been eliminated by regular inspections and cleanings.

As a further effort to minimize potential errors in feedwater flow rate, in 1992 TVA installed leading-edge flow meters (LEFMs), which use ultrasonic pulses to measure the velocity, and hence the flow rate (see Reference (36)). TVA is currently using the LEFMs as a check to determine if the venturis are fouling.

Venturi Bypass Flow

In addition to venturi fouling, which has affected many plants including Callaway and Sequoyah 1 in this study, a separate problem consisting of bypass flow around the venturi meter can cause measured values to be erroneously low rather than high. This problem can result from corrosion and/or cracking of the circumferential welds that secure the venturi to the feedwater pipe. Because feedwater flow measurements are used in the secondary calorimetric calculation to calibrate reactor thermal power, this error can potentially lead to >100% reactor power. If severe enough, the operating license for thermal power might be violated. At least one US plant has experienced this problem.

Temporal Nature of Reported Data

There are two basic ways that plants can report data measurements. The most straightforward method is to record instantaneous measurements of various quantities. The second method involves time averaging the instantaneous measurements recorded during a certain interval and then reporting the resulting averaged values. In this study, the following is true of the measured data used in the fouling factor calculations:

- Callaway measurements are assumed to be instantaneous.
- Sequoyah 1 measurements are known to be instantaneous readings until March 1992. After that time, measured values are time averaged over an unspecified length of time.
- South Texas 1 measurements are instantaneous. For each day on which data were provided, numerous readings were provided, typically once per hour for 8 to 16 hours. Care was taken to use a set of measurements as close together in time on a particular day as possible.
- SONGS 2 measurements are assumed to be instantaneous.

Either type of measurement is believed to be acceptable. However, the use of averaged values will avoid the problem of using several instantaneous measurements taken at different times to calculate a single fouling factor, an inconsistency that can introduce additional scatter and uncertainty to the calculated fouling factor above what is computed in Chapter 4.

Pressure and Fouling Factor Transients

All of the plants in this study have experienced SG steam pressure transients in some manner. Many of these transients do not appear to reflect any consistent pattern and are probably due to normal scatter in the data values and measurements. However, some appear to be connected to plant restarts after outages and trips. Based on the available data, transient behavior at each plant in this study is discussed below. It is important to note that missing data, data scatter, and the frequency of available data might be masking non-random transient behavior not reported here.

Callaway

After restart from the EOC 2, EOC 3, and EOC 4 outages, SG steam pressure exhibited notable decreases, as is evident in Figure 4-6. The fouling factor (Figure 4-18b) exhibited less significant transients after EOC 2, EOC 4, and EOC 7. Neither parameter seems to show any non-random transient behavior during the other outages based on

the available data. The transients following the EOC 2, EOC 3, EOC 4, and EOC 7 outages may be summarized as follows:

EOC 2: There is a restart pressure loss of about 25 psi in SG A and about 5 psi in SG B (other SGs unaffected). Recovery of this loss appeared to take almost all of Cycle 3.* The SG A fouling factor increased about 30 to 40 10^{-6} h-ft^2-°F/BTU upon restart, and then gradually decreased to a value close to that at the end of Cycle 2. The fouling factors for the other SGs show no clear transient pattern following the EOC 2 outage.

EOC 3: All 4 SGs exhibited a step decrease in SG pressure following this outage. The decrease ranges from 5 psi (SG B) up to 30 psi (SG A). In this case, no long-term recovery is apparent; pressure for all 4 SGs remained relatively constant during Cycle 4. In contrast, there is no indication of a step change in the fouling factor following the EOC 3 outage, except for a slight increase for SG D (15 10^{-6}).

EOC 4: There was a large SG pressure decrease following this outage for all four SGs (20 psi up to 40 psi for SG A). However, it is noteworthy that just prior to the outage, the pressure increased almost this same amount; the net decreases were modest (0 to 10 psi). There is only a limited apparent pressure recovery during the beginning of Cycle 5, which is subsequently lost in the latter half of the cycle, perhaps due to increases in the fouling factor during Cycle 5. Only the fouling factor for SG A exhibited a matching step change after EOC 4; the others did not change much. In fact, SG D's fouling factor decreased following the outage.

EOC 7: The fouling factor for all four loops increased notably after restart from the EOC 7 outage, during which SG chemical cleaning was performed. The increase was about 20 10^{-6} h-ft^2-°F/BTU in SGs A and B and 50 10^{-6} in SGs C and D. As discussed previously, the fouling factor increase is most likely due to removal of heat-transfer-enhancing scale from the tube OD surfaces. Although less prominent, there is an accompanying step decrease in SG pressure in SG C (10–15 psi) and SG D (about 5 psi). (The pressures in SGs A and B do not seem to exhibit a step decrease following the EOC 7 outage.) As indicated on pp. 7-1 and 7-2, part of the reason why the pressure decrease is not in better agreement with the fouling factor increase after chemical cleaning may be variations in primary temperatures among the four loops.

Since the transient behavior of SG pressure and fouling factor described above do not agree all that well, it is likely that fluctuations in T_{ave} are partially responsible for the

---

* Due to the power uprate during Cycle 3, it is difficult to tell exactly how long the pressure recovery took.

pressure transients (see Figure 7-3). In addition, SG A generally exhibited much more severe transients than the other SGs, indicating a phenomenon unique to that loop (e.g., differences in temperature control).

Sequoyah 1

The only discernible restart transient for Sequoyah 1 occurred after the most recent outage, during which the SGs were chemically cleaned. Per Figure 4-19d, all four SG pressures exhibited a step decrease of about 5–10 psi, and all four fouling factors increased about 25 10^{-6} h-ft^2-°F/BTU. This behavior may have been due to a change in the degree of hot-leg streaming or possibly the removal of deposits that were slightly heat-transfer enhancing.* Note that a portion of the pressure decrease following the EOC 7 outage (about 3 psi) is due to significant tube plugging that took place.

South Texas 1

Pressure and fouling factor transients for South Texas 1 were discussed in the last chapter (p. 7-6). There were two notable transients apparent from the data. Neither coincided with a refueling outage, although both followed decreases in plant thermal power.

Recommendations for Standardized Measurements

Based on the uncertainty analyses performed in Chapter 4 and the above discussion of measurement practices at the plants involved in this study, we recommend that utilities consider several improvements that will facilitate more accurate fouling factor calculations and allow more easily direct comparison of different plants on a common basis:

- Install pressure transducers accurate to within ±2 psi or better as near to the SG outlets as possible, or at some location on the SG shell. This will reduce the uncertainty directly associated with the measurement and will also eliminate the need to correct pressure measurements for the friction losses between the SGs and the current locations of these measurements. Note that such additional instruments need not be qualified for use in calorimetric calculations; the measurements can be reported "for information only."

- Because the fouling factor is rather sensitive to T_{cold}, take steps to assure an actual measurement uncertainty of less than 1.0°F for this quantity. Keep records of the

* As indicated earlier, the deposits at Sequoyah 1 prior to chemical cleaning are believed to have been slightly resistive although this conclusion is not certain.

actual uncertainty for each cycle of operation to facilitate future fouling calculations.

- Install redundant temperature elements for T_{hot} and T_{cold}. Such instruments would reduce the uncertainty of primary temperatures and aid in evaluating hot-leg streaming. Like the accurate pressure transducers mentioned above, such measurements could be for information only to avoid costly qualification procedures.

- Consider installation of instruments to measure primary loop flow rate to aid in calibrating thermal power. In particular, this action will help in evaluating potential hot-leg streaming problems.

- Inspect and clean the feedwater flow venturis. If fouling is present, perform tests or otherwise determine approximately how much error the fouling was contributing to the flow measurements. This practice will allow more accurate accounting for venturi fouling in the fouling factor calculations. Also consider installing redundant LEFMs to aid in calibrating the venturis.

- Although current allowable tolerances may exist on measurements of steam pressure, primary temperatures, and feedwater flow rate, these values probably do not reflect the actual variability of the instruments (e.g., Sequoyah). Perform analyses or tests to determine the actual tolerances associated with the measurements. (More accurate instruments such as those described above could be used to aid this effort.) This will significantly reduce the calculated fouling factor uncertainty. For moderate calculated fouling levels (e.g., 30 to 50 10^{-6} h-ft^2-°F/BTU), achieving a low uncertainty will increase the chance that secondary tube fouling (or other sources of pressure degradation) can be conclusively identified early.

- For preheater units, install instrumentation to aid in determining flow rates and temperatures characterizing the preheater area. Reference (37) provides guidance on this topic.

- The fouling factor calculation is most meaningful when measurements are provided frequently. The authors recommend recording at least the following quantities *for each loop* at least once per operating week to facilitate future fouling factor calculations.*

---

* Note that the calculated fouling factor will be most meaningful if all measurements reflect the same operating condition (i.e., all measurements are recorded at the same time). Relatively short time lags (e.g., several minutes) are probably not significant.

1. Narrow-range (or most accurate) T_{hot} and T_{cold}. T_{ave}-controlled plants should also record the value of T_{ave} used by the computer and its calculation basis.
2. SG steam pressure. Indicate any corrections necessary for converting raw measurements to outlet, dome, or average bundle pressure.
3. Feedwater mass flow rate.
4. Feedwater temperature.
5. Feedwater pressure.
6. Blowdown flow rate.
7. Steam mass flow rate, condensate mass flow rate, and/or HP inlet or first stage turbine pressure. These quantities can be used as independent checks for consistency of feedwater flow rate measurements.
8. Total NSSS thermal power.

The first three items above are absolutely essential for computing a meaningful fouling factor.

9

REMEDIAL MEASURES FOR IMPROVING HEAT TRANSFER

This chapter includes elements of a remedial strategy that utilities could use to address future thermal performance degradation. Certain items in the list below will be more or less important for a particular plant depending on plant-specific thermal performance and remaining heat-transfer margin.

Information Gathering

a. Gather and analyze available thermal performance data from previous operating cycles (especially Cycle 1). The presence of thermally resistive secondary tube deposits can be revealed by the fouling factor history. In addition, calculated fouling factors for early operation are instrumental in determining whether the SGs initially performed at the level indicated by thermal-hydraulic design values.

b. Track the fouling factor over future operating cycles. Calculation of the fouling factor requires the quantities listed at the end of Chapter 8; primary temperatures, SG steam pressure, and feedwater mass flow rate are the most important. As discussed in Chapter 8, the greater the frequency of data, the more meaningful the calculated results. In addition, data on the actual precision of the above measurements are required to perform an uncertainty analysis for the calculated fouling factor (see Chapter 4).

c. Add instrumentation to measure additional quantities, such as the pressure drop between the tube bundle and the current measurement location, recirculation ratio, and flow distribution (for preheater units). This information can help identify higher-than-design separator/dryer pressure drop, tube support fouling and/or blockages, and preheater flow maldistribution, all of which can degrade thermal performance. Note that several methods have been used for measuring recirculation, including: 1) measuring the velocity in the downcomer with ultrasonic techniques, 2) measuring the downcomer fluid temperature, and 3) using tracer techniques.

d. At every opportunity, make tube scale property measurements, including thickness, bulk and skeletal density, pore size distribution, and structure (e.g., metallographic cross sections). These measurements can be performed on flakes collected each time the SGs are opened for secondary-side access (e.g., sludge lancing). They can also be performed each time tubes are pulled for other reasons (e.g., corrosion). Experience with SONGS 2 indicates that scale thicknesses of 10–14 mils can cause significant heat-transfer degradation. Collecting information at multiple times will help in evaluating how tube scale morphology and thickness are changing over time, which can lead to a projection of future fouling rates.

e. Perform visual inspections of the interior of the tube bundle for information on secondary tube scale, including thickness uniformity and tube support blockages. Also, use low-frequency eddy current testing (ECT) to investigate the relative thickness of deposits throughout the tube bundle.

f. Track impurity ingress concentrations (particularly iron and copper, although lesser impurities like silicates can also be relevant to heat transfer) to provide information for an independent assessment of deposit loading. Independent deposit thickness estimates can be calculated with this information, thereby helping to confirm thickness measurements that might be available for a limited number of flake samples that are not necessarily representative of the entire tube bundle. Time histories of impurity concentrations can also be used to evaluate the effects of alternate amines (e.g., DMA or ETA). Impurity ingress information will help lead to industry correlations among water chemistry, impurity concentrations, and heat-transfer performance.

g. Implement changes in instrumentation that will reduce the uncertainty associated with calculated fouling factors. See the end of Chapter 8 for more details.

Implementation of Countermeasures

Any and all feasible countermeasures against performance degradation can be evaluated for possible implementation, including the following:

a. Turbine modifications (e.g., enlarging the HP turbine diaphragm)
b. Feedwater heater bypass
c. Piping modifications
d. Throttle valve changes

Many of these countermeasures are being employed by individual utilities who have been forced to deal with performance degradation in past years. Participation in EPRI-sponsored workshops and communication with other utilities are effective ways of obtaining information about countermeasures that may be of primary interest for a particular plant.

Implementation of Actions to Slow Heat Transfer Reduction

Several actions that may reduce the rate of thermal performance loss are listed below. Plants that have experienced rapid fouling or have limited remaining thermal margin would potentially benefit most from these actions, although all utilities should consider them.

a. Switch to DMA or ETA as the pH control additive in the feed and condensate system. The experience at Comanche Peak (see Appendix D) indicates that DMA can lower feedwater iron concentrations and in some cases break up and/or remove scale. In addition, limited evidence from Callaway suggests that ETA may reduce fouling rates. Note, however, that data from other plants do not in general substantiate this benefit as yet (8).

b. Improve makeup water treatment system practices, thereby lowering impurity transport (e.g., silica) to the SGs.

c. Replace plant components that incorporate copper alloys and prevent operation at optimal feedwater pH (e.g., MSRs). Optimizing pH has been shown to reduce corrosion-product transport by reducing flow accelerated corrosion (FAC).

Cost-Benefit Evaluation

An effective means of selecting the most appropriate remedial strategy includes development of a cost-benefit model which determines the net costs of various options and also considers the likelihood of success. A number of options are currently available:

a. SECONDARY-CYCLE MODIFICATIONS. Turbine modifications (which can allow near-100% electrical power generation at lower steam pressures) and feedwater heater bypasses (which increase heat transfer by increasing feedwater subcooling) can mitigate electrical power losses.

b. ALTERNATE REPAIR CRITERIA FOR TUBE DEGRADATION (E.G., AT SUPPORTS). For plants with limited remaining thermal margin, this strategy can prolong the life of the SGs by preserving heat-transfer area, allowing the plant to generate 100% power for a longer period of time.

c. SLEEVING. For plants that are approaching the VWO condition, the use of sleeves rather than plugs for tube defects preserves heat-transfer area, potentially prolonging the ability to generate 100% power. This approach is generally more practical for top of tube sheet (TTS) defects than for defects in other areas, but can be considered for all defects affecting the straight segments of the tubes.

d. PRIMARY TEMPERATURE INCREASE. For plants with small thermal margins and limited tube degradation, an increase in primary temperature will provide additional thermal margin. However, there are two major disadvantages that

might hinder a T_{hot} increase: i) changes to technical specifications or safety analyses that are potentially required by such an increase, and ii) the resulting increase in the rates of degradation mechanisms that affect SG tubes and other primary-pressure-boundary Alloy 600 components. Note that the first problem may be avoidable if the plant in question is operating below the original design temperatures.

e. CHEMICAL CLEANING. The results of the fouling factor calculations presented earlier in this report for Callaway, Sequoyah 1, and SONGS 2 (see Chapter 7) suggest that chemical cleaning can restore the thermal performance of the SG tube bundle to a level near its original operating level. This is because chemical cleaning is the most effective of the deposit removal processes, resulting in the dissolution and removal of as much as 20,000 pounds of deposits from each SG.* Note that pre-planning at utilities that have used chemical cleaning has resulted in cost savings and greater levels of assurance that the application will be successful with no unacceptable consequences (e.g., high carbon steel corrosion or high waste processing costs).

   On the other hand, chemical cleaning is considered to be the most expensive of the available sludge management options, costing as much as $4 million to $10 million per plant for "off-line" cleaning processes. Off-line cleaning processes are typically performed during scheduled refueling outages after the plant has been placed in cold shutdown. "On-line" cleaning involves injection of chemical solutions into the SGs while the plant is in the process of shutting down or starting up. The main advantages of the on-line processes are that heating of the chemical solutions is achieved by primary to secondary side heat transfer and higher temperatures can usually be achieved than by off-line processes. On-line processes are typically less expensive than off-line processes in terms of the cost of procuring the service from a vendor, but they inevitably result in some lost critical path time during an outage. Off-line processes may or may not affect critical path, depending on the nature of other outage activities. In either case, chemical cleaning is now a generally accepted maintenance option for deposit removal. The principal downsides to chemical cleaning are the slight corrosion of the carbon and low alloy steel pressure boundary and internal structural materials and the cost of treating, disposing, and storing the chemical cleaning wastes, which may be hazardous if heavy metals concentrations exceed regulatory limits.

f. LOW-RISK MECHANICAL CLEANING. For utilities that decide that an aggressive scale removal option like chemical cleaning is not a viable option, immediate use of technology for mechanically cleaning the SGs might provide short-term

---

* The chemical cleaning at SONGS Unit 3 resulted in the removal of about 20,000 pounds of corrosion products from each SG. Note that Westinghouse SGs, which are in general smaller than SONGS' CE 3410's, would only accumulate this quantity of corrosion products if the average scale thickness reached 20–30 mils.

thermal performance benefits, thereby delaying more costly and difficult measures until a future outage. Such options include upper-bundle water jetting with preparatory scale softening (e.g., ultrasonic cleaning with a scale softening agent). Preliminary testing of such methods to determine the amount of scale that could be removed would be necessary to accurately assess the impact on future thermal performance.

g. SG REPLACEMENT. For many plants, increasing rates of tube corrosion have made replacement a strong consideration, or even a necessity. In this case, the optimal time to replace the SGs becomes a primary concern.

The feasibility and costs of the above options that are relevant for a particular plant must be considered in order to identify the most economically attractive action(s) for combating thermal performance degradation. It is probably in the interest of most utilities (even those not immediately threatened with electrical generating losses) to begin a preliminary evaluation of this type.

10

REFERENCES

1. "Causes of PWR Steam Generator Thermal Performance Degradation," G. A. White, M. A. Kreider, and R. D. Varrin, Dominion Engineering, Inc., paper presented at the EPRI Nuclear Plant Performance Improvement Seminar, Asheville, NC, September 3-4, 1996.

2. "Predicting the Steam Pressure Recovery Following Chemical Cleaning at San Onofre Unit 2," M. A. Kreider, G. A. White, and R. D. Varrin, Jr., paper presented at the Seventh EPRI PSE Nuclear Plant Performance Improvement Seminar, San Antonio, TX, August 11-12, 1997.

3. "Steam Generator Thermal Performance Degradation Case Studies," M. A. Kreider, G. A. White, and R. D. Varrin, Jr., paper presented at the Seventh EPRI PSE Nuclear Plant Performance Improvement Seminar, San Antonio, TX, August 11–12, 1997.

4. *Ginna Station Steam Generator U-Bend Tube Analysis for Chemical Cleaning Data*, Electric Power Research Institute Project S413-01, Final Report, EPRI TR-100866, July 1992.

5. *User's Guide for Steam Generator Analysis Package*, Electric Power Research Institute Projects RPS415-02 and S541-01, Report TR-105253, 1995.

6. "Application of the ATHOS3 Code for Steam Generator Thermal Hydraulics and Fouling Analysis," Srikantiah, G. S., and Chappidi, P. R., Proceedings of the ASME/JSME 4th International Conference on Nuclear Engineering, Vol. 5, New Orleans, LA, March 10-14, 1996.

7. *Statistical Analysis of Steam Generator Tube Degradation*, Electric Power Research Institute Project S405-9, Final Report, NP-7493, September 1991.

8. "Steam Generator Pressure Loss Survey 95-016," Electric Power Research Institute (EPRI) Plant Support Engineering P^{2}EP (Plant Performance Enhancement Program). Survey results distributed to survey initiators and respondents in Plant Support Engineering letter dated November 30, 1995. Survey results also presented by A. L. Matheny at the Steam Generator Performance Degradation Meeting, Charlotte, NC (February 6, 1996).

9. *Steam Generator Performance Degradation*, Electric Power Research Institute Project S403-11, Final Report, EPRI NP-7524, September 1991.

10. *Characterization of PWR Steam Generator Deposits*, Electric Power Research Institute Project S523-01, Final Report, EPRI TR-106048, February 1996.

11. *Thermal Analysis of Pressurized Water Reactors*, Third Edition, Tong, L. S. and Weisman, Joel, American Nuclear Society, 1996.

12. *Verification of the ATHOS3 Code Against Feedring and Preheat Steam Generator Test Data*, Electric Power Research Institute Project 1066-10, Final Report, EPRI NP-5728, May 1988.

13. *Thermal-Hydraulic Characteristics of a Westinghouse Model F Steam Generator*, Vol. 1, Electric Power Research Institute Project S129-1, Interim Report, EPRI NP-1719, March 1981.

14. *Nuclear Power Experience*, Vol. PWR-1, published by Stoller Power, Inc., Boulder, CO, 1986-1995.

15. Dominion Engineering Steam Generator Database, compiled from various sources.

16. ASME Performance Test Code PTC 19.1-1985, American Society of Mechanical Engineers, 1985.

17. Sequoyah Nuclear Plant Set Point and Scaling Document No. 1-T-68-2, Rev. 3, November 30, 1995.

18. Sequoyah Nuclear Plant Set Point and Scaling Document No. 1-F-3-35-A, Rev. 3, March 21, 1995.

19. Sequoyah Nuclear Plant Set Point and Scaling Document No. 1-T-3-36, Rev. 2, October 26, 1995.

20. Sequoyah Nuclear Plant Set Point and Scaling Document No. 1-P-3-92, Rev. 0, September 24, 1995.

21. "PWR Units – Steam Generator ID Oxide Layers' Thickness and Chemical Composition," [translated from French], Cattant, François, Electricité de France Doc. No. D.5004/CTT/RA.90.128, December 3, 1990.

22. *Examination of Three Steam Generator Tubes From the Ginna Nuclear Power Plant*, Electric Power Research Institute Project S138-2, Final Report, EPRI NP-2534-LD, August 1982.

23. *Evaluation of Steam Generator U-Bend Tubes from the Trojan Nuclear Power Plant*, Electric Power Research Institute Project S138-4, Final Report, EPRI NP-2629-LD, September 1982.

24. *Destructive Examination of Tube R31C66 From the Ginna Nuclear Plant Steam Generator*, Electric Power Research Institute Project S407-40, Final Report, EPRI NP-7371-M, June 1991.

25. *Metallurgical and Chemical Evaluation of Tubes R17C85, R28C32, and R26C50 From a Doel Unit 2 Steam Generator*, Electric Power Research Institute Project S304-3, Final Report, EPRI NP-5022-LD, December 1986.

26. *Examination of Tubes R3C41HL and R9C58HL of Steam Generator C, North Anna Unit 1*, Electric Power Research Institute Project S304-20, Final Report, EPRI NP-5420-LD, October 1987.

27. *The Oxide Handbook*, Second Edition, Samsonov, G.V., ed., IFI/Plenum Data Company, New York, 1982.

28. "Thermal Conductivity of Magnetite and Hematite," Malgaard, Journal of Applied Physics, Vol. 42, No. 9, pp. 3644-3647, August 1971.

29. Bruggeman, D.A.G., *Annalen der Physik* [in German], Vol. 24, pp. 636-679, 1935.

30. "Thermochemical and Physical Properties," Version 2.2 for Macintosh, E.S. Microware, Hamilton, OH, 1994.

31. *Characterization and Examination of Steam Generator Sludge Deposits*, Varrin, R. D., Esposito, J. E., et al. [contact first author for more information].

32. Pan, C., Jones, B. G., and Machiels, A. J., "Wick Boiling Performance in Porous Deposits with Chimneys," Paper presented at the ASME/AIChE/ANS National Heat Transfer Conference Symposium on Multiphase Flow and Heat Transfer, Denver, CO (August 1985).

33. "Westinghouse Experience with Performance Degradation," presentation to the EPRI Performance Degradation Meeting, Charlotte, NC, February 6, 1996.

34. *Fundamentals of Heat and Mass Transfer*, Second Edition, Incropera, F. P., and DeWitt, D. P., John Wiley & Sons, New York, 1985.

35. "Using a Flow Correction Factor to Compensate for Feedwater Venturi Bias and Increase Plant Generation," Lestina, T. (MPR Associates) and Contard, C. (Niagara Mohawk Power Corp.), paper presented at the EPRI Nuclear Plant Performance Improvement Seminar, Asheville, NC, September 3-4, 1996.

36. "The Application of Externally-Mounted Leading Edge Flow Meter (LEFM) for the Measurement of Sequoyah Feedwater Flow," Bennett, Edgar B. Jr. (TVA), Augenstein, Donald (MPR Associates, Inc.), Proceedings of the American Power Conference, Chicago, IL, April 1993, pp. 1446-1451.

37. "Inbetriebsetzungsmessungen zur Bestimmung des Betriebsverhaltens von Dampferzeugern mit Vorwärmkammer" [in German], Th. Schwarz, published by Siemens Forsch-Entwicklungsber, 1985.

38. "Steam Generator Feedwater Nozzle Fouling at Duke Power's Oconee Unit 2," G. L. Ward, P. W. Downing, et al. (Duke Power), paper presented at the EPRI Sludge Management Workshop, Myrtle Beach, South Carolina, August 19–21, 1996 (cf. EPRI TR-108047, July 1997).

39. "Dimethylamine Technology to Remove Deposits and Reduce Fouling of Nuclear Steam Generators," R. L. Trent (Calgon Corporation) and B. D. Fellers (Texas Utilities Electric), paper presented at the EPRI Sludge Management Workshop, Myrtle Beach, South Carolina, August 19–21, 1996 (cf. EPRI TR-108047, July 1997).

40. "Dimethylamine Chemistry Demonstration: Nuclear Steam Cycle Application," B. D. Fellers (Texas Utilities Electric) and D. S. Shenberger (Calgon Corporation), paper presented at the 55th Annual International Water Conference, Pittsburgh, PA, October 1–November 2, 1994.

41. "Dimethylamine (DMA) Demonstration to Augment Morpholine Chemistry," B. Fellers, J. Stevens, and G. Nichols (Texas Utilities Electric), paper presented at the EPRI Amine Workshop, New Orleans, LA, September 13–14, 1993.

42. "Characterization of Comanche Peak 2 Steam Generator Sludge," W. A. Byers, J. M. Partezana, et al., Westinghouse Electric Company, February 1998.

43. "Steam Generator Performance Trends, Apparent Cause(s), Solutions," B. D. Fellers (Texas Utilities Electric), paper presented at the EPRI Workshop, Charlotte, NC, February 6, 1996.

Additional Related Reference Materials

44. "Utility Experience with Steam Generator Chemical Cleaning," Electric Power Research Institute Project S523-03, Final Report, EPRI TR-104553, December 1994.

45. Collier, J. G. and Thome, J. R. *Convective Boiling and Condensation,* Clarendon Press–Oxford, Third Edition 1994, pp. 259-64.

46. "Steam Generator Tube Fouling Characteristics and Mechanisms," Baum, A., SG-94-05-007, presented at the EPRI Sludge Management Workshop, May 10-12, 1994, Norfolk, VA.

A

DEI CALCULATION C-5055-00-1

Purpose

This calculation documents the units associated with the equation used by Callaway to compute the pressure drop in the steam piping that exits the steam generators (SGs).

Conclusions

The equation used by Callaway to compute the pressure drop in main steam piping downstream of the SGs is a modified form of the Darcy Equation used for flow of incompressible fluids that includes a correction based on the fluid density. The equation is used in other DEI calculations to determine actual SG outlet pressure from main steam pressure measurements.

Input Data

The equation of interest is reported in Reference (1) and is as follows:

$$\Delta P = \frac{0.00000336(0.0115)(464)}{(26.132)^5} \times \frac{m^2}{\rho} - 0.3076\rho \qquad \text{(eq. A-1)}$$

The above equation is applicable to Loops 1 and 2. A similar equation with "383" in place of "464" is used for Loops 3 and 4.

Calculation and Results

It is believed that Eq. [3-1] is a form of the Darcy Equation with a correction for variable density (the linear term). To confirm this, we begin with the most common form of the Darcy Equation and manipulate it to resemble the first term in Eq. [A-1]. Note that f is the friction factor, L is the pipe length, D is the pipe ID, V is the fluid velocity, Q is the volumetric flow rate, A is the pipe cross-sectional flow area, ρ is the density of the fluid, g_c is the gravitational constant (no units), and $\dot{m}$ is the mass flow rate:

$$\Delta P = f\,\frac{L}{D}\,\frac{V^2}{2g_c}\,\rho$$

$$= f\,\frac{L}{D}\,\frac{\left(Q/A\right)^2}{2g_c}\,\rho = f\,\frac{L}{D}\,\frac{Q^2}{2g_c}\,\frac{\rho}{\left(\frac{\pi}{4}D^2\right)^2} = f\,\frac{L}{D^5}\,\frac{Q^2}{g_c}\,\frac{8}{\pi^2}\,\rho \qquad \text{(eq. A-2)}$$

$$= \frac{8}{\pi^2 g_c}\,f\,\frac{L\dot{m}^2}{\rho D^5}$$

If we postulate that the following units are used in Eq. [A-2],

$[\dot{m}]$ = lb_m/h

$[L]$ = ft

$[g_c]$ = $\dfrac{lb_m - ft}{lb_f - s^2}$

$[D]$ = in

$[\rho]$ = lb_m/ft^3

then the units of Eq. [A-2] may be written as:

$$[\Delta P] = \left(\frac{8}{\pi^2}\right)\left(\frac{lb_f - s^2}{32.2\ lb_m - ft}\right)(ft)\left(\frac{lb_m}{h}\right)^2\left(in^{-5}\right)\left(\frac{ft^3}{lb_m}\right)$$

$$= 0.02517\left(\frac{s^2}{h^2}\right)\left(\frac{ft^3}{in^3}\right)(psi) \qquad \text{(eq. A-3)}$$

Thus, in order for the result of Eq. [A-3] to be "psi," the coefficient that must be multiplied by the term $f\,\dfrac{L\dot{m}^2}{\rho D^5}$ in Eq. [A-2] is given by:

$$C = 0.02517 \times \left(\frac{h^2}{3600^2\,s^2}\right)\left(\frac{12^3\,in^3}{ft^3}\right) = 3.357\ 10^{-6} \qquad \text{(eq. A-4)}$$

(The units in Eq. [A-4] cancel the explicit units in Eq. [A-3] and are thus not taken as part of the constant *C*.) Note that this value is identical to that found in Eq. [A-1]. Thus, it is clear that Eq. [A-1] is a modified form of Eq. [A-2], with the following values:

f = 0.0115

L = 464 ft (or 383 ft for Loops 3 and 4)

D = 26.132 in

The mass flow rate and density vary depending on measured values.

References

1. Fax Transmittal Memo No. 7672, from Steve Ewens (Union Electric) to Glenn White (DEI), June 13, 1996, p. 3.

B

DEI CALCULATION C-5055-00-2

Purpose

This calculation estimates the magnitude of steam pressure decrease associated with a postulated partial secondary tube deposit exfoliation at South Texas 1.

Conclusions

Partially exfoliated deposits (assumed to produce a 0.001" steam-filled gap) that cover 4% of the OD heat-transfer surface at South Texas 1 are sufficient to induce a 20 psi steam pressure loss.

Input Data

The sensitivity of secondary steam pressure at South Texas 1 to changes in fouling factor is equal to –0.235 psi per 10^{-6} h-ft^2-°F/BTU. This information is per calculations performed on South Texas 1 data. The thermal conductivity of steam at 550°F is taken from Reference (1).

Calculation and Results

For the purposes of this calculation, it is assumed that the OD surfaces of the tubes are covered with corrosion deposits. Due to plant transients, it is postulated that the deposits covering some fraction of the tube OD surfaces partially exfoliate, thereby creating a 0.001" annular steam-filled gap between the tube surface and the deposit. If this gap is relatively small and thus not subject to convection heat transfer, then the added thermal resistance associated with the annular gaps is approximately given by the following equation:

$$\Delta R_f'' = \frac{\delta}{k} A_f \qquad \text{(eq. B-1)}$$

where $\Delta R_f''$ is the added resistance, δ is the thickness of the annular gap, k is the thermal conductivity of the steam in the gap, and A_f is the fraction of the tube surface area covered by such partially exfoliated deposits.

In order to relate this change in resistance to a postulated pressure decrease, say 20 psi, we first must calculate the associated resistance increase associated with this pressure decrease:

$$\Delta R_f'' = \frac{\partial R_f''}{\partial p_{sat}} \Delta p_{sat}$$

$$= \frac{1}{-0.235} \left(10^{-6}\, h - ft^2 - {}^\circ F / BTU \; per \; psi\right) \times (-20 \; psi) \qquad \text{(eq. B-2)}$$

$$= 85 \; 10^{-6}\, h - ft^2 - {}^\circ F / BTU$$

Substituting values into Eq. [B-1], we have:

$$85 \; 10^{-6} \; h - ft^2 - {}^\circ F / BTU = \frac{0.001/12 \; ft}{0.038 \; BTU / h - ft - {}^\circ F} A_f \qquad \text{(eq. B-3)}$$

Solving for A_f yields:

$$A_f = 0.039 \qquad \text{(eq. B-4)}$$

Thus, only 4% of the OD surface area of the STP 1 SG tubes would have to be covered by partially exfoliated deposits that create a 0.001" steam-filled gap in order to induce a 20 psi steam pressure decrease.

References

1. ASME Steam Tables, Sixth Edition, American Society of Mechanical Engineers, 1993.

C

PAN MODEL FOR HEAT AND MASS TRANSPORT BY WICK BOILING IN POROUS SURFACE LAYERS

In a series of three papers from the mid-1980s, Pan, Jones, and Machiels (Reference (32) in Chapter 10) (hereafter referred to as Pan) published a fully two-dimensional model of heat and mass transfer for boiling on a porous deposit with evenly spaced chimneys. They assume that vaporization takes place along the chimney wall and that liquid does not enter the chimney directly from the bulk fluid phase. In order to allow the heat, momentum, and mass transfer equations to be written in two dimensions rather than three, Pan replaced the rectangular unit chimney cell with a cylindrical cell of equivalent volume. Figure C-1 illustrates the Pan model and its cylindrical unit cell. His control volume is the "porous shell" of the cylindrical unit cell outside the chimney. Because the convective terms in the heat and momentum equations are neglected, the temperature and pressure inside the shell both satisfy Laplace's equation.

The Schrage model is used to formulate the important expression for the liquid flux at the chimney wall. If the frictional pressure drop in the chimney and any boiling point elevation due to the solute concentration are neglected (as well as any fluid property effects from the solute), then the temperature and velocity fields can be written as infinite series of analytic expressions involving Bessel functions. Because the convective term cannot be neglected for the mass transfer equation, the concentration field must be found using a numerical routine. Pan recommends using a successive over-relaxation method where the diffusive terms are discretized using the central-difference scheme and the convective terms are written using upwind methods. Pan's most complete model considers the effect of boiling-point elevation by coupling the heat- and mass-transport equations.

Advantages of the Pan model include

1. The model predicts heat transfer resistance in addition to concentration factor.

2. Coupling of the heat and mass transfer can be considered.

3. The model can be modified to consider effects such as precipitation in the porous shell or at the heating surface.

4. The one-dimensional simplification of the model, the Cohen model, yields reasonable and well-behaved concentration factors over a wide range of conditions.

5. The physical picture of the model is quite plausible, provided that the interiors of steam chimneys are in fact dry.

Model Assumptions

The Pan model is based on the following assumptions:

- Chimneys are always dry and all evaporation is along the chimney wall.
- Non-axisymmetric effects may be neglected and the problem can be described in two dimensions.
- Vapor temperature in chimneys may be estimated using the pressure drop for a series of chimney segments with uniform wall injection (plus back-pressure due to the chimney mouth bubble).
- The process is assumed to be quasi-steady.
- The thermal boundary condition for the deposit-bulk flow interface may be described by a constant temperature or convection coefficient.
- Volatility of the solute at the chimney wall has a negligible effect on the solute concentration field.
- The evaporative heat-transfer coefficient (or evaporation coefficient) is assumed to be constant along the chimney wall.
- Any variation in the imposed heat flux along the base of the control volume is negligible.

Control Volume/Governing Equations

Pan's control volume is the region of the deposit unit cell outside the chimney. The square cross section of the unit cell is replaced by a circular cross section with the same area. The heat, momentum, and mass transport equations written for the control volume along with their boundary conditions form the mathematical basis of the model.

Pan developed the following scheme for solving the equations when the heat and mass transfer are coupled through the boiling point elevation:

1. Neglect the boiling point elevation and frictional pressure drop in the chimney and calculate the two-dimensional temperature distribution using the eigenvalue solution.

2. Calculate the water flux distribution at the chimney wall using the radial temperature gradient calculated from the temperature distribution.

3. Calculate the flow field within the porous shell using the chimney wall water flux calculated in Step 2 and the eigenvalue solution equation.

4. Calculate the solute concentration field using the numerical over-relaxation method.

5. Estimate the axial vapor pressure distribution in the chimney by applying the perturbation solution for pipe flow with uniform injection for several chimney regions.

6. Return to Step 1 and include the boiling point elevation and frictional pressure drop terms as given by Steps 4 and 5 and the assumed dependence of boiling point elevation on solute concentration. Because the chimney wall water flux distribution is key to the model, changes in it between iterations are used to determine convergence.

In cases of strong coupling between the heat and mass transfer, Pan used predictor-corrector techniques to improve the convergence rate.

Inputs and Intermediate Quantities

Inputs: Environment

q_0'' = imposed heat flux at heating surface (W/m^2)

p_{sat} = system pressure (from which T_{sat} and water properties are calculated) (Pa)

C_b = the bulk solute concentration (mol/m^3)

ΔT_{be} = boiling point elevation as function of solute concentration and temp. (°C)

Inputs: Properties of the Solute

D_l = the molecular diffusivity of the solute in water (m^2/s)

Inputs: Properties of Deposit

δ = deposit thickness (m)

f = fraction of heating surface not occupied by heating surface (–)

ε = the porosity of the porous medium (outside the chimney) (–)

τ = the tortuosity of the porous medium (outside the chimney) (–)

N_v = chimney population density (m^{-2})

r_v = chimney radius (m)

k_m = effective thermal conductivity of porous medium saturated with liquid water (W/m-K) (may be calculated using Maxwell's formula or Bruggeman's equation)

Bruggeman's Equation:

$$\left(\frac{k_m - k'}{k_{sk} - k'}\right)\left(\left|\frac{k_{sk}}{k_m}\right|\right)^{1/3} = 1 - \varepsilon$$

where

k_{sk} = skeletal thermal conductivity of deposit

Intermediate: Properties of Water

ρ_l = density of saturated liquid (kg/m^3)

h_{fg} = latent heat of vaporization (J/kg)

v_{fg} = specific volume change upon vaporization (m^3/kg)

k' = thermal conductivity of saturated liquid (W/m-K)

Intermediate: Nondimensional Quantities

ξ = normalized axial coordinate along chimney
$= z/\delta$

Pe_δ = Peclet number based on layer thickness
$= \delta U_l / D$ (a measure of convective to diffusive effects)

Bi_m = modified Biot number
$$= \delta\sqrt{\frac{2\pi N_v}{f} \cdot \frac{h_e r_v}{k_m}}$$

Other Intermediate

U_l = scaling velocity (m/s)

$$= \frac{q_0^{''}}{fh_{fg}\rho_l}$$

D = effective diffusion coefficient of solute in porous matrix (m^2/s)

$= \tau\varepsilon D_l$

h_e = evaporative heat transfer coefficient at chimney wall (W/m^2-K)

$$= \left(\frac{2E}{2-E}\right)\left(\frac{M}{2\pi R}\right)^{\frac{1}{2}} \frac{h_{fg}^2}{T_{sat}^{3/2} v_{fg}}$$

according to the Schrage model from kinetic theory, which is valid for small evaporation rates, where

E = evaporation coefficient constant (conservative value 0.04)

M = molecular mass of water

R = universal gas constant

T_{sat} = absolute saturation temperature at system pressure

Output: Concentration Factor

ΔT = temperature drop through the porous layer (°C)

ϕ_c = the two-dimensional concentration factor (–)

C = the two-dimensional solute concentration field (mol/m^3)

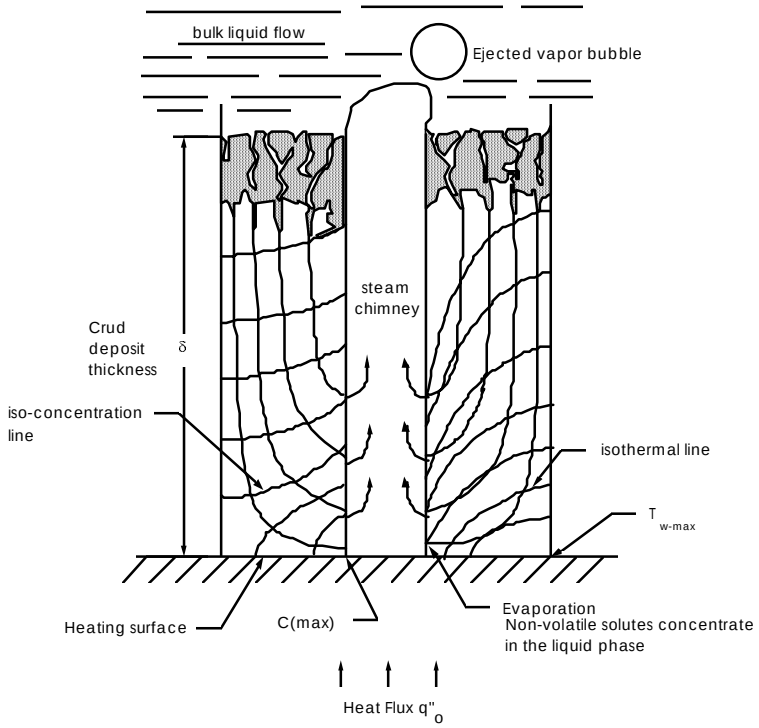

Figure C-1
The Pan Model of Heat and Mass Transport for Wick Boiling

D

ADDITIONAL CASE STUDY: EFFECTS OF DMA ADDITION ON THERMAL PERFORMANCE AT COMANCHE PEAK 2

This appendix serves two primary purposes. First, results analogous to those presented in Chapters 4 through 8 are presented for Comanche Peak Unit 2. The added results augment the database of fouling factor and pressure loss information presented for Callaway, Sequoyah 1, South Texas 1, and SONGS 2 earlier in this report. Second, an analysis of the effects of dimethylamine (DMA) addition on the histories of global fouling factor and SG steam pressure at Comanche Peak 2 is presented. By comparing the history of DMA application with the fouling factor and pressure loss histories, this appendix seeks to establish a correlation between DMA usage and reduced fouling or fouling rates at Comanche Peak 2.

Usage of DMA at Comanche Peak 2 has consisted of both off-line soaks and on-line addition. Specifically, DMA was first used at Comanche Peak 2 during the Cycle 1 mid-cycle outage (MCO 1) in April 1994, followed by on-line additions starting in August 1994 and continuing to the present. A second soak was also instituted during the second refueling outage (RFO 2) in April 1996. The analysis presented in this appendix resulted in a number of significant conclusions regarding the fouling behavior at Comanche Peak 2 and its relationship to DMA addition:

- A major change in SG fouling behavior at Comanche Peak 2 due to DMA was not observed and should not have been expected due to the low level of fouling (calculated at $9 \pm 31\ 10^{-6}$ h-ft^2-°F/BTU as of mid-1997).

- A transient decrease in the fouling factor after the DMA soak during the second refueling outage suggests that DMA can alter the heat-transfer properties of SG scale. Analyses of scale samples taken from the Maine Yankee SGs before and after soaking with DMA suggest that DMA can increase scale porosity, providing independent support for this hypothesis.

- The transient fouling factor decrease mentioned above was followed by a slightly larger fouling factor increase over the succeeding months. This behavior

may reflect a two-step process: a) DMA-induced increases in the scale porosity, which temporarily increased heat transfer (and decreased the fouling factor) by enhancing the efficiency of boiling heat transfer, followed by b) breakup and exfoliation of many of these porous deposits over subsequent operation, resulting in a decrease in boiling heat-transfer efficiency (and an increase in the fouling factor).

- The presence of small transient fouling factor increases correlates well with plant trips. Perhaps the most likely explanation for these transients is small changes in hot-leg temperature streaming associated with temporary changes in core flow patterns after trips. Hot-leg temperature streaming can cause inaccurate primary temperature measurements which result in an apparent increase in the fouling factor. Two other possible explanations—partial deposit exfoliation/steam blanketing and cyclic fouling and de-fouling of the preheater—are unlikely to be responsible for these transients at Comanche Peak 2 in view of the very low level of fouling observed during visual inspections of the tube bundle and the preheater.

- Lower-than-expected heat-transfer margin at Comanche Peak 2 has made the plant susceptible to potential future decreases in electrical generating capacity as a result of modest future decreases in SG thermal performance. Tube plugging and fluctuation in primary temperatures, for example, can cause such performance decreases.

- The effect of DMA on SG thermal performance at plants with high levels of SG fouling (e.g., SONGS 2 prior to chemical cleaning) could be significantly greater than that observed at Comanche Peak 2.

- Due to the differences in heat transfer in SGs with integral preheaters, the effects of DMA on fouling in feedring-type SGs could potentially be significantly different than at Comanche Peak 2 or at other plants with preheater SGs.

The remainder of this appendix is divided into a number of subsections covering the following:

- A brief background on the use of DMA in SGs.

- A detailed discussion of the fouling factor calculations and uncertainty analysis performed for the Comanche Peak 2 SGs.

- A summary of available information on tube scale deposit properties for Comanche Peak 2.

- A breakdown of the observed steam pressure loss at Comanche Peak 2 according to potential causal factors.
- A description of the fouling factor transients observed at Comanche Peak 2 including potential causes.
- A brief discussion of thermal performance measurements at Comanche Peak 2.
- A history of secondary water chemistry at Comanche Peak 2, including the use of morpholine and DMA and the resultant feedwater iron transport.
- The correlation between DMA treatments (including the prolonged soaks during the Cycle 1 mid-cycle outage and the second refueling outage) and subsequent SG fouling behavior.
- A list of suggested follow-up actions to further investigate the potential of DMA for ameliorating SG fouling due to secondary tube scale.

Use of DMA in SG Secondary Feedwater

DMA is an alternate amine that can be used as an additive to control SG feedwater pH. It is also believed to have potential benefits concerning SG fouling that are unrelated to pH control. In particular, it is believed to

a. Have a softening effect on secondary tube scale, thereby allowing the existing scale to be more easily destabilized and dislodged by the passing secondary fluid. Successful use of DMA at Oconee to de-foul feedwater nozzles (38) and DMA application in conjunction with pressure pulse cleaning (PPC) at Farley, which resulted in heavier flake release than previous PPC applications without DMA, tend to confirm this hypothesis.

b. Increase the porosity of tube scale layers, potentially increasing boiling heat-transfer efficiency. Laboratory experiments consisting of soaking scale samples from the Maine Yankee SGs in a DMA solution were performed by the authors. Results of before-and-after observations of the samples indicated an increase in porosity, supporting this hypothesis. DMA injections at Comanche Peak 1 (39, 40, 41), which resulted in the removal of compounds rich in silica and calcium-, magnesium-, and alumino-silicates (see Reference (40) for more detail), provide further evidence. These compounds have been found in dense tube scale at other plants (e.g., Ginna and San Onofre) and are believed to be partly responsible for reducing scale porosity and increasing scale thermal resistance.

c. Reduce the rate of iron transport to the SGs. Several plants in the industry, including Comanche Peak 2, have experienced a decrease in feedwater iron concentration after incorporating DMA in the feedwater chemistry.

d. Alter the local SG water chemistry environment, potentially changing particle sizes and/or deposition mechanisms, which affect the buildup of new tube scale. Analysis of filtered feedwater at Comanche Peak 1 before and after use of DMA revealed a notable decrease in the average particle size (see Tables 1 and 2 in Reference (41)).

As is implied by the above list, DMA may have effects on scale that already exists on tubes and may also slow and/or alter the manner in which new scale is deposited. Separating these effects based on indirect evidence such as global fouling factors is somewhat difficult.

Chapter 4 Analysis for Comanche Peak 2

In this part of Appendix D, the required data and resulting fouling factor calculations for Comanche Peak Unit 2 are presented. The information parallels that provided for Callaway, Sequoyah 1, and South Texas 1 starting on p. 4-7.

Design Data

The relevant thermal-hydraulic design data for the Comanche Peak 2 SGs are used to develop a baseline for the fouling factor and are summarized in the rightmost column of Table D-1. (Values for the other plants in the study are repeated from Table 4-1 for comparative purposes.) Note that the average bundle pressure (1010 psia) is calculated from the outlet pressure (1000 psia) and an estimate of the pressure difference between the middle of the bundle and the outlet. In the absence of a design value, this estimate is based on experience with other plants in the industry.

Measured Operating Data

Full-power measurements at Comanche Peak 2 were provided by Texas Utilities Electric (TUE) for all periods of commercial operation (August 1993 until April 1997). On average, 16 sets of measurements per month were provided, with no gaps longer than 0.1 EFPY between data sets. Measurements were provided either in electronic spreadsheet format or as primary and secondary calorimetric computer printouts. Note that all reported values are two-hour averages.

Listed below are the items used in fouling factor calculations for Comanche Peak 2. These categories are the same as those discussed in Chapter 4:

OUTAGE DATES AND EFPY. The start and end dates of major outages (i.e., refueling outages, mid-cycle outages, and planned in-service inspections) were compiled from References (14) and (15). The effective full-power years (EFPY) of operation at the start of each refueling outage were provided by TUE.

NUMBER OF PLUGGED TUBES. The tube plugging history at Comanche Peak 2 is included in the calculations. Per TUE and Reference (15), a total of only 8 tubes have been plugged (all prior to commercial operation).

PRIMARY TEMPERATURES. For each date, T_{hot}, T_{cold}, and T_{ave} were reported by TUE for each SG. However, because the T_{hot} values are wide-band measurements subject to significant uncertainty, the T_{ave} and T_{cold} values were used to back-calculate T_{hot} for the purposes of the fouling factor calculations.

FEEDWATER TEMPERATURE. Single measurements were reported for each SG; all values are incorporated in the fouling factor calculations.

FEEDWATER PRESSURE. Single measurements of feedwater pressure were provided for each loop; all values were incorporated into the fouling factor calculations.

FEEDWATER FLOW RATE. Single feedwater mass flow rates were provided for each loop.

STEAM MASS FLOW RATE. Single steam flow rates were available from the calorimetric printouts only (December 1996 though April 1997); none was included in the electronic files.

BLOWDOWN FLOW RATE. Total blowdown measurements were provided by TUE for most dates. (When necessary, average values from other operating periods were used.) As with Callaway and Sequoyah 1, blowdown is assumed to be evenly distributed among the four loops.

STEAM PRESSURE. Secondary steam pressure is measured downstream of the SG outlets. Therefore, the measured values must be corrected for the pressure drop from the SG to the location of the measurement. (Note that all measurements reported as gage pressures (psig) are converted to absolute pressures (psia) for the purposes of the fouling factor calculations.)

The main steam pressure recorded by instrumentation is converted to the pressure at the middle of the tube bundle (i.e., average tube bundle pressure) by applying the following corrections:

1. The loss due to flow through the piping between the SG outlet and the pressure transducers. The Comanche Peak 2 transducers are located immediately outside the containment building although the exact distance from the SGs was not provided. Based on data from other plants, including another with model D5 SGs, the pressure loss through this piping is estimated to be 7 psi.

2. Pressure drop between the middle of the tube bundle and the SG outlet nozzle. In the absence of measured data or a plant-specific design value, this is estimated to be 10 psi based on values characteristic of other plants in the industry (e.g., 11.5 psi for Wolf Creek/Callaway, 8 psi for Sequoyah 1, 7 psi for South Texas 1).

CALORIMETRIC THERMAL POWER. Plant-computed thermal power measurements were provided on the hard-copy calorimetric printouts (one value using venturi-meter values for feedwater mass flow rate and a second value using LEFM values for feedwater mass flow rate).

Graphical representations for histories of the above measured parameters are provided at the end of this appendix. They include:

Figure D-1. Historical Steam Generator Outlet Steam Pressure at Comanche Peak 2
Figure D-2a. Historical Hot and Cold Leg Temperatures at Comanche Peak 2
Figure D-2b. Historical Hot Leg Temperature at Comanche Peak 2
Figure D-2c. Historical Cold Leg Temperature at Comanche Peak 2
Figure D-3. Historical Feedwater Mass Flow Rate at Comanche Peak 2
Figure D-4. Historical Feedwater Temperature at Comanche Peak 2

Detailed discussions of these figures are provided at relevant locations in the remainder of the appendix.

With the data described above, the fouling factor is calculated for the operating history of Comanche Peak 2 relative to the design value for the clean thermal resistance. The results are shown in Figure D-5. Key characteristics of the fouling factor history include the following:

- Similarly to Callaway and Sequoyah 1, early Cycle 1 operation at Comanche Peak 2 suggests a *possible* decrease in fouling factor. Note, however, that the decrease is modest (only 10 to 15 10^{-6} h-ft^2-°F/BTU) and is based only on two or three data points taken during the first month of operation and therefore may reflect measurement inaccuracies or normal scatter. Unlike Callaway and Sequoyah 1, no decrease in fouling factor is discernible during the remainder of Cycle 1. Note that this difference in fouling behavior is consistent with the observed feedwater iron transport rates during early operation at the three plants: Callaway (10–20 ppb during Cycle 1) and Sequoyah (10 ppb average over the first four cycles) had substantially higher transport rates than Comanche Peak 2 (about 1.3 ppb during Cycle 1).

- Much like South Texas 1, the startup fouling factor is calculated to be significantly higher than the design values would suggest (approximately 75 10^{-6} h-ft^2-°F/BTU).

- The long-term change in the fouling factor—about +9 10^{-6} h-ft^2-°F/BTU—is very small, suggesting little or no fouling due to secondary tube deposits.

- Short-term transients in the fouling factor correlate well with plant trips, as illustrated in Figure D-5. Most of these transients are marked by a temporary increase in the fouling factor after restart followed by a gradual decrease to approximately the original level. As discussed later under **Fouling Factor and Pressure Transients**, the most likely explanation for these transients may be variations in the degree of hot-leg temperature streaming associated with changes in core flow patterns.

- Comparing one-month periods before and after the second refueling outage, during which a high-concentration DMA soak was applied to the SGs, the fouling factor decreased by about 20 10^{-6} h-ft^2-°F/BTU. However, over the succeeding 0.75 EFPY, the fouling factor increased by roughly 30 10^{-6}, more than offsetting the initial decrease.* Possible connections to the DMA treatment are discussed later in this appendix.

Fouling Factor Uncertainty Analysis

The uncertainty associated with the Comanche Peak 2 fouling factor is calculated using the methodology described in Chapter 4. The input measurement uncertainties are listed in Table D-2. Note that the T_{hot} uncertainty is based on the T_{cold} uncertainty plus a 3°F allowance for hot-leg streaming.† The results of the uncertainty analysis are shown in Table D-3. The uncertainties in primary temperature are the main contributors to the total uncertainty while uncertainties in steam pressure and feedwater flow rate play minor roles. Including the uncertainty, the Comanche Peak 2 fouling factor as of April 1997 is given by

$$R''_{f-CP2} = 9 \pm 31\ 10^{-6} h - ft^2 - ^\circ F / BTU \qquad \text{(eq. 10-5)}$$

---

* Note that this comparison reflects full-power operation. The month immediately following the outage, during which Comanche Peak 2 operated at 96% power, reflects even lower fouling factors but is not part of the comparison. However, because the power level—96%—was so close to full power, it is believed that the variation in power did not significantly affect the fouling factor and that the actual magnitudes of the decrease and subsequent increase in fouling factor may have been closer to -30 10^{-6} and +40 10^{-6}, respectively.

† Although the extent of hot-leg streaming at Comanche Peak 2 is not clear, it is a T_{ave}-controlled plant potentially susceptible to the phenomenon. The 3°F value is believed to be a reasonable bound on the uncertainty due to streaming.

Deposit Properties

In Chapter 5, the properties of secondary tube scale at Callaway, Sequoyah 1, South Texas 1, and SONGS 2 were discussed. For Comanche Peak 2, some chemical characterization data for sludge were available from analyses performed on samples taken during RFO 3 in November 1997 (see Reference (42)). These samples contained little loose powder or typical tube scale; most of the samples included large amounts of debris from other plant components (screen wires, gasket material, etc.). X-ray diffraction (XRD) tests on the sludge material that could be isolated indicated that the predominant component of the sludge particles was magnetite, or Fe_3O_4 (65 to near 100%), with smaller amounts of maghemite, or γ-Fe_2O_3 (trace up to 33%). One sample exhibited 26% silica (SiO_2). Some scale samples were determined to contain copper and agglomerations of alumino-silicates sandwiched between thin layers of iron oxide. These samples were low in porosity.*

No data were available concerning the thickness of the scale samples analyzed or the details of the scale morphology. In fact, historically, deposit loading at Comanche Peak 2 has been so small that tube scale flakes have been very difficult to gather from the routine sludge lancing operations during which samples are normally collected, precluding direct measurements.† As a result, the estimated scale thickness at Comanche Peak 2 is less than 0.5 mils. In fact, the feedwater iron concentration history suggests an average thickness of about 0.2 mils. Due to the extremely small thickness suggested by the feedwater iron transport history, the exact combination of physical and chemical properties of the scale is not expected to have a great impact on heat transfer.‡ The water chemistry and impurity ingress rates at Comanche Peak 2 which have led to this small scale thickness are discussed later in this appendix.

---

* It is unknown whether these dense scale samples reflect tube scale or deposits from tube supports or the TTS.

† According to TUE personnel, sludge lancing operations on the Comanche Peak 2 SGs have netted sludge weights as small as 2 lb per SG.

‡ For example, a 0.2-mil layer of magnetite, with a thermal conductivity of 2.0 BTU/h-ft-°F (28) and purely conductive heat transfer, provides a thermal resistance of only $8\ 10^{-6}$ h-ft^2-°F/BTU. Even a significant error in this calculated resistance would not dramatically affect the resulting global fouling factor. It should also be noted that a 0.2-mil layer is believed to be too thin to result in a significant increase in boiling efficiency, meaning no significant enhancement would be expected either.

Causes of SG Steam Pressure Loss at Comanche Peak 2

Using the techniques outlined in Chapter 6, the best-estimate and bounding pressure losses due to each potential cause were calculated for Comanche Peak 2 as of April 1997. The results for variables which appear in the overall heat-transfer equation (Q, U, A, and T_{cold}/T_{ave}) were computed with the aid of the appropriate partial derivatives, which are reported in Table D-4. The results for these and the other potential causes of pressure loss are shown in the rightmost column of Table D-5. Key observations for Comanche Peak 2 are the following:

- The long-term change in T_{ave} over the operating history, a decrease of 0.7°F, is responsible for a steam pressure decrease of nearly 6 psi. This represents the single largest portion of the total 11-psi decrease observed since the beginning of Cycle 1.

- Secondary tube deposits, believed to be very thin (0.2 mils best estimate), are estimated to have no appreciable net effect on heat transfer. It is possible, in light of the slight net increase in fouling factor following the prolonged DMA soak during RFO 2 (see **Correlation Between SG Fouling Behavior and DMA Addition** below), that the deposits present prior to the soak were slightly beneficial to heat transfer.

- The only other factor estimated to have an effect on steam pressure is hot-leg streaming (4 psi). TUE personnel have indicated that hot-leg streaming is likely, based on the loop asymmetry observed during recent operation. Although no data were available on the magnitude of such streaming, it is judged likely to be at least 0.5°F based on the size of the fouling factor transients in Figure D-5 and experience with streaming at other plants. The corresponding best-estimate pressure loss is 4 psi.

- As noted at the bottom of Table D-5, the best-estimate pressure loss (11 psi) matches the actual observed loss versus the unit's initial performance (11 psi). When calculated relative to the design new pressure, however, the estimated and observed losses are significantly different (11 psi versus 41 psi). This discrepancy suggests a higher-than-expected initial thermal resistance in the SGs. This conclusion is supported by the initial positive fouling factor in Figure D-5 and the initial startup steam pressure of 1003 psia, which is about 30 psi below the expected clean pressure calculated from other design operating values (and only 3 psi above the design VWO pressure). This lack of heat-transfer margin is important because small subsequent decreases in SG thermal performance could result in decreased electrical generating capacity.

- Of the factors listed in Table D-5 which can alter initial performance versus design, only the primary velocity, calculated to be about 10% higher than the design value, is predicted to have had an appreciable effect (a 5-psi *increase*). Pre-service tube plugging and initial primary temperatures each had a very minor effect on the initial pressure compared to design.

  It should also be noted that the fraction of flow sent to the preheater (with the balance sent to the upper internals) was adjusted at Comanche Peak 2 at initial startup from a design value of 90% to 85%. Because the preheater tends to increase the efficiency of the SG, a lower fraction of flow sent through it will decrease the steam pressure. The utility estimates this effect to have decreased the initial steam pressure at Comanche Peak 2 compared to the design pressure by 5–10 psi.

Per Table D-5, the steam pressure losses at Comanche Peak 2 (as of April 1997) can be summarized as follows:

Reported Primary Temperature Variation	6 psi
Total - Well-Known Causes	**6 psi**
Actual Observed Loss	**11 psi**

The remaining 5 psi is probably due to a combination of minor causes, including hot-leg temperature streaming and primary deposits. It is unlikely that secondary deposits (best-estimate average thickness of 0.2 mils) are currently causing a significant decrease (or increase) in steam pressure.*

Fouling Factor and Pressure Transients

The Comanche Peak 2 fouling factor history is marked by a number of transient increases and decreases, as noted briefly earlier and illustrated in Figure D-5. These transient changes correlate well with plant trips, also marked on Figure D-5. The magnitude of these transients ranges from less than 10 10^{-6} h-ft^2-°F/BTU up to about 15 10^{-6}, which is considerably smaller than the largest such transients observed at South Texas 1 (see Chapter 7).

Three plausible explanations for such periodic increases and decreases in fouling factor, as described in Chapter 7, are

* A limited region of significantly thicker deposits (e.g., 1–2 mils or more) is possible. However, the effect on heat transfer of such thicker-than-average deposits (even if they are resistive) is expected to be minimal because more heat would be transferred through the thinner deposits, offsetting the effect of the thicker deposits.

- Cyclic variations in hot-leg temperature streaming associated with reactor trips and outages. In particular, the formation (during operation) and release (after a trip) of corrosion deposits on fuel cladding within the reactor have been noted at Comanche Peak 2. It is possible that the changes in reactor flow patterns (and consequently changes in the flow fields in the hot-leg pipes) induced by these corrosion layers cause variations in primary temperature measurement error. Note that a small change in primary temperature error (on the order of 0.5°F) would result in the apparent transient changes in fouling noted in Table D-5.

- Cyclic fouling and de-fouling of the preheater (either the tubes within the preheater or the preheater baffle plates). As discussed in Chapter 3, fouling in the preheater can increase its thermal resistance and/or alter the flow distribution, both of which can increase the global fouling factor for the SG as a whole. However, visual inspection data from the Comanche Peak 2 preheaters recorded in December 1997 indicate very low levels of fouling, making this explanation unlikely.

- Partial deposit exfoliation accompanied by steam blanketing. As demonstrated in Appendix B, a 1-mil steam gap covering only 4% of the tube bundle could be responsible for the transients observed at South Texas 1. The smaller transients at Comanche Peak 2 could be explained by an even smaller portion of the tube surface area affected by partial exfoliation. It should be noted, however, that visual inspections and sludge retrieval efforts at Comanche Peak 2 revealed very few, if any, flakes on the TTS and TSP surfaces. Thus, this explanation is also judged unlikely to be responsible for the transients observed at Comanche Peak 2.

Based on the above discussions, it appears that transient changes in reactor flow patterns (or some as-yet undetermined phenomenon) is responsible for the transients at Comanche Peak 2. Verifying this explanation conclusively would require detailed measurement of the primary fluid temperature in the hot-leg pipe cross sections before and after reactor trips.

Thermal Performance Measurements at Comanche Peak 2

Like the other plants in this study, steam pressure measurements are taken downstream of the SGs on the main steam piping (32" diameter in this case). Comanche Peak 2 P&IDs indicate that three transducers record the pressure in each of the four loops.* The pressure transducers are located just outside the containment

* Note that reported thermal-hydraulic data include only one value per loop, which may reflect an average of the three transducers or a single transducer value.

building. Based on utility information, the accuracy of the loop pressure measurements is ±3.0 psi, a significantly lower tolerance than at the other plants in the study.

Feedwater mass flow rates at Comanche Peak 2 are measured using both venturis and LEFMs. Unlike the other plants in this study, the LEFMs are typically used as the basis for secondary calorimetric calculations, although the venturi readings are used (usually with a correction factor) if the LEFMs are out of service. The stated tolerance for the venturis is ±1.3% of the design value while the LEFMs are calculated to be accurate within 0.5%. According to TUE personnel, the effects of venturi fouling tend to vary day to day. However, recent LEFM and venturi measurements in early 1997 agreed very well, suggesting minimal venturi fouling.

History of Secondary Water Chemistry at Comanche Peak 2

In order to determine whether the addition of DMA has had an appreciable effect on SG fouling, we now examine briefly the water chemistry history at Comanche Peak 2 and the corresponding feedwater iron concentration. Since the beginning of operation, morpholine has been added to the feedwater as indicated in Figure D-6. Note that the concentration increased from about 10 ppm during the first part of Cycle 1 up to 30 or 40 ppm during more recent operation.

The DMA history at Comanche Peak 2 is illustrated in Figure D-7 (versus operating time in EFPYs) and in Figure D-8 (versus calendar time). DMA was first added to the SG feedwater during the Cycle 1 mid-cycle outage (MCO 1) in April 1994. Over a span of about 10 days during this outage, the SGs were soaked in a solution of approximately 1000 ppb DMA. On-line additions of DMA were begun in August 1994 (0.8 EFPY) and have continued to the present.* A second soak, characterized by the following, was instituted during the second refueling outage (RFO 2) in April 1996:

- A much higher DMA concentration than the first soak (about 7000 ppb)
- A thermal cycle caused by a reactor trip following the initial restart from the refueling outage. After the trip, the DMA concentration was again raised to approximately 7000 ppb (see Figure D-8).

The iron concentration history corresponding to the above water chemistry is illustrated in Figure D-9. Figures D-10 and D-11 show the iron concentration history in combination with the morpholine and DMA histories, respectively. Noteworthy observations regarding these plots include:

---

* Data were only available through mid-1996.

- The overall average feedwater iron concentration since the beginning of commercial operation—between 0.75 and 1 ppb—is lower than for many other plants in the industry, which have typically experienced much higher concentrations early in life (10 ppb or more in some cases).

- The average iron concentration prior to on-line DMA addition (and prior to the higher morpholine concentrations of 30–40 ppb) was approximately 1.3 ppb while the average since the beginning of on-line DMA has been nearly 0.7 ppb. Although not conclusive, this result suggests that the combination of morpholine and on-line DMA is effective at reducing feedwater iron transport rates to very low levels.

Correlation Between SG Fouling Behavior and DMA Addition

One of the major aims of this appendix is to determine any correlations between the apparent fouling behavior of the SGs at Comanche Peak 2 and the DMA additions employed there, particularly the soaks instituted during MCO 1 and RFO 2. Towards this end, the fouling factor history was calculated (Figure D-5) and the history of DMA input was documented (Figure D-7). In Figure D-12, the two histories are superimposed to allow direct comparison. Key observations regarding this plot are the following:

- The MCO 1 DMA soak does not appear to have significantly affected the fouling factor. Discounting the period of low-power operation indicated in Figure D-12, the average fouling factor remained unchanged for the two-month periods preceding and succeeding the MCO 1 soak.

- The on-line DMA addition (500 to 600 ppb) which started in August 1994 (at about 0.8 EFPY) and continued until RFO 2 (2.1 EFPY) also appears to have had no noticeable effect on SG fouling.*

- The high-concentration DMA soak applied during RFO 2 (7000 ppb) was accompanied by a decrease in fouling factor of about 23 10^{-6} h-ft^2-°F/BTU.† However, over the following nine months (0.75 EFPY), the average fouling factor increased by 33 10^{-6} (i.e., to a level 10 10^{-6} higher than the level recorded before the outage) before stabilizing in recent months.

---

* It should be noted that the two significant transients visible in Figure D-12 (at 1.3 EFPY and 1.9 EFPY) occurred immediately after reactor trips. It is judged unlikely that the on-line DMA addition was responsible for these fluctuations in fouling factor.

† This decrease reflects the last two weeks of full-power operation prior to RFO 2 and the first two weeks of full-power operation after the outage. The last two weeks prior to RFO 2 and the first four weeks after the outage were marked by reduced power operation and are consequently not included in the comparison.

This behavior may reflect a two-step process. First, the DMA soak may have induced increases in the scale porosity by selectively dissolving portions of the tube scale layer (40, 43). This increase in porosity enhanced boiling heat-transfer efficiency, temporarily lowering the fouling factor. Second, subsequent operation with DMA caused the total breakup and exfoliation of this porous scale layer, reducing boiling heat-transfer efficiency and increasing the fouling factor.

While the above points seem to suggest that DMA did not significantly increase long-term SG thermal performance at Comanche Peak 2, it should be noted that:

- DMA has aided in keeping the Comanche Peak 2 tubes quite clean, reducing the potential for some forms of severe tube corrosion and helping to prevent the buildup of thick tube scale layers which could in the future be thermally resistive (as at SONGS 2).

- Because the net change in average fouling factor at Comanche Peak 2 has been so small—actually decreasing by a negligible $2\ 10^{-6}$ just prior to RFO 2 compared to early operation—no significant improvement in fouling factor should have been expected from the DMA soaks because the secondary tube scale layer that is present is already having a small effect on heat transfer.

- As discussed before, the temporary decrease in fouling after RFO 2 may have resulted from DMA-induced increases in scale porosity which increased heat transfer through wick boiling (capillary force effects) and changes in bubble nucleation and growth dynamics. This hypothesis is further supported by the fact that the net fouling factor just after RFO 2 was significantly negative compared to early operation ($-24\ 10^{-6}$).

- For plants with significant increases in heat-transfer resistance due to secondary deposits (e.g., SONGS 2 prior to the chemical cleaning), the effects of DMA on subsequent fouling could be significantly more pronounced than for Comanche Peak 2. In particular, since DMA has been shown to be capable of increasing the porosity of a scale layer in some circumstances, there is the potential for creating a heat-transfer enhancing (or less thermally resistive) layer of scale from a previously resistive layer, thereby reducing the SG fouling factor. Such a change might also last longer than at Comanche Peak 2 if DMA is capable of increasing the porosity of dense, consolidated scale layers. On the other hand, it is also possible that DMA could strip away the porous, enhancing outer few mils of a thick deposit layer, leaving unchanged a thermally resistive layer below and thereby increasing the fouling factor.

Possible Follow-Up Activities Concerning Industry Application of DMA Treatments

The foregoing analysis does not provide definitive evidence regarding the potential for DMA applications to permanently reduce SG fouling factors, largely because Comanche Peak 2 has exhibited such small net fouling factors over its operating life. In spite of this conclusion, the results of the high-concentration soak during RFO 2 indicate the potential that DMA could enhance thermal performance at more heavily fouled plants. Consequently, the following steps are suggested from a steam generator thermal performance standpoint:*

1. Consider further high-concentration DMA soaks at Comanche Peak 2 during future refueling outages in order to determine whether the transient fouling factor decrease observed after RFO 2 is repeatable. By also tracking the iron transport to the SGs between soaks, confirmation of the hypothesis that prolonged DMA soaks first increase scale porosity and then cause the scale to exfoliate might be possible.

2. Investigate the effects of DMA, especially high-concentration soaks, on a plant with SGs that exhibit significant fouling (i.e., a level at least approaching that of SONGS 2 prior to chemical cleaning—100 10^{-6} h-ft^2-°F/BTU or more). Such a study will help determine whether DMA is capable of effecting a significant *in situ* change in the heat-transfer properties of such resistive tube scale. Metallographic cross sections of tube scale flakes collected before and after the application of DMA soaks could reveal whether the inner, consolidated tube scale layer can be affected by DMA. As discussed for SONGS 2 in Chapter 5, the inner, primarily nonporous layer can cause high SG fouling factors.

   Because integral preheaters increase the uncertainty of the fouling factor calculation and also because preheater fouling can affect the overall performance of the SGs irrespective of any changes in secondary tube scale in the remainder of the bundle, it is recommended that any plant chosen for such a study have feedring-type SGs.

* Please note that these suggestions do not reflect any evaluation of the costs or potential effects of DMA on other plant components. Utilities considering DMA for the first time must account for these factors before deciding to proceed with such treatments.

Table D-1
Design Steam Generator Heat-Transfer Parameters (Including Comanche Peak 2)

Parameter	Units	Callaway	Sequoyah 1	South Texas 1	Comanche Peak 2
T_{hot}	°F	620	609.7	626.1	618.8
T_{cold}	°F	557	546.7	559.7	559.3
Steam Generator Dome Pressure	psia	1000	857	1100	1000
Steam Generator Avg. Bundle Pressure	psia	1012	865	1107	1010
Saturation Temp. for Avg. Bundle Pressure	°F	546.1	527.3	557.1	545.8
Thermal Power (per SG)	MWt	895	856	954	856
Thermal Power (per SG)	BTU/h	3.053E+09	2.920E+09	3.256E+09	2.922E+09
Heat Transfer Area (OD)	ft^2	55,000	51,500	68,000	48,300
Average Heat Flux (Based on OD Area)	BTU/h-ft^2	55,509	56,698	47,882	60,489
Design Plugging Margin	–	15%	0%	0%	0%
Number of Tubes (per SG)	–	5626	3388	4864	4570
Feedwater Temperature	°F	446.0	434.5	440.0	440.0
Feedwater Pressure	psia	1025	876	1129	1021
Secondary Mass Flow Rate	lb_m/h	3.963E+06	3.749E+06	4.240E+06	3.785E+06
Flow Split (Preheater/Upper Internals)	%	–	–	100/0	90/10
Blowdown Flow Rate	lb_m/h	31,250	20,000	NA[†]	NA[†]

[†] Not available; average actual values were 39,000 and 46,500, respectively.

Table D-2
Comanche Peak 2 Measurement Uncertainties

Symbol	Quantity	Tolerance	Source
T_{hot}	Hot-Leg Temperature	±4.2°F	Best Estimate[2]
T_{cold}	Cold-Leg Temperature	±1.2°F	TUE Personnel
p_{sat}	SG Steam Pressure	±3.0 psi	TUE Personnel
m_{FW}	Feedwater Flow Rate	±1.3% design (±4.9 10^4 lb_m/h)	TUE Personnel
T_{FW}	Feedwater Temperature	±2°F	Bounding Estimate
Q_{BD}	Blowdown Flow Rate	±2% (930 lb_m/h)	TUE Personnel
p_{FW}	Feedwater Pressure	±0.25% FS (±5 psi)	TUE Personnel
x	Steam Quality	±0.10%	Bounding Estimate
A	Heat-Transfer Area	0.25% (±121 ft^2)[1]	Bounding Estimate

NOTES

1. This tolerance reflects the possibility that plugged tubes may be longer or shorter on average than the average-lengtl tube in the whole bundle.
2. Includes 3°F allowance for hot-leg temperature streaming.

Table D-3 (p. 1 of 2)
Fouling Factor Uncertainty Analysis for Comanche Peak 2

Quantity	Description	Units	Design Value (VWO)	Bilateral Tolerance	Δx
Measured quantities					
T_{hot}	hot leg temperature	°F	618.8	4.2	4.2
T_{cold}	cold leg temperature	°F	559.3	1.2	1.2
T_{FW}	feedwater temperature	°F	440	2.0	2.0
m_{FW}	feedwater flow rate	lb/h	3.785E+06	1.29%	4.883E+04
Q_{BD}	blowdown volumetric flow rate	gpm	125	2%	3
p_{FW}	feedwater pressure	psia	1021	5.0	5.0
p_{sat}	steam generator dome pressure	psia	1000	3.0	3.0
x	steam quality	%	99.90	0.10	0.10
A	heated outside-tube surface area	ft^2	48,300	0.25%	121
Intermediate quantities					
$T_{sat,out}$	outlet saturation temperature	°F	544.6		
p_{bundle}	mid-bundle pressure	psia	1010		
T_{sat}	bundle saturation temperature	°F	545.8		
DT_{lm}	log-mean temperature difference	°F	35.24		
v_f	saturated liquid specific volume	ft^3/lb	0.02164		
m_{BD}	blowdown mass flow rate1	lb/h	46,500		
m_{steam}	steam flow rate	lb/h	3.739E+06		
h_f	saturated liquid specific enthalpy	Btu/lb	544.1		
h_g	saturated vapor specific enthalpy	Btu/lb	1192.6		
$h_f(T_{FW})$	feedwater saturated spec. enthalpy	Btu/lb	419.0		
$v_f(T_{FW})$	feedwater saturated spec. volume	ft^3/lb	0.01926		
$p_{sat}(T_{FW})$	saturation pressure at feedwater T	psia	381.54		
h_{FW}	feedwater specific enthalpy	Btu/lb	421.2		
Q	steam generator heat transfer rate	Btu/h	2.887E+09		
R	global resistance to heat transfer	h-°F/Btu	1.221E-08		
U	global heat transfer coefficient	Btu/h-ft^2-°F	1696		
Calculated quantity					
R"	global area-based resistance	10^{-6} h-ft^2-°F/Btu	589.6		
Other quantities required for partial derivatives					
$c_{p,FW}$	feedwater specific heat	Btu/lb-°F	1.103		
v_{FW}	feedwater specific volume	ft^3/lb	0.01926		
h_{fg}	latent heat of vaporization at psat	Btu/lb	648.5		
v_g	saturated vapor specific volume	ft^3/lb	0.4412		
v_{fg}	specific volume change upon vap.	ft^3/lb	0.4195		
$\partial h_g/\partial p_{sat}$	partial derivative of vapor enthalpy	(Btu/lb)/psi	-0.03473		
$\partial h_f/\partial p_{sat}$	partial derivative of liquid enthalpy	(Btu/lb)/psi	0.1533		
$\partial(h_{fg}/v_f)/\partial p_{sat}$	partial derivative of h_{fg}/v_f ratio	(Btu/ft^3)/psi	-13.86		
$\partial Q/\partial p_{sat}$	partial derivative of thermal power	(Btu/h)/psi	-116,818		

Table D-3 (p. 2 of 2)
Fouling Factor Uncertainty Analysis for Comanche Peak 2

Partial derivatives of area-based resistance		Units for ∂R''/∂x	**∂R''/∂x**	**Δ(x)**	**(∂R''/∂x)Δ(x)**
$\partial R''/\partial T_{hot}$	partial deriv. wrt hot leg temp.	$(10^{-6}$ h-ft^2-°F/Btu)/°F	5.125	4.2	21.52
$\partial R''/\partial T_{cold}$	partial deriv. wrt cold leg temp.	$(10^{-6}$ h-ft^2-°F/Btu)/°F	15.976	1.2	19.17
$\partial R''/\partial T_{FW}$	partial deriv. wrt feedwater temp.	$(10^{-6}$ h-ft^2-°F/Btu)/°F	0.853	2.0	1.71
$\partial R''/\partial m_{FW}$	partial deriv. wrt feedwater flow	$(10^{-6}$ h-ft^2-°F/Btu)/(lb/h)	-1.574E-04	4.883E+04	-7.69
$\partial R''/\partial Q_{BD}$	partial deriv. wrt blowdown flow	$(10^{-6}$ h-ft^2-°F/Btu)/gpm	0.049	3	0.12
$\partial R''/\partial p_{FW}$	partial deriv. wrt feedwater press.	$(10^{-6}$ h-ft^2-°F/Btu)/psi	0.003	5	0.01
$\partial R''/\partial p_{sat}$	partial deriv. wrt steam gen. press.	$(10^{-6}$ h-ft^2-°F/Btu)/psi	-2.516	3	-7.55
∂R''/∂x	partial deriv. wrt outlet quality	$(10^{-6}$ h-ft^2-°F/Btu)/%	-4.952	0.10	-0.50
∂R''/∂A	partial deriv. wrt heated area	$(10^{-6}$ h-ft^2-°F/Btu)/ft^2	0.012	121	1.47
				$\Sigma\lvert(\partial R''/\partial x)\Delta(x)\rvert$	59.74
				$\Sigma[(\partial R''/\partial x)\Delta(x)]^2$	952.27
				$\{\Sigma[(\partial R''/\partial x)\Delta(x)]^2\}^{1/2}$	30.86
Final results of error analysis			**Design**	$\Delta_{worst\ case}(R'')$	$\Delta_{statistical}(R'')$
R''	global area-based resistance	10^{-6} h-ft^2-°F/Btu	589.6	59.7	30.9

Notes
1. The average reported blowdown flow rate is used in lieu of a design value.

Table D-4
Sensitivity of Comanche Peak 2 SG Pressure to Other Parameters in Overall Heat Transfer Equation

Quantity	Description	Units	Design VWO	Early Operation	Recent Operation (Cycle 3)
nominal values of parameters in overall heat transfer coefficient equation (inputs)					
T_{hot}	hot leg temperature	°F	618.8	616.2	615.7
T_{cold}	cold leg temperature	°F	559.3	561.9	561.0
p_{sat}	steam generator dome pressure	psia	1000	1003	992
A	total outside-tube surface area	ft^2	48,300	48,279	48,279
N_{tot}	total number tubes	--	4570	4568	4568
Q	steam generator thermal power	MWt	856	852	856
nominal values of parameters in overall heat transfer coefficient equation (calculated)					
p_{bundle}	mid-bundle pressure	psia	1011	1014	1003
T_{sat}	bundle saturation temperature	°F	545.9	546.29	544.93
Q	steam generator thermal power	Btu/h	2.922E+09	2.906E+09	2.920E+09
ΔT_{lm}	log-mean temperature difference	°F	35.09	36.19	36.91
R	global resistance to heat transfer	h-°F/Btu	1.201E-08	1.246E-08	1.264E-08
U	global heat transfer coefficient	Btu/h-ft^2-°F	1724	1663 (1)	1639
R''	global area-based resistance	10^{-6} h-ft^2-°F/Btu	580.1	601.3	610.2
calculation of dp_{sat}/dT_{sat} using Clapeyron relation: $dp_{sat}/dT_{sat} = h_{fg}/(Tv_{fg})$					
h_f	saturated liquid specific enthalpy	Btu/lb	544.2	544.7	543.0
h_g	saturated vapor specific enthalpy	Btu/lb	1192.5	1192.4	1192.9
h_{fg}	latent heat of vaporization at p_{sat}	Btu/lb	648.3	647.7	649.9
T	absolute bundle saturation temp.	°R	1005.6	1006.0	1004.6
v_f	saturated liquid specific volume	ft^3/lb	0.0216	0.0216	0.0216
v_g	saturated vapor specific volume	ft^3/lb	0.4407	0.4392	0.4448
v_{fg}	specific volume change upon vap.	ft^3/lb	0.4191	0.4176	0.4232
$\partial p_{sat}/\partial T_{sat}$	partial deriv. of sat. press. with T	psi/°F	8.31	8.33	8.26
partial derivatives of steam generator pressure					
effect of variations in reactor coolant loop temperature					
$\partial p_{sat}/\partial T_{cold/ave}$	partial deriv. wrt RCL temperature	psi/°F	8.31	8.33	8.26
effect of tube plugging					
$\partial p_{sat}/\partial A$	partial deriv. wrt heated area	psi/ft^2	0.00478	0.00519	0.00528
$\partial p_{sat}/\partial N_{plug}$	partial deriv. wrt no. tubes plugged	psi/tube plugged	-0.051	-0.055	-0.056
$\partial p_{sat}/\partial \%_{plug}$	partial deriv. wrt % tubes plugged	psi/1% plugged	-2.31	-2.51	-2.55
effect of variations in steam generator thermal power					
$\partial p_{sat}/\partial Q$	partial deriv. wrt thermal power	psi/(Btu/h)	-1.23E-07	-1.23E-07	-1.23E-07
$\partial p_{sat}/\partial Q$	partial deriv. wrt thermal power	psi/MWt	-0.419	-0.418	-0.419
effect of variations in overall heat transfer coefficient (fouling factor)					
$\partial p_{sat}/\partial U$	partial deriv. wrt overall HT coeff.	psi/(Btu/h-ft^2-°F)	0.134	0.151	0.156
$\partial p_{sat}/\partial R_f$''	partial deriv. wrt fouling factor	psi/(10^{-6} h-ft^2-°F/Btu)	-0.398	-0.417	-0.418

NOTES
1. The corresponding heat-transfer coefficient calculated for clean conditions is 1914.

Table D-5
Sources of Steam Generator Pressure Degradation (Including Comanche Peak)

		Callaway Just Before Chem Clean			Callaway After CC (1/96-4/96)			Sequoyah 1 Just Before Chem Clean			Sequoyah 1 After CC (3/96-5/96)			South Texas 1 (2/96-6/96)			SONGS 2 Just Before CC			Comanche Peak 2 (2/97-4/97)		
Steam generator type		Westinghouse Model F						Westinghouse Model 51						W Model E2			CE Model 3410			West. Model D5		
Current EFPYs		8.63			9.54			7.49			7.91			5.02			10.02			3.01		
Design plugging margin for heat transfer		0%						0%						0%			10%			0%		
Current plugging level		0.63%			0.80%			1.32%			2.53%			1.32%			3.70% (EOC 8)			0.04%		
Current fouling factor (10^{-6} h-ft^2-°F/Btu)		-28 ± 19			-5 ± 19 (1)			21 ± 24			42 ± 24 (1)			30 ± 62			172 ± 48			9 ± 31		
Nominal design dome pressure (psia)		1000						857						1100			900			1000		
Design start-up dome pressure (psia)		1009						878						1106			941			1033		
Actual start-up dome pressure (psia)		1003						877						1115			933			1002		
Current dome pressure (psia)		986			975			852			841			1052			855			991		
Current total pressure loss vs. Initial Perf. (psi)		17			28			25			36			63			77			11		
Deposit Fouling Factors from Local Heat Transfer Analyses (10^{-6} h-ft^2-°F/Btu)		Lower Bound	Best Estimate	Upper Bound	Lower Bound	Best Estimate	Upper Bound	Lower Bound	Best Estimate	Upper Bound	Lower Bound	Best Estimate	Upper Bound	Lower Bound	Best Estimate	Upper Bound	Lower Bound	Best Estimate	Upper Bound	Lower Bound	Best Estimate	Upper Bound
Secondary freespan deposits		-30.0	-15.0	0.0	2.4	9.7	29.1	-15.0	28.8	107.0	2.4	9.7	29.1	-15.0	0.0	5.0	51.1	185.1	363.6	-5.0	0.0	10.0
Secondary flow blockage and extra friction	lower recirc ratio (2)	-5.8	5.3	17.8	flow paths open &			-11.2	0.0	11.2	flow paths open &			-4.3	0.0	4.3	-4.5	6.0	19.5	flow paths open &		
	greater Δp in bundle		(3)		little extra friction				(3)		little extra friction				(3)			(3)		little extra friction		
Primary deposits		0.4	2.1	30.9	0.4	2.1	30.9	0.4	2.1	30.9	0.4	2.1	30.9	0.4	2.1	30.9	0.4	2.1	31.4	0.4	2.1	30.9
Total (10^{-6} h-ft^2-°F/Btu)		*-35.4*	*-7.6*	*48.8*	*2.8*	*11.8*	*60.1*	*-25.8*	*30.8*	*149.1*	*2.8*	*11.8*	*60.0*	*-18.8*	*2.1*	*40.1*	*47.0*	*193.2*	*414.5*	*-4.6*	*2.1*	*40.9*
SOURCES OF PRESSURE LOSS (psi)		Lower Bound	Best Estimate	Upper Bound	Lower Bound	Best Estimate	Upper Bound	Lower Bound	Best Estimate	Upper Bound	Lower Bound	Best Estimate	Upper Bound	Lower Bound	Best Estimate	Upper Bound	Lower Bound	Best Estimate	Upper Bound	Lower Bound	Best Estimate	Upper Bound
Sources That Affect Initial Performance vs. Ideal Design Performance (But Not Pressure Loss Since Start-Up)																						
Pre-service tube plugging		0.3	0.3	0.3	0.3	0.3	0.3	0.0	0.0	0.0	0.0	0.0	0.0	0.1	0.1	0.1	0.4	0.4	0.4	0.1	0.1	0.1
Initial RCL temps. different than design		-0.6	8.6	17.8	-0.6	8.6	17.8	-5.1	6.8	18.6	-5.1	6.8	18.6	-49.3	-13.8	21.7	-23.8	-1.5	20.8	-35.7	0.4	36.5
Primary tube velocity different than design		-4.0	-3.1	-1.7	-5.2	-2.9	-0.5	-0.4	1.1	2.7	-0.4	1.1	6.9	-3.4	-2.2	-0.3	-5.8	-3.5	-2.9	-8.3	-4.8	0.1
Tube thickness variation from nominal		-12.3	0.0	12.5	-12.3	0.0	12.5	-15.2	0.0	15.4	-15.2	0.0	15.4	-8.6	0.0	8.7	-16.1	0.0	16.3	-15.3	0.0	15.5
Tube thermal cond. variation from nominal		-5.5	0.0	6.1	-5.5	0.0	6.1	-6.8	0.0	7.6	-6.8	0.0	7.6	-3.9	0.0	4.3	-7.2	0.0	8.0	-6.9	0.0	7.6
Subtotal (psi) (not included in Total below)		*-22.2*	*5.8*	*35.0*	*-23.3*	*6.0*	*36.2*	*-27.5*	*7.9*	*44.3*	*-27.5*	*7.9*	*48.4*	*-65.2*	*-15.9*	*34.5*	*-52.5*	*-4.6*	*42.5*	*-66.0*	*-4.3*	*59.8*
Sources That are Due to Deposits within the Tube Bundle																						
Secondary freespan deposits		-10.8	-5.4	0.0	0.9	3.5	10.5	-5.3	10.3	38.2	0.9	3.5	10.4	-3.5	0.0	1.2	19.8	71.9	141.2	-2.1	0.0	4.2
Secondary flow blockage and extra friction	lower recirc ratio (2)	-2.1	1.9	6.4	flow paths open &			-4.0	0.0	4.0	flow paths open &			-1.0	0.0	1.0	-1.7	2.3	7.5	flow paths open &		
	greater Δp in bundle		(3)		little extra friction				(3)		little extra friction				(3)			(3)		little extra friction		
Primary deposits		0.1	0.7	11.2	0.1	0.7	11.2	0.1	0.7	11.0	0.1	0.7	11.0	0.1	0.5	7.3	0.2	0.8	12.2	0.2	0.9	12.9
Subtotal (psi)		*-12.8*	*-2.7*	*17.6*	*1.0*	*4.3*	*21.7*	*-9.2*	*11.0*	*53.2*	*1.0*	*4.2*	*21.4*	*-4.4*	*0.5*	*9.4*	*18.3*	*75.0*	*160.8*	*-1.9*	*0.9*	*17.1*
Sources That are NOT Due to Deposits within the Tube Bundle which are Captured in the Fouling Factor Calculation																						
Uncertainty in steam generator press. meas.		-6.5	0.0	6.5	-6.5	0.0	6.5	-4.8	0.0	4.8	-4.8	0.0	4.8	-7.5	0.0	7.5	-6.0	0.0	6.0	-3.0	0.0	3.0
Extra separator/dryer pressure drop		3.5	4.0	4.4	3.5	4.0	4.4	0.0	0.0	4.0	0.0	0.0	4.0	0.0	0.0	13.0	0.0	4.0	13.0	0.0	0.0	3.0
Error in applied primary temperature due to	$T_{cold/ave}$ meas. error	-4.6	0.0	4.6	-4.6	0.0	4.6	-5.9	0.0	5.9	-5.9	0.0	5.9	-17.8	0.0	17.8	-22.3	0.0	22.3	-18.0	0.0	18.0
	Hot leg streaming	0.0	4.0	5.9	0.0	4.0	5.9	0.0	14.7	22.0	0.0	14.7	22.0	0.0	12.9	25.9	T_{cold} control plant			0.0	4.1	12.4
	Divider plate leakage	0.00	0.02	2.4	0.00	0.02	2.4	0.00	0.02	2.3	0.00	0.02	2.3	0.00	0.03	2.8	0.00	0.04	3.9	0.00	0.02	2.3
Error in reactor power calibration due to uncertainty in	FW flow including venturi fouling	-2.2	0.0	3.9	-2.2	0.0	3.9	-2.2	0.0	4.1	-2.2	0.0	4.1	-1.6	0.0	3.2	-1.9	0.5	3.8	-4.6	0.0	6.4
	FW temperature	-0.5	0.0	0.5	-0.5	0.0	0.5	-0.8	0.0	0.8	-0.8	0.0	0.8	-0.5	0.0	0.5	-0.8	0.0	0.8	-1.0	0.0	1.0
	Outlet steam quality	-0.5	0.0	0.5	-0.5	0.0	0.5	-0.5	0.0	0.5	-0.5	0.0	0.5	-0.4	0.0	0.4	-0.3	0.0	0.3	-0.3	0.0	0.3
	Blowdown flow	-0.02	0.0	0.02	-0.02	0.0	0.02	-0.2	0.0	0.2	-0.2	0.0	0.2	-0.2	0.0	0.2	-0.01	0.0	0.0	-0.1	0.0	0.1
Subcooling (feedwater temp. variations) (2)		-2.1	-0.7	0.0	-10.1	-3.4	0.0	-2.0	0.0	2.0	-1.0	0.0	1.0	-1.0	0.0	1.0	-4.3	-1.4	0.0	-1.0	0.0	1.0
Flow maldistribution in preheater														0.0	3.0	15.0				0.0	0.0	3.0
Subtotal (psi)		*-12.9*	*7.2*	*28.8*	*-20.9*	*4.5*	*28.8*	*-16.4*	*14.7*	*46.6*	*-15.4*	*14.7*	*45.6*	*-28.9*	*16.0*	*87.2*	*-35.6*	*3.1*	*50.1*	*-28.1*	*4.2*	*50.5*
Apparent fouling factor corresponding to this pressure loss (10^{-6} h-ft^2-°F/Btu)		*-36*	*20*	*80*	*-58*	*13*	*80*	*-46*	*41*	*131*	*-43*	*41*	*128*	*-123*	*68*	*371*	*-92*	*8*	*129*	*-67*	*10*	*121*
Net fouling factor after subtracting this component (10^{-6} h-ft^2-°F/Btu)		*8*	*-48*	*-108*	*53*	*-18*	*-85*	*66*	*-21*	*-110*	*85*	*1*	*-86*	*153*	*-38*	*-341*	*264*	*164*	*43*	*76*	*-1*	*-112*
Sources That are Accounted for by the Fouling Factor Calculation																						
Tube plugging since start-up		1.2	1.2	1.2	1.6	1.6	1.6	3.6	3.6	3.6	6.9	6.9	7.0	1.5	1.5	1.5	11.6	11.7	11.8	0.0	0.0	0.0
T_{cold}/T_{ave} variations vs. design temperatures		4.5	9.1	13.7	6.9	11.5	16.1	0.7	6.6	12.5	1.4	7.3	13.3	20.2	37.9	55.7	-28.2	-5.9	16.3	-11.8	6.2	24.2
T_{cold}/T_{ave} variations vs. initial temperatures		-3.8	0.8	5.4	-1.3	3.3	7.9	-5.9	0.0	5.9	-5.2	0.7	6.7	33.9	51.7	69.5	-26.7	-4.5	17.8	-12.3	5.8	23.8
Variations in thermal power		-4.5	-3.6	-2.7	-3.6	-2.7	-1.8	-3.7	-2.8	-1.9	-2.8	-1.9	-0.9	-1.6	-0.8	0.0	-1.3	-0.7	0.0	-0.9	0.0	0.9
Power uprate		13.9	15.4	17.0	13.9	15.4	17.0	No Uprate			No Uprate			No Uprate			No Uprate			No Uprate		
Subtotal vs. Design (psi)		*15.1*	*22.1*	*29.2*	*18.8*	*25.9*	*32.9*	*0.5*	*7.4*	*14.3*	*5.5*	*12.4*	*19.3*	*20.0*	*38.6*	*57.2*	*-17.9*	*5.1*	*28.2*	*-12.7*	*6.2*	*25.1*
Subtotal vs. Initial Perf. (psi)		*6.8*	*13.9*	*20.9*	*10.6*	*17.7*	*24.7*	*-6.1*	*0.8*	*7.7*	*-1.1*	*5.8*	*12.7*	*33.8*	*52.4*	*70.9*	*-16.4*	*6.6*	*29.7*	*-13.2*	*5.8*	*24.7*
Summary																						
Best-Est. Total Loss vs. Design New (psi) (4)		***27***			***35***			***33***			***31***			***55***			***83***			***11***		
Actual Total Loss vs. Design New (psi)		***23***			***34***			***26***			***37***			***54***			***85***			***42***		
Best-Est. Total Loss vs. Initial Perf. (psi) (4)		***18***			***26***			***27***			***25***			***69***			***85***			***11***		
Actual Total Loss vs. Initial Perf. (psi)		***17***			***28***			***25***			***36***			***63***			***77***			***11***		

(1) The fouling factor has been decreasing at Callaway and Sequoyah 1 since just after chemical cleaning. Callaway's has decreased about 11 10^{-6} and Sequoyah's has decreased about 4 10^{-6}.
(2) The values for Callaway and SONGS 2 are preliminary results of a one-dimensional heat transfer model of the steam generator using the Chen correlation for secondary resistance. The values for Sequoyah 1 and South Texas 1 are estimates based on engineering judgment.
(3) This effect may be evaluated using ATHOS modeling.
(4) These estimates include calculated pressure losses due to secondary deposits based on available tube scale characterization data.

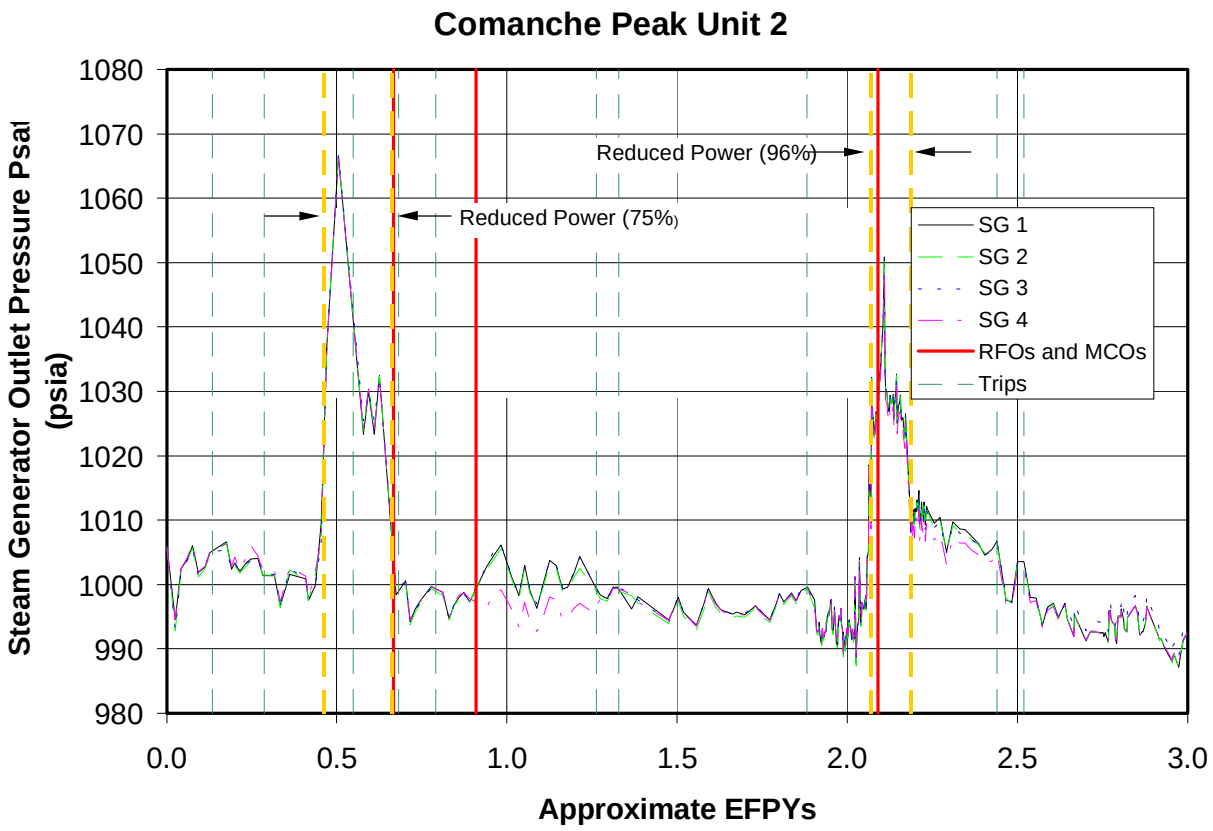

Figure D-1
Historical Steam Generator Outlet Steam Pressure at Comanche Peak 2

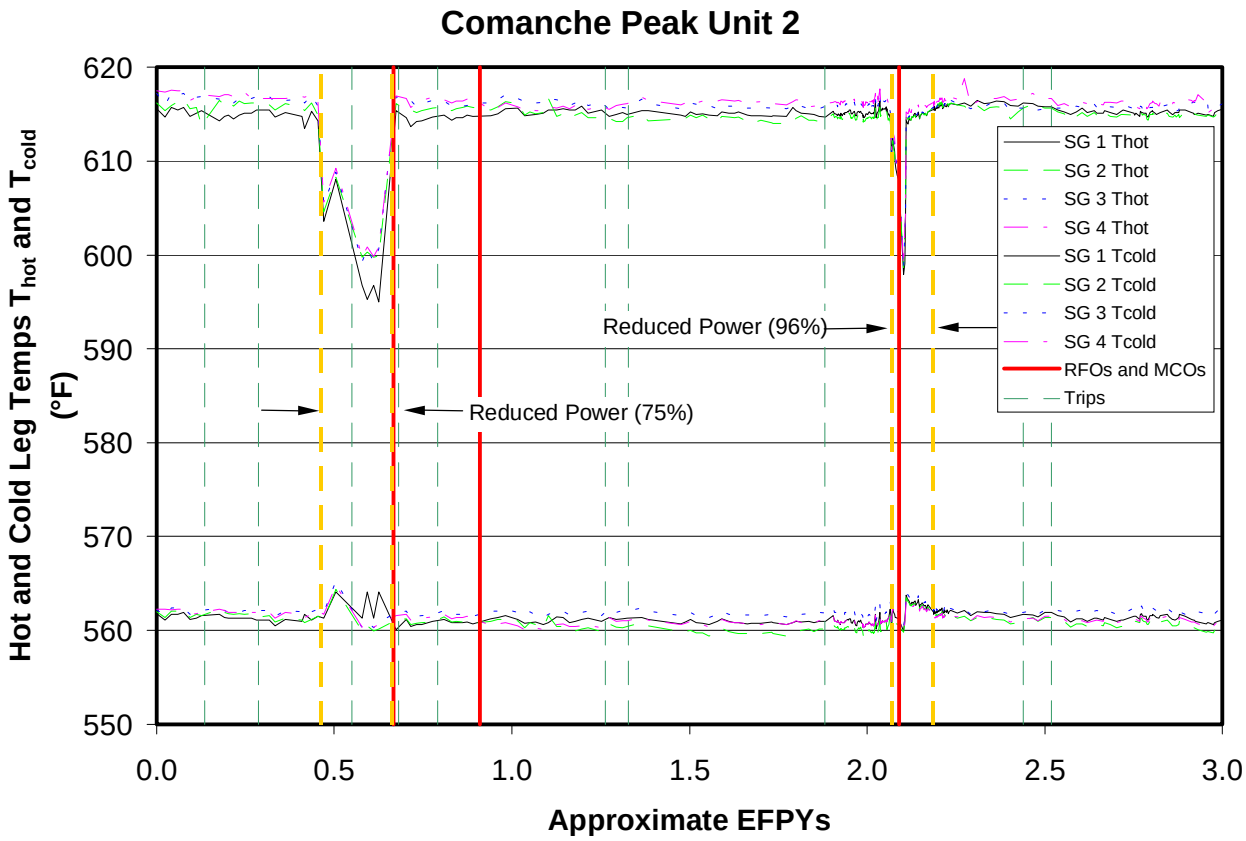

Figure D-2a
Historical Hot and Cold Leg Temperatures at Comanche Peak 2

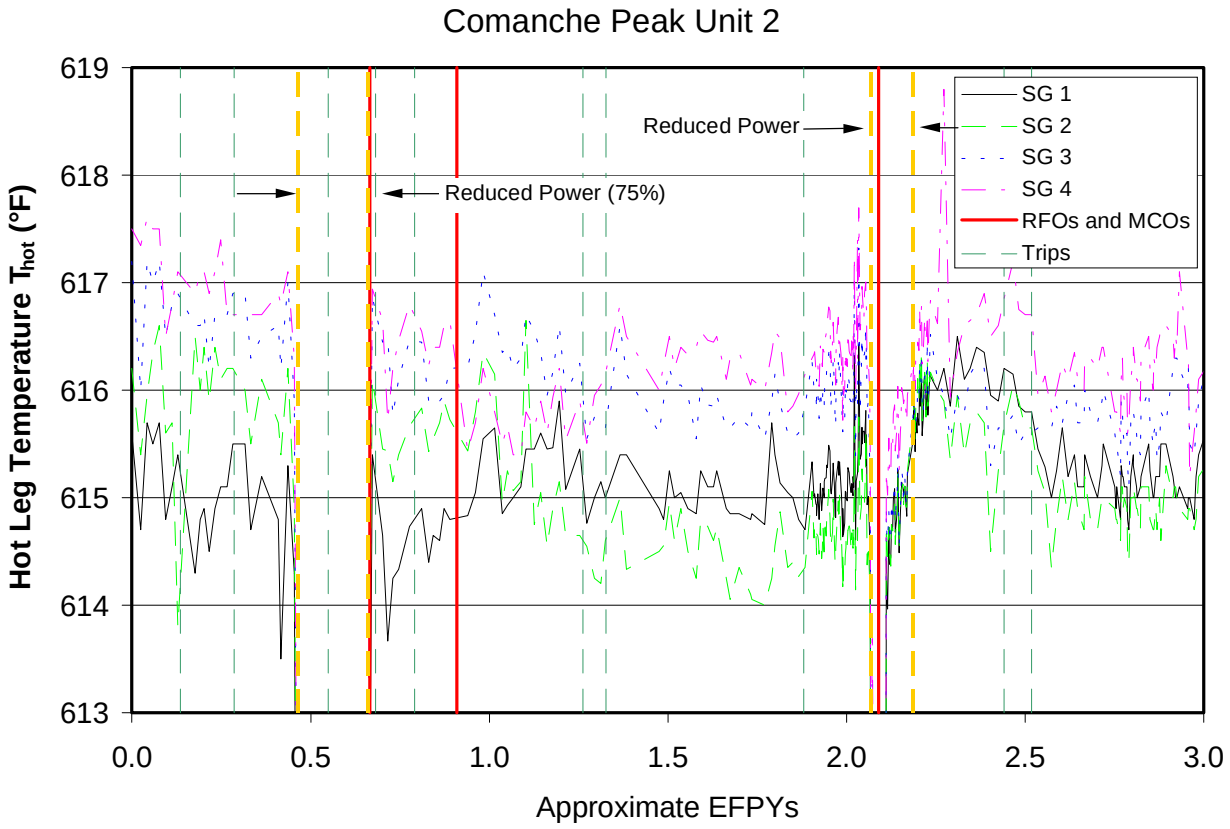

Figure D-2b
Historical Hot Leg Temperature at Comanche Peak 2

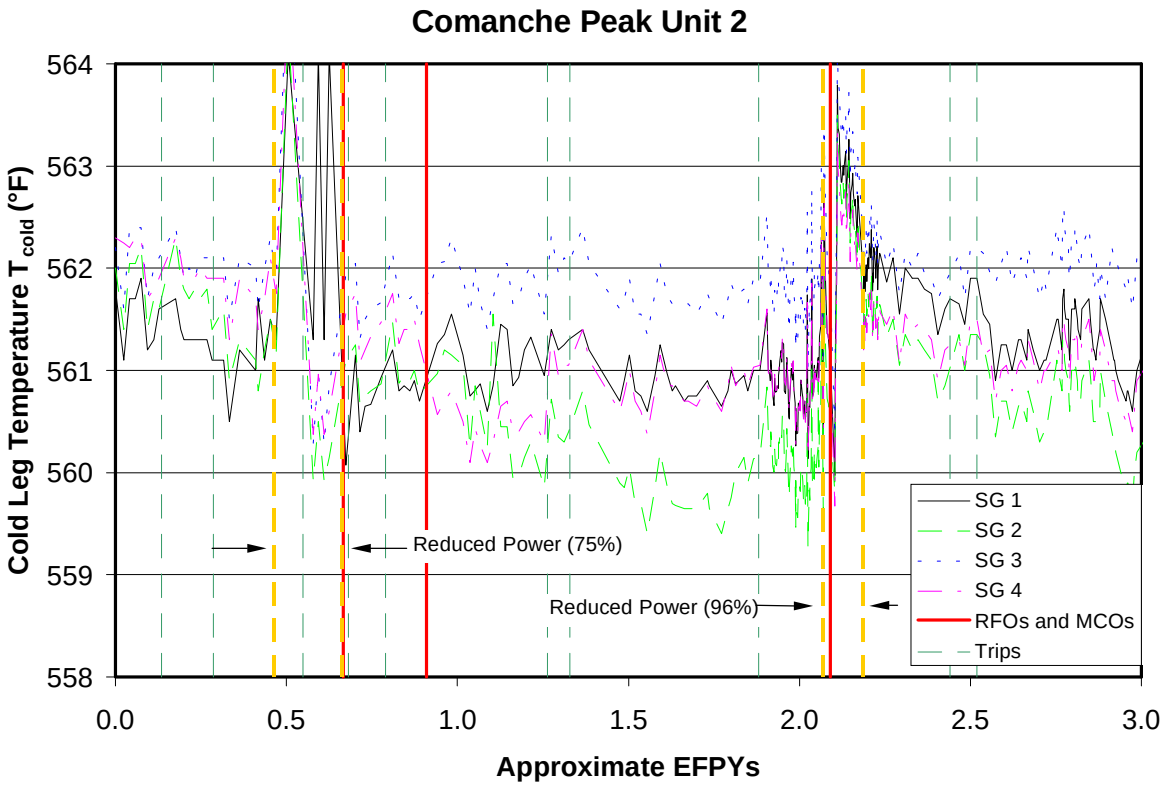

Figure D-2c
Historical Cold Leg Temperature at Comanche Peak 2

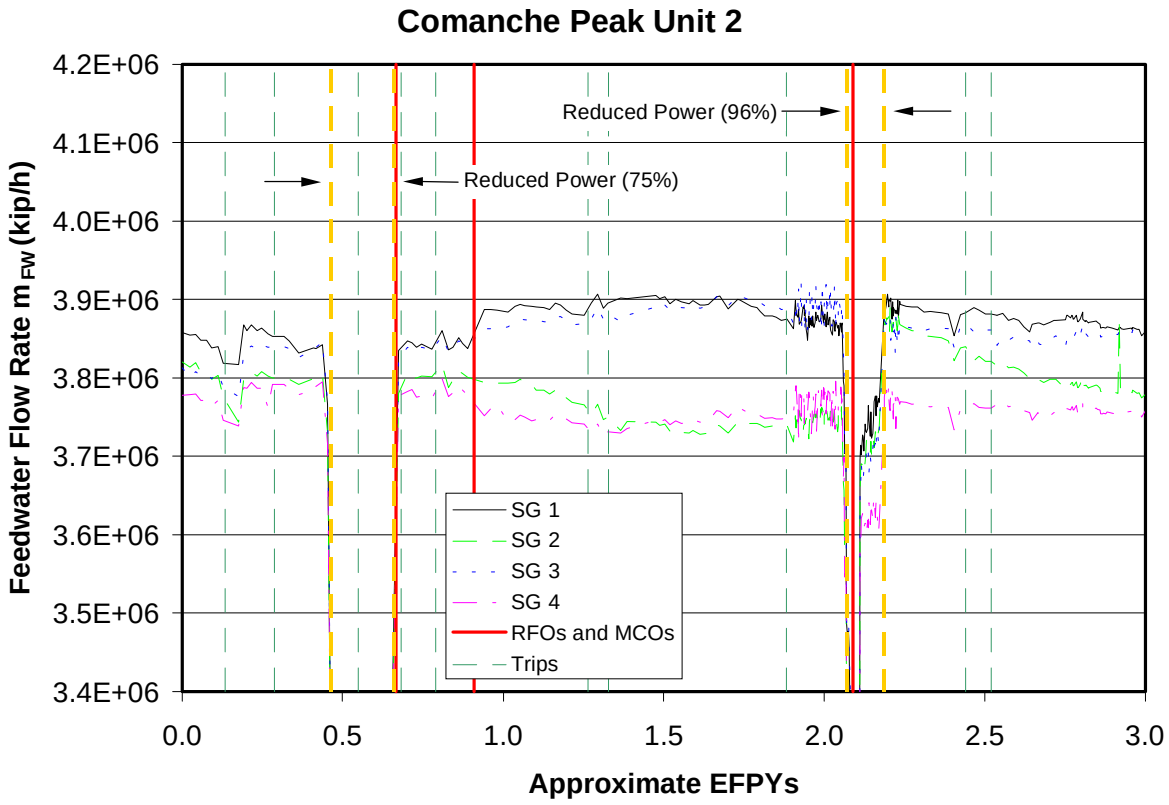

Figure D-3
Historical Feedwater Mass Flow Rate at Comanche Peak

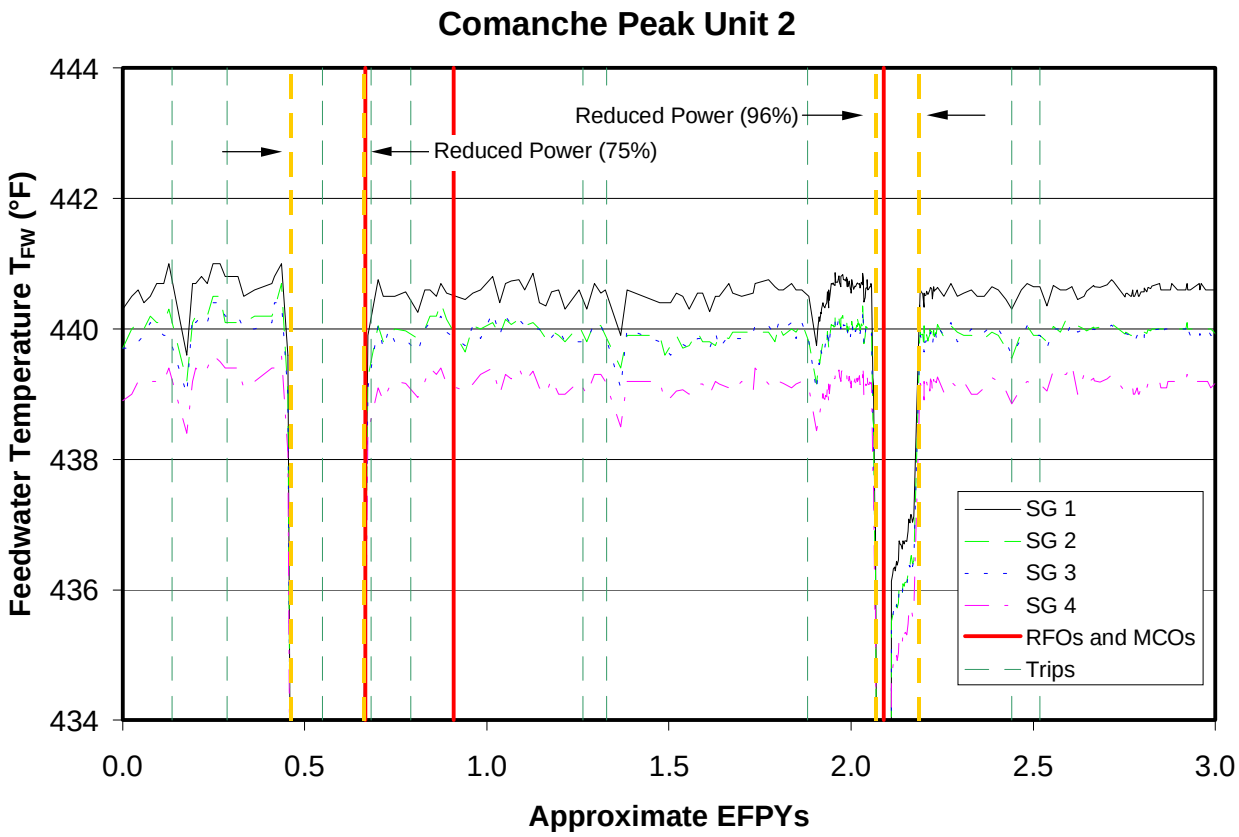

Figure D-4
Historical Feedwater Temperature at Comanche Peak 2

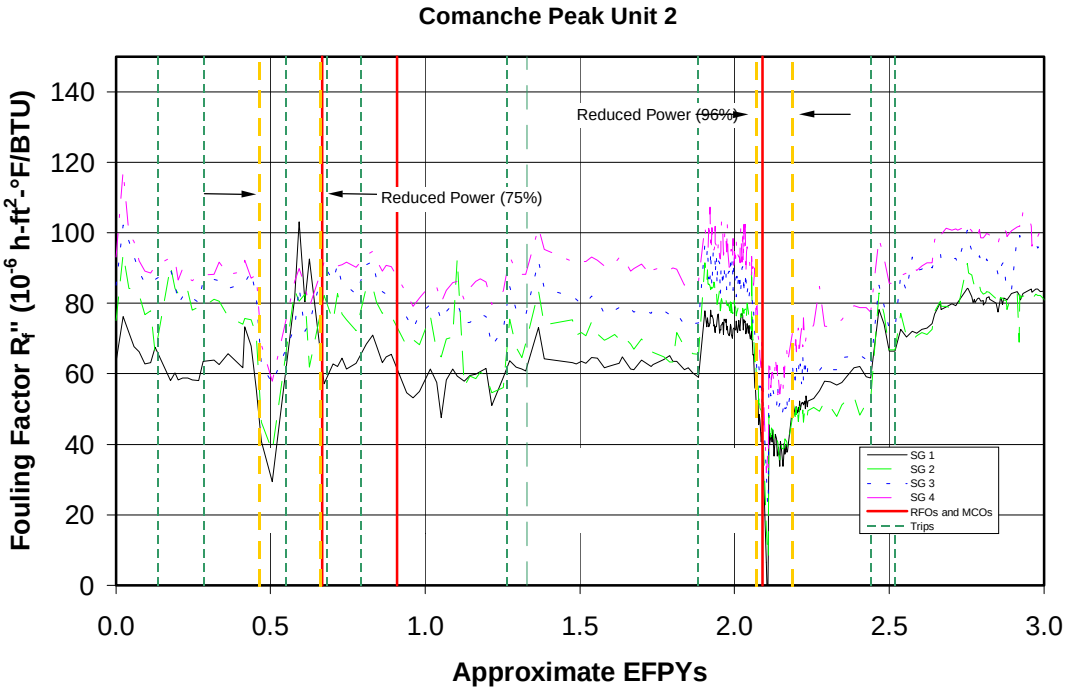

Figure D-5
Historical Fouling Factor at Comanche Peak 2
(Using Feedwater Flow Measurements)

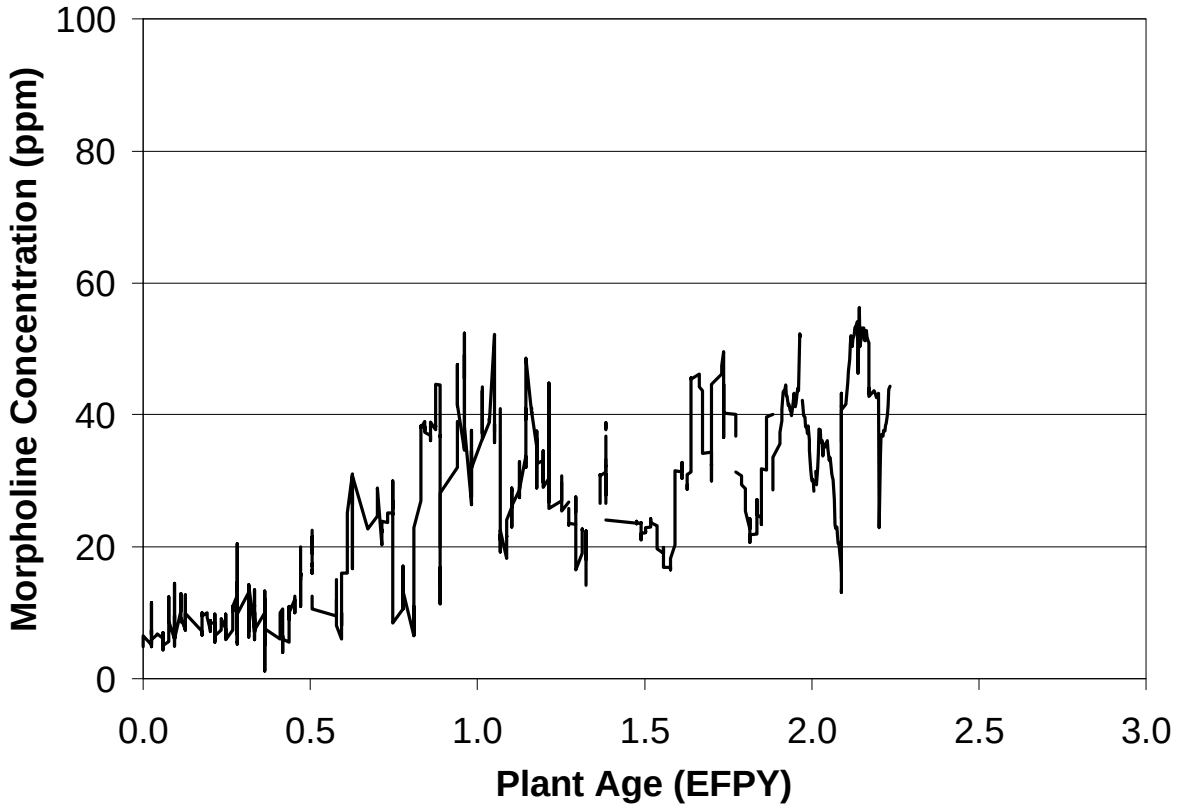

Figure D-6
Historical Feedwater Morpholine Concentration at Comanche Peak 2

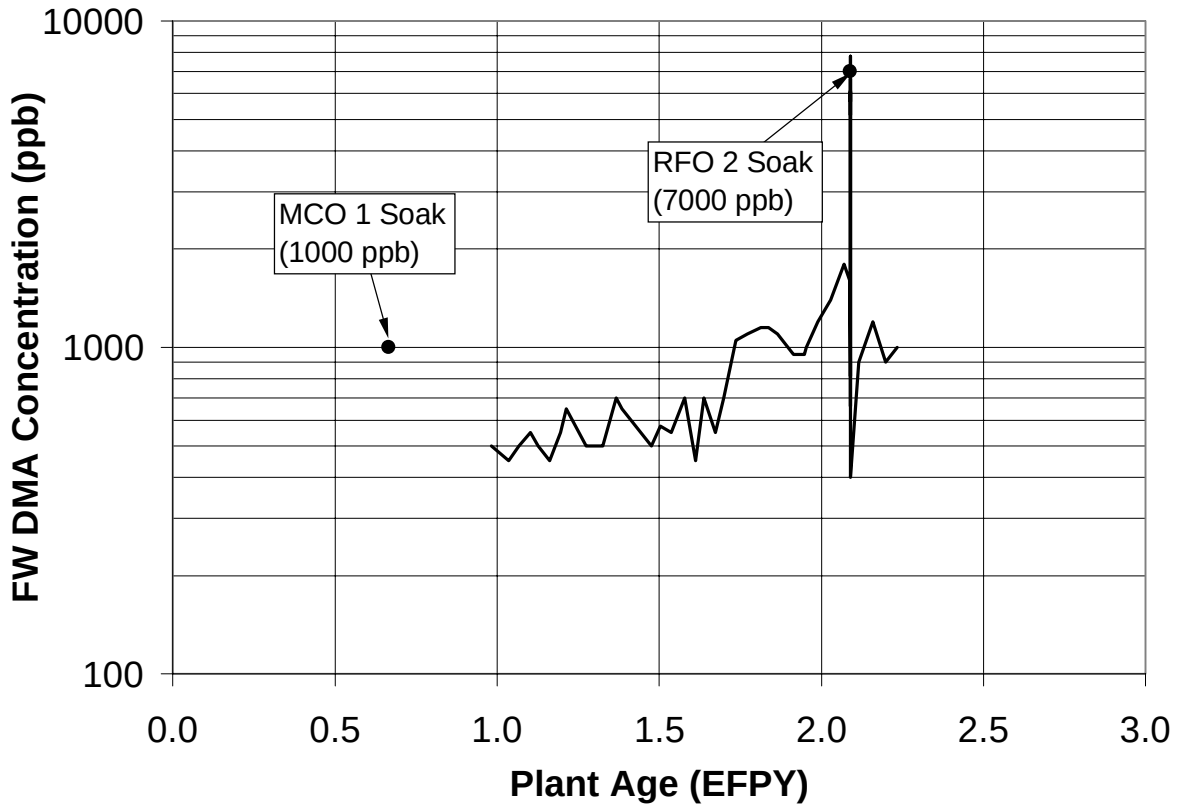

Figure D-7
Historical Feedwater DMA Concentration at Comanche Peak 2 Versus Operating Time

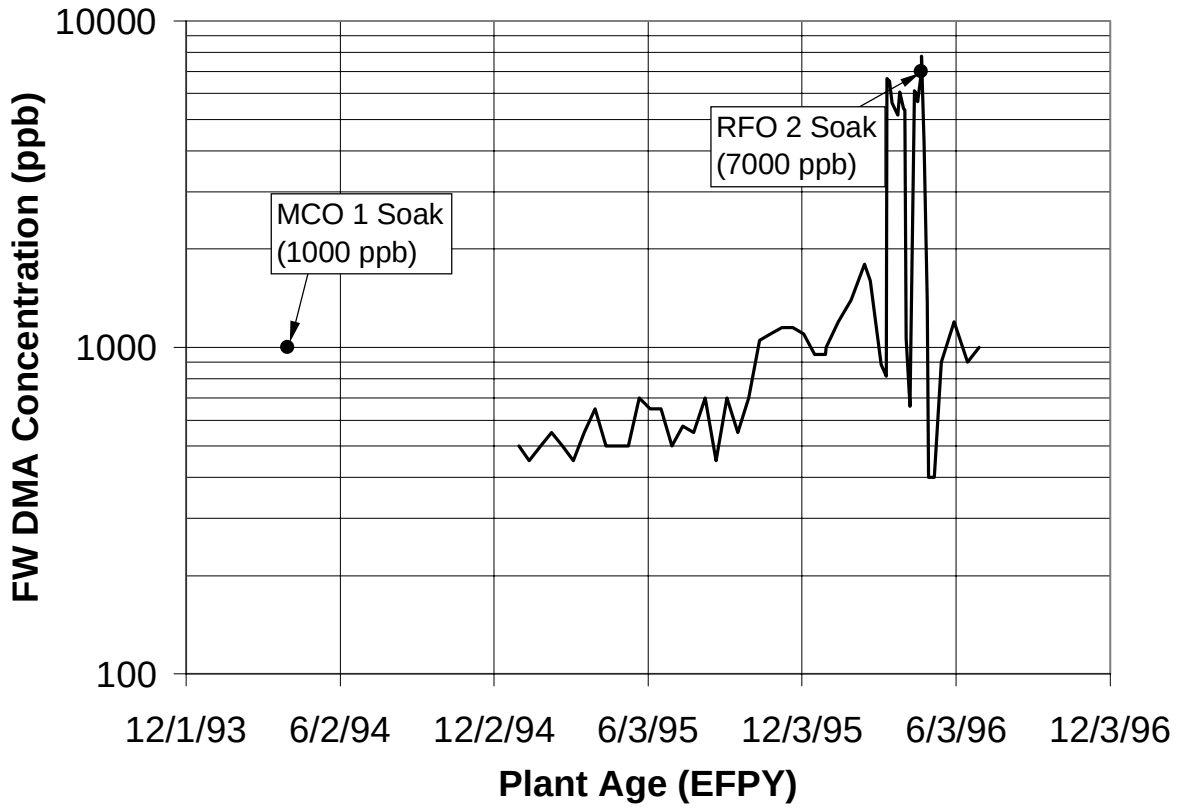

Figure D-8
Historical Feedwater DMA Concentration at Comanche Peak 2 Versus Calendar Time

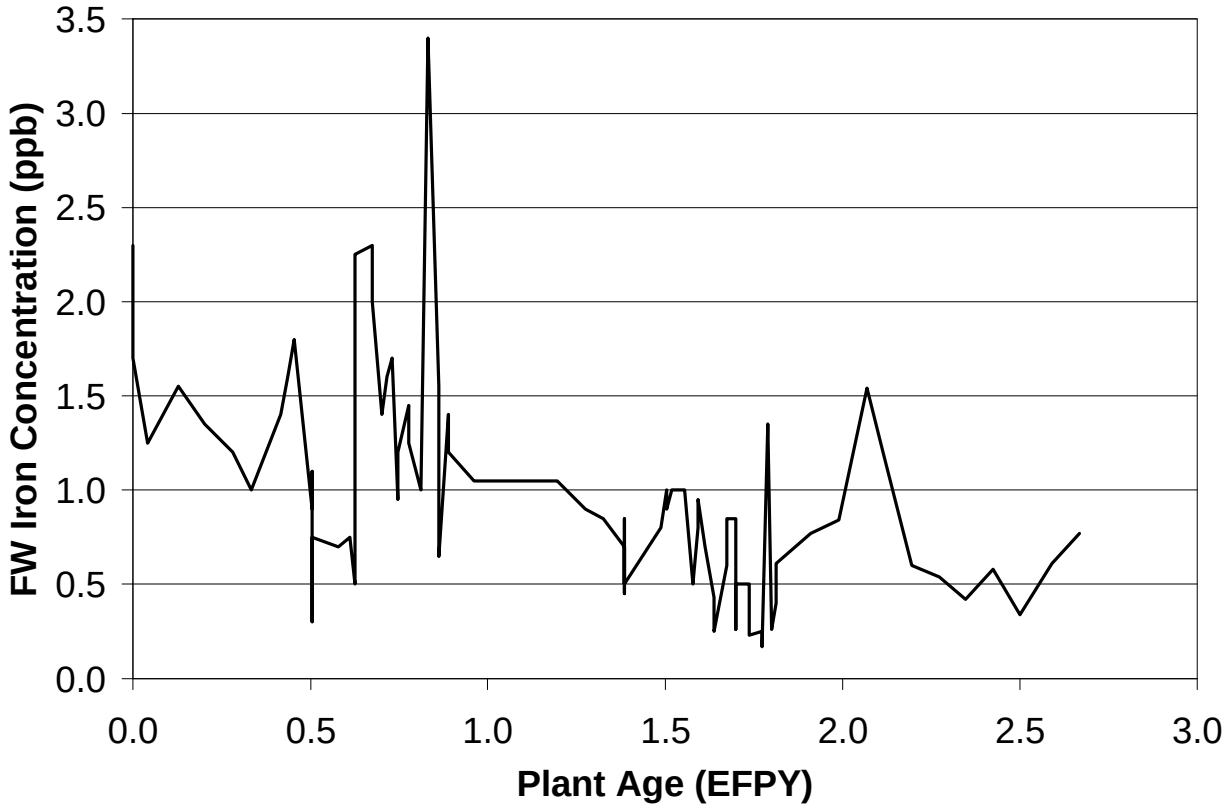

Figure D-9
Historical Feedwater Iron Concentration at Comanche Peak 2

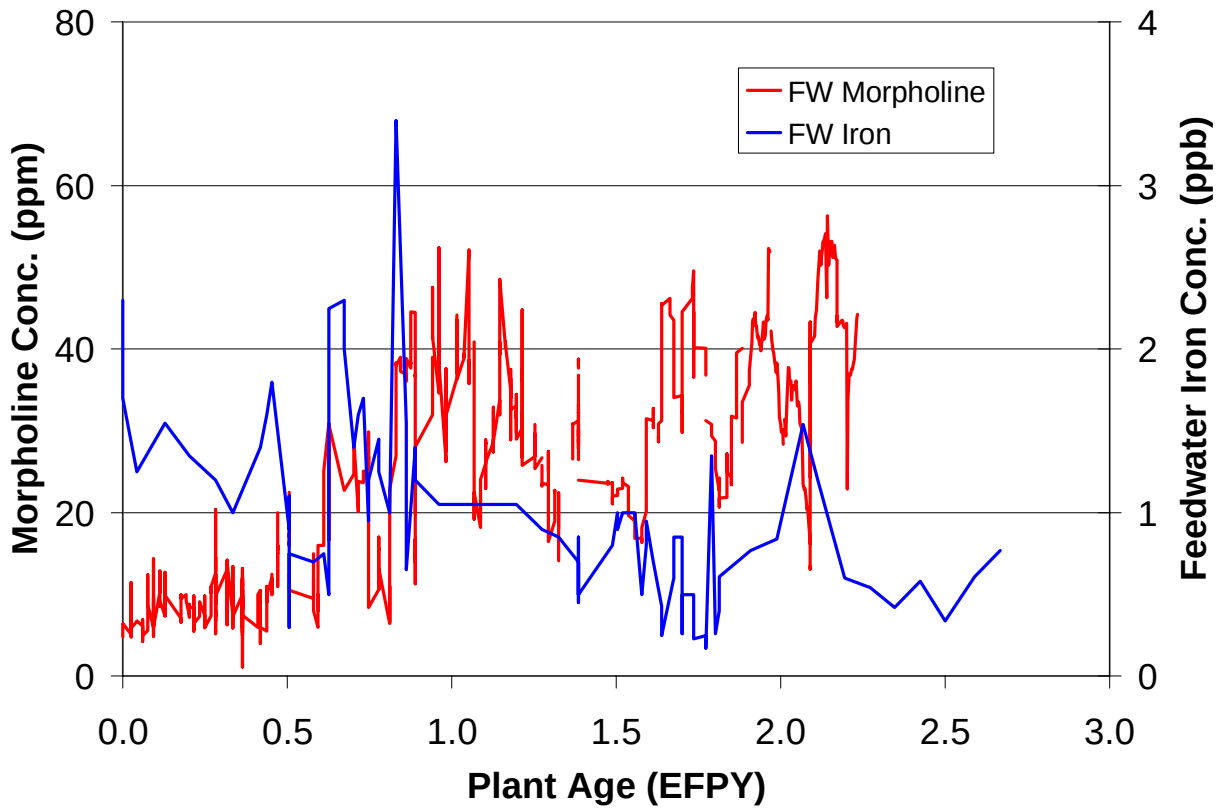

Figure D-10
Historical Feedwater Morpholine and Iron Concentrations at Comanche Peak 2

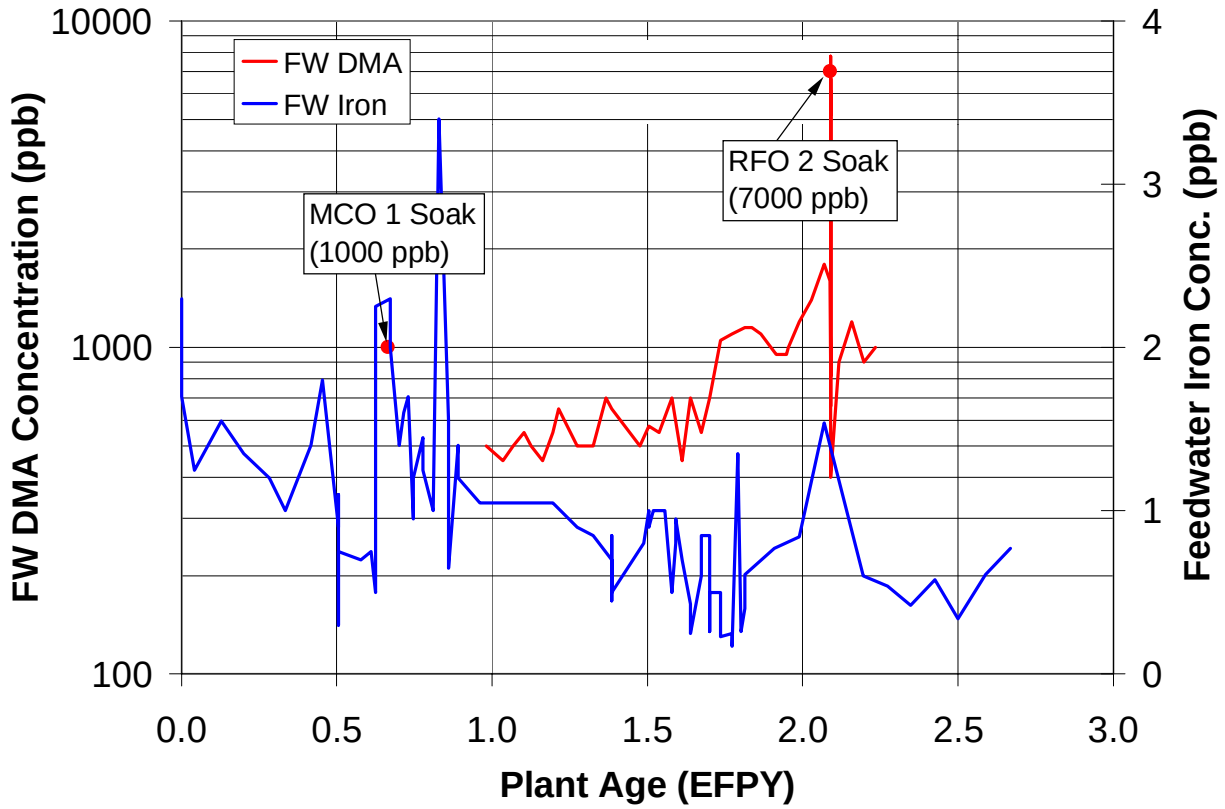

Figure D-11
Historical Feedwater DMA and Iron Concentrations at Comanche Peak 2

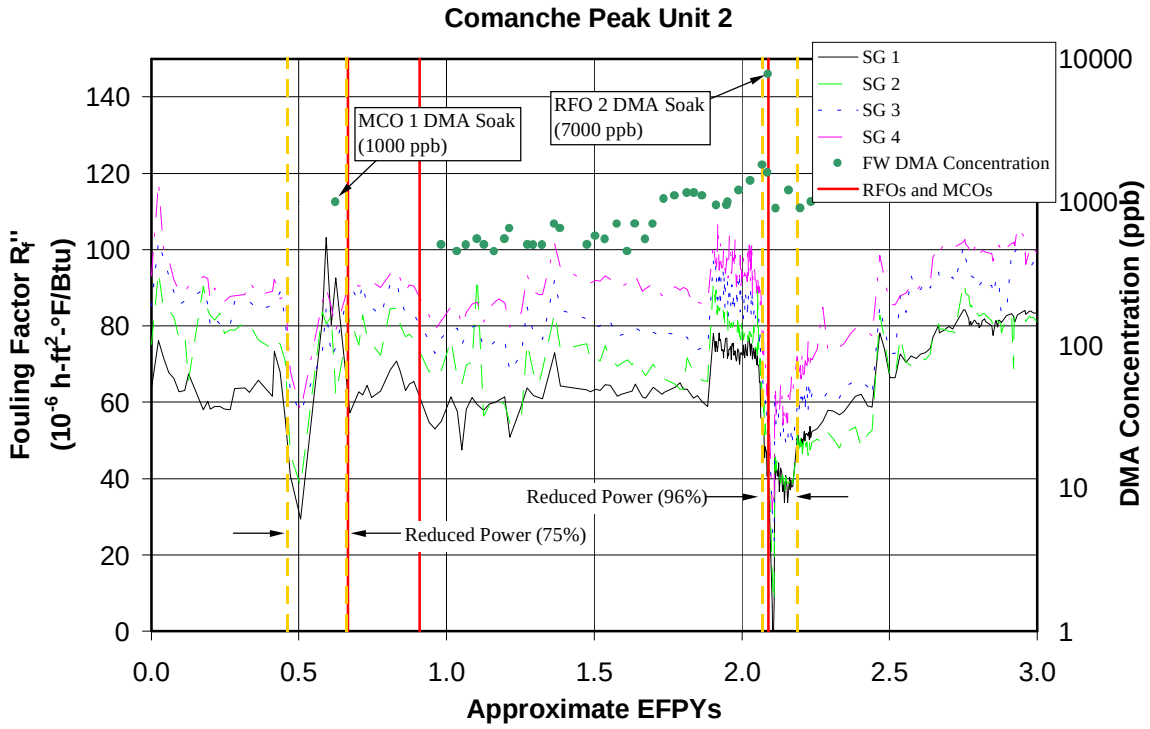

Figure D-12
Historical Fouling Factor and DMA Concentration at Comanche Peak 2

E

MEMORANDUM ON SG PRIMARY FILMS

Date: December 1, 1995

Subject: Telecons with Charles Laire (Laborelec), François Cattant (EPRI/NMAC*) and Kjell Norring (Studsvik Energy)

Charles Laire (Laborelec-Belgium) – November 29, 1995

Based on his experimental work on numerous tubes, he indicated the following information regarding primary-side (ID) corrosion:

- Oxide layers were very thin - typically 1 micron or less.
- IGA on the ID surface penetrated only 15-20 microns at the most. The IGA surfaces, he believes, are oxide filled (not steam spaces). He doesn't believe that the IGA has a significant effect on heat transfer.
- In his experiments, no data on primary-side film composition was collected.
- Doel 4 had a similar experience to Callaway, i.e., chemical cleaning did not result in a significant steam pressure improvement, despite the success in removing corrosion products. Laire indicated that the theory why no pressure recovery was realized is that corrosion products may have been blocking preheater bypass flow prior to chemical cleaning. This blockage increased heat transfer. After chemical cleaning, this blockage may have been cleared, counteracting the beneficial effect of deposit removal.

François Cattant (EPRI/NMAC) – November 30, 1995

Based on his experimental work on numerous tubes from French SGs, he indicated the following information regarding primary-side (ID) corrosion:

- Primary-side oxide thickness depends somewhat on tube manufacturer:

---

* Believed to be currently at EdF.

Vallourec/Inphy:	1.5 microns average
Westinghouse/Huntington:	0.92 microns average
Vallourec/Huntington:	1.1 microns average

A maximum thickness from all samples was recorded to be 4 to 5 microns thick. These tubes were from Dampierre, Gravelines, and Tricastin, plants that had been in operation for about 10 years at the time of the tube pulls (ca. 1990).

Further details are available in EdF Document No. D5004/CTT/RA.90.128, dated Dec. 3, 1990, and titled "PWR Plants SGs: Composition and Thickness of Layers on ID Surfaces" [approximate translation from French].

- The main components of the film were oxides of Cr, Ni, and Fe.
- IGA on the primary side varied in thickness from 5-10 microns above the TS to 10-20 microns in the TS. No tests were performed to determined IGA composition. The grain-boundary thicknesses on the primary side were ≈0.5 microns.

Kjell Norring (Studsvik Energy - Sweden) – December 1, 1995

Based on his examination of tubes from Ringhals 3 and 4 (ca. 1990), he indicated the following information regarding primary-side (ID) corrosion:

- Oxide thickness averages approximately 1 micron; the thickness tends to be very uniform.
- No spalling of ID films has been observed.
- He does not believe that the structure of primary-side IGA is likely to be a source of reduced heat transfer.